BULK DC-DC CONVERSION FOR MVDC APPLICATIONS

Prof. D. Dujić, Dr. J. Kucka*, Dr. G. Ulissi, N. Djekanović, R. Barcelos**
École Polytechnique Fédérale de Lausanne (EPFL)
Power Electronics Laboratory (PEL)
*Large Drives Applications, SIEMENS AG, Germany
**Roland Berger, Zurich, Switzerland

INTRODUCTION

Power Electronics Laboratory at EPFL

Prof. Drazen Dujic, Head of the Power Electronics Laboratory at EPFL, Lausanne, Switzerland

Education:

- 2008 PhD, Liverpoool John Moores University, Liverpool, United Kingdom
- 2005 M.Sc., University of Novi Sad, Novi Sad, Serbia
- 2002 Dipl. Ing., University of Novi Sad, Novi Sad, Serbia

Dr. Jakub Kucka, was with EPFL as Postdoc., now with SIEMENS AG, Large Drives Application, Erlangen, Germany

Education:

- 2019 PhD, Leibniz University Hannover, Hannover, Germany
- 2014 M.Sc., Czech Technical University, Prague, Czech Republic

Dr. Gabriele Ulissi, with Roland Berger, Zurich, Switzerland

Education:

- 2022 PhD, École Polytechnique Fédérale de Lausanne (EPFL), Lausanne, Switzerland
- 2018 M.Sc., École Polytechnique Fédérale de Lausanne (EPFL), Lausanne, Switzerland

Ms. Nikolina Djekanovic, PhD student with Power Electronics Laboratory at EPFL

Education:

- 2023 PhD, École Polytechnique Fédérale de Lausanne (EPFL), Lausanne, Switzerland
- 2018 M.Sc., Technische Universität Wien (TUW), Wien, Austria

Mr. Renan Pillon Barcelos, PhD student with Power Electronics Laboratory at EPFL

Education:

- 2025 PhD, École Polytechnique Fédérale de Lausanne (EPFL), Lausanne, Switzerland
- 2021 M.Sc., Universidade Federal de Santa Catarina (UFSC), Florianópolis, Brasil

École Polytechnique Fédérale de Lausanne

School of Engineering

EPFL — STI — IEM — PEL

Institute of Electrical and Micro Engineering

- Online since February 2014
- Currently: 10 PhD students, 4 Post Docs, 1 Administrative Assistant
- Funding CH: SNSF, SFOE, Innosuisse
- Funding EU: H2020, S2R JU, ERC CoG
- Funding Industry: OEMs
- `https://www.epfl.ch/labs/pel/`

ECPE Competence Centre

▲ PEL Medium Voltage Laboratory

RESEARCH FOCUS

MVDC Technologies and Systems
- System Stability
- Protection Coordination
- Power Electronic Converters

MVDC
ENERGY CONVERSION TECHNOLOGIES AND SYSTEMS

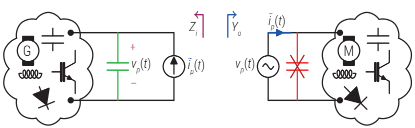

High Power Electronics
- Multilevel Converters
- Solid State Transformers
- Medium Frequency Conversion

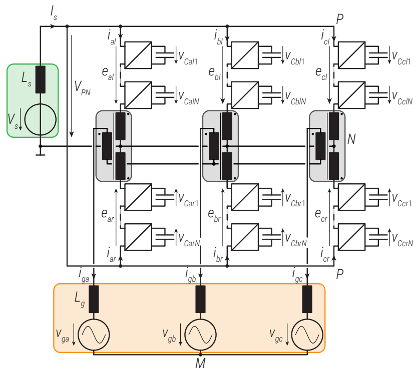

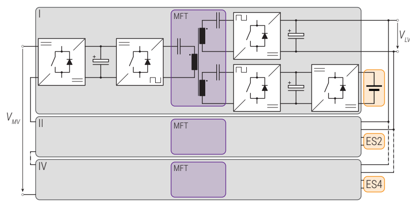

Components
- Semiconductor devices
- Magnetics
- Modeling, Characterization

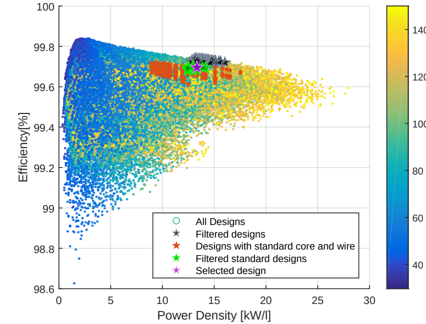

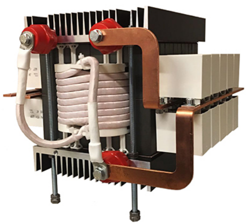

Before the coffee break

1) Introduction
- MVDC Applications
- Motivation and Challenges
- Power Electronics Converters

2) Bulk vs Modular Power Conversion
- High Power DC-DC Conversion
- Modular DC-DC Conversion
- Bulk DC-DC Conversion – DC Transformer

3) Resonant Conversion
- Resonant DC-DC Converters
- Modeling
- Control Principles

After the coffee break

4) HV Semiconductors
- High Voltage Devices
- IGBT versus IGCT
- Design with IGCTs

5) Gate Drivers for IGCT
- Operating Principles
- Optimization for the Resonant Operation
- High Frequency Operation

6) IGCT Resonant Switching
- ZVS versus ZCS
- Series-connection of IGCTs
- High Frequency Operation

⇒ Tutorial pdf can be downloaded from: *(Source:* `https://www.epfl.ch/labs/pel/publications-2/publications-talks/`*)*

Before the coffee break

7) MFT Design Challenges

- MW Design Challenges
- Technologies and Materials
- Electrical and Thermal Modeling

8) MFT Design Examples

- MFTs for SST
- MFTs for Bulk Power
- Special Designs

9) MFT Design Optimization

- Design Optimization
- Practical 1MW 5kHz Design Experience
- Experimental Results

After the coffee break

10) MVDC Power Distribution Networks

- MVDC Network Modelling
- DC Transformer in MVDC Power Distribution Networks
- Operational Performance Assessment

11) Direct Current Transformer Features

- Operating Principles
- Power Reversal Methods
- Practical Examples

12) Summary and Conclusions

- Why MVDC?
- How MVDC?
- When MVDC?

⇒ Tutorial pdf can be downloaded from: *(Source:* `https://www.epfl.ch/labs/pel/publications-2/publications-talks/`*)*

INTRODUCTION

MVDC Applications, Systems and Technologies

WHY DC?

- No reactive power

  Example: @ $cos(\varphi) = 0.95$

  $$\frac{P}{Q} \approx \frac{3}{1}$$

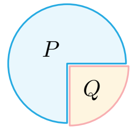

  - No constraints imposed upon transmission distance
  - Transmission capacity increase
  - Lower transmission losses
  - Alleviated stability problems

- No skin effect ($R_\gamma \downarrow \Longrightarrow P_\gamma \uparrow$)
- Cheaper solution ("Break-even distance")
- Underwater cable transmission
- No need for synchronization (Marine applications)
- Direct integration of Renewable Energy Sources
- Challenges $\Longrightarrow$ DC Transformer/Protection?

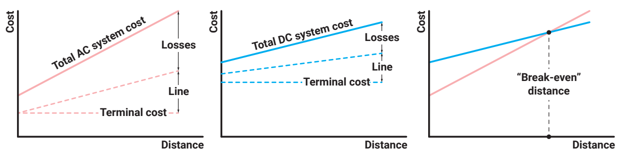

▲ Cost comparison between AC and DC systems

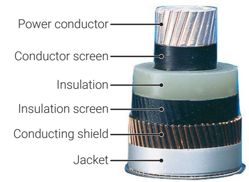

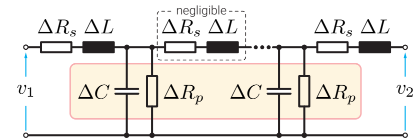

▲ High voltage cable

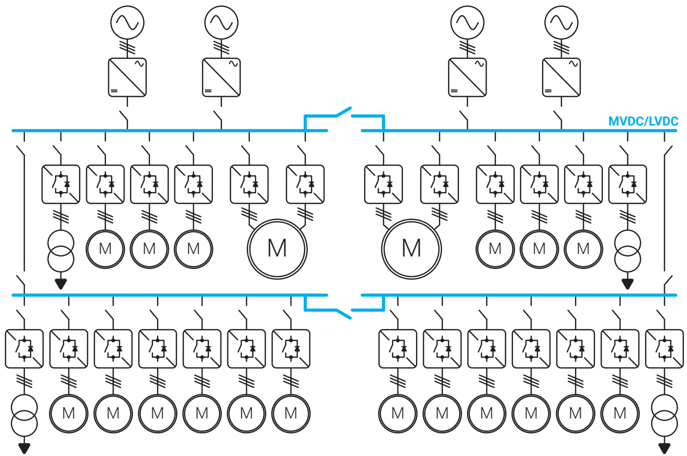

▲ DC Ship distribution system - frequency decoupling through a DC distribution [1]

[1] Uzair Javaid et al. "MVDC supply technologies for marine electrical distribution systems." *CPSS Transactions on Power Electronics and Applications* 3.1 (2018), pp. 65–76

CONVERSION OF AC LINES INTO DC

- Transmission capacity increase
- Employment of the existing conductors
- No change in tower foundations
- Possible tower head adjustment
- Possible isolator assemblies adjustment

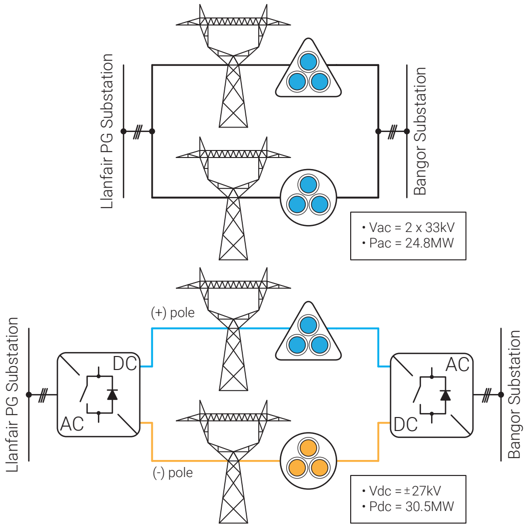

▲ Angle DC Project - UK

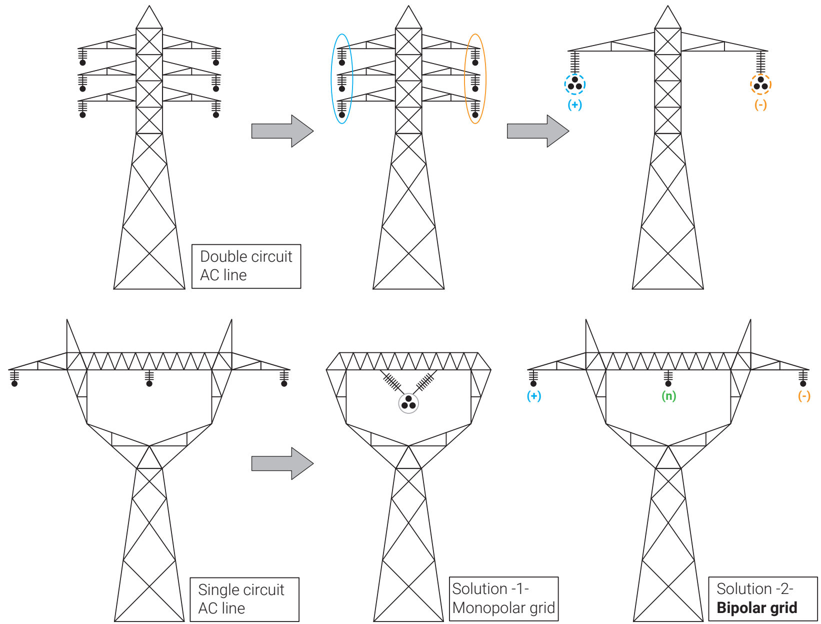

▲ Conversion of two typical AC lines into DC [2], [3], [4], [5]

MVDC POWER DISTRIBUTION NETWORKS

MVDC Power Distribution Networks

- Feasibility (Applications)
- System Level Gains
- Dynamic Stability

Conversion

- Passive and Stable
- Flexible, Modular and Scalable
- Efficient

Protection

- DC Breaker?
- Fault Current Limiting by Converters
- Protection Coordination

▲ Power electronics constituents

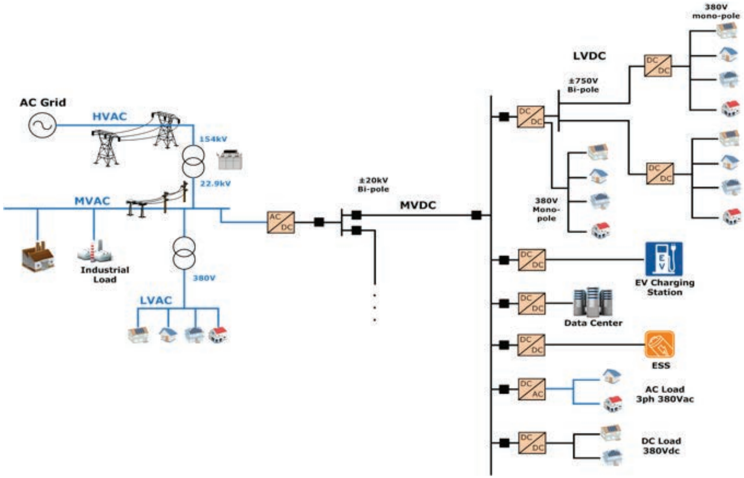

▲ Envisioned future MVDC grids and its links with existing grids

A TREND TOWARDS DC

Bulk power transmission

- Break even distance against AC lines
- ~ 50 – 100 km for subsea cables or 600 km for overhead lines
- Long history since 1950s
- Interconnection of asynchronous grids

▲ From mercury arc rectifiers to modern HVDC systems

LVDC ships

- Variable frequency generators ⇒ maximum efficiency of the internal combustion engines
- Commercial products by ABB & Siemens

▲ Specialized vessels with LVDC distribution

Datacenters

- 380 V_{dc}
- DC loads (including UPS)
- Expected efficiency increase

Large PV powerplants

- 1500 V_{dc} PV central inverters
- Higher number of series-connected panels per string

▲ 1500V PV inverter - step towards the MVDC

Open challenges

- DC breaker
- Conversion blocks missing
- Protection coordination
- Business case

A TREND TOWARDS DC

Bulk power transmission

- Break even distance against AC lines
- ~ 50 – 100 km for subsea cables or 600 km for overhead lines
- Long history since 1950s
- Interconnection of asynchronous grids

▲ From mercury arc rectifiers to modern HVDC systems

LVDC ships

- Variable frequency generators ⇒ maximum efficiency of the internal combustion engines
- Commercial products by ABB & Siemens

▲ Specialized vessels with LVDC distribution

Datacenters

- 380 V_{dc}
- DC loads (including UPS)
- Expected efficiency increase

Large PV powerplants

- 1500 V_{dc} PV central inverters
- Higher number of series-connected panels per string

▲ 1500V PV inverter - step towards the MVDC

Open challenges

- DC breaker
- Conversion blocks missing
- Protection coordination
- Business case

⇒ DC is beneficial for medium / high power applications

EMERGING MVDC APPLICATIONS

Installations

- ABB HVDC Light demo: 4.3 km/$\pm$9 kV_{dc} [6]
- Tidal power connection: 16 km/10 kV_{dc} (based on MV3000 & MV7000) [7]

- Unidirectional oil platform connection in China: 29.2 km/$\pm$15 kV_{dc} [8]

Projects

- Angle DC: conversion of 33 kV MVac line to $\pm$27 kV MVdc [9]

Universities

- Increased number of laboratories active in high power domain
- China, Europe, USA,...

Products

- Siemens MVDC Plus
  - 30 - 150 MW
  - < 200 km
  - < $\pm$50 kV_{dc}

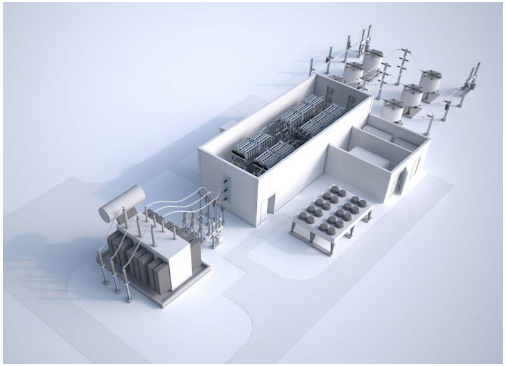

- RXPE Smart VSC-MVDC
  - 1 - 10 MVAr
  - $\pm$5 - $\pm$50 kV_{dc}
  - 40 - 200 km

EMERGING MVDC APPLICATIONS

Installations

- ABB HVDC Light demo: 4.3 km/$\pm$9 kV$_{dc}$ [6]
- Tidal power connection: 16 km/10 kV$_{dc}$ (based on MV3000 & MV7000) [7]

- Unidirectional oil platform connection in China: 29.2 km/$\pm$15 kV$_{dc}$ [8]

Projects

- Angle DC: conversion of 33 kV MVac line to $\pm$27 kV MVdc [9]

Universities

- Increased number of laboratories active in high power domain
- China, Europe, USA,...

Products

- Siemens MVDC Plus
  - 30 - 150 MW
  - < 200 km
  - < $\pm$50 kV$_{dc}$

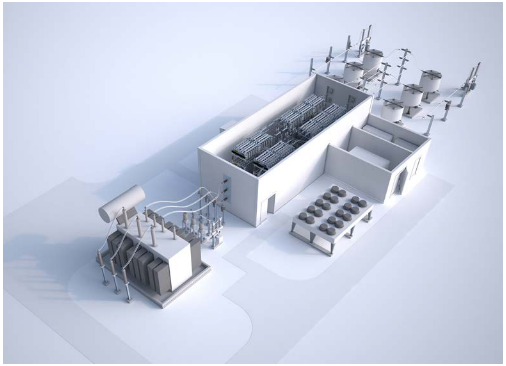

- RXPE Smart VSC-MVDC
  - 1 - 10 MVAr
  - $\pm$5 - $\pm$50 kV$_{dc}$
  - 40 - 200 km

⇒ MVDC is gaining momentum through early pilot and demonstration projects!

A TREND TOWARDS HIGHLY MODULAR CONVERTER TOPOLOGIES

HVDC

- Decoupled semiconductor switching frequency from the converter apparent switching frequency
- Improved harmonic performance ⇒ less / no filters
- Series-connection of semiconductors still possible
- Fault blocking capability depending on the cell type

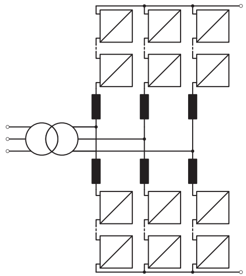

MV drives

- Monolithic ML topologies (NPC, NPP, FC, ANPC) are not scalable
- Robicon drive → everyone offers it
- Siemens & Benshaw: MMC drive
- Low dv/dt → motor friendly

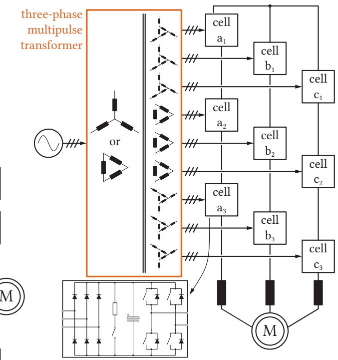

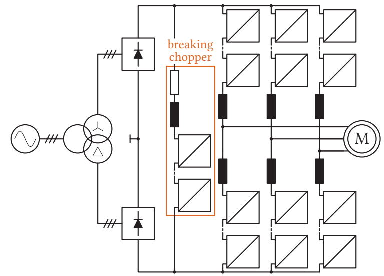

Solid-state transformers (SSTs)

- Power density increase w/ conversion & isolation at higher frequency
- Grid applications / traction transformer w/ different optimization objectives
- MFT design / isolation are the bottlenecks

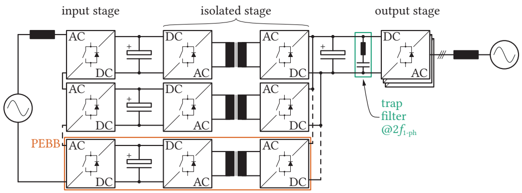

FACTS

- SFC for railway interties (direct catenary connection)
- STATCOM
- BESS (split batteries)

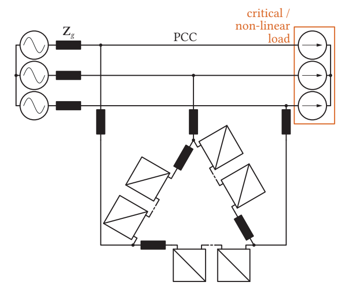

A TREND TOWARDS HIGHLY MODULAR CONVERTER TOPOLOGIES

HVDC

- Decoupled semiconductor switching frequency from the converter apparent switching frequency
- Improved harmonic performance ⇒ less / no filters
- Series-connection of semiconductors still possible
- Fault blocking capability depending on the cell type

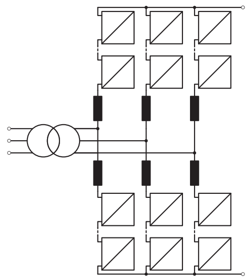

Solid-state transformers (SSTs)

- Power density increase w/ conversion & isolation at higher frequency
- Grid applications / traction transformer w/ different optimization objectives
- MFT design / isolation are the bottlenecks

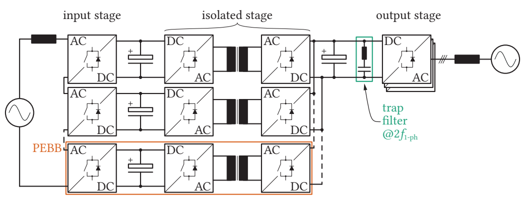

MV drives

- Monolithic ML topologies (NPC, NPP, FC, ANPC) are not scalable
- Robicon drive → everyone offers it
- Siemens & Benshaw: MMC drive
- Low dv/dt → motor friendly

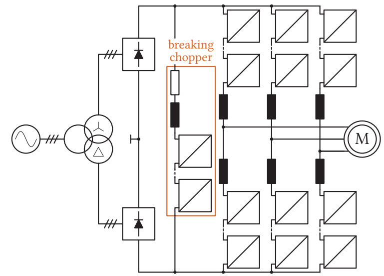

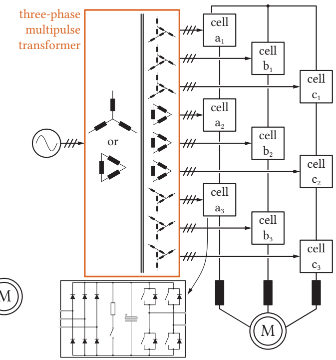

FACTS

- SFC for railway interties (direct catenary connection)
- STATCOM
- BESS (split batteries)

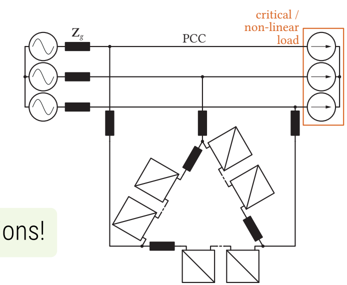

⇒ Modularity provides obvious benefits in high power AC-DC applications!

SOLID STATE TRANSFORMER FOR TRACTION (ABB - 1.2MW PETT)

Characteristics

- 1-Phase MVAC to MVDC
- Power: 1.2MVA
- Input AC voltage: 15kV, 16.7Hz
- Output DC voltage: 1500 V
- 9 cascaded stages (n + 1)
- input-series output-parallel
- double stage conversion

99 Semiconductor Devices

- HV PEBB: 9 x (6 x 6.5kV IGBT)
- LV PEBB: 9 x (2 x 3.3kV IGBT)
- Bypass: 9 x (2 x 6.5kV IGBT)
- Decoupling: 9 x (1 x 3.3kV Diode)

9 MFTs

- Power: 150kW
- Frequency: 1.75kHz
- Core: Nanocrystalline
- Winding: Litz
- Insulation / Cooling: Oil

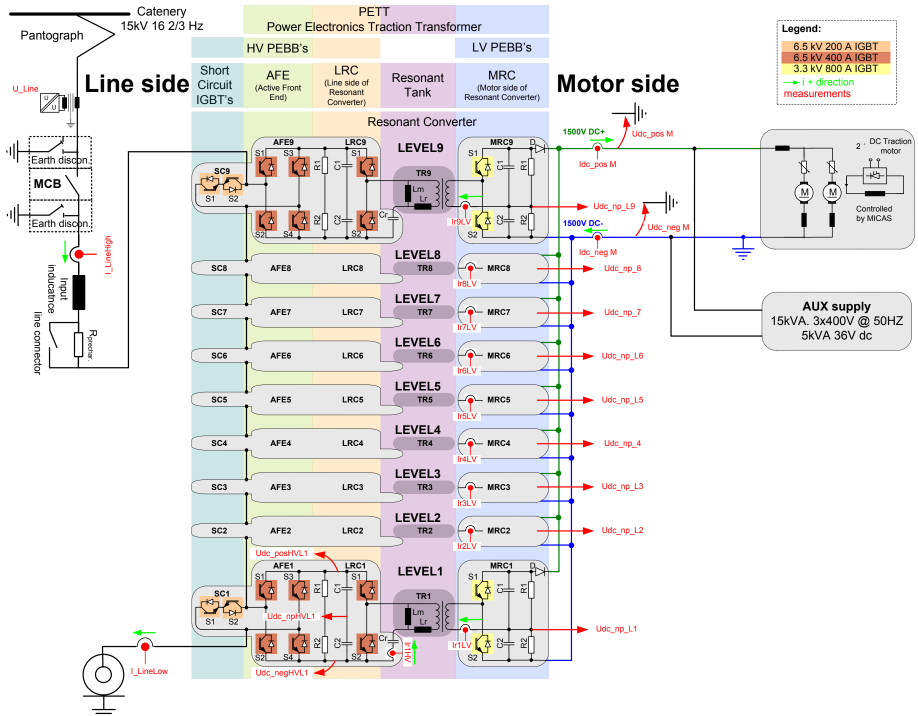

▲ ABB PETT scheme [10], [11]

Retrofitted to shunting locomotive

- Replaced LFT + SCR rectifier
- Propulsion motor - 450kW
- 12 months of field service
- No power electronic failures
- Efficiency around 96%
- Weight: ≈ 4.5 t

Technologies

- Standard 3.3kV and 6.5kV IGBTs
- De-ionized water cooling
- Oil cooling/insulation for MFTs
- n + 1 redundancy
- IGBT used for bypass switch

Displayed at:

- Swiss Museum of Transport
- https://www.verkehrshaus.ch

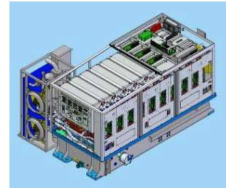





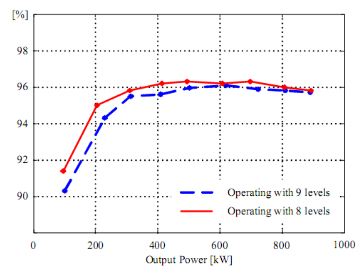

▲ ABB PETT prototype [10], [11]

[10] D. Dujic et al. "Power Electronic Traction Transformer-Low Voltage Prototype." *IEEE Transactions on Power Electronics* 28.12 (Dec. 2013), pp. 5522–5534

[11] C. Zhao et al. "Power Electronic Traction Transformer-Medium Voltage Prototype." *IEEE Transactions on Industrial Electronics* 61.7 (July 2014), pp. 3257–3268

UNIFLEX-PM

- Reduced scale prototypes

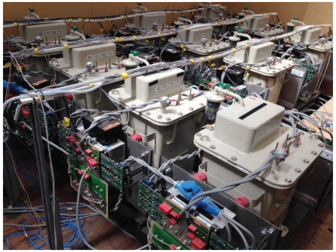

▲ UNIFLEX-PM prototype

FREEDM

- Reduced scale prototypes

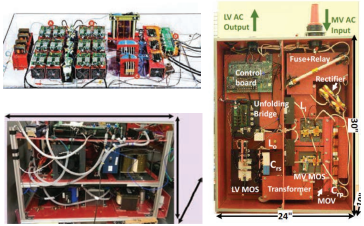

▲ FREEDM SSTs [13]

HEART

- Reduced scale prototypes

▲ HEART project

GE

- Full scale prototype

▲ GE prototype [12]

HUST

- Full scale prototype

▲ HUST SST [14]

XD Electric Company

- Full scale prototype

▲ XD Electric Company SST [15]

SOLID-STATE TRANSFORMER (SST)

Concept and motivation?

- SST = Switching stages + Isolation
- Firstly envisioned within AC grids
- Power Electronic Building Blocks (PEBBs)
- Conventional transformer vs SST?
- Operating frequency increase **(MFT)**

	Grid Tx	SST
Controlability	No	Yes
Efficiency	$\eta \geq 99\%$	$P_?$
Q compensation	No	Yes
Fault tolerance	No	Yes
Size	Bulky	Compact
Cost	Low	High

Advantages at the expense of cost and reduced efficiency!

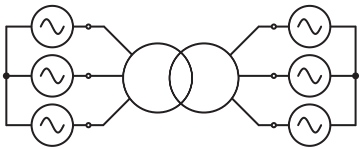

▲ Conventional AC grid transformer

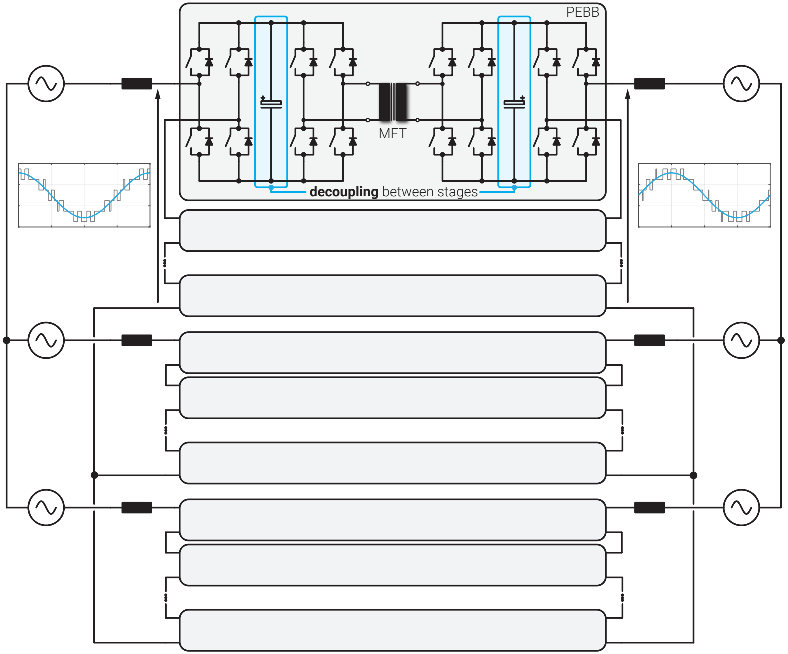

▲ Solid-State Transformer employed with the aim of interfacing two AC systems [16], [17]

- Inherent part of the almost all SST topologies
- Expansion of the existing power system
- Enabling technology for MVDC
- Penetration of renewable energy sources
- Fast / Ultra Fast EV charging
- **Medium Frequency conversion**

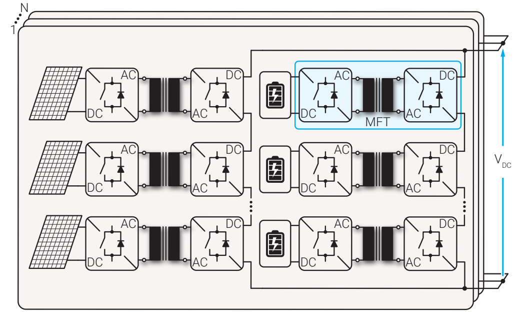

▲ Employment of a DC-DC SST within RES-based systems

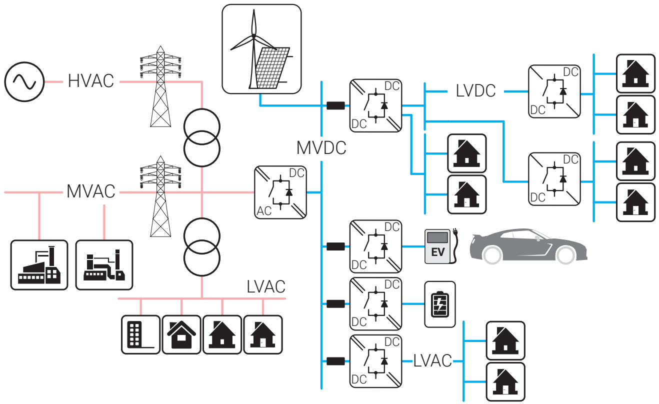

▲ Concept of a modern power system

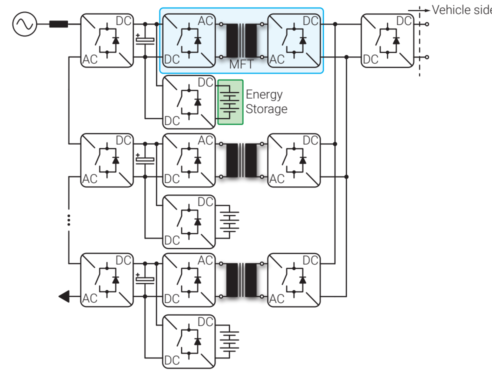

▲ Fast EV charging concept

MEDIUM FREQUENCY TRANSFORMER (MFT) CHALLENGES

- **Skin and proximity effect losses:** impact on efficiency and heating
- **Cooling:** increase of power density ⇒ decrease in size ⇒ less cooling surface ⇒ higher R_{th} ⇒ higher temperature gradients
- **Non-sinusoidal excitation:** impact on core and winding losses and insulation
- **Insulation:** coordination and testing taking into account high $\frac{dV}{dt}$ characteristic for power electronic converters
- **Accurate electric parameter control:** especially in case of resonant converter applications

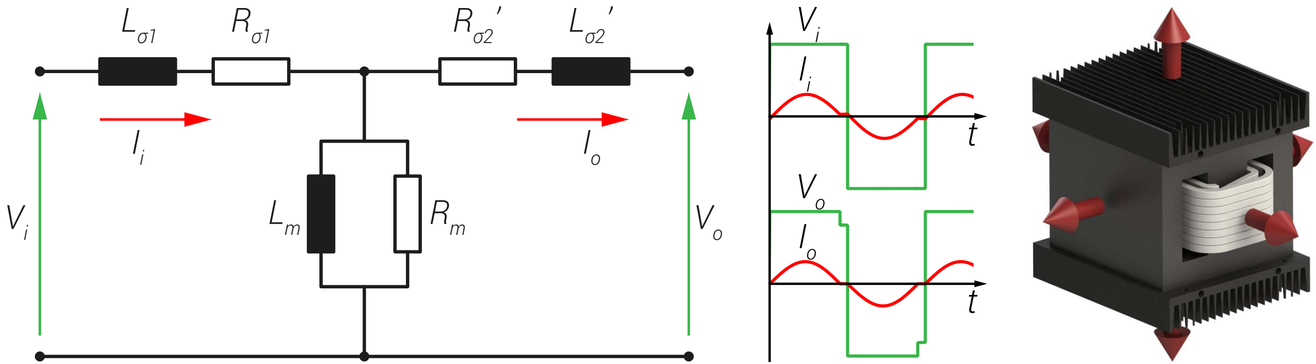

▲ Medium Frequency Transformer challenges

⇒ MFT design is generally challenging and requires multiphysics considerations and multiobjective optimization

MFT NONSINUSOIDAL POWER ELECTRONIC WAVEFORMS

DAB Converter:

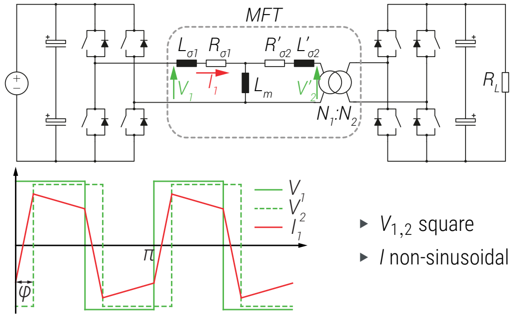

- $V_{1,2}$ square
- I non-sinusoidal

Series Resonant Converter:

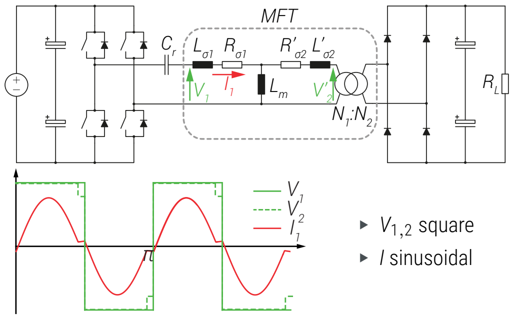

- $V_{1,2}$ square
- I sinusoidal

Core Losses:

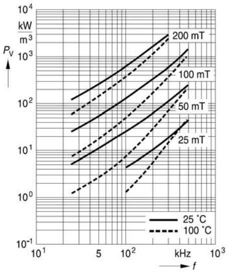

▲ Specific AC core losses

- Data-sheet - sinusoidal excitation
- Steinmetz - sinusoidal excitation losses
- Core is excited with square pulses!
- Losses must be correctly evaluated
- Generalization of Steinmetz model

Winding Losses:

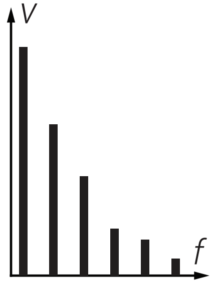

▲ Harmonics impacting winding losses

- Current waveform impacts the winding losses
- Copper is a linear material
- Losses can be evaluated in harmonic basis
- Current harmonic content must be evaluated
- Losses are the sum of the individual harmonic losses

MFT ACCURATE PARAMETERS CONTROL

DAB Converter:

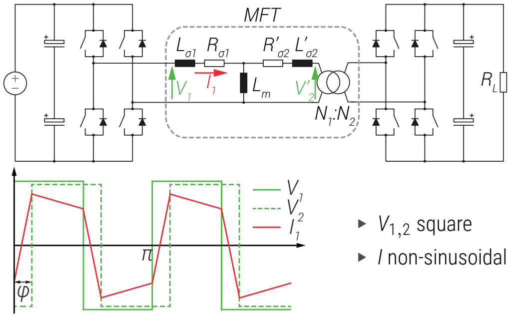

- $V_{1,2}$ square
- I non-sinusoidal

Series Resonant Converter:

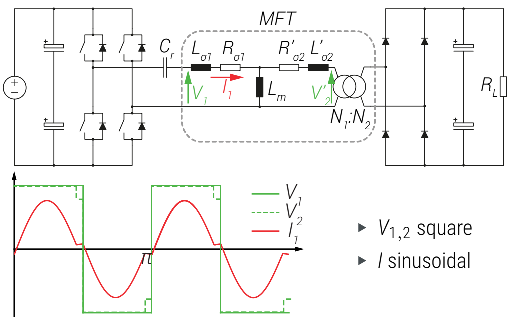

- $V_{1,2}$ square
- I sinusoidal

DAB

- Leakage inductance
- Controllability of the power flow
- Higher than $L_{\sigma.min}$:

$$L_{\sigma.min} = \frac{V_{DC1} V_{DC2} \varphi_{min}(\pi - \varphi_{min})}{2 P_{out} \pi^2 f_s n}$$

- Magnetizing Inductance is normally high

SRC

- Leakage inductance is part of resonant circuit
- Must match the reference:

$$L_{\sigma.ref} = \frac{1}{\omega_0^2 C_r}$$

- Magnetizing inductance is normally high
- Reduced in case of LLC
- Limits the magnetization current to the reference $I_{m.ref}$
- Limits the switch-off current and losses

$$L_m = \frac{n V_{DC2}}{4 f_s I_{m.ref}}$$

- $I_{m.ref}$ has to be sufficiently high to maintain ZVS

MFT VARIETY OF DESIGNS...

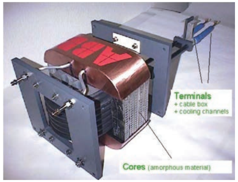

ABB: 350kW, 10kHz

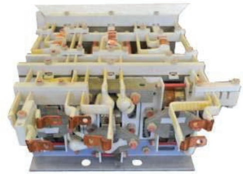

ABB: 3x150kW, 1.8kHz

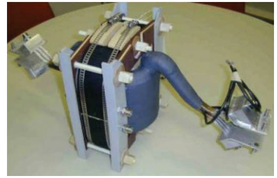

BOMBARDIER: 350kW, 8kHz

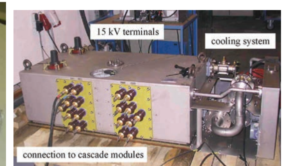

ALSTOM: 1500kW, 5kHz

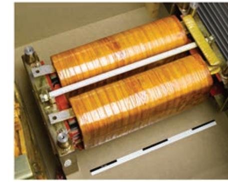

IKERLAN: 400kW, 5kHz

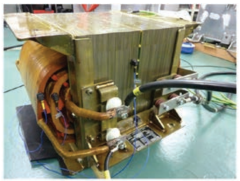

IKERLAN: 400kW, 1kHz

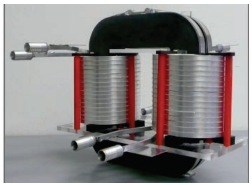

FAU-EN: 450kW, 5.6kHz

CHALMERS: 50kW, 5kHz

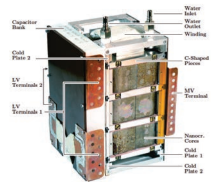

ETHZ: 166kW, 20kHz

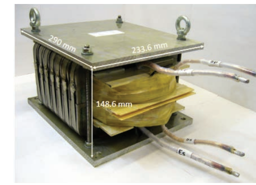

EPFL: 300kW, 2kHz

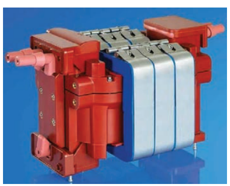

STS: 450kW, 8kHz

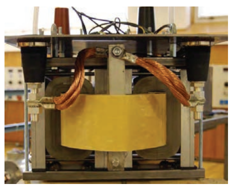

KTH: 170kW, 4kHz

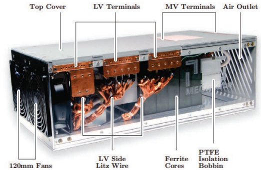

ETHZ: 166kW, 20kHz

EPFL: 100kW, 10kHz

?

ACME: ???kW, ???kHz

ENERGY CONVERSION TECHNOLOGIES AND SYSTEMS

▲ EMPOWER-ing the future energy systems

MVDC Grids

- DC Transformer
- Flexibility
- Stability

DC-DC Conversion

- Resonant principles
- Medium frequency conversion
- Absence of the control loops

DC Protection

- HV semiconductors
- Active protection
- Selectivity

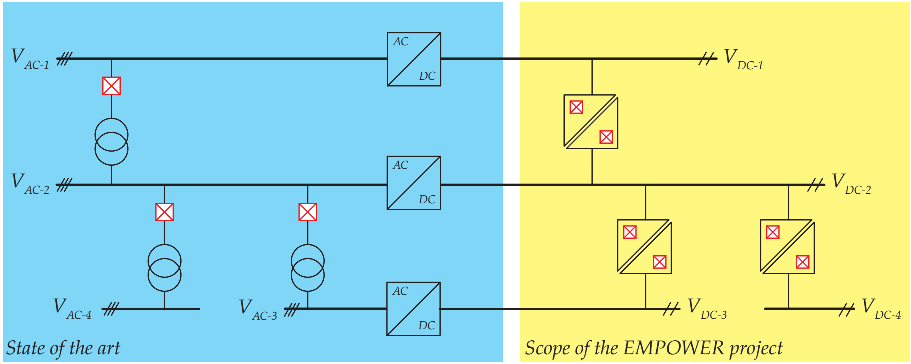

▲ Today's AC and tomorrow's DC power distribution networks enabled by DC Transformers

▲ The EMPOWER - Holistic and Integrated

EMPOWER - A EUROPEAN RESEARCH COUNCIL CONSOLIDATOR GRANT

ENERGY CONVERSION TECHNOLOGIES AND SYSTEMS

▲ EMPOWER-ing the future energy systems

MVDC Grids

- DC Transformer
- Flexibility
- Stability

DC-DC Conversion

- Resonant principles
- Medium frequency conversion
- Absence of the control loops

DC Protection

- HV semiconductors
- Active protection
- Selectivity

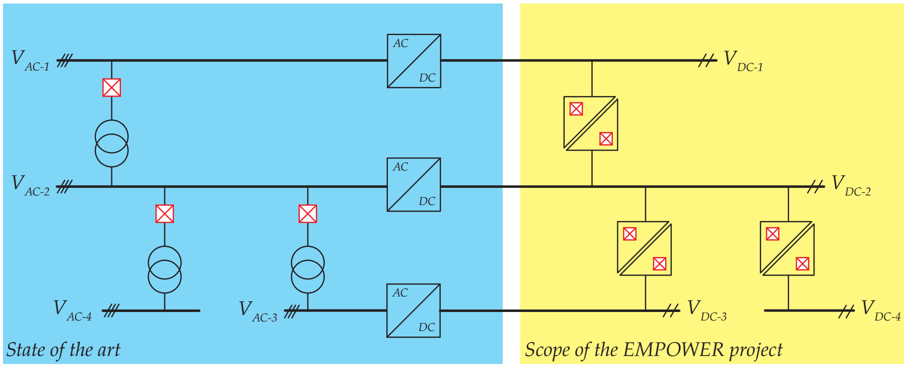

▲ Today's AC and tomorrow's DC power distribution networks enabled by DC Transformers

▲ The EMPOWER - Holistic and Integrated

⇒ Can we make a simple DC Transfomer behaving as much as possible as equivalent AC transformer?

BULK VS. MODULAR POWER CONVERSION

The same conversion function, but many implementation differences

Fractional power processing

- Multiple MFTs
- Equal power distribution among PEBBs
- MFT isolation?
- Various PEBB configurations

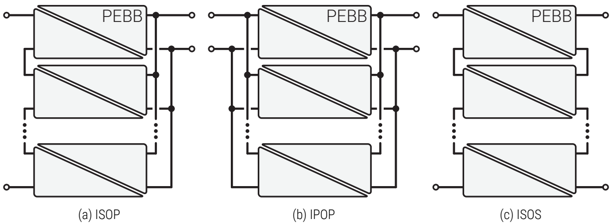

▲ Different structures employed depending upon the voltage level

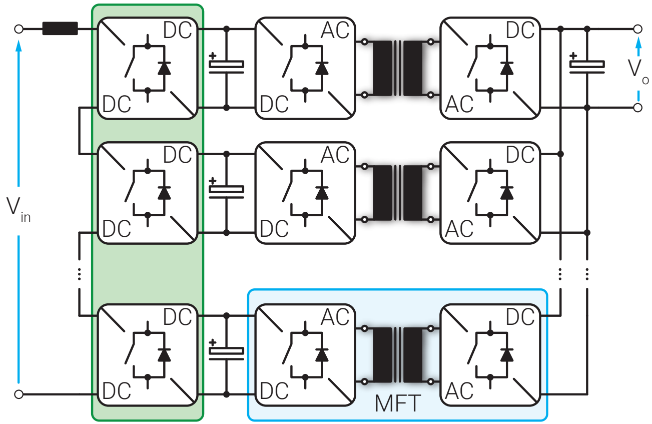

▲ ISOP Structure

Bulk power processing

- Single MFT
- Isolation solved only once
- Various configurations/operating principles

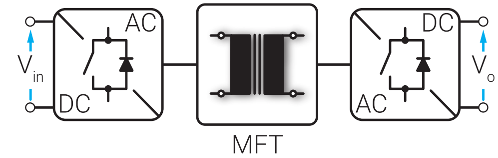

▲ Bulk power processing concept

DC-DC SST - BASIC CONCEPTS

Fractional power processing

- Multiple MFTs
- Equal power distribution among PEBBs
- MFT isolation?
- Various PEBB configurations

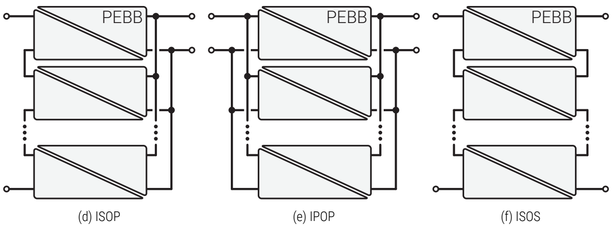

▲ Different structures employed depending upon the voltage level

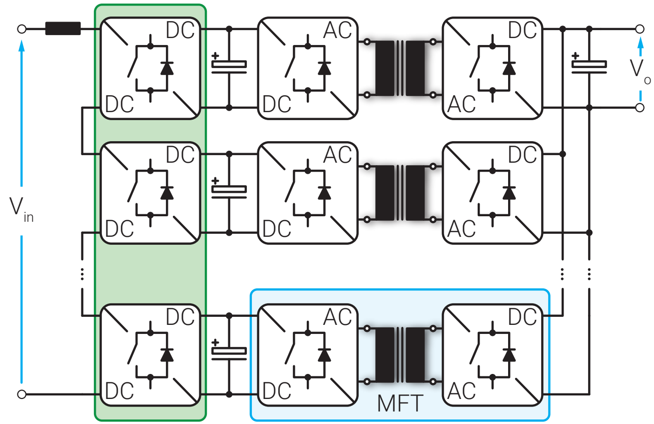

▲ ISOP Structure

Bulk power processing

- Single MFT
- Isolation solved only once
- Various configurations/operating principles

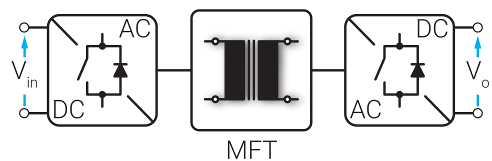

▲ Bulk power processing concept

⇒ Both design approaches are valid, and have their pros and cons! Many factors should be considered!

COMMON PEBB CONFIGURATIONS

Dual-Active Bridge

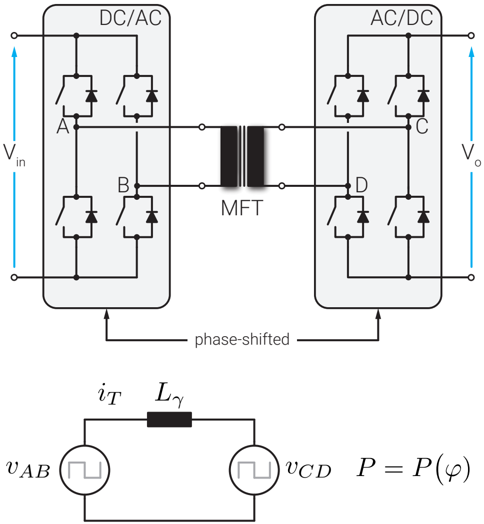

▲ Dual Active Bridge [18]

Resonant Converters

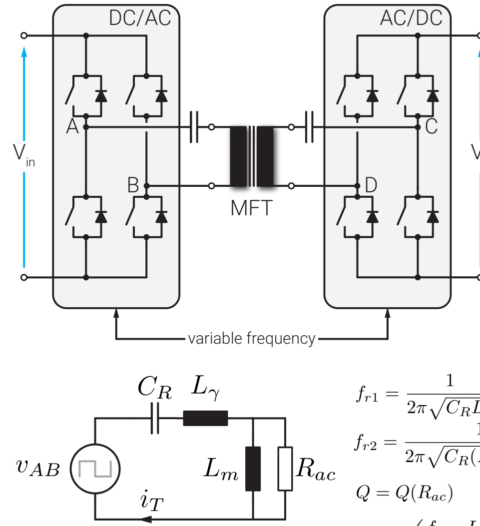

$$f_{r1} = \frac{1}{2\pi\sqrt{C_R L_\gamma}}$$

$$f_{r2} = \frac{1}{2\pi\sqrt{C_R(L_\gamma + L_m)}}$$

$$Q = Q(R_{ac})$$

$$G = G\left(\frac{f_{sw}}{f_{r1}}, \frac{L_m}{L_\gamma}, Q\right)$$

▲ LLC Resonant Converter

1-PHASE DAB

Basic operating principles

SINGLE-PHASE (1PH) DUAL ACTIVE BRIDGE (DAB)

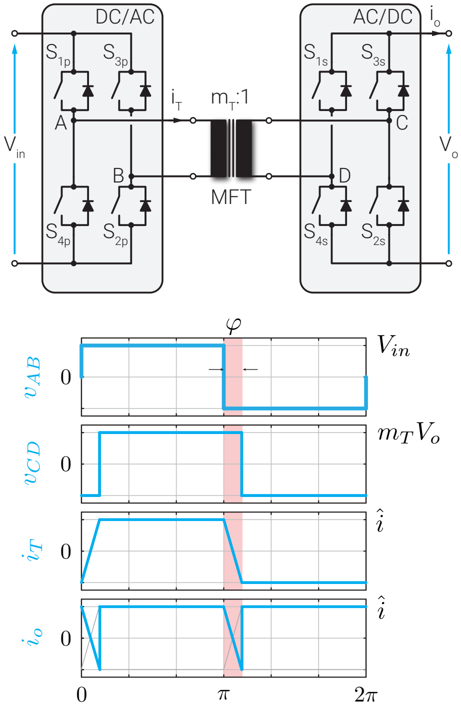

▲ 1PH-DAB with its relevant waveforms

Power equation

$$P = \frac{1}{T}\int_0^T v_{AB} i_T dt$$

$$= m_T \frac{V_{in} V_o}{\omega L_\Sigma} \varphi \left(1 - \frac{|\varphi|}{\pi}\right)$$

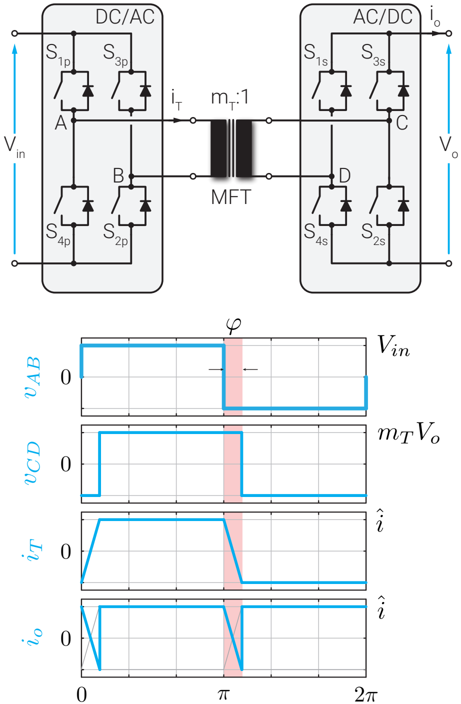

▲ 1PH-DAB with its relevant waveforms

Power equation

$$P = \frac{1}{T}\int_0^T v_{AB} i_T dt$$

$$= m_T \frac{V_{in} V_o}{\omega L_\Sigma} \varphi \left(1 - \frac{|\varphi|}{\pi}\right)$$

Switching cycle

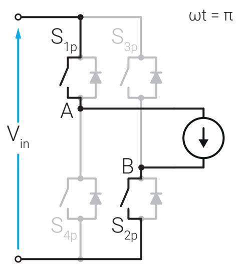

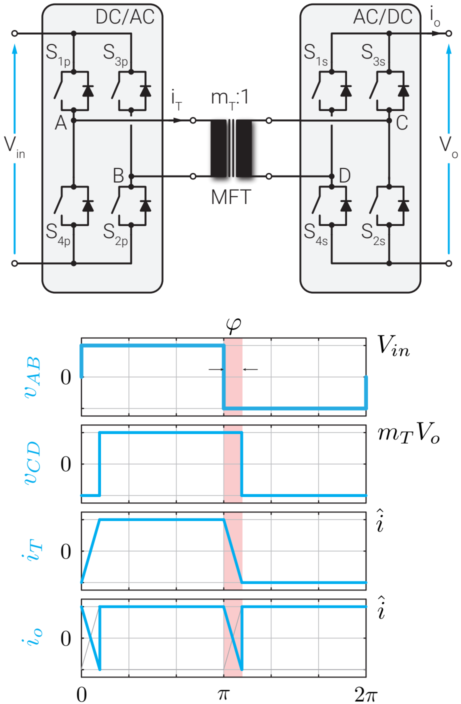

▲ 1PH-DAB with its relevant waveforms

Power equation

$$P = \frac{1}{T}\int_0^T v_{AB} i_T dt$$

$$= m_T \frac{V_{in} V_o}{\omega L_\Sigma} \varphi \left(1 - \frac{|\varphi|}{\pi}\right)$$

Switching cycle

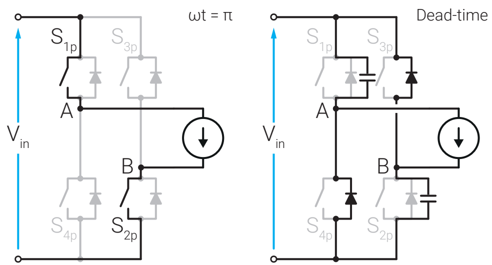

SINGLE-PHASE (1PH) DUAL ACTIVE BRIDGE (DAB)

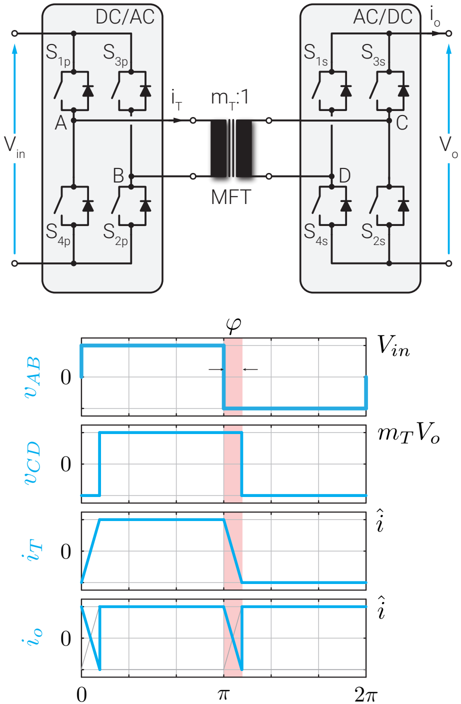

▲ 1PH-DAB with its relevant waveforms

Power equation

$$P = \frac{1}{T}\int_0^T v_{AB} i_T dt$$

$$= m_T \frac{V_{in} V_o}{\omega L_\Sigma} \varphi \left(1 - \frac{|\varphi|}{\pi}\right)$$

Switching cycle

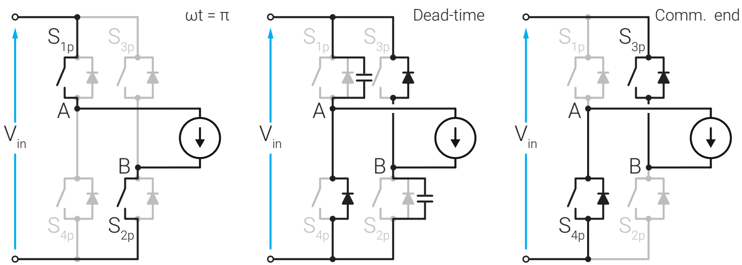

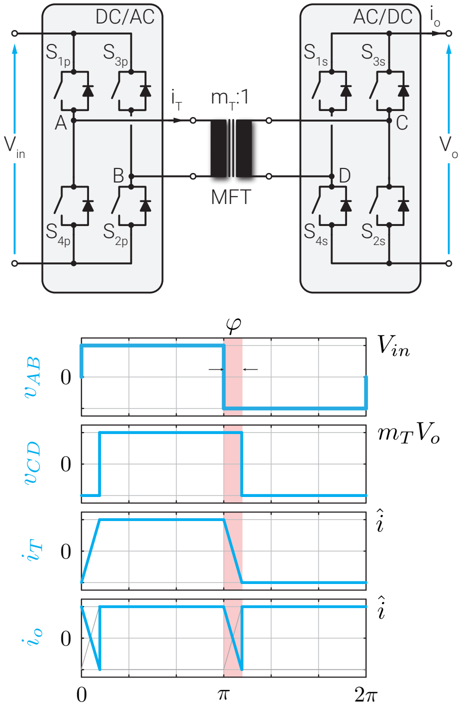

▲ 1PH-DAB with its relevant waveforms

Power equation

$$P = \frac{1}{T}\int_0^T v_{AB} i_T dt$$

$$= m_T \frac{V_{in} V_o}{\omega L_\Sigma} \varphi \left(1 - \frac{|\varphi|}{\pi}\right)$$

Switching cycle

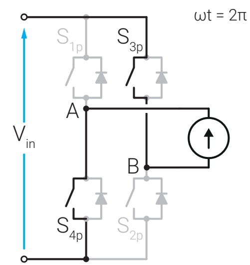

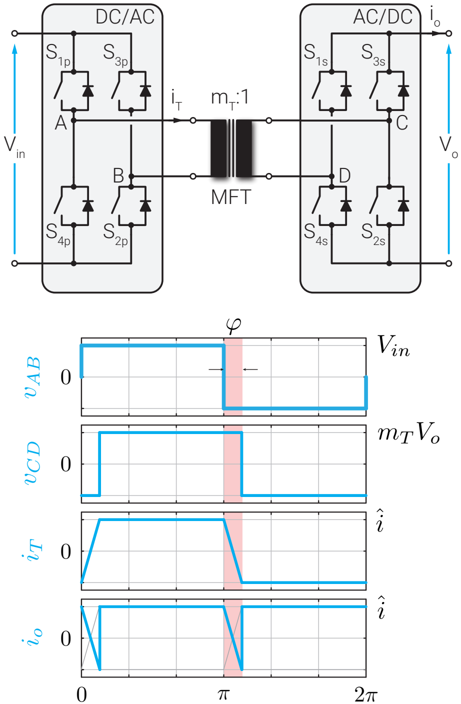

▲ 1PH-DAB with its relevant waveforms

Power equation

$$P = \frac{1}{T}\int_0^T v_{AB} i_T dt$$

$$= m_T \frac{V_{in} V_o}{\omega L_\Sigma}\varphi\left(1 - \frac{|\varphi|}{\pi}\right)$$

Switching cycle

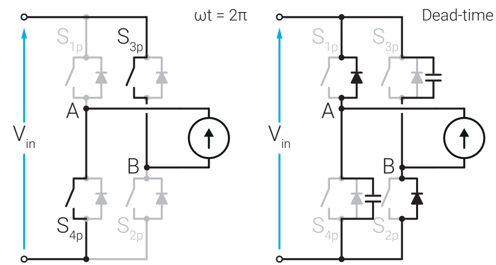

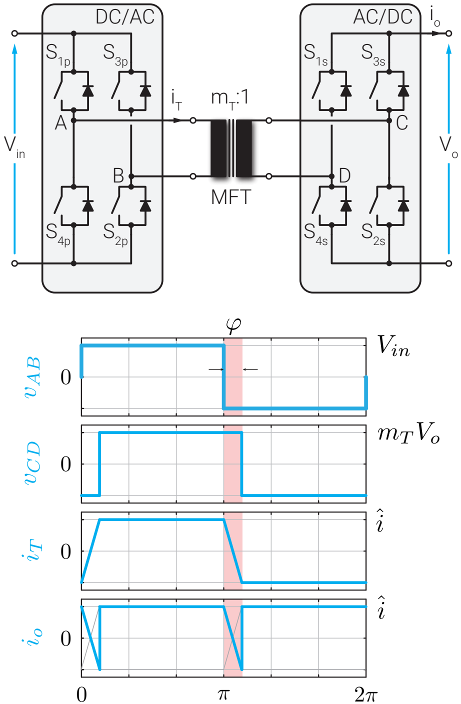

▲ 1PH-DAB with its relevant waveforms

Power equation

$$P = \frac{1}{T}\int_0^T v_{AB} i_T dt$$
$$= m_T \frac{V_{in} V_o}{\omega L_\Sigma} \varphi \left(1 - \frac{|\varphi|}{\pi}\right)$$

Switching cycle

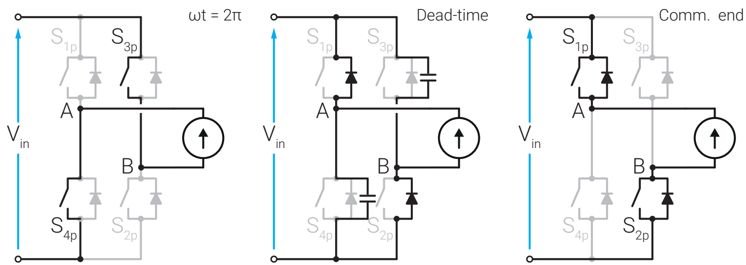

Main features

- Phase-Modulated converter
- Simple power flow control
- Soft-switching capability
- Many other advanced modulation schemes are known

3-PHASE DAB

Somewhat more complicated...

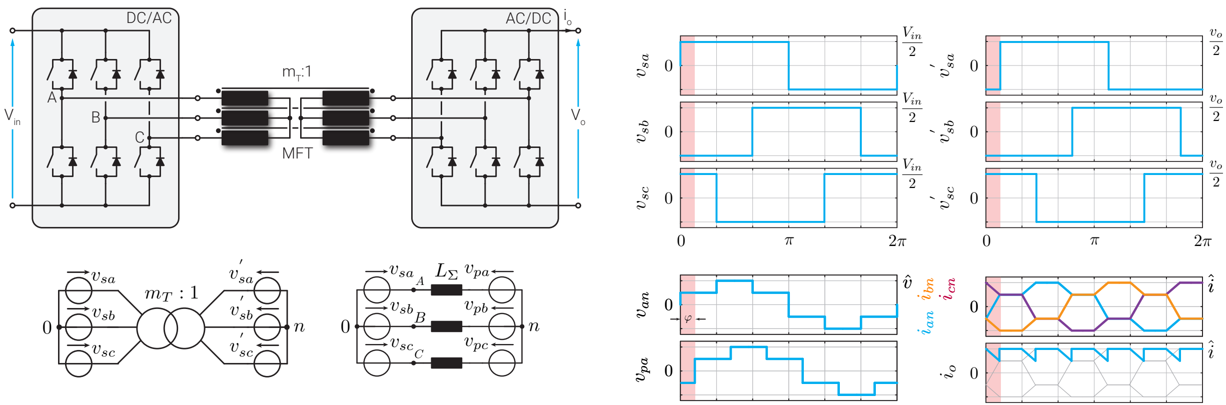

$$v_{an} = \frac{2v_{sa} - v_{sb} - v_{sc}}{3} \qquad v_{pa} = m_T\frac{2v'_{sa} - v'_{sb} - v'_{sc}}{3}$$

▲ 3PH-DAB with its relevant waveforms

Power Equation

$$P = \frac{3}{T}\int_0^T v_{an} i_{an} dt$$

$$= m_T \frac{4}{3} \frac{V_{in} V_o}{\omega L_\Sigma} \varphi \left(\frac{1}{2} - \frac{3|\varphi|}{8\pi}\right)$$

1-PH vs 3-PH DAB

	Control Simplicity	Tx utilization	Soft Switching	In/Out current ripple
1-PH DAB	☺	☹	☺	☹
3-PH DAB	☺	☺	☺	☺

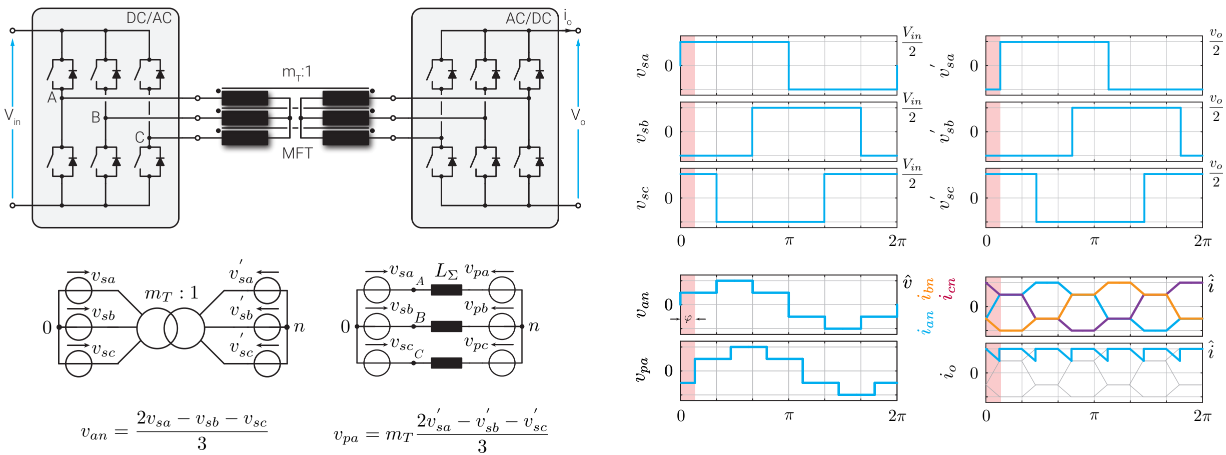

▲ 3PH-DAB with its relevant waveforms

Power Equation

$$P = \frac{3}{T}\int_0^T v_{an} i_{an} dt$$

$$= m_T \frac{4}{3} \frac{V_{in} V_o}{\omega L_\Sigma} \varphi \left(\frac{1}{2} - \frac{3|\varphi|}{8\pi} \right)$$

1-PH vs 3-PH DAB

	Control Simplicity	Tx utilization	Soft Switching	In/Out current ripple
1-PH DAB	☺	☹	☺	☹
3-PH DAB	☺	☺	☺	☺

⇒ 3PH-DAB is considered favorable!

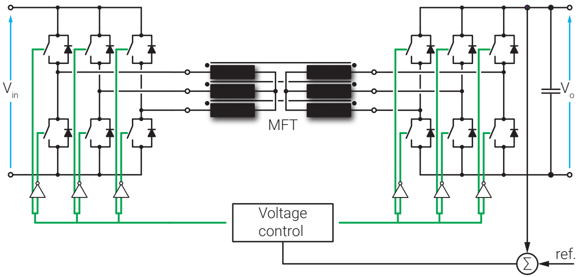

▲ Observed DAB-based system

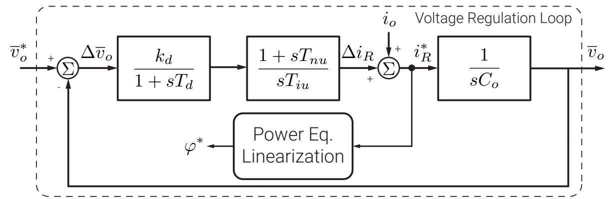

▲ Output voltage control loop

Assuming $P_{in} = P_{out}$:

$$\cancel{V_o} i_o = \frac{4 m_T V_{in} \cancel{V_o}}{3\omega L}\varphi\left(\frac{1}{2} - \frac{3|\varphi|}{8\pi}\right)$$

$$\Rightarrow i_o = \frac{4 m_T V_{in}}{3\omega L}\varphi\left(\frac{1}{2} - \frac{3|\varphi|}{8\pi}\right)$$

⇒ Controlled current source behavior!

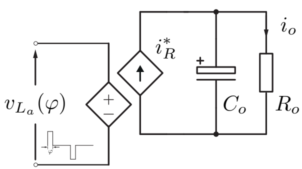

▲ DAB equivalent circuit seen from the controlled side

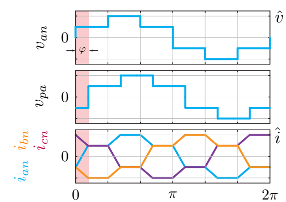

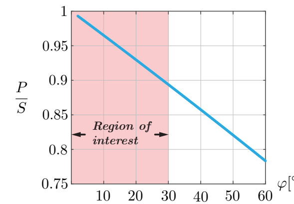

$$\frac{P}{S} = \frac{4\pi - 3\varphi}{2\pi\sqrt{\frac{4\pi-\varphi}{\pi}}}$$

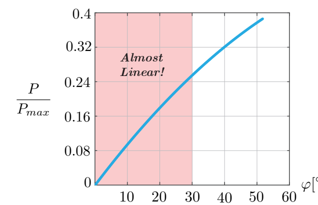

ABRUPT PHASE ANGLE CHANGES? (I)

- Six step modulation
- Limited number of voltage states

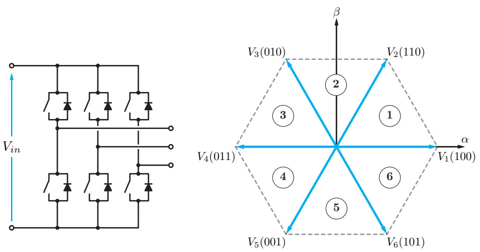

▲ Either side of the 3PH-DAB

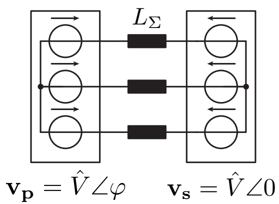

▲ DAB equivalent circuit

? Current shape in the $\alpha\beta$ plane?

For $\omega t \in [(k-1)\frac{\pi}{3}, k\frac{\pi}{3}]$

$$\mathbf{V_p} = \mathbf{V_k}$$

$$\mathbf{V_s} = \begin{cases} \mathbf{V_{k-1}}, & \omega t \in [(k-1)\frac{\pi}{3}, (k-1)\frac{\pi}{3}+\varphi] \\ \mathbf{V_k}, & \omega t \in [(k-1)\frac{\pi}{3}+\varphi, k\frac{\pi}{3}] \end{cases}$$

$$L\frac{d\mathbf{i}}{dt} = \mathbf{V_p} - \mathbf{V_s}$$

$$= \begin{cases} \hat{V}e^{j(k+1)\frac{\pi}{3}}, & \omega t \in [(k-1)\frac{\pi}{3}, (k-1)\frac{\pi}{3}+\varphi] \\ 0, & \omega t \in [(k-1)\frac{\pi}{3}+\varphi, k\frac{\pi}{3}] \end{cases}$$

$$\mathbf{i} = \begin{cases} \mathbf{i_{0,k}} + \frac{\hat{V}}{L_\Sigma} t e^{j(k+1)\frac{\pi}{3}}, & \omega t \in [(k-1)\frac{\pi}{3}, (k-1)\frac{\pi}{3}+\varphi] \\ \mathbf{i_{0,k}} + \frac{\hat{V}}{\omega L_\Sigma}\varphi\ e^{j\ (k+1)\frac{\pi}{3}}, & \omega t \in [(k-1)\frac{\pi}{3}+\varphi, k\frac{\pi}{3}] \end{cases}$$

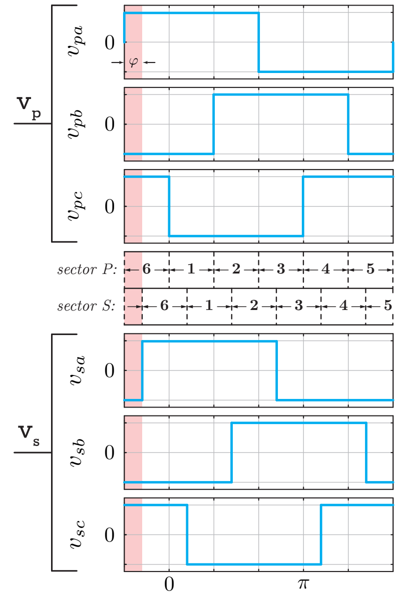

▲ DAB switching signals

ABRUPT PHASE ANGLE CHANGES? (I)

- Six step modulation
- Limited number of voltage states

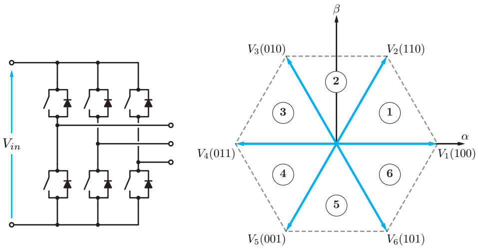

▲ Either side of the 3PH-DAB

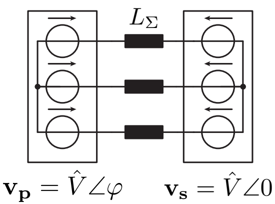

▲ DAB equivalent circuit

? Current shape in the $\alpha\beta$ plane?

For $\omega t \in [(k-1)\frac{\pi}{3}, k\frac{\pi}{3}]$

$$\mathbf{V_p} = \mathbf{V_k}$$

$$\mathbf{V_s} = \begin{cases} \mathbf{V_{k\text{-}1}}, & \omega t \in [(k-1)\frac{\pi}{3}, (k-1)\frac{\pi}{3}+\varphi] \\ \mathbf{V_k}, & \omega t \in [(k-1)\frac{\pi}{3}+\varphi, k\frac{\pi}{3}] \end{cases}$$

$$L\frac{d\mathbf{i}}{dt} = \mathbf{V_p} - \mathbf{V_s}$$

$$= \begin{cases} \hat{V}e^{j(k+1)\frac{\pi}{3}}, & \omega t \in [(k-1)\frac{\pi}{3}, (k-1)\frac{\pi}{3}+\varphi] \\ 0, & \omega t \in [(k-1)\frac{\pi}{3}+\varphi, k\frac{\pi}{3}] \end{cases}$$

$$\mathbf{i} = \begin{cases} \mathbf{i_{0,k}} + \frac{\hat{V}}{L_\Sigma} t e^{j(k+1)\frac{\pi}{3}}, & \omega t \in [(k-1)\frac{\pi}{3}, (k-1)\frac{\pi}{3}+\varphi] \\ \mathbf{i_{0,k}} + \frac{\hat{V}}{\omega L_\Sigma}\varphi\, e^{j(k+1)\frac{\pi}{3}}, & \omega t \in [(k-1)\frac{\pi}{3}+\varphi, k\frac{\pi}{3}] \end{cases}$$

- Amplitude of the change proportional to φ
- Phase change in 60° steps

⇒ Current slides along a hexagon!

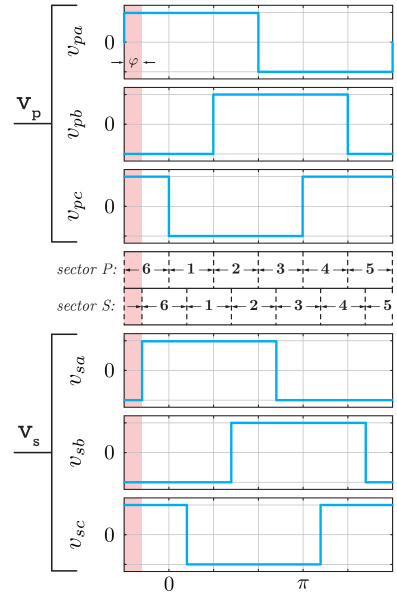

▲ DAB switching signals

ABRUPT PHASE ANGLE CHANGES? (II)

Recap

- Limited number of voltage states V_p and V_s
- Current vector stepwise phase changes (60°)
- Current vector magnitude directly proportional to phase angle
- Current vector slides along the hexagon [19], [20]

ABRUPT PHASE ANGLE CHANGES? (II)

Recap

- Limited number of voltage states V_p and V_s
- Current vector stepwise phase changes (60°)
- Current vector magnitude directly proportional to phase angle
- Current vector slides along the hexagon [19], [20]

> ? What if the phase angle gets abruptly changed?

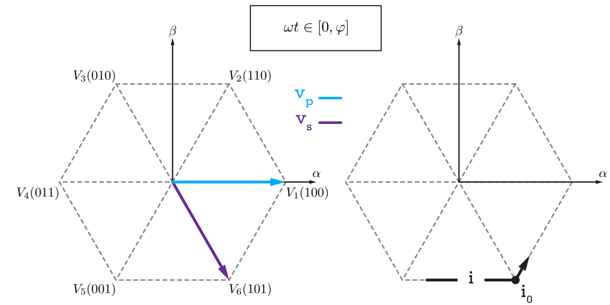

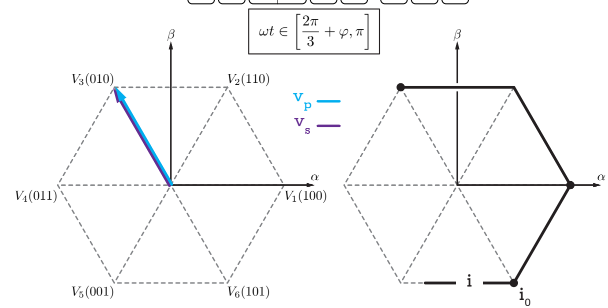

ABRUPT PHASE ANGLE CHANGES? (II)

Recap

- Limited number of voltage states V_p and V_s
- Current vector stepwise phase changes (60°)
- Current vector magnitude directly proportional to phase angle
- Current vector slides along the hexagon [19], [20]

> ? What if the phase angle gets abruptly changed?

- New current vector trajectory
- Hexagon decentralization $\Rightarrow$ Transformer currents asymmetry!

Inverse $\alpha\beta0$ transformation:

$$\begin{bmatrix} i_a^{off} \\ i_b^{off} \\ i_b^{off} \end{bmatrix} = \begin{bmatrix} 1 & 0 & 1 \\ -\frac{1}{2} & \frac{\sqrt{3}}{2} & 1 \\ -\frac{1}{2} & -\frac{\sqrt{3}}{2} & 1 \end{bmatrix} \cdot \begin{bmatrix} i_{\alpha,hex}^{off} \\ i_{\beta,hex}^{off} \\ 0 \end{bmatrix}$$

> ϟ Time constant L_Σ / R_Σ determines asymmetric components decay!

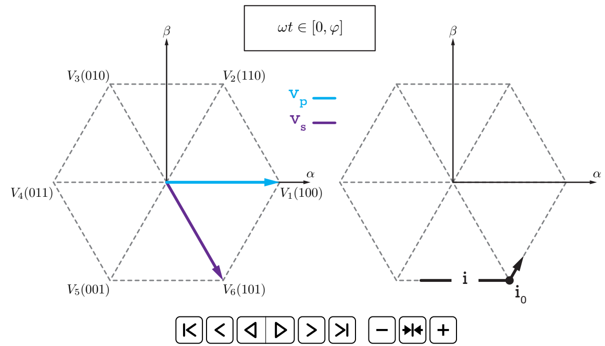

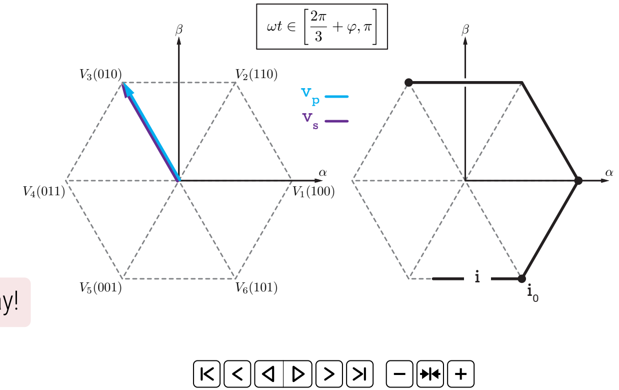

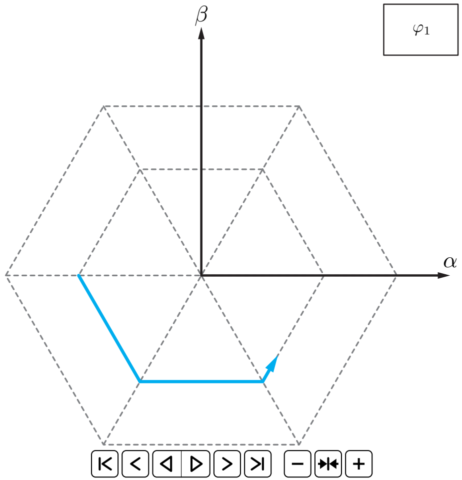

▲ Safe way of achieving phase angle change (I)

Applied phase angle sequence:

$$\underbrace{\varphi_1}_{\textit{Angle change!}} \Rightarrow \underbrace{\underbrace{\frac{\varphi_1+\varphi_2}{2}}_{\frac{T}{6}} \Rightarrow \underbrace{\frac{\varphi_1+\varphi_2}{2}}_{\frac{T}{6}} \Rightarrow \underbrace{\frac{\varphi_1+\varphi_2}{2}}_{\frac{T}{6}}}_{\textit{Transition time} = \frac{T}{2}} \Rightarrow \underbrace{\varphi_2}_{\textit{Transition end}}$$

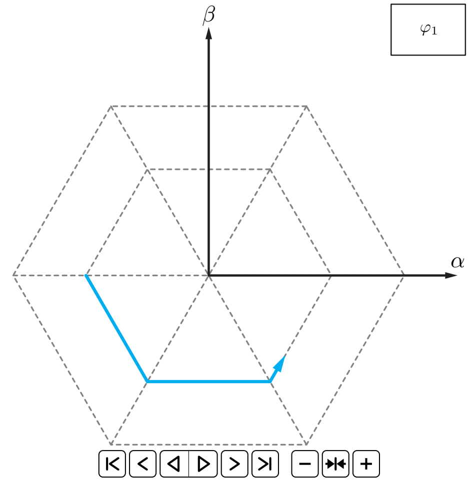

▲ Safe way of achieving phase angle change (II)

Applied phase angle sequence:

$$\underbrace{\varphi_1}_{\textit{Angle change!}} \Rightarrow \underbrace{\underbrace{\varphi_2}_{\frac{T}{6}} \Rightarrow \underbrace{\varphi_1}_{\frac{T}{6}}}_{\textit{Transition time} = \frac{T}{3}} \Rightarrow \underbrace{\varphi_2}_{\textit{Transition end}}$$

MEDIUM VOLTAGE DC-DC

Extending previously presented concepts...

HOW TO HANDLE HIGH/MEDIUM VOLTAGES?

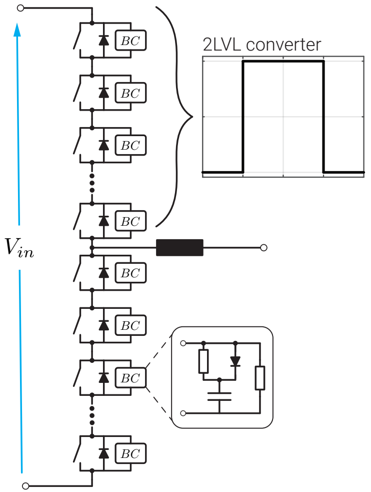

▲ Series connection of switches [21]

- Series connection of switches with snubbers
- Two voltage levels ($n_{LVL} = 2$)
- Two-Level voltage waveforms

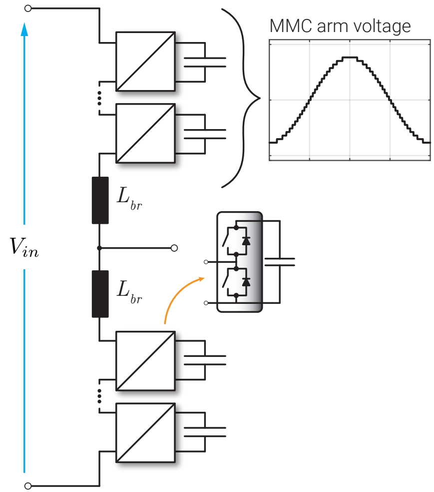

▲ Modular Multilevel Converter (MMC)

- Series connection of Submodules (SM)
- n_{LVL} depending upon number of SMs
- Arbitrary voltage waveform generation

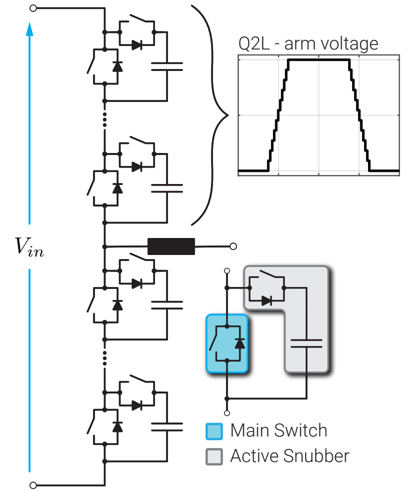

▲ Quasi Two-Level (Q2L) Converter [22], [23]

- Series connection of MMC-alike SMs
- n_{LVL} depending upon number of SMs
- Quasi Two-Level (trapezoidal) voltage waveform

- Variety of conversion possibilities
- Variety of modulations
- Different types of submodules (SMs)
  - Half-Bridge (HB)
  - Full-Bridge (FB)
  - Others...
- Arbitrary voltage waveform generation

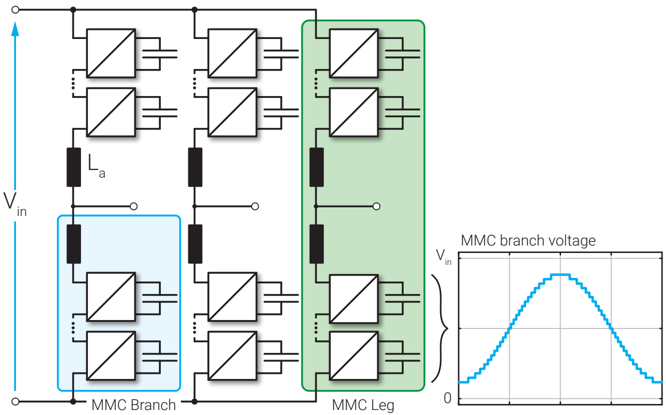

▲ Modular Multilevel Converter (MMC)

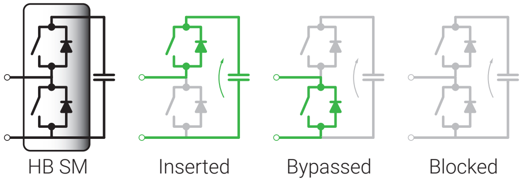

▲ Half-Bridge submodule and its allowed states

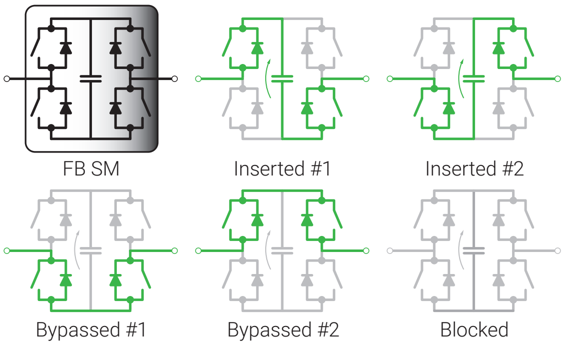

▲ Full-Bridge submodule and its allowed states

- Basic operation principles are retained
- Easy to comprehend (AC equivalent)

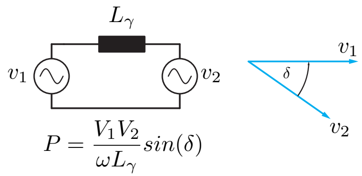

Challenges?

- Modulation choice (sine, square, etc ... ?)
- System design (*N* vs V_{grid})
- Energy balancing
- Q2L mode & capacitors sizing
- Engagement within bipolar grids

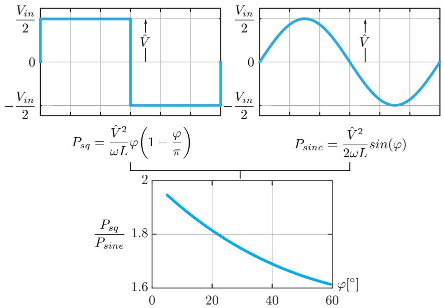

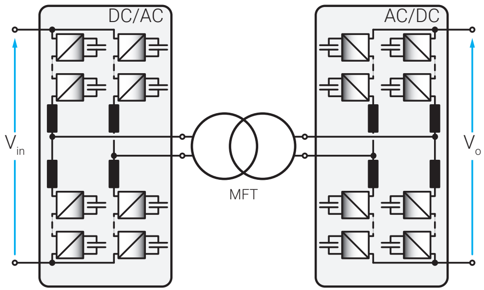

▲ MMC-based 1PH-DAB [24]

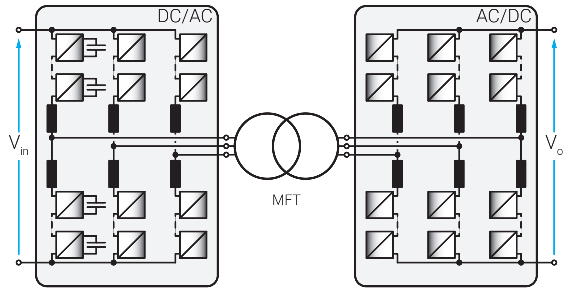

▲ MMC-based 3PH-DAB

[24] Stephan Kenzelmann et al. "Isolated DC/DC structure based on modular multilevel converter." *IEEE Transactions on Power Electronics* 30.1 (2015), pp. 89–98

- Basic operation principles are retained
- Easy to comprehend (AC equivalent)

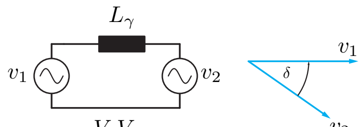

$$P = \frac{V_1 V_2}{\omega L_\gamma} sin(\delta)$$

Challenges?

- Modulation choice (sine, square, etc ... ?)
- System design (N vs V_{grid})
- Energy balancing
- Q2L mode & capacitors sizing
- Engagement within bipolar grids

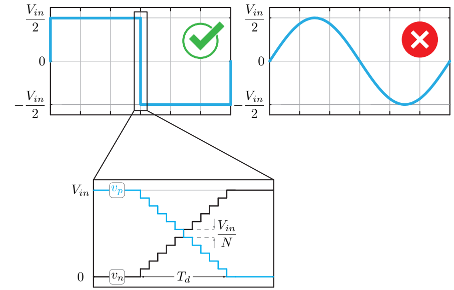

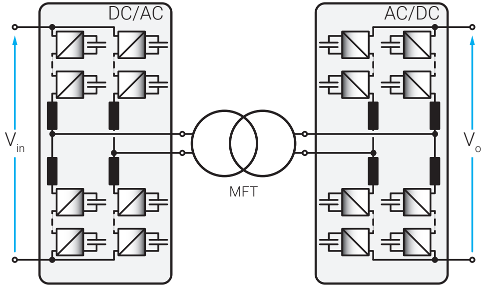

▲ MMC-based 1PH-DAB [24]

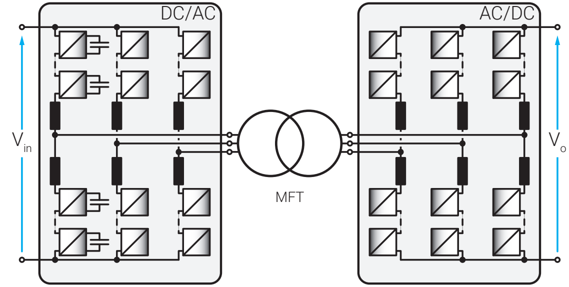

▲ MMC-based 3PH-DAB

[24] Stephan Kenzelmann et al. "Isolated DC/DC structure based on modular multilevel converter." *IEEE Transactions on Power Electronics* 30.1 (2015), pp. 89–98

MMC ENERGY BALANCING AND QUASI SQUARE WAVE OPERATION (I)

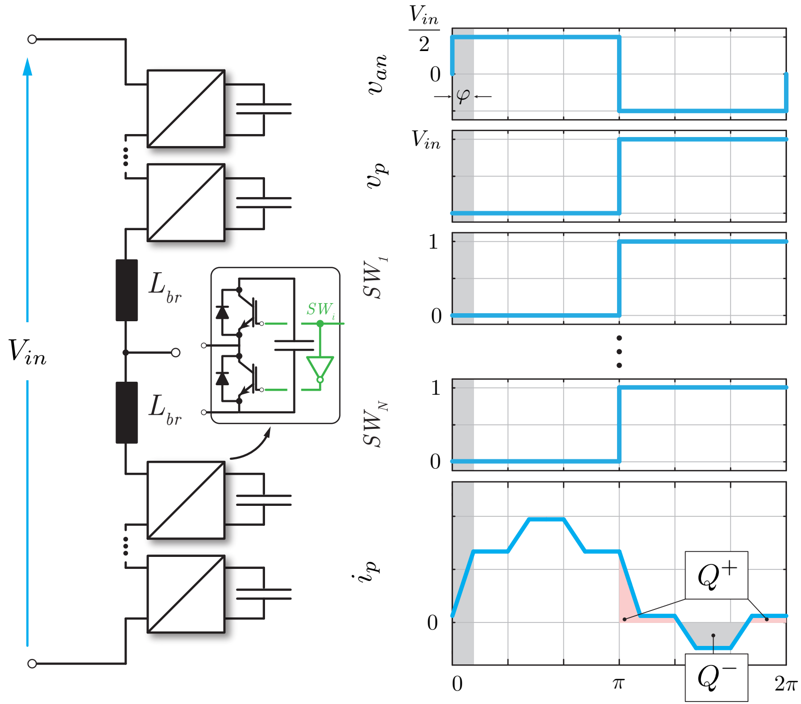

▲ MMC operating as a two level converter and its relevant waveforms

Ideally, $Q^+ = Q^-$ ⇒ **Natural balancing**

However, reality is different...

- Branch resistances affect the MMC current
- Not all the switches are gated at the same time

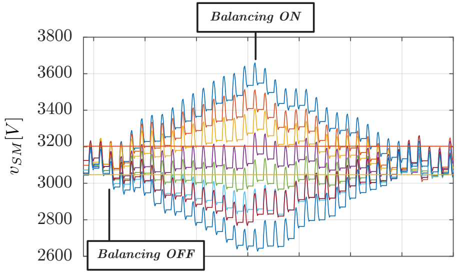

MMC ENERGY BALANCING AND QUASI SQUARE WAVE OPERATION (I)

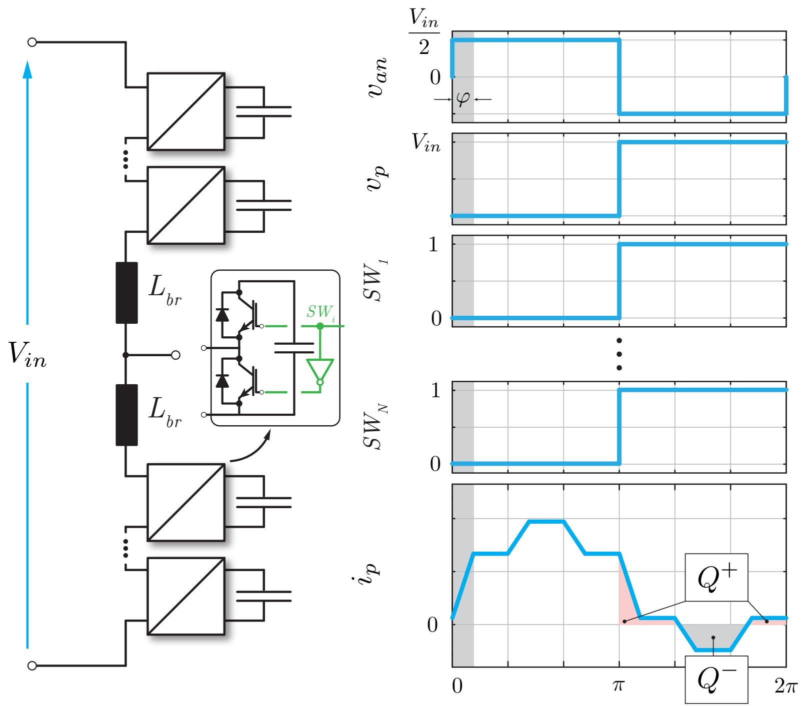

▲ MMC operating as a two level converter and its relevant waveforms

Ideally, $Q^+ = Q^-$ ⇒ **Natural balancing**

However, reality is different...

- Branch resistances affect the MMC current
- Not all the switches are gated at the same time

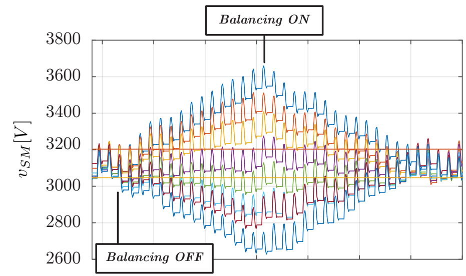

Balancing algorithm must be employed!

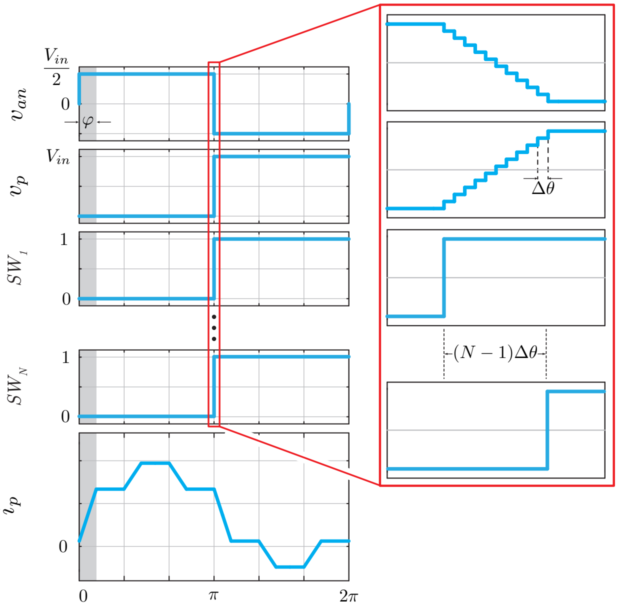

▲ MMC operating with quasi square voltages and its relevant waveforms

Quasi Square Wave operation

- Intentional displacement among gating signals
- Control of MFT voltage slopes (dV/dt)
- Control of SMs' voltages!

$$G = \frac{V_o m_T}{V_{in}}$$

For G = 1, SMs charge distribution can be derived.

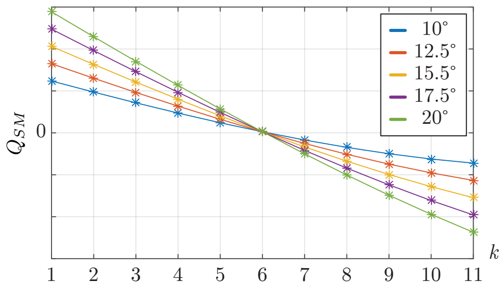

▲ Charge received by a SM depending upon the gate signal [25]

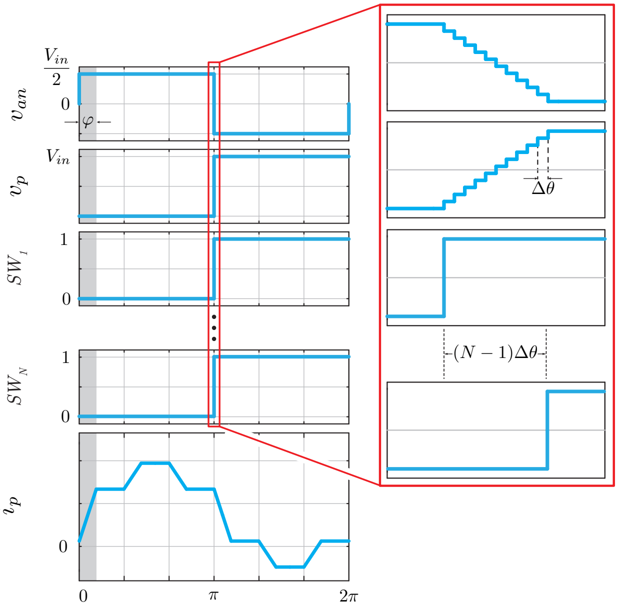

▲ MMC operating with quasi square voltages and its relevant waveforms

Quasi Square Wave operation

- Intentional displacement among gating signals
- Control of MFT voltage slopes (dV/dt)
- Control of SMs' voltages!

$$G = \frac{V_o m_T}{V_{in}}$$

For G = 1, SMs charge distribution can be derived.

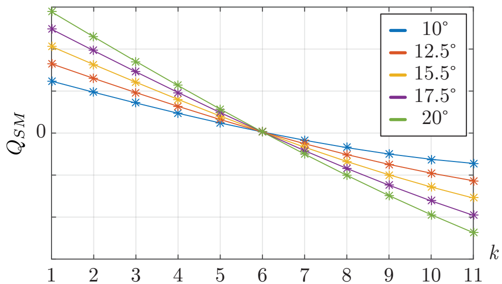

▲ Charge received by a SM depending upon the gate signal [25]

⇒ Different charge distribution enables balancing!

QUASI TWO-LEVEL (Q2L) CONVERTER

- MMC-alike structure
- Branch inductors removed!
- SM = Main Switch + Active Snubber
- Sequential insertion/bypassing of SMs [26]

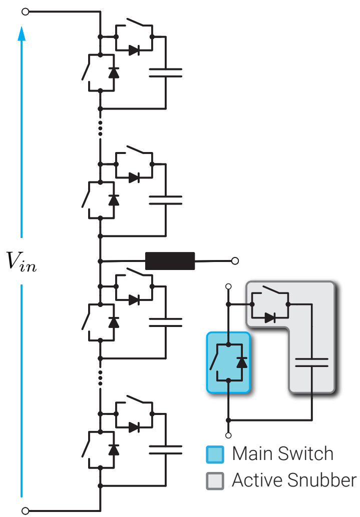

▲ Quasi Two-Level Converter

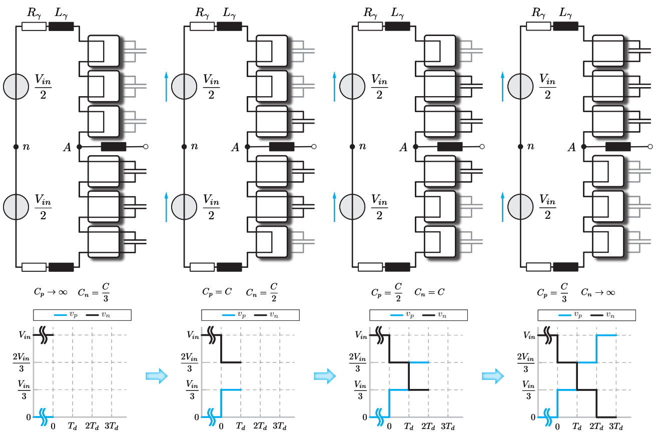

▲ Example of the Q2L Converter transition (N=3)

[26] Stefan Milovanovic and Drazen Dujic. "Comprehensive analysis and design of a quasi two-level converter leg." *CPSS Transactions on Power Electronics and Applications* 4.3 (2019), pp. 181–196

QUASI TWO-LEVEL (Q2L) CONVERTER

- MMC-alike structure
- Branch inductors removed!
- SM = Main Switch + Active Snubber
- Sequential insertion/bypassing of SMs [26]

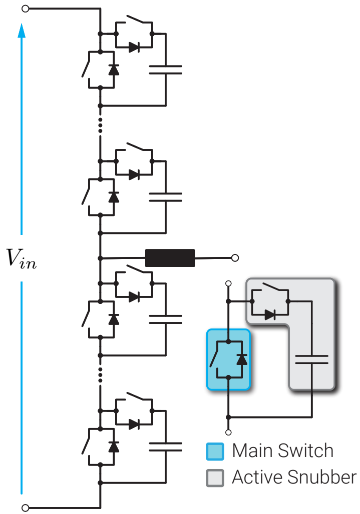

▲ Quasi Two-Level Converter

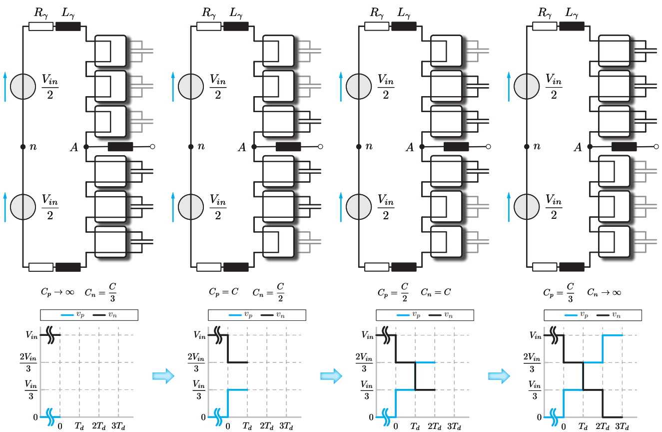

▲ Example of the Q2L Converter transition (N=3)

Every dwell interval introduces new resonant parameters to the circuit!

[26] Stefan Milovanovic and Drazen Dujic. "Comprehensive analysis and design of a quasi two-level converter leg." *CPSS Transactions on Power Electronics and Applications* 4.3 (2019), pp. 181–196

QUASI TWO-LEVEL (Q2L) CONVERTER

- MMC-alike structure
- Branch inductors removed!
- SM = Main Switch + Active Snubber
- Sequential insertion/bypassing of SMs [26]

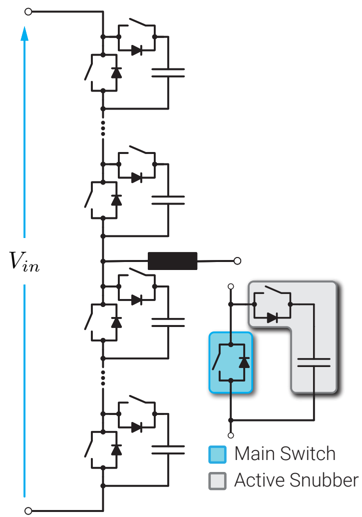

▲ Quasi Two-Level Converter

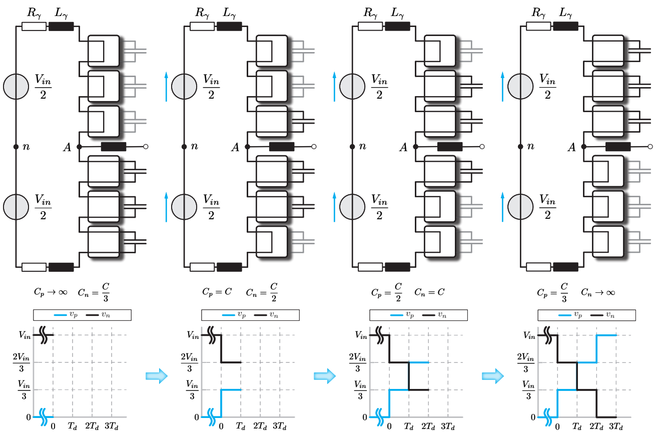

▲ Example of the Q2L Converter transition (N=3)

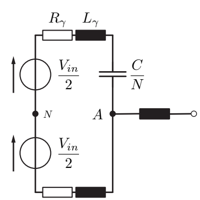

[26] Stefan Milovanovic and Drazen Dujic. "Comprehensive analysis and design of a quasi two-level converter leg." *CPSS Transactions on Power Electronics and Applications* 4.3 (2019), pp. 181–196

- MMC-alike structure
- Branch inductors removed!
- SM = Main Switch + Active Snubber
- Sequential insertion/bypassing of SMs [26]

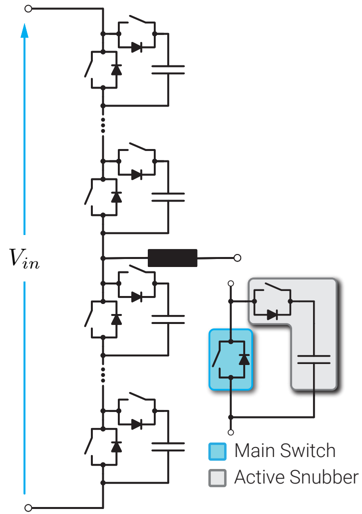

▲ Quasi Two-Level Converter

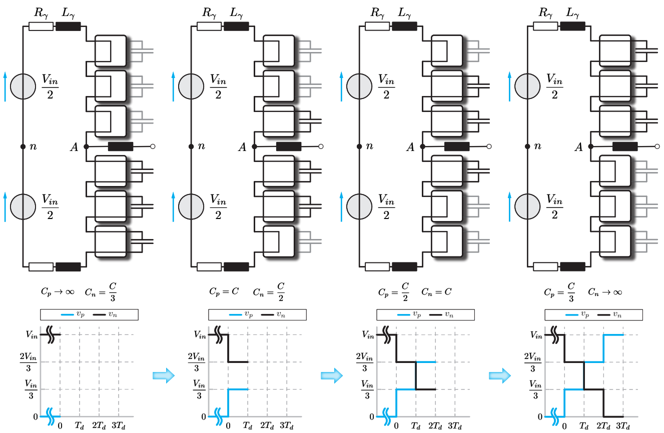

▲ Example of the Q2L Converter transition (N=3)

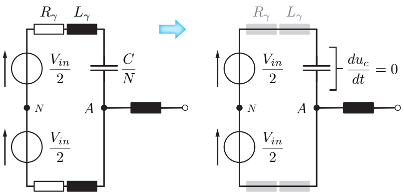

[26] Stefan Milovanovic and Drazen Dujic. "Comprehensive analysis and design of a quasi two-level converter leg." *CPSS Transactions on Power Electronics and Applications* 4.3 (2019), pp. 181–196

- MMC-alike structure
- Branch inductors removed!
- SM = Main Switch + Active Snubber
- Sequential insertion/bypassing of SMs [26]

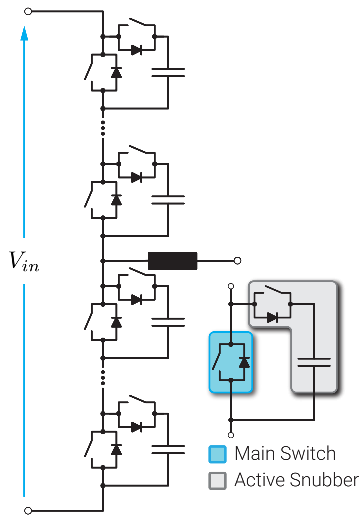

▲ Quasi Two-Level Converter

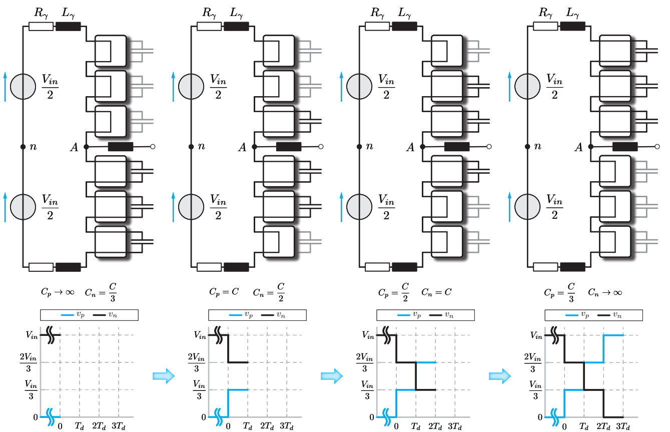

▲ Example of the Q2L Converter transition (N=3)

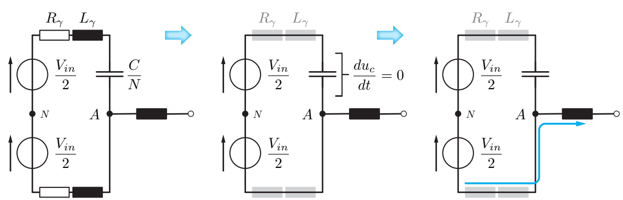

⇒ Output current drifts to a single branch. Common mode current does not exist!

[26] Stefan Milovanovic and Drazen Dujic. "Comprehensive analysis and design of a quasi two-level converter leg." *CPSS Transactions on Power Electronics and Applications* 4.3 (2019), pp. 181–196

Q2L CONVERTER - PROS AND CONS

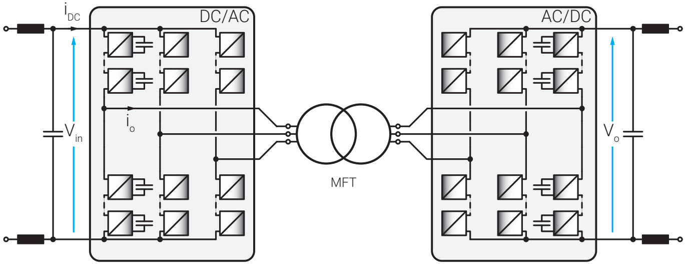

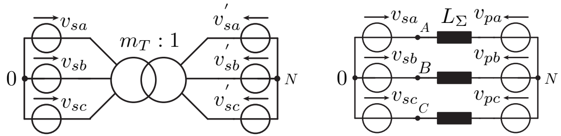

▲ Observed Q2L configuration

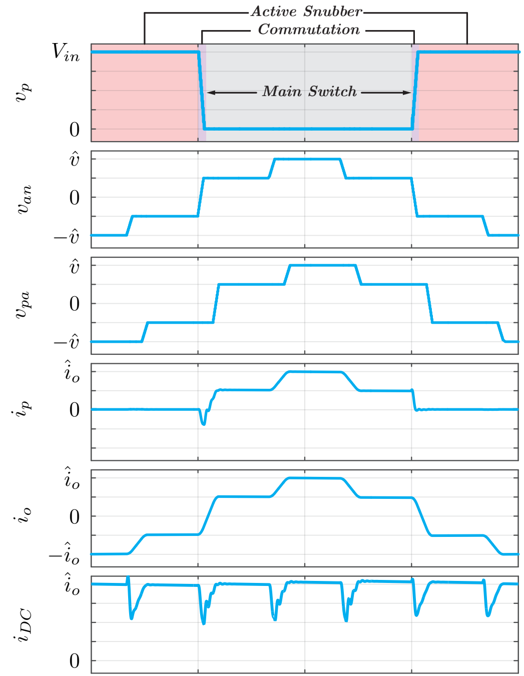

▲ Relevant waveforms of the Q2L converter operating as the 3PH-DAB

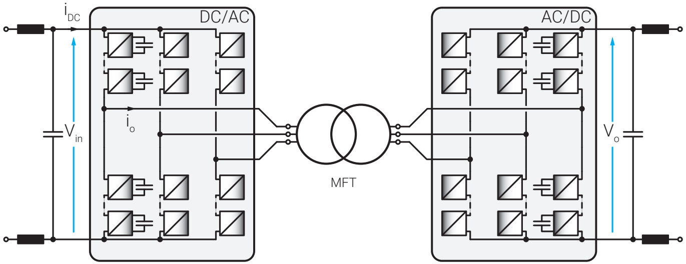

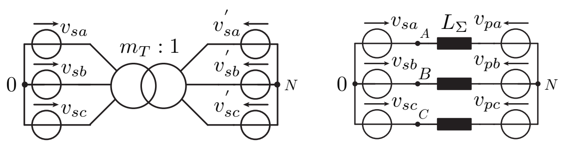

▲ Observed Q2L configuration

⇒ SM capacitor = ”short-interval” energy buffer

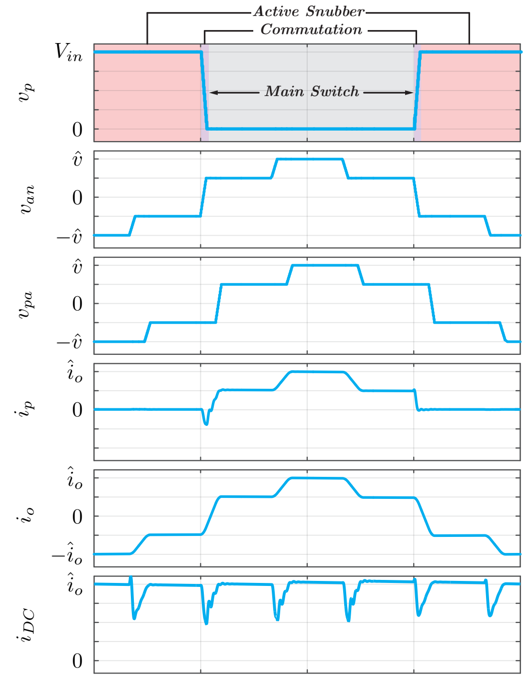

▲ Relevant waveforms of the Q2L converter operating as the 3PH-DAB

Q2L CONVERTER - PROS AND CONS

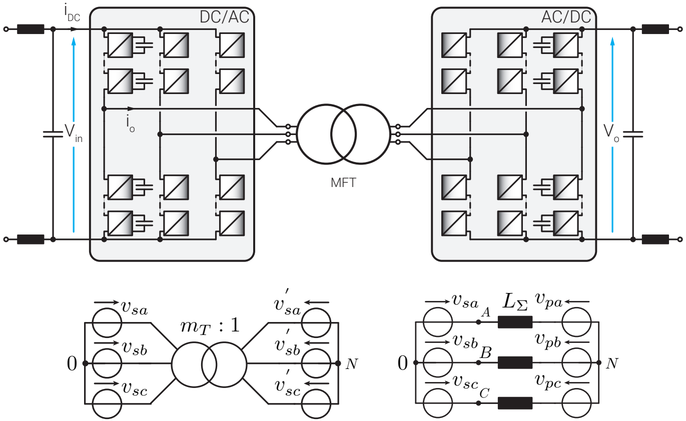

▲ Observed Q2L configuration

Pros

- Significant reduction in submodule capacitance
- Converter size reduction (no branch inductors, small SM capacitance)
- Active snubber switch can be sized for half the rated current

Cons

- Need for HV/MV input/output capacitor
- Complicated analysis of transition process/SM capacitance sizing
- SM capacitance sizing influenced by the branch stray inductance

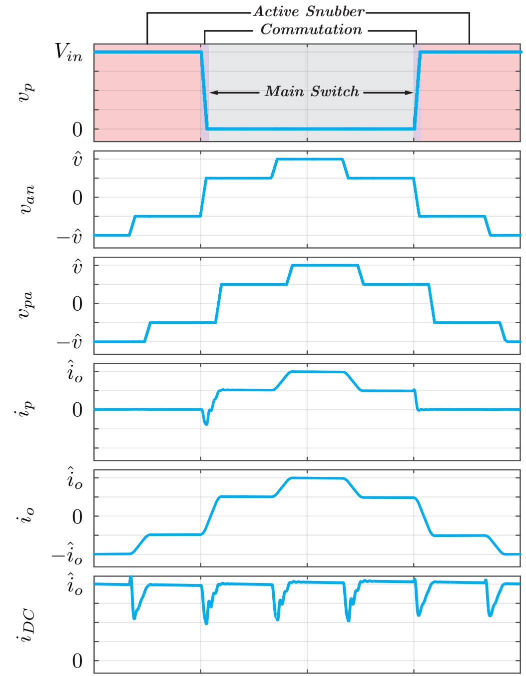

▲ Relevant waveforms of the Q2L converter operating as the 3PH-DAB

SCOTT MFT BASED DC-DC

Medium Frequency Conversion, High Power, Redundancy ...

- Provided ratings

Parameter	Value
Input voltage (V_{in})	±20kV
Output voltage (V_o)	1.5kV
Rated power (P_{nom})	10MW
Operating frequency (f)	1kHz

- **Redundancy**
- Converter structure considering given grid nature?
  - Topology
  - Operating principles and control
  - Operating frequency
  - Sizing principles considering given ratings
  - Constraints
  - Behavior under faults

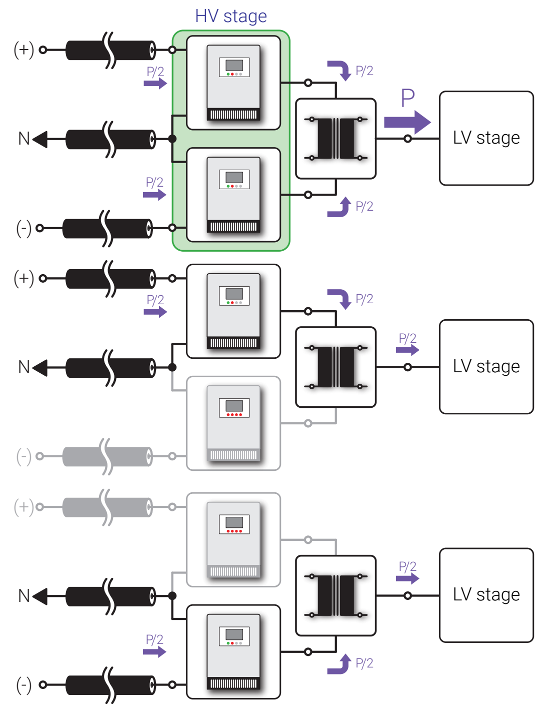

▲ Generic structure of a converter to be employed within a bipolar grid

SIX-STEP MMC-BASED HIGH POWER DC-DC CONVERTER

Features:

- Both stages switching at MFT operating frequency
- DAB operating principles
- Independent operation of the MMCs (ideally)
- Bidirectional topology
- Bipolar DC grids interface
- Redundant under faulty operating conditions
- Medium frequency operation

Drawbacks?

- Twelve arm inductors (or six coupled inductors)
- Magnetic coupling (circulating currents)

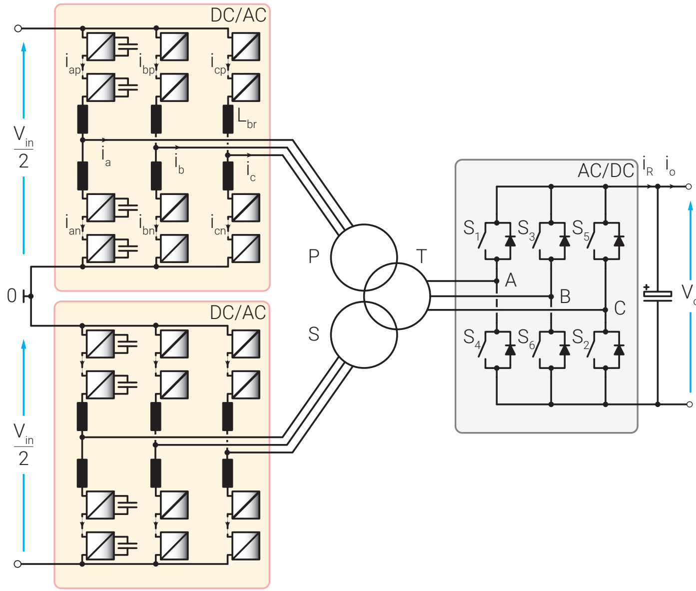

▲ Six-Step MMC-Based High Power DC-DC Converter [27]

[27] Stefan Milovanovic and Drazen Dujic. "Six-Step MMC-Based High-Power DC-DC Converter." *The 2018 International Power Electronics Conference-IPEC 2018 ECCE Asia*. CONF. 2018

MMC-BASED BIDIRECTIONAL DC-DC CONVERTER EMPLOYING STC

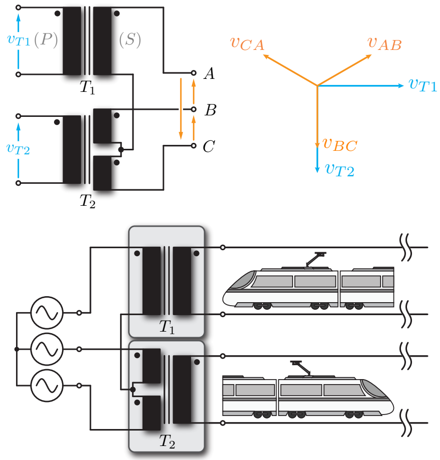

▲ Scott Transformer Connection

- 3PH 3W Tx ⟹ 2 x 1PH Tx
- Number of MMC branches reduction (N_L ↓)
- Ability to operate in a pure rectifier mode
- Medium frequency operation

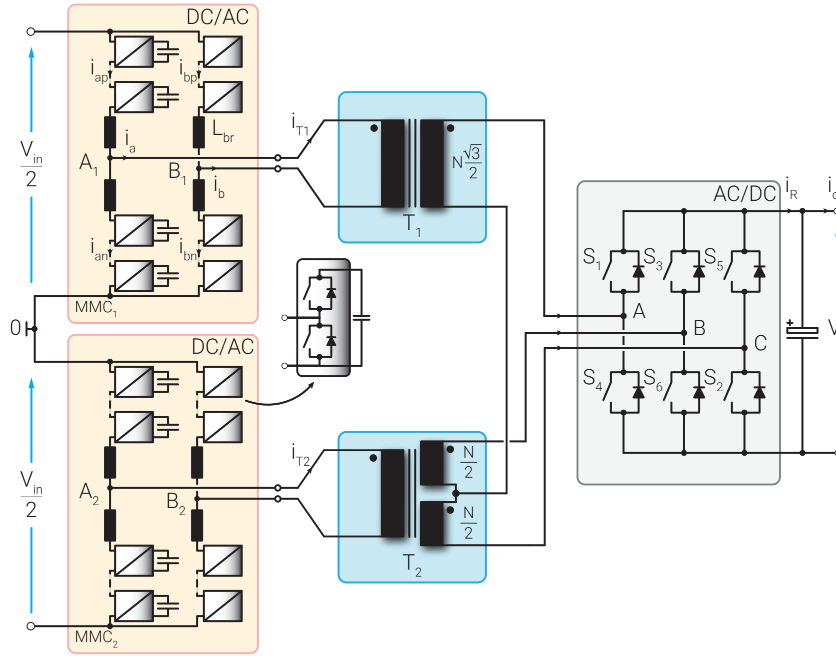

▲ MMC-Based High Power DC-DC Converter Employing Scott Transformer Connection [28]

[28] S. Milovanovic and D. Dujic. "MMC-Based High Power DC-DC Converter Employing Scott Transformer." *PCIM Europe 2018*. June 2018, pp. 1–7

- MMCs independent operation

$$V_{T1} = m_{T1}\frac{V_{AB} - V_{CA}}{2}$$
$$V_{T2} = m_{T2}V_{BC}$$

- Suitable HV side voltages (V_{c1}, V_{c2})?
- DAB behavior (phase modulated converter)

$$P_1 = \frac{V_o^2 m_{T1}^2}{\omega L_a}\varphi_1\left(\frac{1}{2} - \frac{3|\varphi_1|}{8\pi}\right)$$
$$P_2 = \frac{V_o^2 m_{T2}^2}{\omega L_a}\varphi_2\left(\frac{2}{3} - \frac{|\varphi_2|}{2\pi}\right)$$

$$\left(m_{T1} == \frac{2}{\sqrt{3}}m_{T2}\right) \wedge \left(\varphi_1 == \varphi_2\right)$$
$$\Rightarrow P_1 = P_2$$

- Bidirectional topology
- Fundamental frequency switching
- Redundant under faults

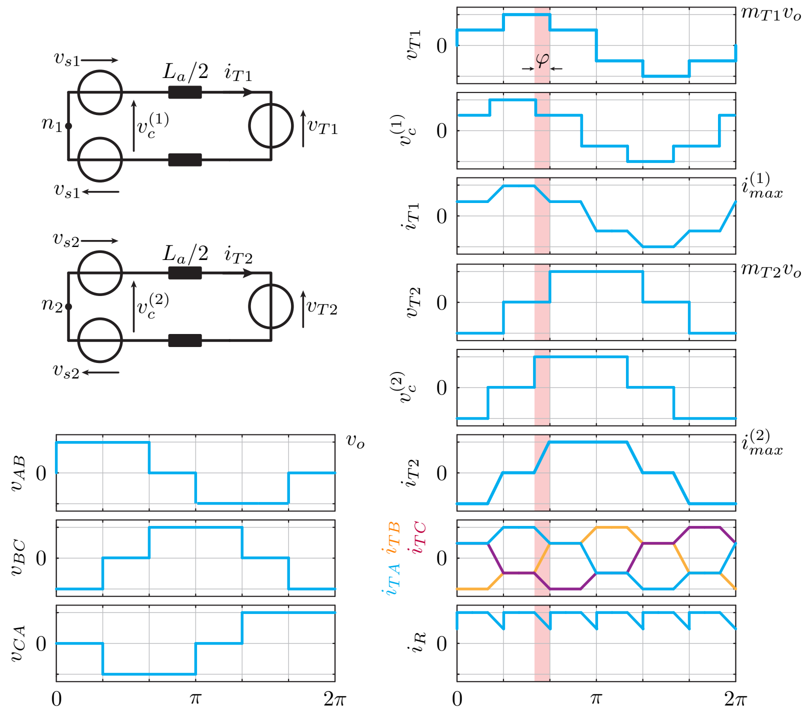

▲ Converter idealized operating waveforms

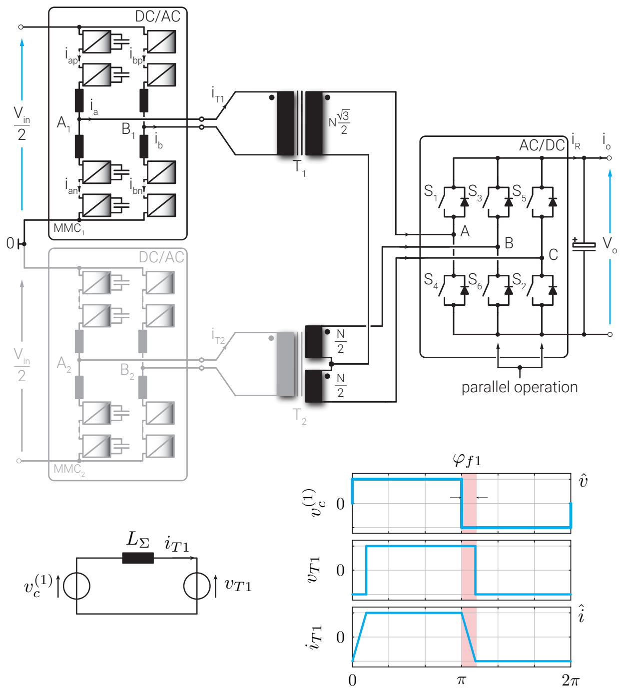

▲ Converter operation in the case of "Minus" DC pole malfunction

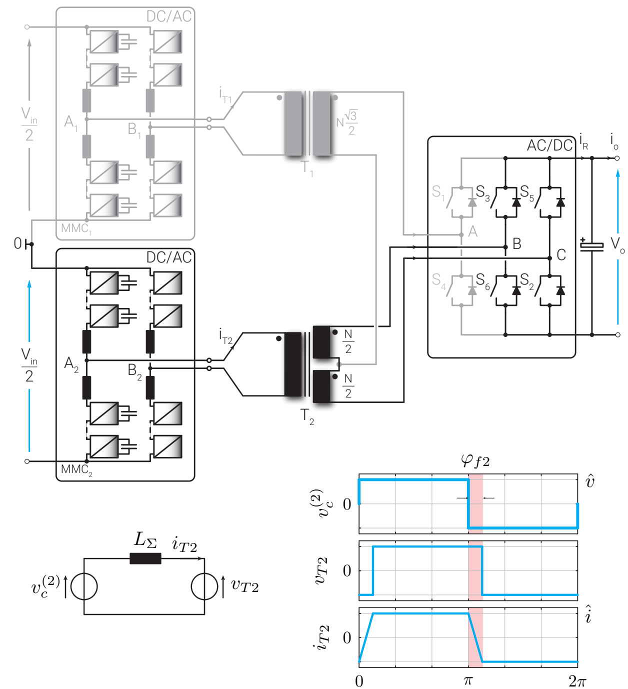

▲ Converter operation in the case of "Plus" DC pole malfunction

SIMULATION RESULTS (I)

Table 1 Simulated system ratings

Parameter	Value
Input voltage (V_{in})	±20kV
Output voltage (V_o)	1.5kV
Rated power (P_{nom})	10MW
Operating frequency (f)	1kHz

- i_{in1} → MMC_1 input current
- i_{in2} → MMC_2 input current
- i_{in} → neutral conductor current
- i_{T1} → T_1 P-winding current
- i_{T2} → T_2 P-winding current
- i_S → LV stage 3PH-currents
- i_R → SSC output current
- V_o → load voltage
- i_o → load current
- i_{rev} → LV side current injection
- V_{T1} → T_1 P-winding voltage
- V_{T2} → T_2 P-winding voltage

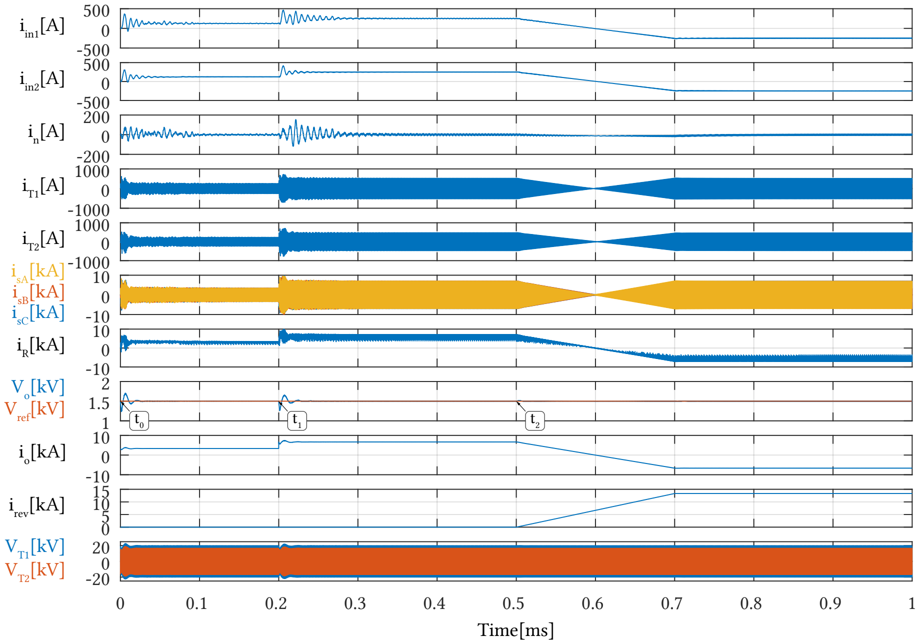

▲ Converter operating waveforms

SIMULATION RESULTS (II)

- i_{in1} → MMC_1 input current
- i_{in2} → MMC_2 input current
- i_{in} → neutral conductor current
- i_{T1} → T_1 P-winding current
- i_{T2} → T_2 P-winding current
- i_S → LV stage 3PH-currents
- i_R → SSC output current
- V_o → load voltage
- i_o → load current
- i_{rev} → LV side current injection
- V_{T1} → T_1 P-winding voltage
- V_{T2} → T_2 P-winding voltage

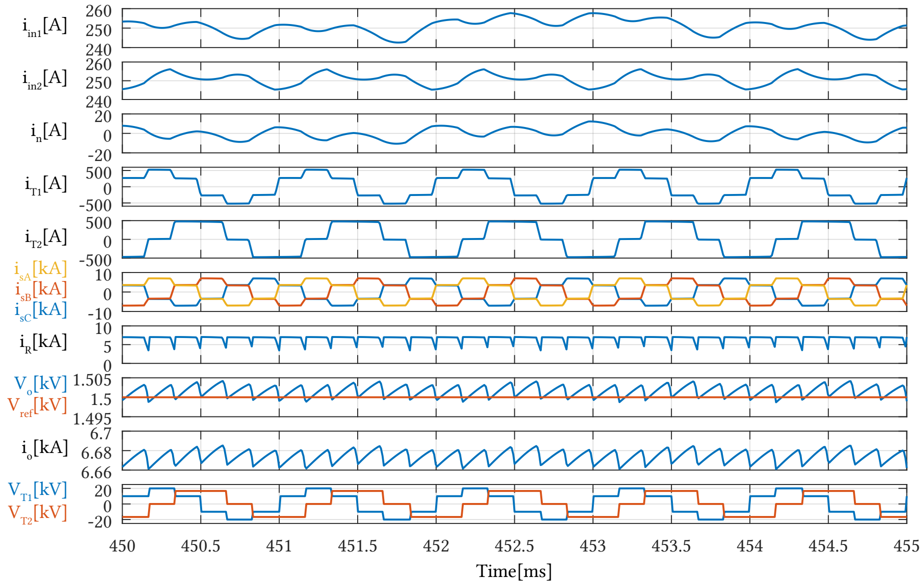

▲ Converter operating waveforms during five fundamental cycles

MMC-BASED HIGH POWER UNIDIRECTIONAL DC-DC CONVERTER

- No magnetic coupling between Tx windings
- Parameters mismatch robustness
- Sinusoidal operation mode!

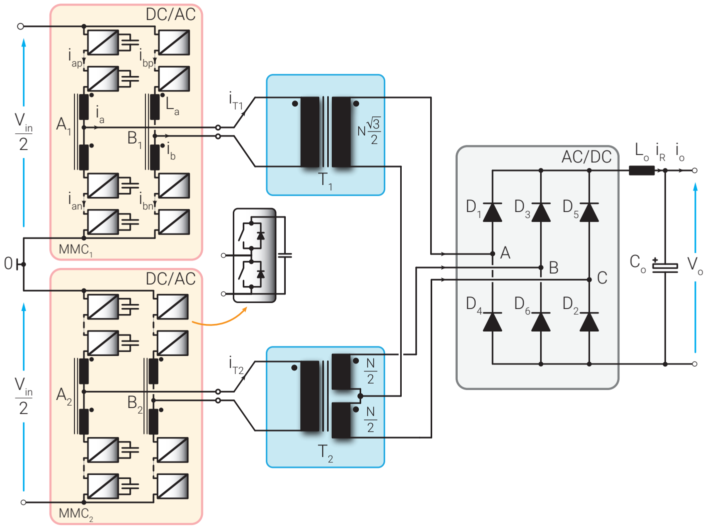

▲ MMC-based High-Power Unidirectional DC-DC Converter

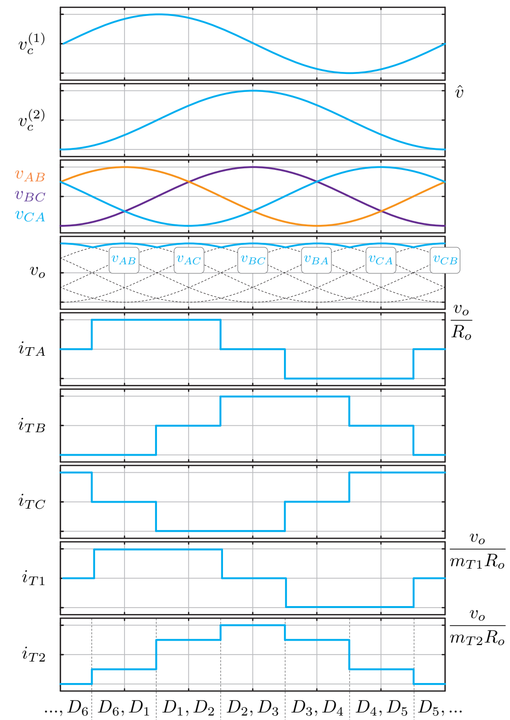

▲ Converter idealized operating waveforms

SIMULATION RESULTS (I)

Table 2 Simulated system ratings

Parameter	Value
Input voltage (V_{in})	±20kV
Output voltage (V_o)	1.5kV
Rated power (P_{nom})	10MW
Operating frequency (f)	250Hz

- i_T → LV-stage 3PH - currents
- i_{in1} → MMC_1 input current
- i_{in2} → MMC_2 input current
- V_1 → MMC_1 AC voltage
- V_2 → MMC_2 AC voltage
- i_R → DR output current
- i_o → load current
- V_o → load voltage
- i_{T1} → T_1 P-winding current
- i_{T2} → T_2 P-winding current
- V_{T1} → T_1 P-winding voltage
- V_{T2} → T_2 P-winding voltage
- V_R → DR output voltage

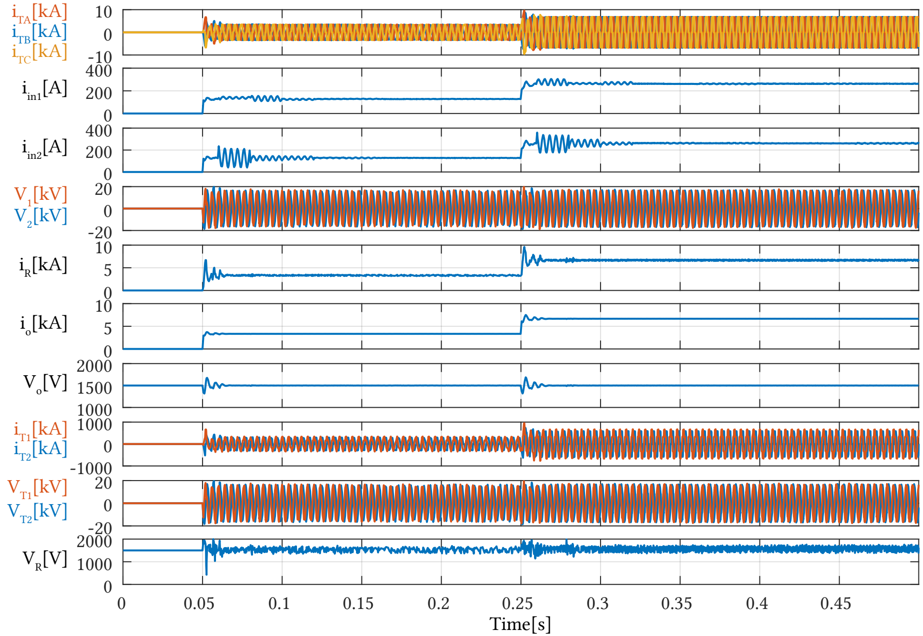

▲ Converter operating waveforms

SIMULATION RESULTS (II)

- i_T → LV-stage 3PH - currents
- i_{in1} → MMC$_1$ input current
- i_{in2} → MMC$_2$ input current
- V_1 → MMC$_1$ AC voltage
- V_2 → MMC$_2$ AC voltage
- i_R → DR output current
- i_o → load current
- V_o → load voltage
- i_{T1} → T$_1$ P-winding current
- i_{T2} → T$_2$ P-winding current
- V_{T1} → T$_1$ P-winding voltage
- V_{T2} → T$_2$ P-winding voltage
- V_R → DR output voltage

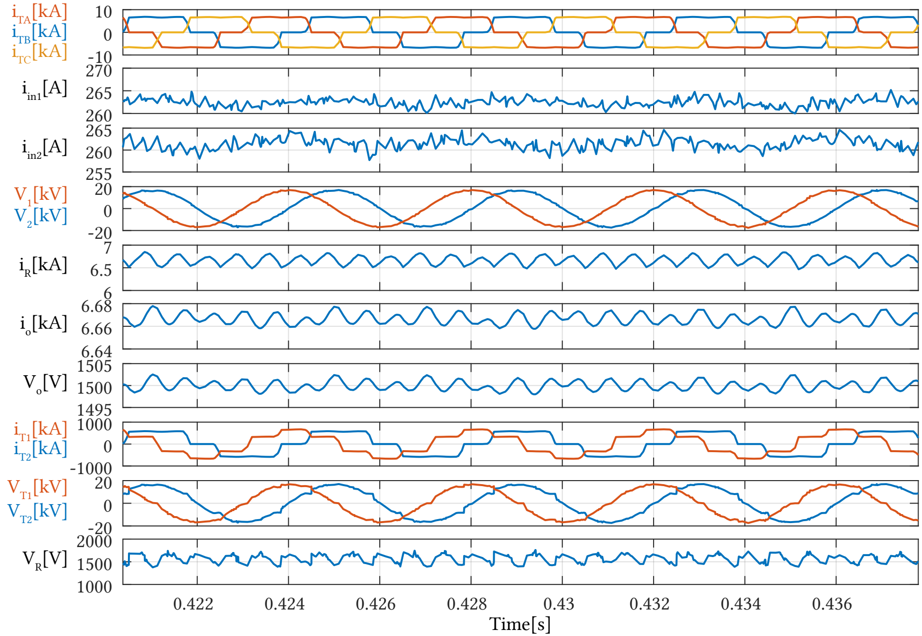

▲ Converter operating waveforms during five fundamental cycles

SUMMARY

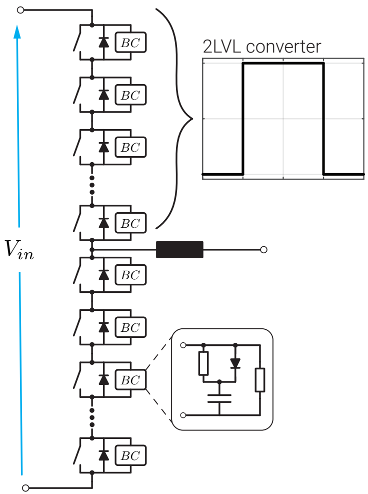

▲ Series connection of switches

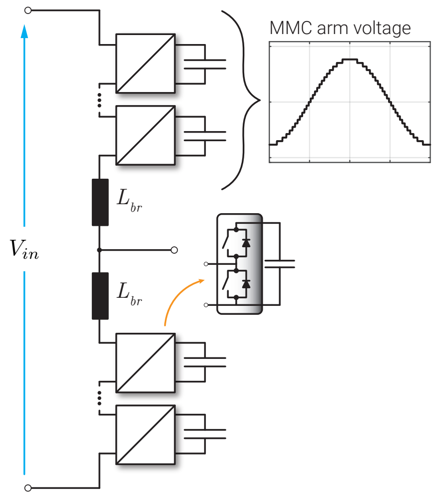

▲ Modular Multilevel Converter (MMC)

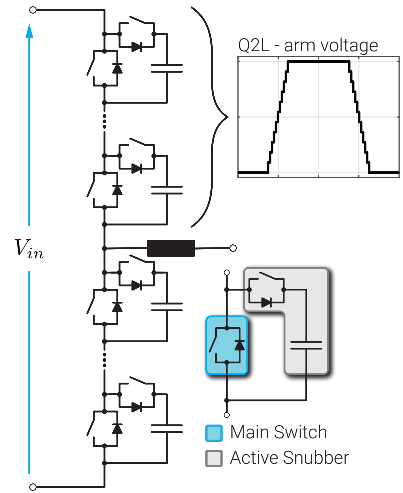

▲ Quasi Two-Level (Q2L) Converter

- Series connection of switches with snubbers
- Two-Level voltage waveforms

- Series connection of Submodules (SM)
- Arbitrary voltage waveform generation

- Series connection of MMC-alike SMs
- Quasi Two-Level (trapezoidal) voltage waveform

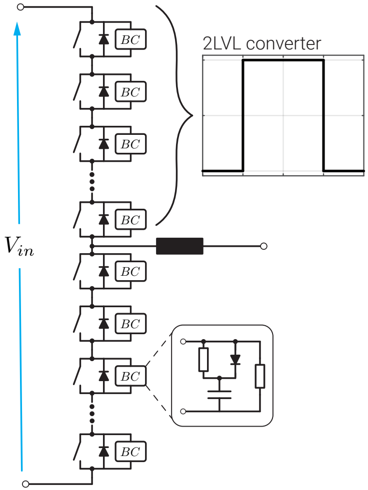

▲ Series connection of switches

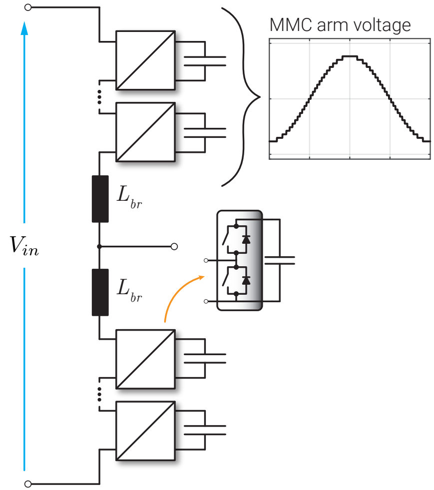

▲ Modular Multilevel Converter (MMC)

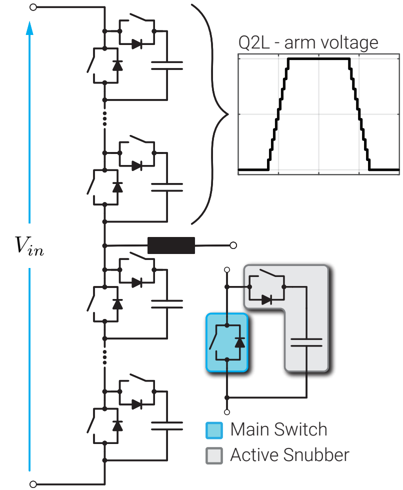

▲ Quasi Two-Level (Q2L) Converter

- Series connection of switches with snubbers
- Two-Level voltage waveforms

- Series connection of Submodules (SM)
- Arbitrary voltage waveform generation

- Series connection of MMC-alike SMs
- Quasi Two-Level (trapezoidal) voltage waveform

⇒ Despite the lack of high voltage semiconductors, we can manage medium/high voltage designs!

RESONANT CONVERSION

DC-DC Converters, Control Principles, Scalability for High Power Applications

Voltage adaptation in AC and DC systems

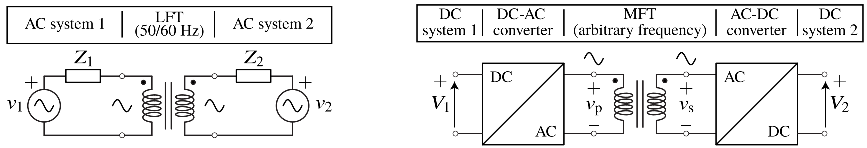

(a) (b)

▲ Principles of interconnecting two networks in case galvanic isolation along with voltage adaptation is needed: (a) Two AC systems; (b) Two DC systems.

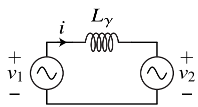

▲ Two AC voltage sources coupled by means of an inductor

$$v_1 = \hat{v}_1 \cos(\omega t)$$

$$v_2 = \hat{v}_2 \cos(\omega t - \delta)$$

$$\downarrow$$

$$P_{12} = \frac{\hat{v}_1 \hat{v}_2}{2\omega L_\gamma} \sin(\delta)$$

Voltage adaptation in AC and DC systems

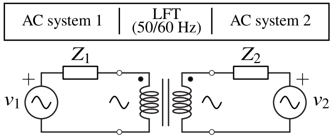

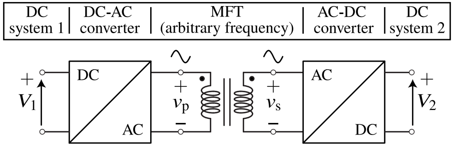

▲ Principles of interconnecting two networks in case galvanic isolation along with voltage adaptation is needed: (a) Two AC systems; (b) Two DC systems.

Dual-Active Bridge

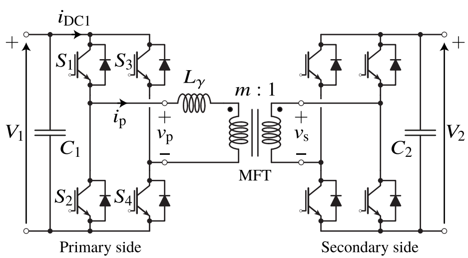

▲ Single-Phase Dual-Active-Bridge DAB.

Resonant Converter

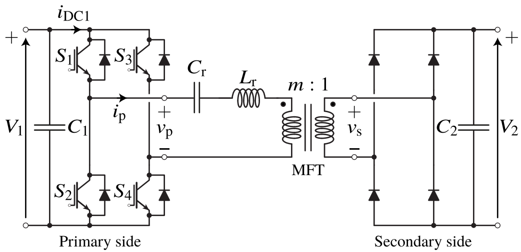

▲ Series resonant converter.

Dual-Active Bridge

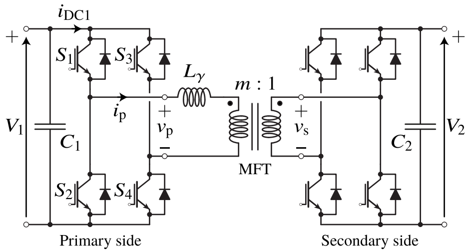

▲ 1PH DAB

Power Transfer

$$P = \frac{1}{2\pi}\int_0^{2\pi} v_p i_p = \frac{V_1^2}{\omega_s L_\gamma}\theta\left(1 - \frac{\theta}{\pi}\right)$$

Presence of high order harmonics

$$\frac{P}{S_{MFT}} = \frac{\frac{1}{2\pi}\int_0^{2\pi} v_p i_p}{V_{p,RMS} I_{p,RMS}} = \frac{1 - \frac{\theta}{\pi}}{\sqrt{1 - \frac{\theta}{2\pi}}}$$

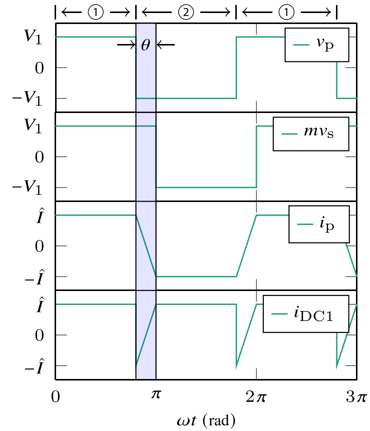

▲ Typical operating waveforms.

⇒ $\theta \uparrow$ PF$\downarrow$

General structure

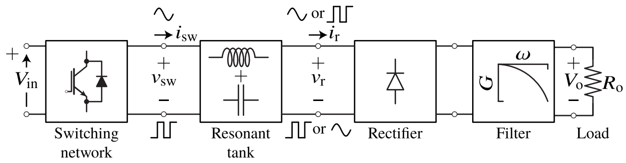

▲ General structure of the resonant converters

$$\hat{V}_{sw}^{(n)} = \begin{cases} \frac{4V_{in}}{\pi n}, & n \text{ is odd} \\ 0, & 0 \text{ is even} \end{cases}$$

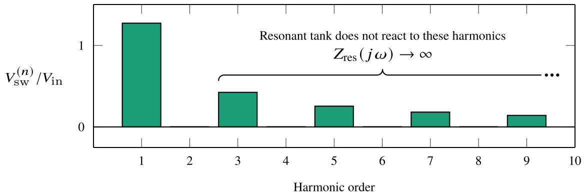

▲ Spectral content of voltage v_{sw} applied to the resonant tank

Resonant converters

- Series resonant
- Parallel resonant
- Series-Parallel resonant (LCC)
- Series-Parallel resonant (LLC)

Modeling

- First Harmonic Approximation - FHA
- Piece-wise sinusoidal analysis
- ...

Switching network

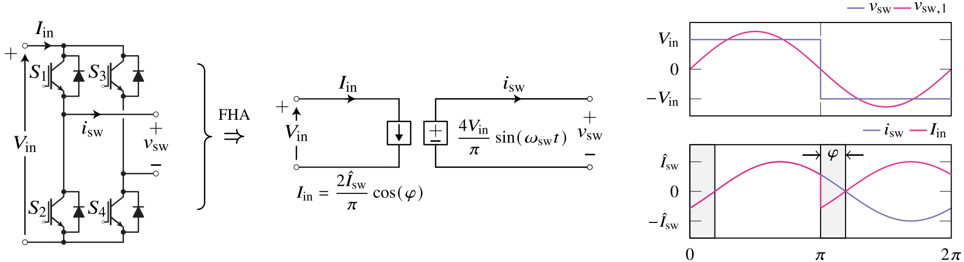

(a) (b) (c)

▲ (a) FB switching network; (b) FHA principle applied to the FB network; (c) Voltage and current waveforms typical for the switching network.

Rectifier and filter

▼ (a) DR with a capacitive filter; (b) DR with an *LC* filter.

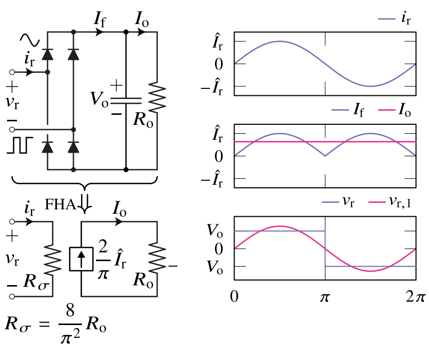

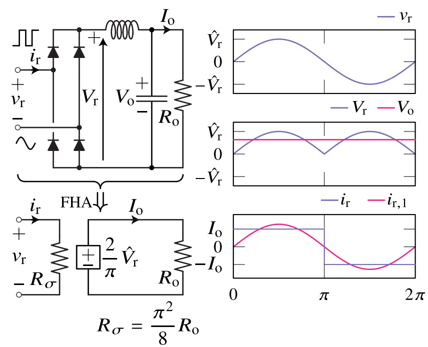

(a) (b)

Averaged Model

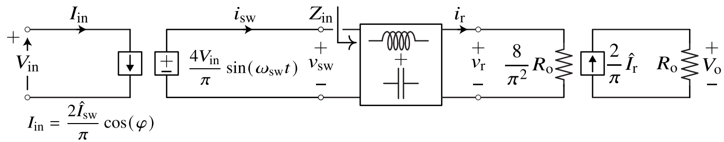

▲ Averaged representation of an arbitrary resonant converter in case rectification stage utilizes purely capacitive filter

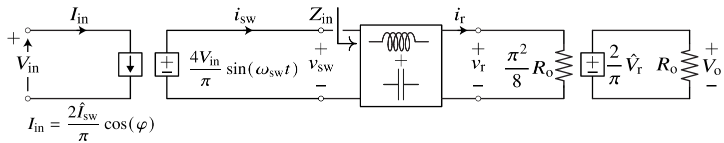

▲ Averaged representation of an arbitrary resonant converter in case rectification stage utilizes an *LC* filter.

Resonant Tank characteristics

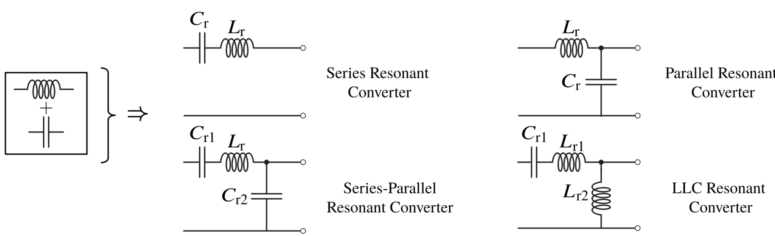

▲ (left) DR with a capacitive filter; (right) DR with an *LC* filter.

Series Resonant Converter

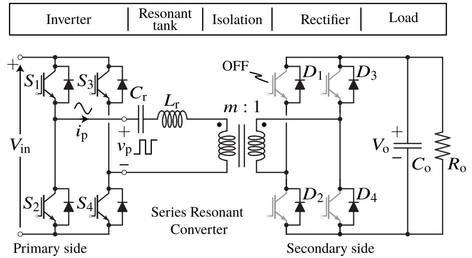

- Series resonant converter
- Typical waveforms of an SRC operating at various switching frequencies.

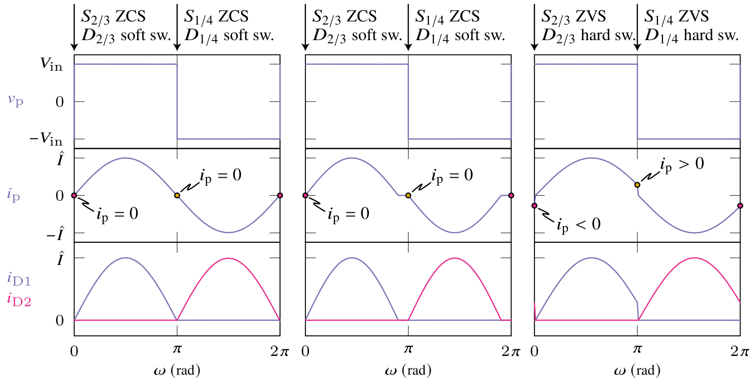

Series Resonant Converter

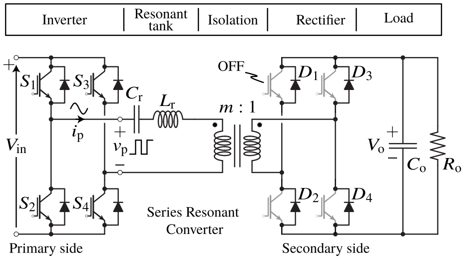

(a)

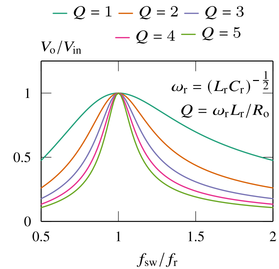

(b)

▲ SRC: (a) Topology; (b) Transfer characteristic derived assuming that $m = 1$;

Parallel Resonant Converter

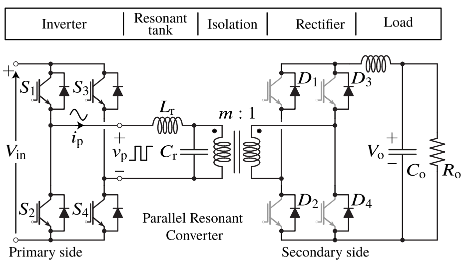

(a)

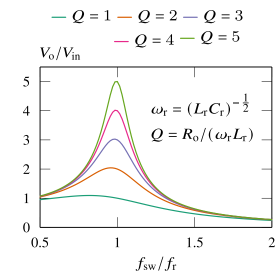

(b)

▲ SRC: (a) Topology; (b) Transfer characteristic derived assuming that $m = 1$;

LCC

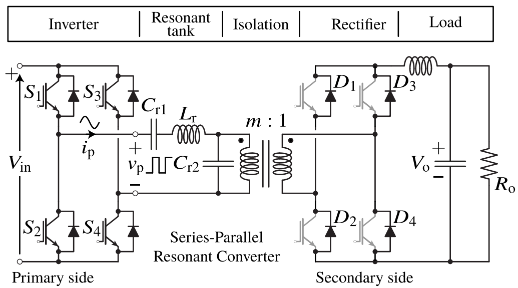

(a)

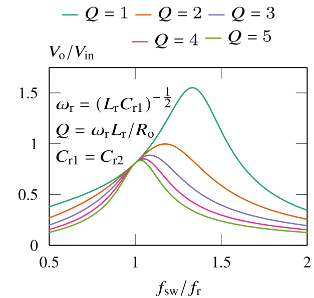

(b)

▲ LCC: (a) Topology; (b) Transfer characteristic derived assuming that $m = 1$;

▼ FHA equivalent of the *LCC* converter.

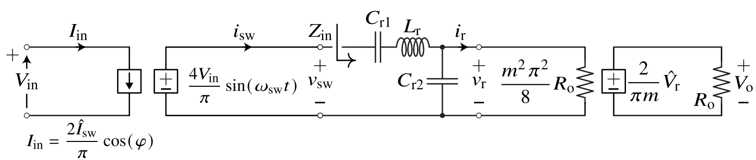

LCC

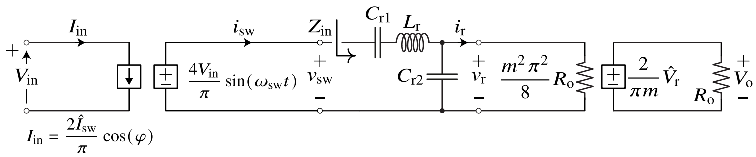

▲ FHA equivalent of the *LCC* converter.

▼ *LCC* converter transfer characteristics for two different ratios of resonant capacitors and different quality factors. Without loss of generality, MFT turns ratio was set as $m = 1$.

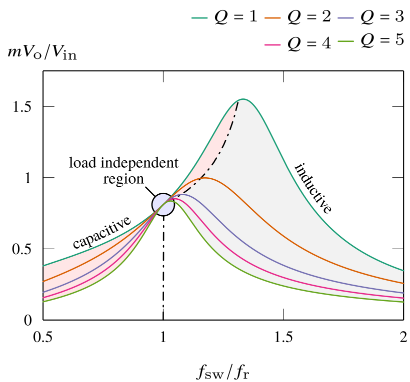

(a)

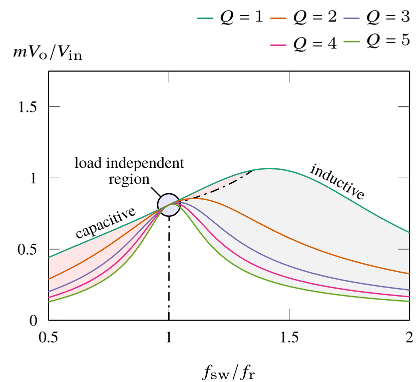

(b)

LLC

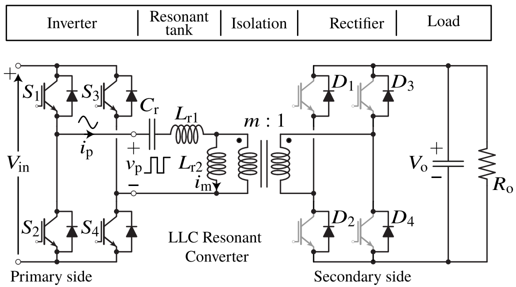

(a)

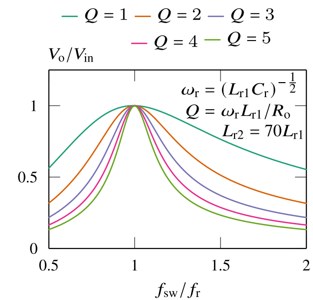

(b)

▲ LLC: (a) Topology; (b) Transfer characteristic derived assuming that $m = 1$;

▼ Typical waveforms of an LLC operating at various switching frequencies.

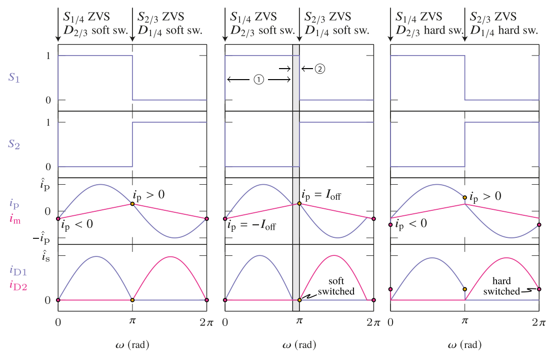

LLC

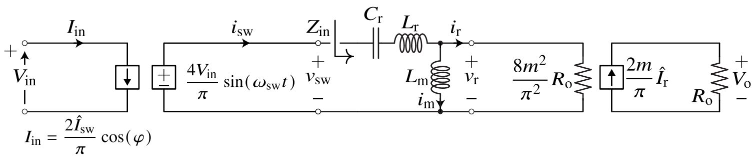

▲ FHA equivalent of the *LLC* converter.

▼ Transfer characteristics of an *LLC* converter for different values of quality factor Q and different ratios of resonant inductors L_r and L_m. Without loss of generality, MFT turns ratio was set as $m = 1$.

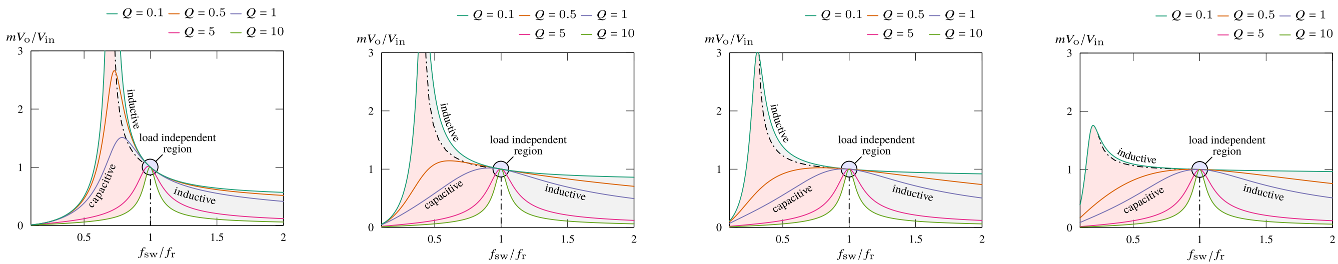

(a) $L_m/L_r = 1$ (b) $L_m/L_r = 5$ (c) $L_m/L_r = 10$ (d) $L_m/L_r = 15$

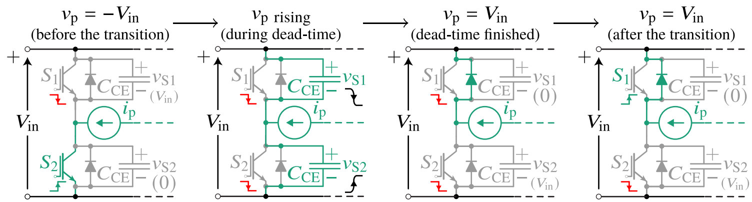

- ▲ One phase-leg of the switching network during the tank voltage transition.
- ▼ Resonant tank current during dead-time.

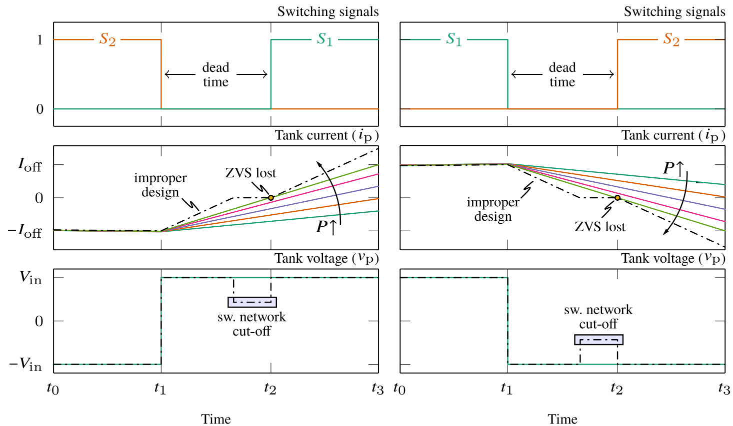

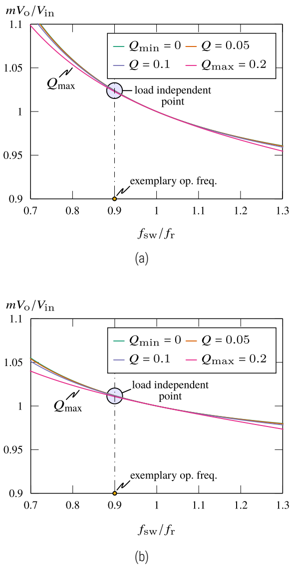

▲ Converter transfer characteristics zoomed around the resonant frequency for two different values of ratio Lm/Lr, $m = 1$.

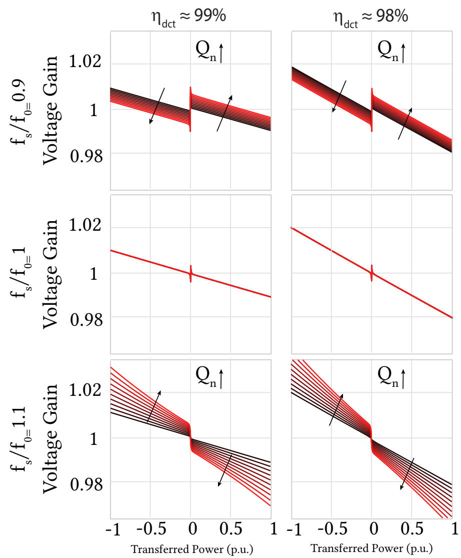

▲ Impact of the switching frequency on the voltage gain for different quality factors ($Q = [0.05, 0.5]$) [29]

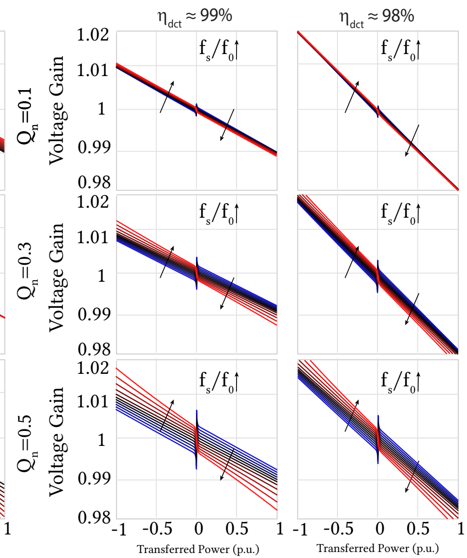

▲ Impact of the quality factor on the voltage gain for different switching frequency ($f_s/f_0 = [0.95, 1.05]$)

[29] Jakub Kucka and Drazen Dujic. "Smooth Power Direction Transition of a Bidirectional LLC Resonant Converter for DC Transformer Applications." *IEEE Transactions on Power Electronics* 36.6 (2021), pp. 6265–6275

LLC CONVERTER - CONTROL PRINCIPLES (III)

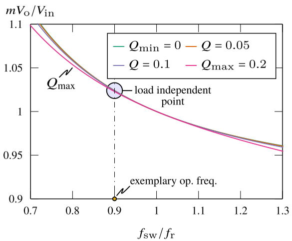

(a)

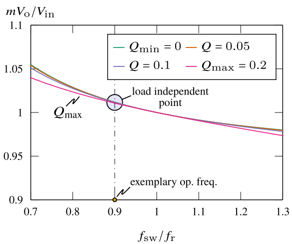

(b)

▲ Converter transfer characteristics zoomed around the resonant frequency for two different values of ratio Lm/Lr, $m = 1$.

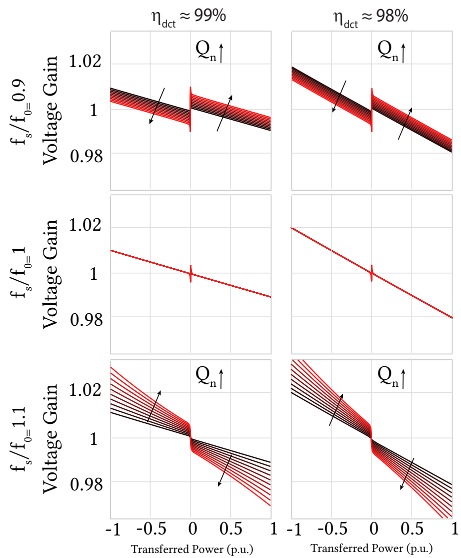

▲ Impact of the switching frequency on the voltage gain for different quality factors ($Q = [0.05, 0.5]$) [29]

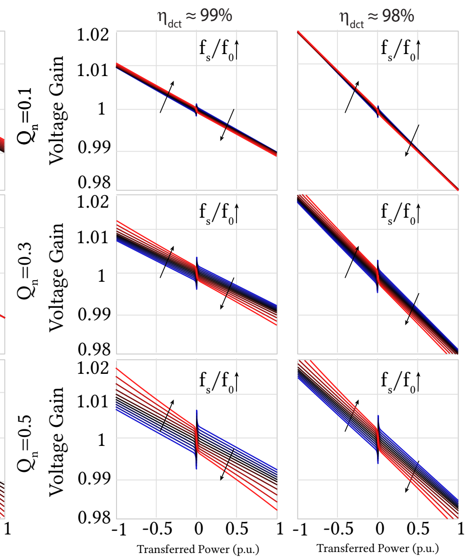

▲ Impact of the quality factor on the voltage gain for different switching frequency ($f_s/f_0 = [0.95, 1.05]$)

⇒ Resonant based Direct Current Transformer has desired features for DC Power Distribution Networks!

[29] Jakub Kucka and Drazen Dujic. "Smooth Power Direction Transition of a Bidirectional LLC Resonant Converter for DC Transformer Applications." *IEEE Transactions on Power Electronics* 36.6 (2021), pp. 6265–6275

COFFEE BREAK

Well deserved...

POWER ELECTRONICS SWITCHES: AN ABUNDANCE OF OPTIONS

Semiconductor devices such as:

- Diodes
- BJTs
- Thyristors
- Triacs
- MOSFETs
- IGBTs
- etc...

Available in:

- Various voltage/current ratings
- Various packages

▲ Power electronics devices exist in a variety of packages and voltage ratings

DEVICES FOR MV APPLICATIONS: FEW MAIN CONTENDERS

Two most used options:

- IGBT
- IGCT
- Thyristors and GTOs are clearly still used

Both devices are:

- Fully controllable
- MV rated

Emerging alternatives:

- HV SiC MOSFETs
- HV SiC IGBTs

Both are slowly emerging, but not mature

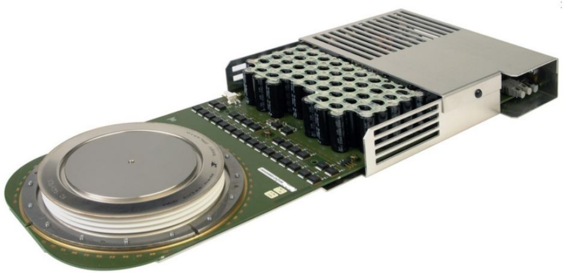

▲ 6.5 kV IGBT module and IGCT

IGBT: CHARACTERISTICS

IGBTs' main characteristics:

- Insulated gate
- Fully controllable
- Voltage controlled
- High power/voltage ratings
- High switching speed
- Simple integration
- Available as module and press-pack

Additional benefits:

- Limitation and turn-off of short circuit current
- Low voltage drop in *ON* state

Device	Voltage Class [kV]	Current Rating [A]	V_{ON} @1kA[V]	V_{ON} @2kA[V]
IGBT/diode	4.5	1600	2.30	3.40
IGBT/diode	4.5	2000	2.55	3.65
IGBT	4.5	2100	1.90	2.70
GTO	4.5	2000	2.20	2.70
Thyristor	4.5	1150	1.35	1.65
IGCT/diode	4.5	2200	2.00	2.50
IGCT	4.5	4000	1.50	1.80

▲ Typical conduction performance of common semiconductor devices

Typical ratings for MV IGBTs:

- 4.5 kV-6.5 kV
- 900 A-1200 A

IGBT: PACKAGING AND GATE DRIVE

Commonly available in:

- Modules
- Press-Pack
- StakPak

Switching performance:

- Can be externally affected by Gate Drive Unit
- Offers controllable di/dt with adequate gate resistance values
- Does not require external circuitry for safe operation

▲ IGBT packaging includes modules, press-pack, and StakPak units

IGCT: CHARACTERISTICS

IGCTs' main characteristics:

- Thyristor based device
- Lowest conduction loss of fully controllable devices
- Integrated in GDU
- Only available as press-pack
- Snubberless turn-off

Traditional IGCT application:

- Low frequency (<1 kHz)
- Hard switched

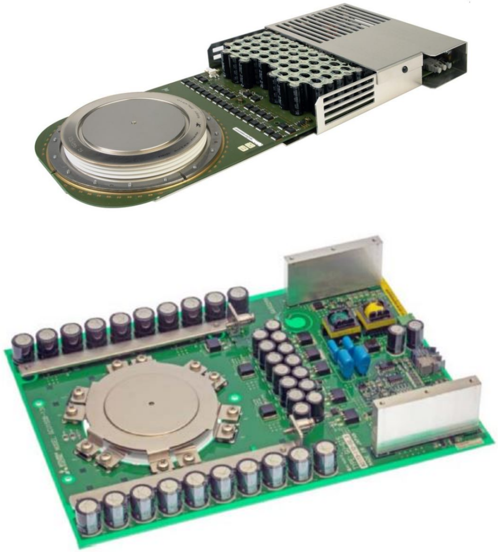

▲ The press-packed GCT is always integrated into the gate driver board to minimise inductance between gate and cathode

The main types of IGCTs:

- Asymmetric
- Reverse conducting - RC-IGCT
- Reverse blocking - RB-IGCT

Ratings of the device can be:

- Up to 6.5 kV (engineering samples up to 10 kV)
- Turn-off current higher for asymmetric devices, due to higher thyristor finger surface (up to 6 kA)
- Hard switched

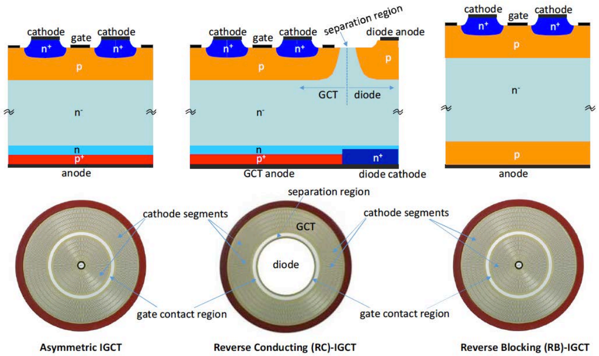

▲ State-of-the-art IGCT device types and their schematic cross sections from top side to bottom side (vertical cross section) [30].

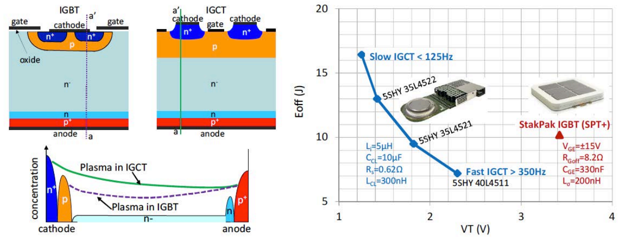

▲ IGCT vs. IGBT. Left: schematic structures of IGCT and IGBT and their plasma distribution during conduction. Right: technology curve comparison between 4.5kV Asymmetric IGCT and StakPak IGBT module at 2.8kV, 2kA, 125°C [30].

IGCT: LIMITATIONS

Compared to the IGBT the IGCT:

- Cannot control turn-on di/dt through GDU
- Requires clamp circuitry
- Cannot turn *OFF* short circuit current
- Has significant GDU power consumption
- Requires bulky GDU capacitors to maintain constant gate-cathode voltage at turn-off

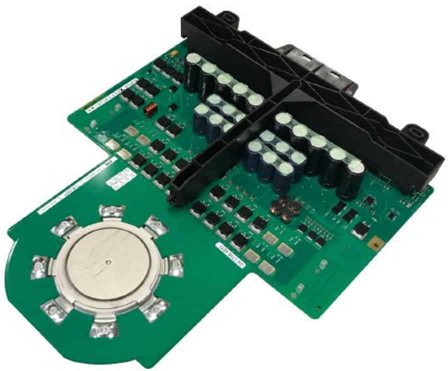

▲ The IGCT GDU allocated a large portion of its surface to capacitors an turn-off MOSFETs

IGCT: CLAMP CIRCUIT

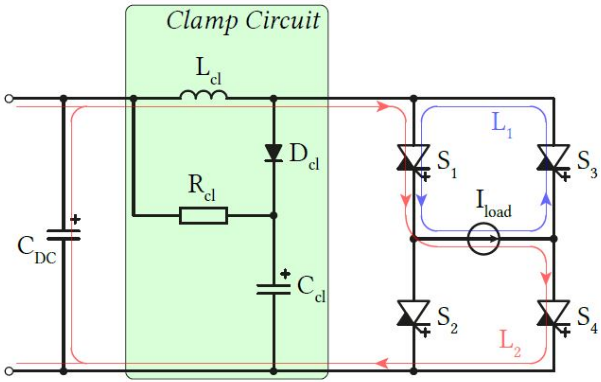

▲ Typical the clamp circuit

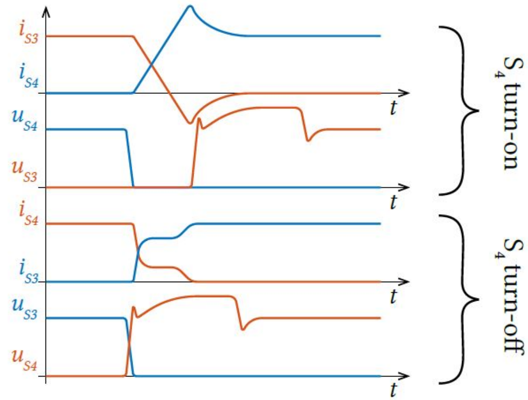

▲ Current and voltage waveforms for the S_3 and S_4 during turn-on and turn-off transients

- IGCT turn-on not fully controlled by GCU action
- Hard IGCT turn-on forces reverse recovery of complementary device antiparallel diode
- Clamp inductor required to limit antiparallel diode reverse recovery di/dt
- RCD snubber limits the overvoltage
- Part of the energy is recovered back to main DC link

IGCT IN RESONANT LLC CONVERTER: HIGH FREQUENCY OPERATION

IGCT frequency limited by:

- Losses and junction temperature
- Gate driver ON/OFF channel capability

Resonant operation implies:

- Lossless turn-on (ZVS or ZCS)
- Low turn-off loss (low turn-off current)
- Limited di/dt

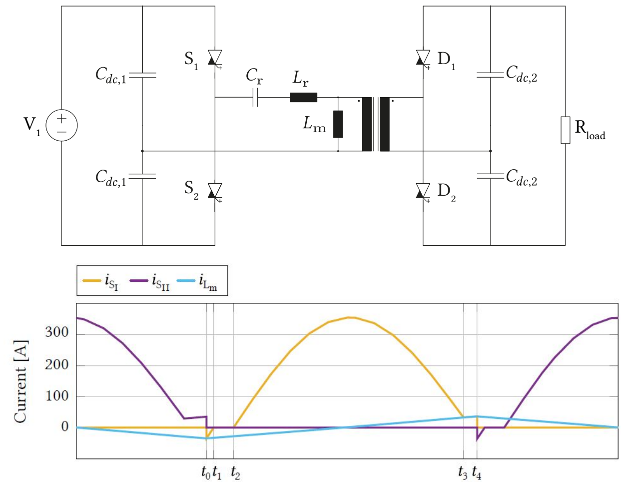

▲ Half-bridge based LLC topology and corresponding current waveforms [31]

[31] Dragan Stamenkovic et al. "Soft Switching Behavior of IGCT for Resonant Conversion." *2019 IEEE Applied Power Electronics Conference and Exposition (APEC)*. 2019, pp. 2714–2719

IGCT IN RESONANT LLC CONVERTER: HIGH FREQUENCY OPERATION

IGCT frequency limited by:

- Losses and junction temperature
- Gate driver ON/OFF channel capability

Resonant operation implies:

- Lossless turn-on (ZVS or ZCS)
- Low turn-off loss (low turn-off current)
- Limited di/dt

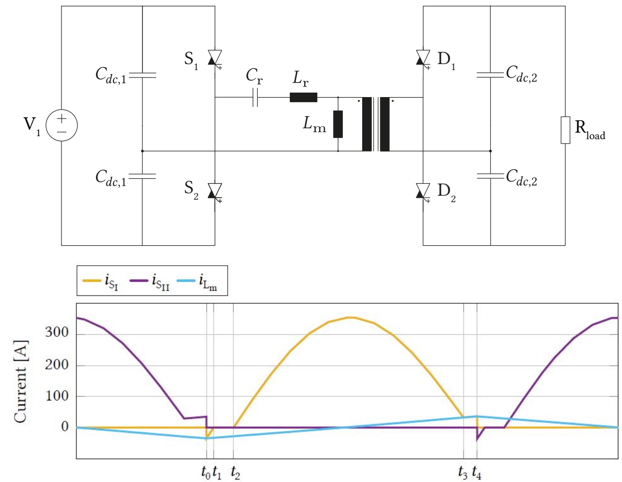

▲ Half-bridge based LLC topology and corresponding current waveforms [31]

⇒ LLC topology can greatly exploit IGCT for high-power designs! High frequency operation must be explored!

[31] Dragan Stamenkovic et al. "Soft Switching Behavior of IGCT for Resonant Conversion." *2019 IEEE Applied Power Electronics Conference and Exposition (APEC)*. 2019, pp. 2714–2719

Hard switched IGCT operation required clamp circuit:

- IGCT turn-on causes reverse recovery of complementary antiparallel diode
- Rate of increase of reverse recovery current must be limited by external means

Soft turn-on removes need for clamp:

- IGCT turn-on occurs while antiparallel diode of the same device is conducting
- Turn-on occurs in ZVS condition
- Current naturally reaches zero in the diode

Removal of clamp circuit is possible for IGCT in LLC topology:

- Significant space saving
- Significant reduction of component count

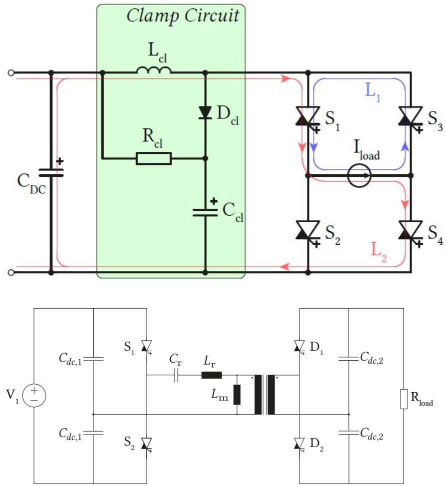

▲ Hard-switched and soft-switched operation differ also by necessity of clamp circuitry [32]

[32] Dragan Stamenković et al. "IGCT Low-Current Switching—TCAD and Experimental Characterization." *IEEE Transactions on Industrial Electronics* 67.8 (2020), pp. 6302–6311

IGCT IN LLC: SERIES CONNECTION IN HARD SWITCHED APPLICATIONS

IGCTs in series connection:

- Dynamic voltage balancing provided by RC or RCD snubbers
- Static voltage balancing provided by passive balancing resistors

Series connection in hard switching:

- Turn-off currents in the kA range
- Snubber capacitance values up to 1 µF

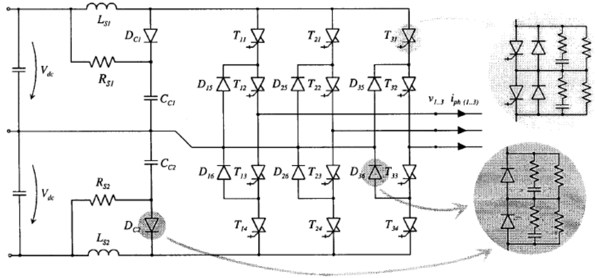

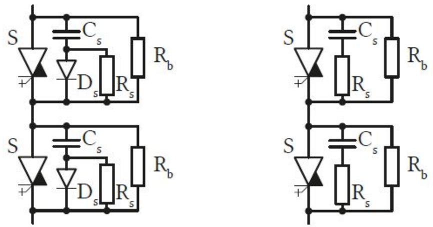

▲ Hard-switched and soft-switched operation differ also by necessity of clamp circuitry

⇒ Large snubber values are needed for hard switched low frequency applications!

IGCT IN LLC: SERIES CONNECTION IN SOFT SWITCHED APPLICATIONS

Challenges in soft switched series connection:

- Low turn-off current increases transitions times
- Large dynamic voltage balancing capacitors unsuitable

For successful series connection in soft switching:

- Ultra-low values of snubber capacitance (<100 nF)
- Purely capacitive snubbers [33]

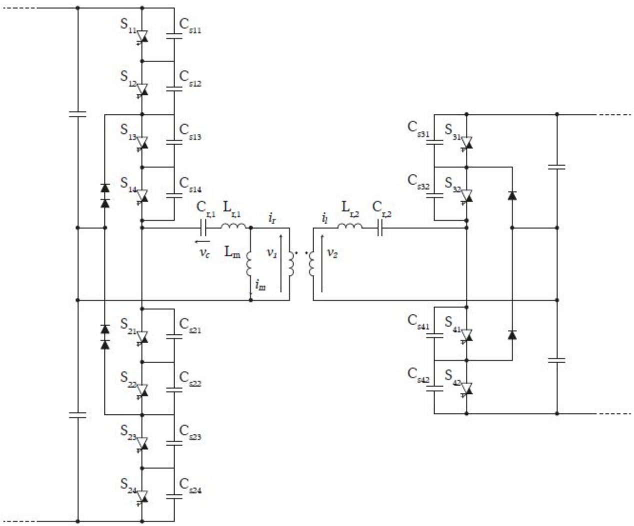

▲ IGCT soft-switching in series connection can employ purely capacitive dynamic voltage sharing snubbers

[33] Gabriele Ulissi et al. "High-Frequency Operation of Series-Connected IGCTs for Resonant Converters." *IEEE Transactions on Power Electronics* 37.5 (2022), pp. 5664–5674

IGCT IN LLC: HIGH FREQUENCY OPERATION IN SERIES CONNECTION

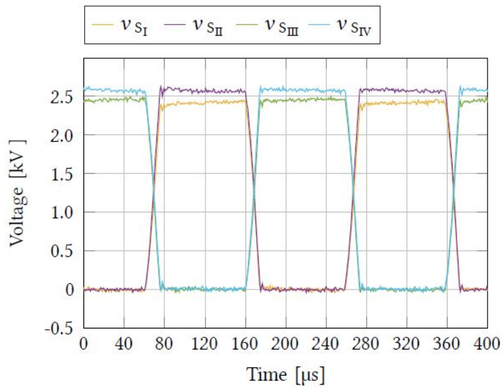

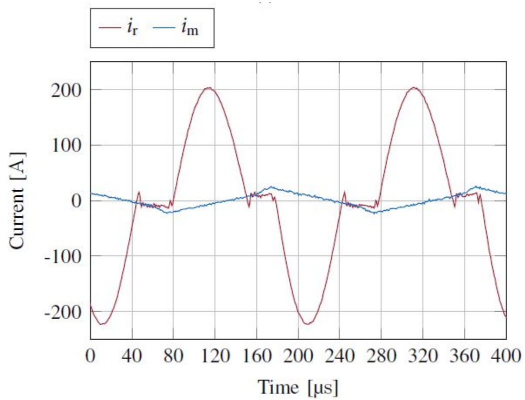

▲ During high-frequency series connected operation the duration of switching transitions is not negligible with respect to the switching period [33]

The duration of switching transitions is significant during high frequency series connected operation due to:

- Presence of snubbers increasing the turn-off an turn-on duration
- Short duration of switching period

Additional factors influencing the switching transition duration are:

- Junction temperature
- Level of current pre-flooding as a result of load level

In resonant IGCT operation the level of current pre-flooding must be accounted for as:

- In increases the duration of the switching transitions
- It may result in loss of ZVS turn-on

Loss of ZVS due to current pre-flooding can be counteracted by:

- Increase of turn-off current level
- Reduction of snubber capacitance value (while still maintaining satisfactory dynamic voltage sharing)
- Increase of dead-time duration

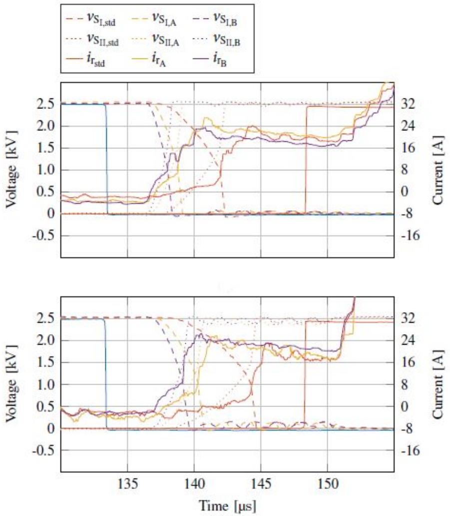

▲ Effect of current pre-flooding in series connected IGCTs during turn-off. Top figure displays transition at peak conduction current of 100 A, bottom figure peak current of 300 A.

Similarly to current pre-flooding level, switching transition duration is also affected by:

- Turn-off current level
- Junction temperature

Increased turn-off current level results in:

- Faster charge carrier sweep-out at turn-off
- Increased turn-off loss

Increased junction temperature results in:

- Increased turn-off duration
- Increased turn-off energy

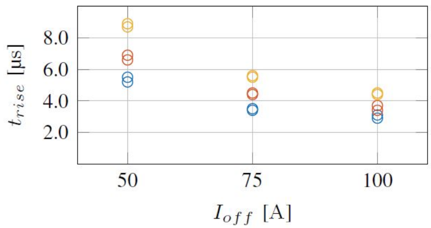

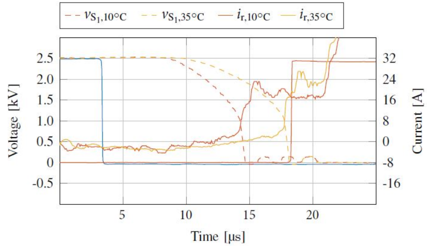

▲ Turn-off duration as a function of turn-off current for series connected IGCTs with snubber capacitance of 40 nF (blue), 70 nF (red), and 100 nF (yellow). IGCT switching transition with a 25 °C difference in junction temperature.

Optimisation of the devices on the technology curve is an additional degree of freedom allowing:

- Custom trade-offs between switching and conduction loss
- Reduction of IGCT switching loss in the LLC-SRC topology

Use of IGCTs in the LLC-SRC topology results in switching loss being most significant:

- IGCTs are oversized for the tested application
- Extremely low conduction loss as a consequence

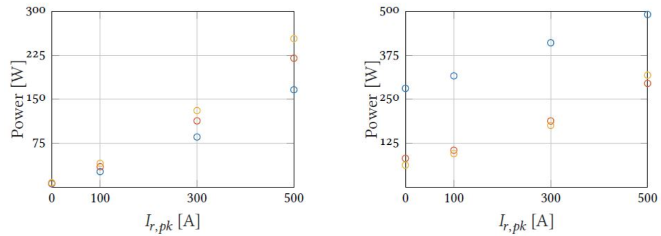

▲ Left: conduction loss and; Right: total loss in the tested application at 5 kHz with standard commercial IGCTs (blue), and devices with respectively +50 % (red), and +95 % increased level of electron irradiation

Trade offs:

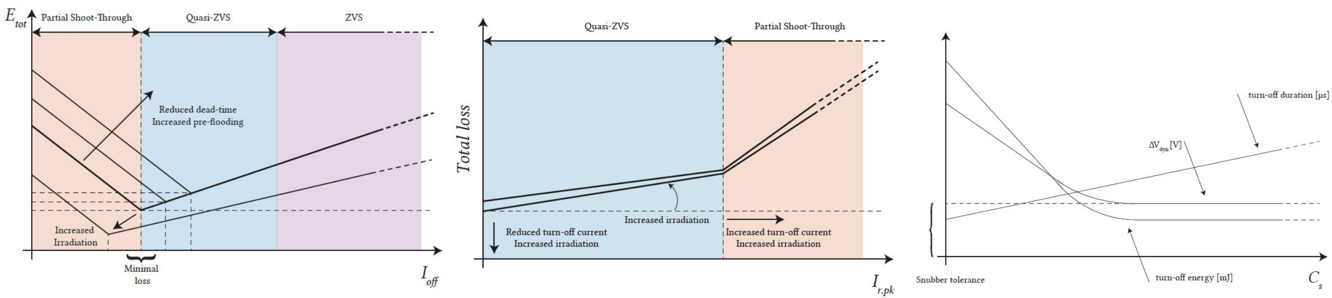

▲ Selecting device and tuning operating conditions require some characterization work

IGCT GATE UNITS FOR SOFT SWITCHING APPLICATIONS

Design, Soft-switching, and Experience

Gate Commuted Thyristor (GCT)

- Thyristor based technology
- Controlled by current
- Hard driving turn off

Necessary functions of the gate unit: [34]

- Turn ON
- Turn OFF
- Backporch operation
- Negative-voltage backporch operation
- Retrigger

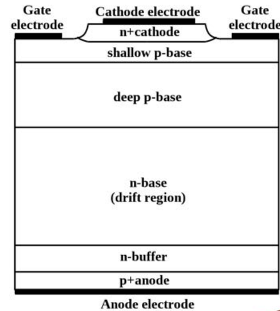

Wikipedia: Integrated gate-commutated thyristor
https://en.wikipedia.org/wiki/Integrated_gate-commutated_thyristor

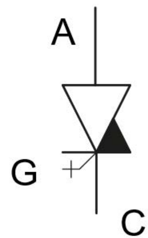

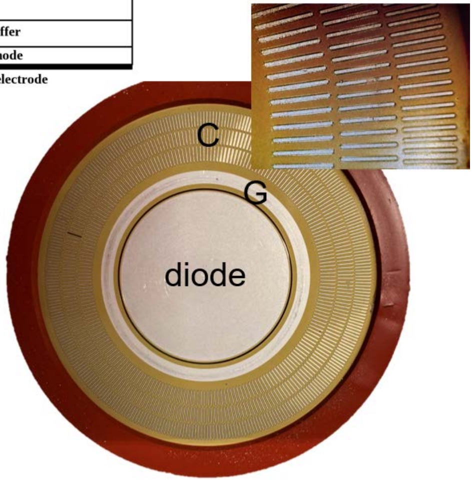

▲ Reverse conducting IGCT structure and symbol

REQUIREMENTS (II)

Turn ON

- Similarly to thyristor the turn on requires steep current into the gate
- The value has to be high enough to turn on all gate cells at once
- Gate current peak is approximately 100 to 300 A
- The device opens practically immediately
- The di/dt is limited only by the external circuit

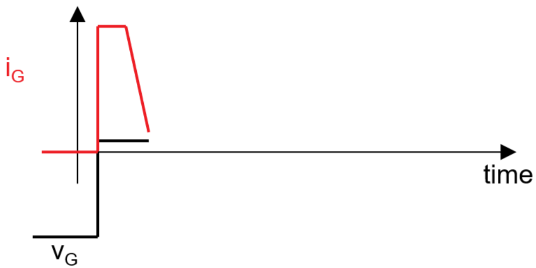

▲ Simplified illustration of a current pulse applied to the gate

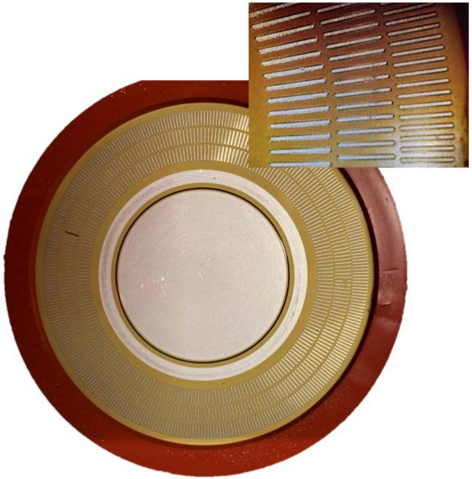

▲ Reverse conducting IGCT structure

REQUIREMENTS (III)

Turn ON

- Similarly to thyristor the turn on requires steep current into the gate
- The value has to be high enough to turn on all gate cells at once
- Gate current peak is approximately 100 to 300 A
- The device opens practically immediately
- The di/dt is limited only by the external circuit

Hence:

- The gate unit cannot impact GCT turn-on behavior
- The only task of the high turn-on pulse is to avoid hot-spots
- It ensures fast and equal activation of all GCT fingers

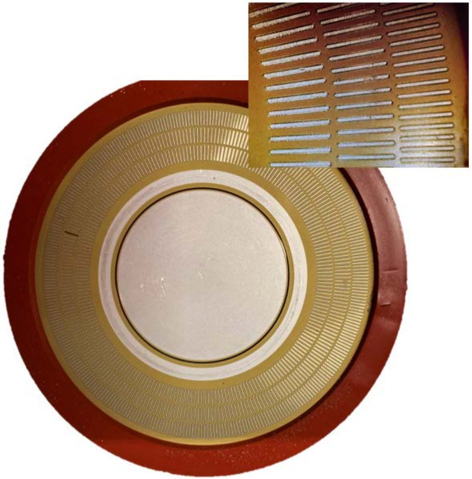

▲ Reverse conducting IGCT structure

REQUIREMENTS (IV)

Backporch Operation:

- A certain value of gate current is necessary to keep the IGCT on (if the anode current would drop below the latching current value)
- This current is typically regulated in relation to temperature conditions

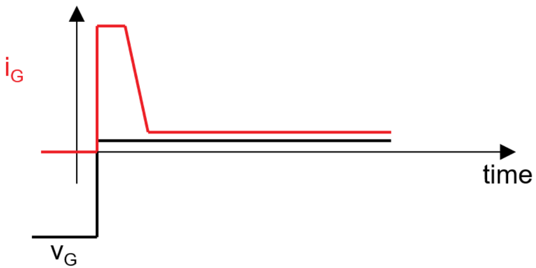

▲ Illustration of backporch current during IGCT conduction

Turn OFF

- Hard-driving the IGCT by clamping the gate voltage to -20 V [35]
- The initial recombination has to happen within a very short time
  → high di/dt of gate current is required
  → low inductance connection of -20 V to gate

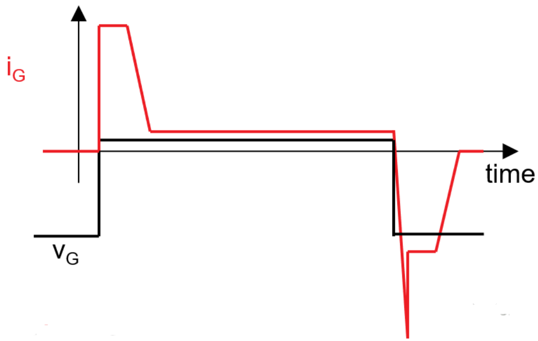

▲ The IGCT turn OFF event - conducted current is commutated to the gate circuitry

- The turn-off dv/dt and di/dt of the switch cannot be impacted by the gate unit
- The lower inductance simply increases the feasible turn-off current

- The current plateau equals the anode current
- High power consumption!

Turn OFF

- Hard-driving the IGCT by clamping the gate voltage to -20 V [35]
- The initial recombination has to happen within a very short time
  → high di/dt of gate current is required
  → low inductance connection of -20 V to gate

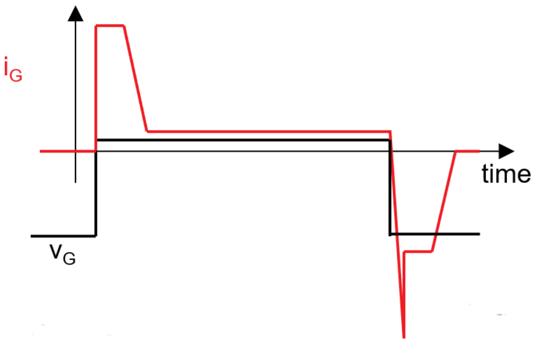

▲ The IGCT turn OFF event - conducted current is commutated to the gate circuitry

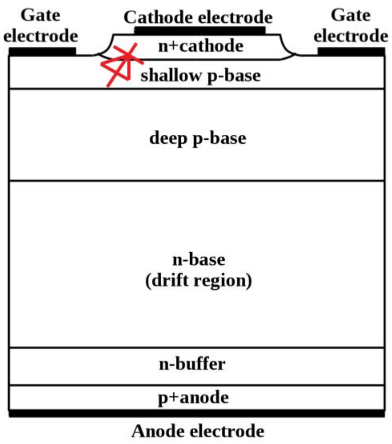

▲ GCT structure

Negative gate voltage Backporch operation

- When the antiparallel diode is conducting, a negative voltage drop over GCT is generated
- The PN junction near anode avalanche breaks and the gate-to cathode voltage becomes negative [36], [37], [38]
- The gate unit typically continues supplying backporch current

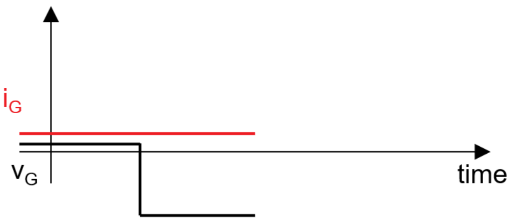

▲ Gate unit during negative gate voltage

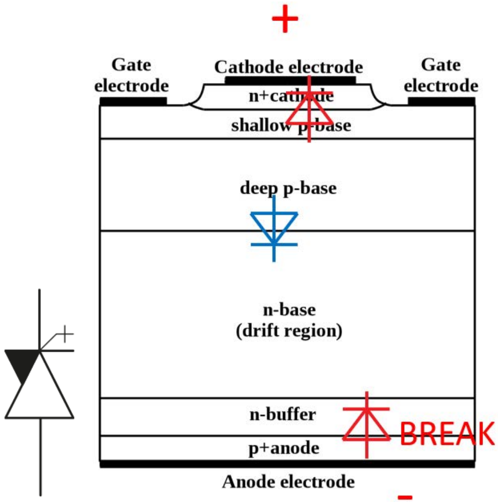

▲ GCT structure

Retrigger Pulse

- Once the anode PN junction closes, a gate current pulse is generated to ensure that all thyristor cells are ready to conduct again
- Problem is eventual high di/dt of the load current
- Retrigger current pulse ensures uniform current take over of the GCT fingers

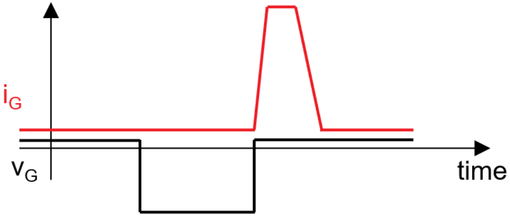

▲ Retrigger pulse applied to the GCT

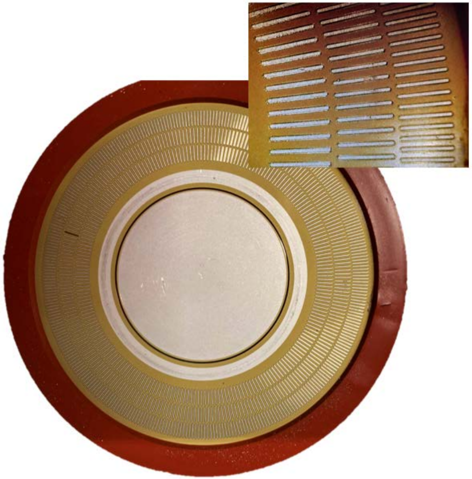

▲ Reverse conducting IGCT structure

Turn OFF Channel

- The solution for the turn off is practically always the same
- A high number of parallel connected MOSFETs connects a high number of capacitors charged to approx. – 20 V to the gate
- High current loading for a very short time
- Parallelization should assure low inductance design

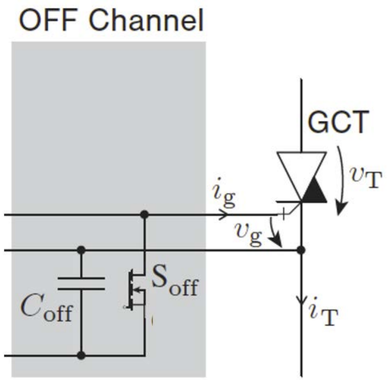

▲ Example of the gate OFF circuit implementation

Turn OFF Channel

- The solution for the turn off is practically always the same
- A high number of parallel connected MOSFETs connects a high number of capacitors charged to approx. – 20 V to the gate
- High current loading for a very short time
- Parallelization should assure low inductance design
- Covers a large area on a typical gate unit

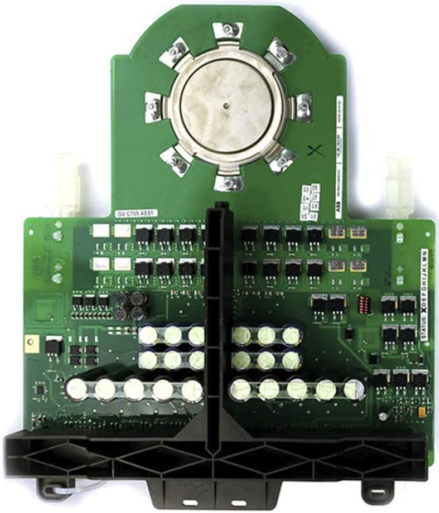

▲ Commercial IGCT - parallel MOSFETs and Capacitors are easily noticable

Turn On & Retrigger Channel

- Typically a single channel for both functions
- High-current inductor with low inductance for current build up
- High current MOSFETs with low switching frequency & a freewheeling diode

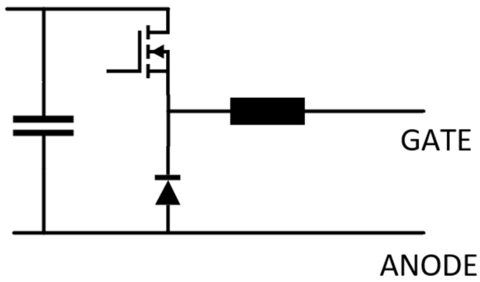

▲ Simplified Gate unit turn ON circuitry

TYPICAL GATE UNIT DESIGNS (IV)

Backporch Channel

- A typical solution is a buck converter closed-loop controlling the current at high switching frequency
- The required current is only several Amperes

Negative-Voltage Backporch Channel

- The standard solution is to reduce the backporch current and consume the energy in non-saturated transistors (and resistors) [36], [37]
- Reference [38] provides another solution where the backporch channel utilizes floating power supply

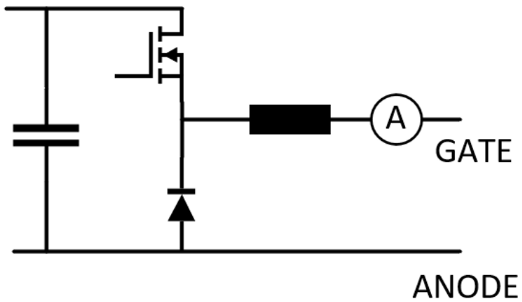

▲ Simplified Gate unit Backporch circuitry

Typical IGCT operating conditions

- Switching at high frequency
- Zero-Voltage turn ON
- Low-Current turn Off
- di/dt during switching is limited by resonant tank

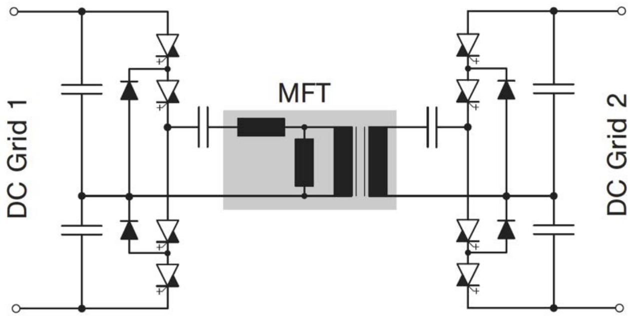

▲ IGCT based DC Transfomer

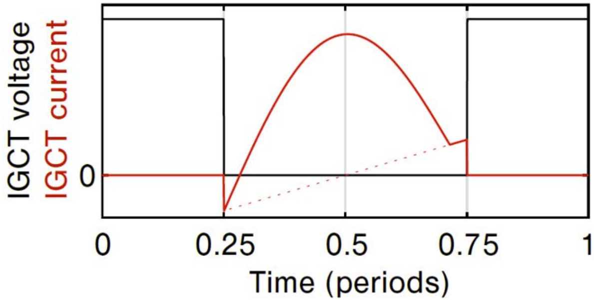

▲ Typical waveforms experienced by IGCT during operation

SOFT-SWITCHING APPLICATION

Typical IGCT operating conditions

- Switching at high frequency
- Zero-Voltage turn ON
- Low-Current turn Off
- di/dt during switching is limited by resonant tank

No clamping circuit is necessary!

Atypical loading for IGCT

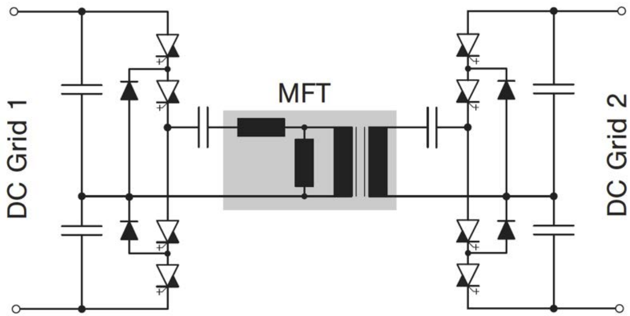

▲ IGCT based DC Transfomer

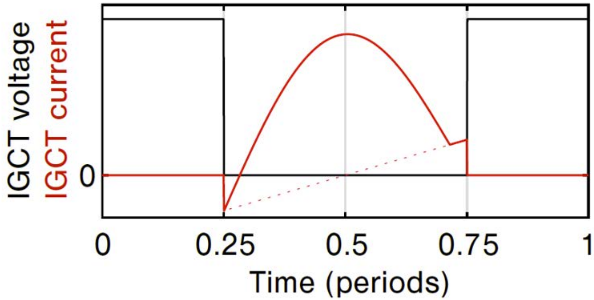

▲ Typical waveforms experienced by IGCT during operation

Main Idea

GATE UNIT DESIGN (I)

Main Idea

- Low turn-off current → Lower consumption → Lower requirements on the turn OFF channel

GATE UNIT DESIGN (I)

Main Idea

- Low turn-off current → Lower consumption → Lower requirements on the turn OFF channel
- Zero-Voltage Turn ON and limited di/dt during retrigger → The magnitude of turn-on gate current pulse can be reduced

Main Idea

- Low turn-off current → Lower consumption → Lower requirements on the turn OFF channel
- Zero-Voltage Turn ON and limited di/dt during retrigger → The magnitude of turn-on gate current pulse can be reduced

> Integration of different channels is possible

GATE UNIT DESIGN (I)

Main Idea

- Low turn-off current → Lower consumption → Lower requirements on the turn OFF channel
- Zero-Voltage Turn ON and limited di/dt during retrigger → The magnitude of turn-on gate current pulse can be reduced

ϟ Integration of different channels is possible

ϟ The size and consumption of the gate unit can be reduced!

GATE UNIT DESIGN (II)

SOFTGATE IGCT Gate Unit

- Gate unit tailored for soft switching

Integration of multiple functions into a single ON channel:

- Turn-ON function
- Retrigger function
- Backporch function
- Negative-Voltage Backporch functions

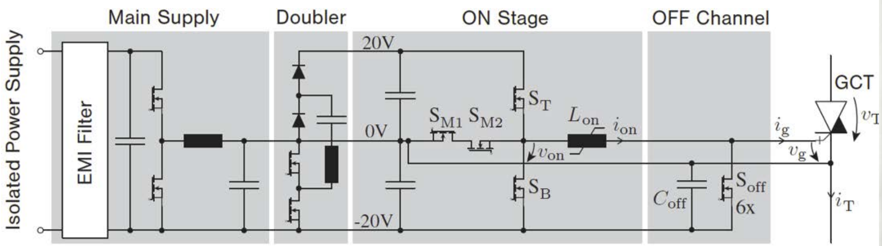

▲ Simplifed SOFTGATE circuitry

▲ Realized SOFTGATE gate unit [39]

[39] Jakub Kucka and Drazen Dujic. "SOFTGATE – An IGCT Gate Unit for Soft Switching." *PCIM Europe 2022; International Exhibition and Conference for Power Electronics, Intelligent Motion, Renewable Energy and Energy Management*. 2022, pp. 1–9

OFF Channel

- Optimized for frequent low-current switching
- Utilizing compact polymer tantalum capacitors and low profile MOSFETs
- Tested up to 1.5 kA emergency turn off

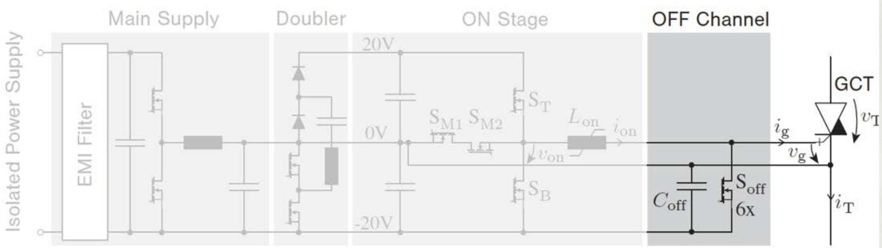

▲ SOFTGATE OFF channel

▲ Realized SOFTGATE gate unit

GATE UNIT DESIGN (IV)

ON Channel

- T-Type NPC topology with nonlinear inductor
- Capable of controlling the gate current by three voltage levels
- Nonlinear inductor enables fast current build-up for turn on and retrigger current pulses

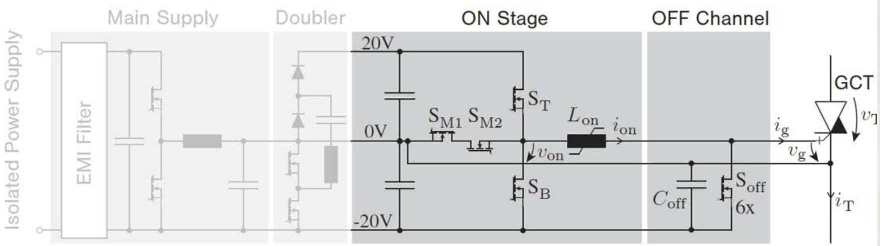

▲ SOFTGATE ON channel

▲ Realized SOFTGATE gate unit

GATE UNIT DESIGN (IV)

ON Channel

- T-Type NPC topology with nonlinear inductor
- Capable of controlling the gate current by three voltage levels
- Nonlinear inductor enables fast current build-up for turn on and retrigger current pulses

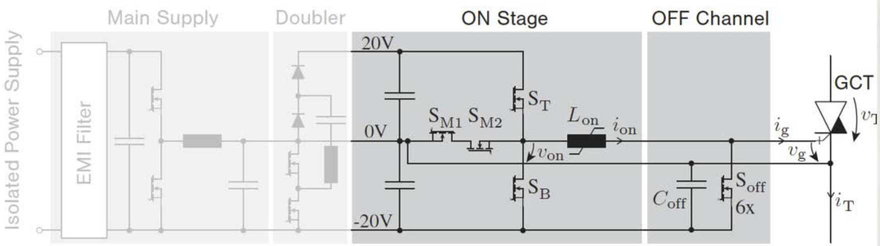

▲ SOFTGATE ON channel

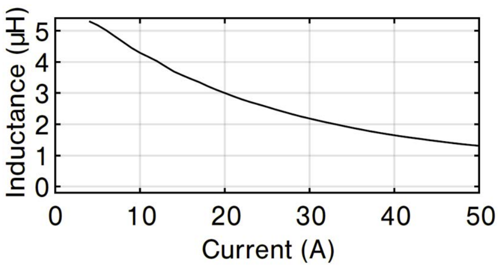

▲ Characteristic of inductor used for the ON channel

▲ Realized SOFTGATE gate unit

SIZE COMPARISON

⇒ The gate unit size can be greatly optimized and reduced for soft-switching applications!

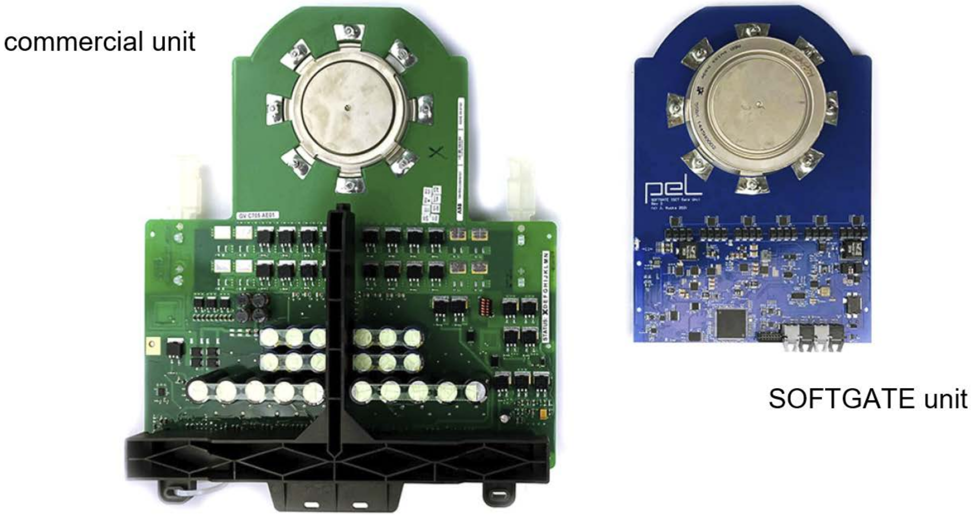

▲ Comparison between commercial and SOFTAGE gate unit [40]

[40] Jakub Kucka and Drazen Dujic. "IGCT Gate Unit for Zero-Voltage-Switching Resonant DC Transformer Applications." *IEEE Transactions on Industrial Electronics* 69.12 (2022), pp. 13799–13807

1.44kHz Resonant Operation

- Full load operation
- 2.5 kV dc link
- 140 A turn off current
- 750 A peak current

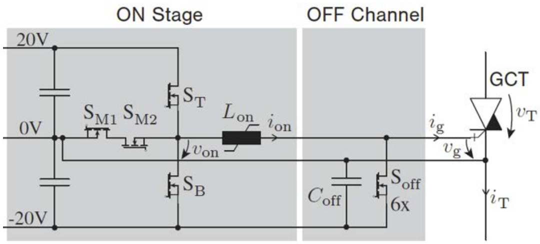

▲ Simplifed SOFTGATE circuitry

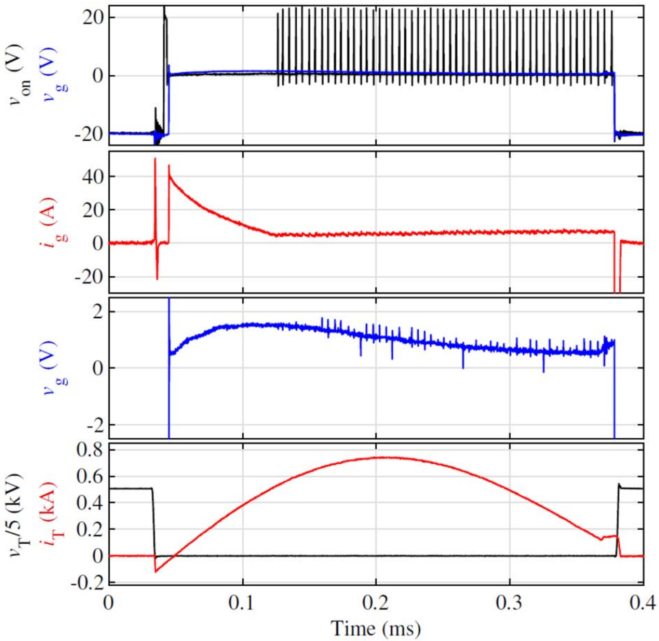

▲ SOFTGATE full load operation

1.44kHz Resonant Operation

- No load operation
- 2.5 kV dc link
- 140 A turn off current

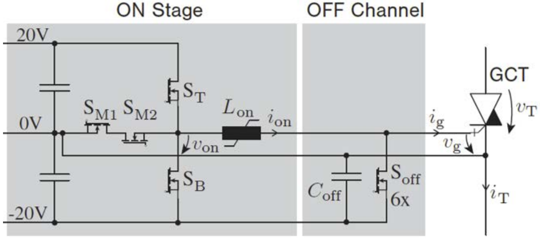

▲ Simplifed SOFTGATE circuitry

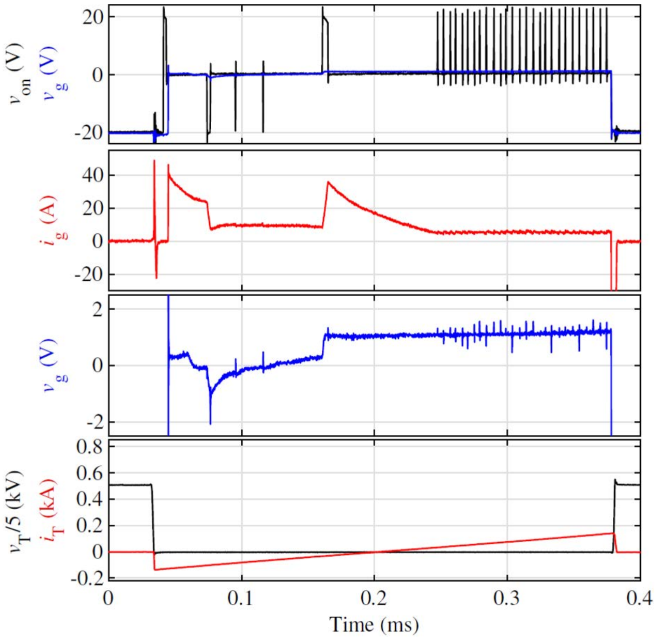

▲ SOFTGATE no load operation

Turn Off Detail

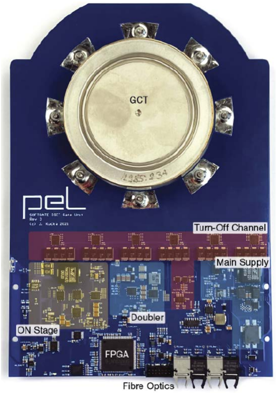

▲ SOFTGATE gate unit

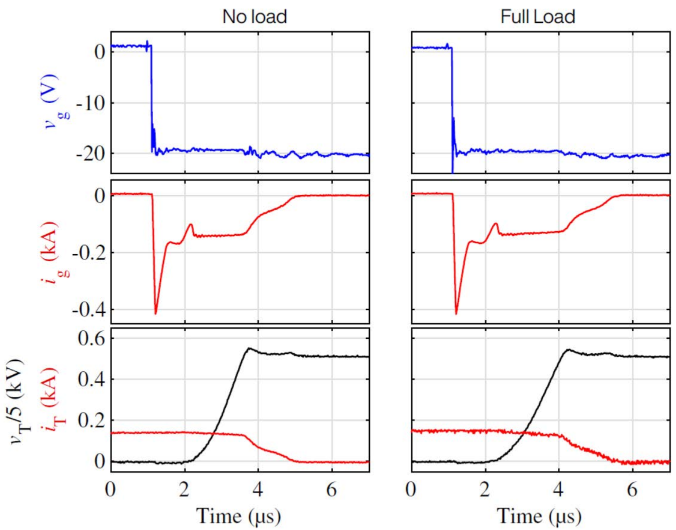

▲ SOFTGATE turn OFF behaviour

High-Current Emergency Turn Off

- 2 kV
- 1.5 kA
- Estimated gate unit turn off inductance: 1.2 nH

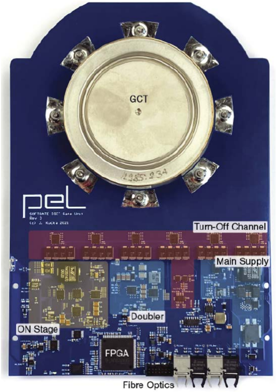

▲ SOFTGATE gate unit

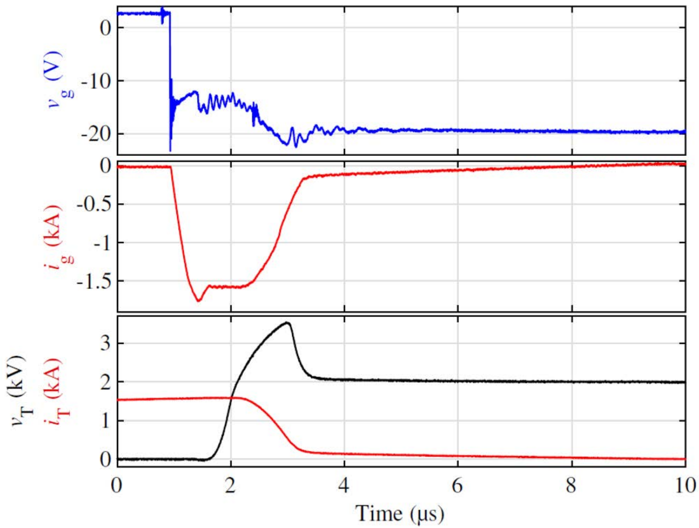

▲ SOFTGATE high current turn OFF

EXPERIMENTAL RESULTS (V)

5kHz Resonant Operation

- 2.5 kV dc link
- 16 A turn off current
- 320 A peak current

Retrigger function had to be disabled!

▲ SOFTGATE gate unit

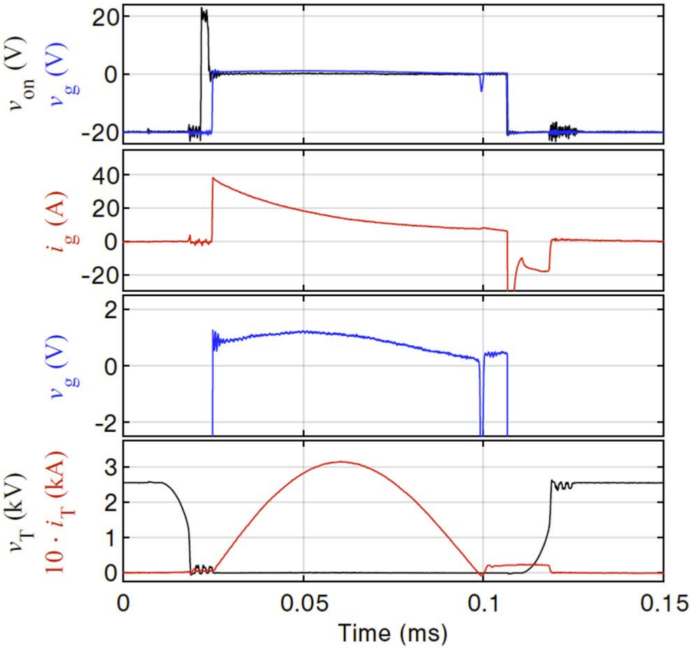

▲ SOFTGATE continuous operation

Consumption

- Only 40 W (compared to commercial 58 W)

Thermal run

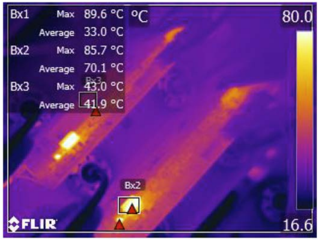

▲ Temperatures in steady state

Turn OFF details

- Long turn off due to low switching current
- Slow voltage build up

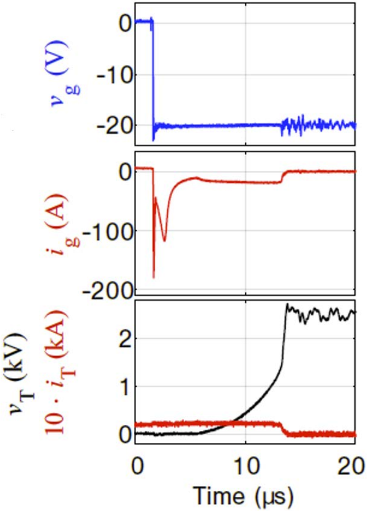

▲ Turn OFF event

Shoot-Through Protection

- Since the application does not require clamping circuit a shoot-through might be fatal
- Idea: measure anode-to-cathode voltage to ensure that the diode is conducting before the turn ON [41]

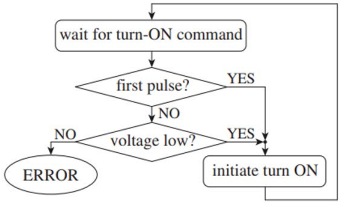

▲ Protection integrated into SOFTGATE

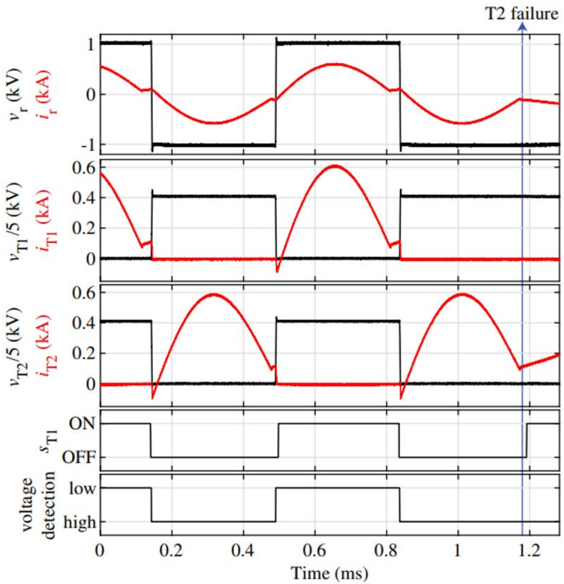

▲ Experimental results

[41] Jakub Kucka and Drazen Dujic. "Shoot-Through Protection for an IGCT-Based ZVS Resonant DC Transformer." *IEEE Transactions on Industrial Electronics* (2022), pp. 1–1

By tailoring the gate unit for soft-switching:

- The size can be minimized
- The consumption ca be reduced
- 5 kHz resonant operation is feasible with IGCTs...
- ...but a special attention should be paid to details
- IGCT is a preferable switch for a resonant medium-voltage dc transformer

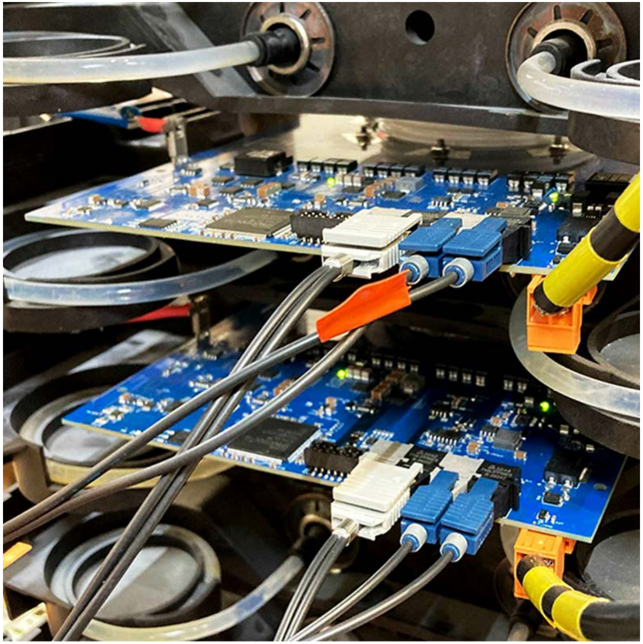

▲ SOFTGATE units inside the IGCT stack

IGCT RESONANT SWITCHING

Increasing switching frequency through resonant topology

SRC-LLC TOPOLOGY AND SUBRESONANT OPERATION (I)

SRC-LLC in subresonant operation

- Often termed as Half-Cycle Discontinuous Mode - HC-DCM

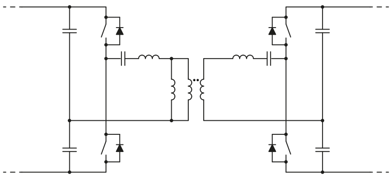

▲ Half bridge SRC-LLC

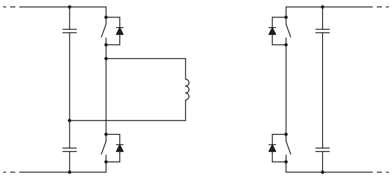

▲ Magnetising circuit component

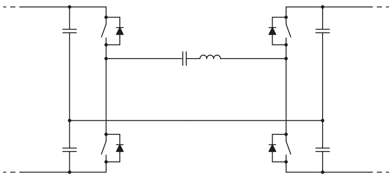

▲ Resonant circuit component

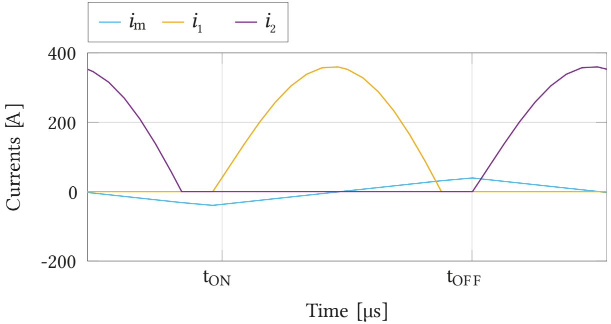

▲ SRC-LLC Subresonant waveforms

Two resonant frequencies adjusted through design:

- $f_r = 1/2\pi\sqrt{C_r L_r}$
- $f_{r2} = 1/2\pi\sqrt{C_r(L_r + L_m)}$

Switching frequency

- f_s - motivated to be high due to MFT

SRC-LLC subresonant operation

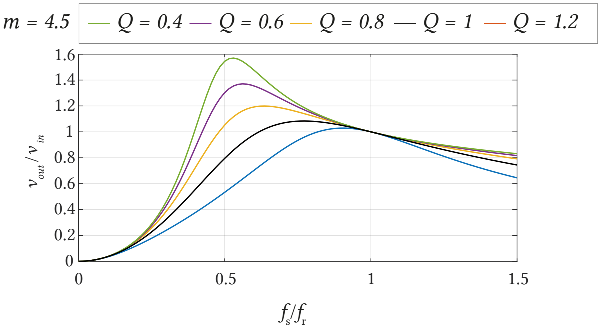

▲ LLC transfer characteristic

Voltage gain transfer function

$$\frac{nV_{out}}{V_{in}} = \frac{mf_n^2}{\sqrt{(f_n^2(m+1)-1)^2 + (f_n mQ(f_n^2-1))^2}}$$

Normalized frequency

- $f_n = f_s/f_r$

Inductance ratio

- $m = L_m/L_r$

Quality factor

- $Q = \frac{\sqrt{L_r/C_r}}{n^2 R_{load}}$

SRC-LLC TOPOLOGY AND SUBRESONANT OPERATION (II)

SRC-LLC subresonant operation

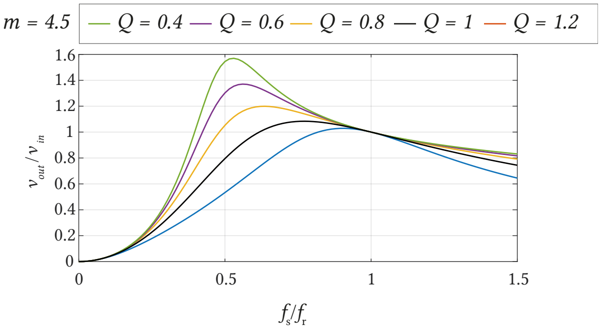

▲ LLC transfer characteristic

Voltage gain transfer function

$$\frac{nV_{out}}{V_{in}} = \frac{mf_n^2}{\sqrt{(f_n^2(m+1)-1)^2 + (f_n mQ(f_n^2-1))^2}}$$

Normalized frequency

- $f_n = f_s/f_r$

Inductance ratio

- $m = L_m/L_r$

Quality factor

- $Q = \frac{\sqrt{L_r/C_r}}{n^2 R_{load}}$

$\Rightarrow$ **No external setpoint**

Transfer characteristic ensures power flow

Principles:

- Switching losses proportional to $V \times I$ at time of switching
- Loss reduction achievable through reduction of V or I
- For ZCS, $I = 0$ at switching instant
- Forward recovery issues [42]

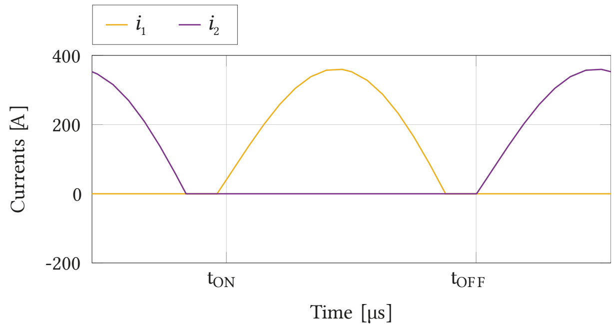

▲ Current magnitude at time of turn off is zero.

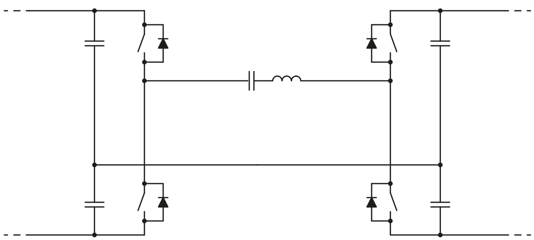

▲ Resonant tank resulting in ZCS switching conditions

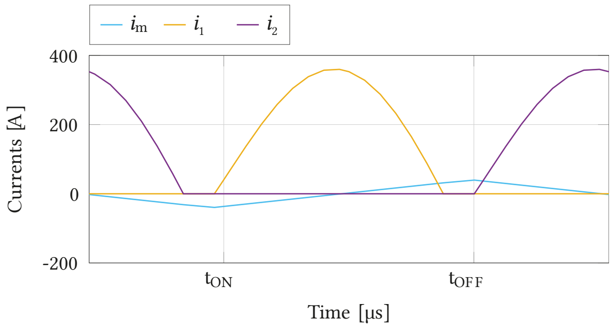

▲ SRC-LLC Subresonant waveforms displaying ZVS operation

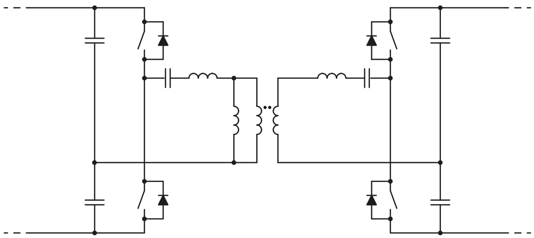

▲ Half bridge SRC-LLC magnetising inductance sustains current in tank until turn-on

Principles:

- Similar principle to ZCS, but loss minimisation through $V = 0$
- Achieved by conduction of antiparalled diode of device to be turned *ON*
- Can be affected by load level in SRC-LLC topology

EXPERIMENTAL IGCT TEST SETUP (II)

PEL IGCT multifunctional test setup:

- Based on 3L-NPC leg
- Characterization of IGCT during low current turn-off
- Characterization of series connected IGCTs during low current turn-off
- Single pulse tests
- Double pulse tests
- Resonant pulse tests
- Continuous operation with power circulation
- DC link voltage of 2.5 kV-5 kV
- Adjustable resonant frequency

▲ Flexible and reconfigurable IGCT test setup [43]

[43] Dragan Stamenkovic. "IGCT Based Solid State Resonant Conversion." PhD thesis. EPFL, 2020

EXPERIMENTAL IGCT TEST SETUP (II)


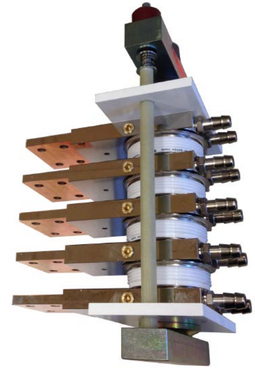


▲ (left) ABB ACS1000 water cooled 3L-NPC IGCT stack (DUT); (middle) Custom-built diodes stack; (right) De-ionised water cooling unit



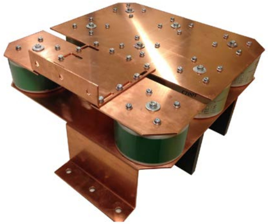

▲ (left) Custom made amorphous alloy core magnetizing inductor; (middle) Configurable array of eight air core resonant inductors; (right) Reconfigurable resonant capacitor bank

Problems to address:

- Minimise total switching energy
- Allow increase of switching frequency
- Ensure safe transitions (dead-time)

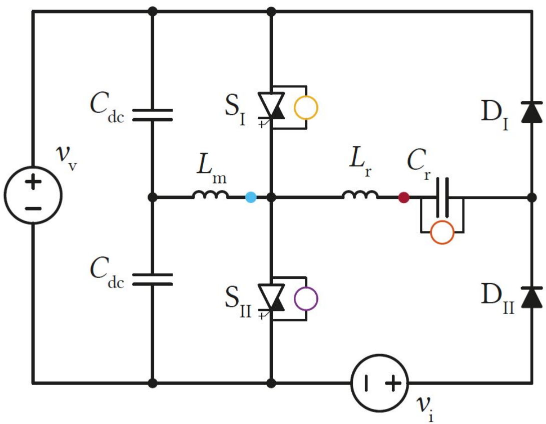

▲ Test setup configuration

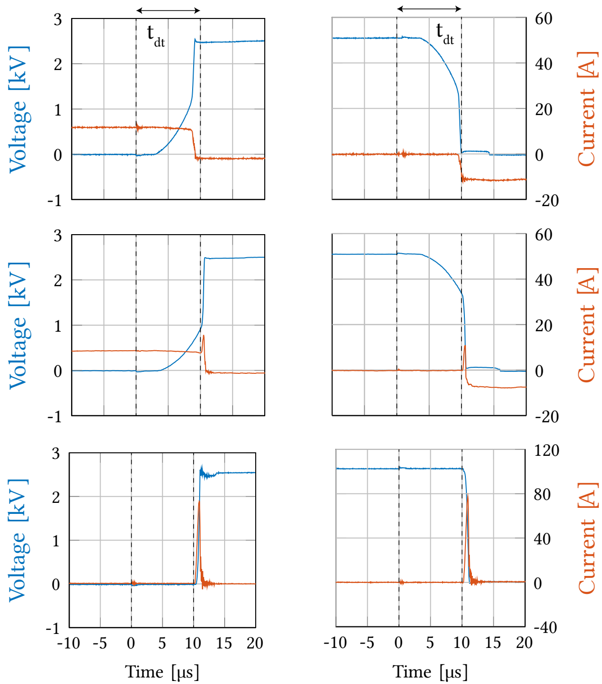

▲ IGCT turn-off and turn-on under (top) ZVS, (middle) non-ZVS, and (bottom) zero-current conditions. The turn-off current values are 17 A, 9 A, and 0 A, respectively. With loss of ZVS partial shoot-though takes place due to incomplete n-base sweep-out.

MINIMISATION OF SWITCHING ENERGY THROUGH ZVS/ZCS (II)

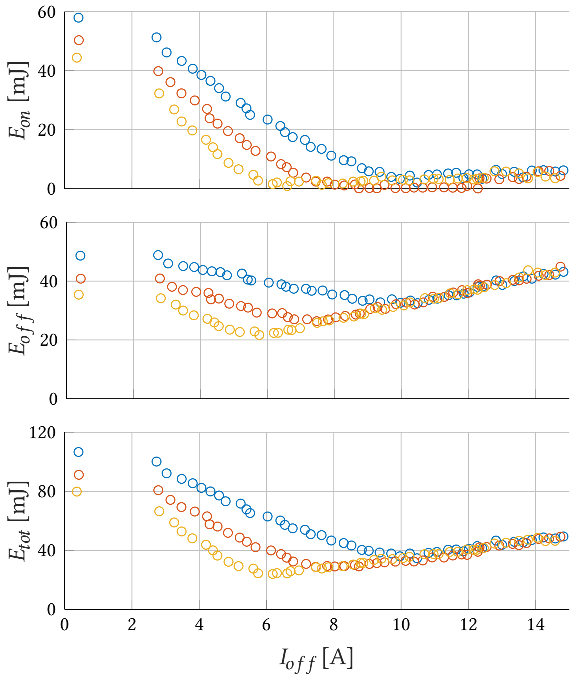

▲ Parametric sweep with different dead-times of o 10 µs, o 12 µs, and o 14 µs, respectively. [44]

Variables:

- Dead-time - from 10 µs to 14 µs
- Turn-off current - from 3 A to 15 A

Temperature has visible effect:

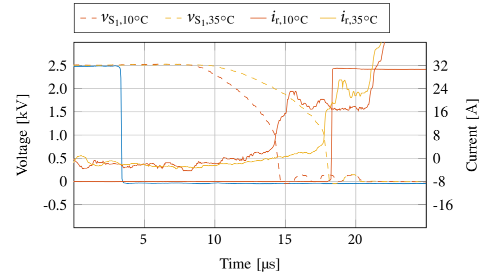

▲ T_j affects and prolongs switching transitions.

[44] Gabriele Ulissi et al. “Resonant IGCT Soft-Switching: Zero-Voltage Switching or Zero-Current Switching?” *IEEE Transactions on Power Electronics* 37.9 (2022), pp. 10775–10783

MINIMISATION OF SWITCHING ENERGY THROUGH ZVS/ZCS (II)

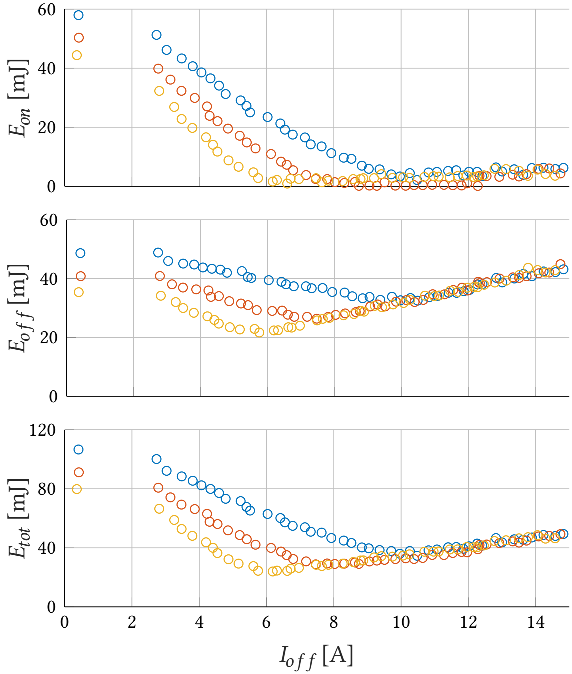

▲ Parametric sweep with different dead-times of o 10 µs, o 12 µs, and o 14 µs, respectively. [44]

Variables:

- Dead-time - from 10 µs to 14 µs
- Turn-off current - from 3 A to 15 A

Temperature has visible effect:

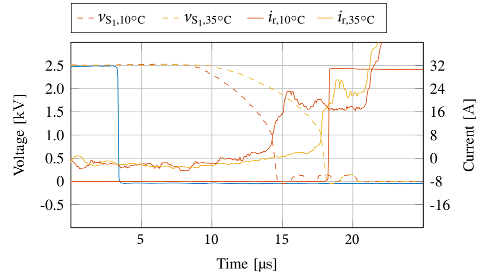

▲ T_j affects and prolongs switching transitions.

⇒ **Minimum loss**

It is achieved at limit of ZVS conditions!

[44] Gabriele Ulissi et al. "Resonant IGCT Soft-Switching: Zero-Voltage Switching or Zero-Current Switching?" *IEEE Transactions on Power Electronics* 37.9 (2022), pp. 10775–10783

MINIMISATION OF SWITCHING ENERGY THROUGH ZVS/ZCS (III)

3 GCTs devices are tested:

- Standard (5SHX 1445H0001)
- +55% irradiated
- +95% irradiated

Enginering samples are irradiated by HITACHI ENERGY Semiconductors

▲ Commercial gate unit is used during testing

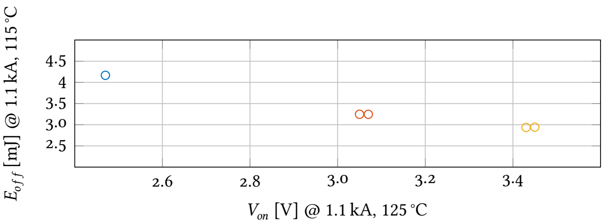

▲ Turn-off energy as a function of on-state voltage under hard switched conditions: o Standard, o +55 % irradiated, and o +95 % irradiated device performance.

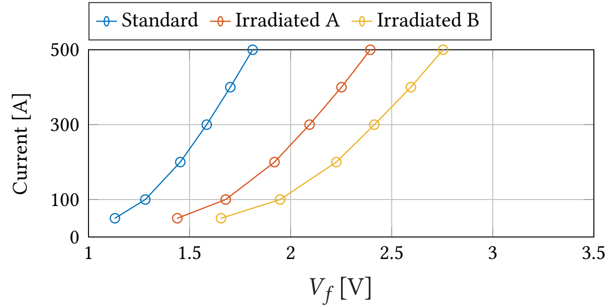

▲ GCT forward voltage

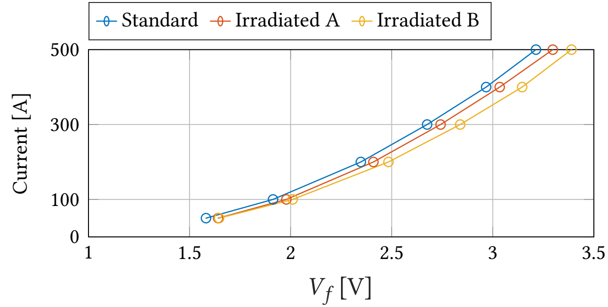

▲ Diode forward voltage

MINIMISATION OF SWITCHING ENERGY THROUGH ZVS/ZCS (IV)

Current pre-flooding:

- How much current resonant peak affects turn OFF event?
- Similar studies have been done for IGBT [45], [46]

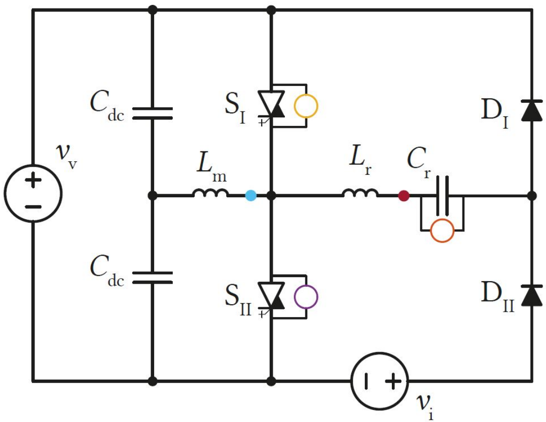

▲ Test setup to evaluate pre-flooding effect

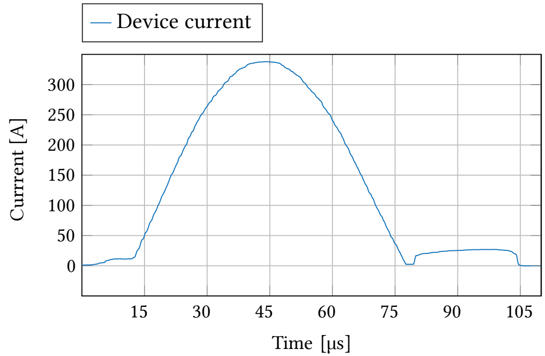

▲ Resonant current pulse

[45] Drazen Dujic et al. "Characterization of 6.5 kV IGBTs for High-Power Medium-Frequency Soft-Switched Applications." *IEEE Transactions on Power Electronics* 29.2 (2014), pp. 906–919

MINIMISATION OF SWITCHING ENERGY THROUGH ZVS/ZCS (V)

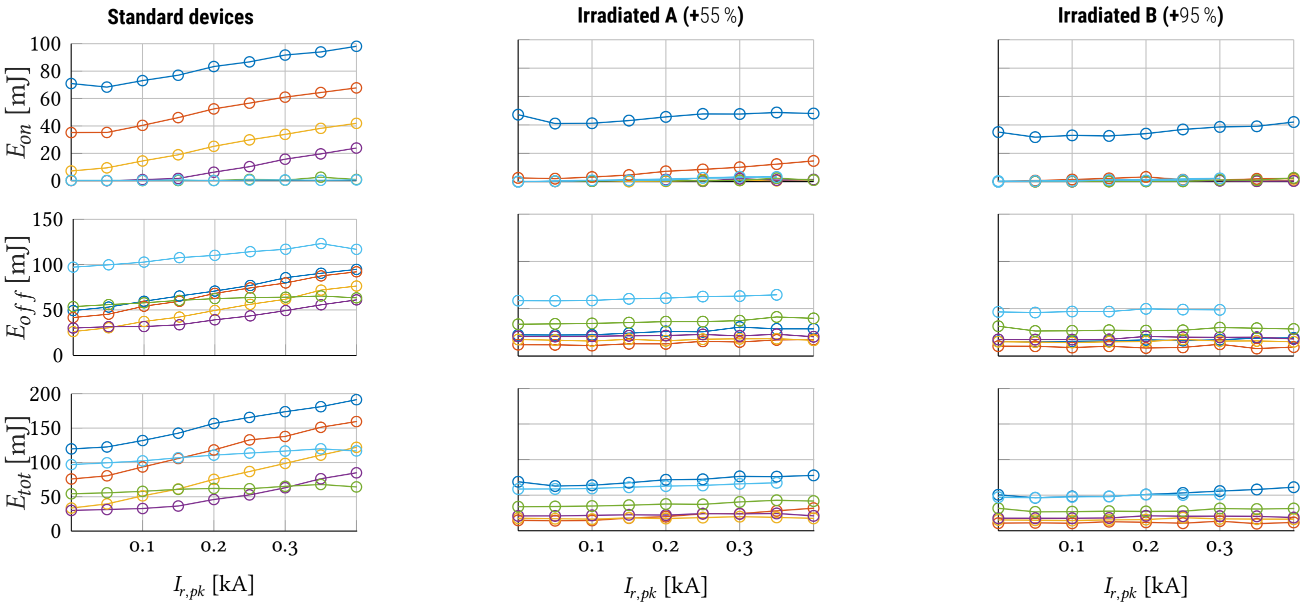

▲ Turn-ON, turn-OFF, and total switching energy for (left) standard commercial RC-IGCTs, (middle) Irradiated A, and (right) Irradiated B devices.

- I_{off} of o 0 A, o 3 A, o 6 A, o 9 A, o 17 A, and o 34 A
- Dead-time of 14 µs

MINIMISATION OF SWITCHING ENERGY THROUGH ZVS/ZCS (V)

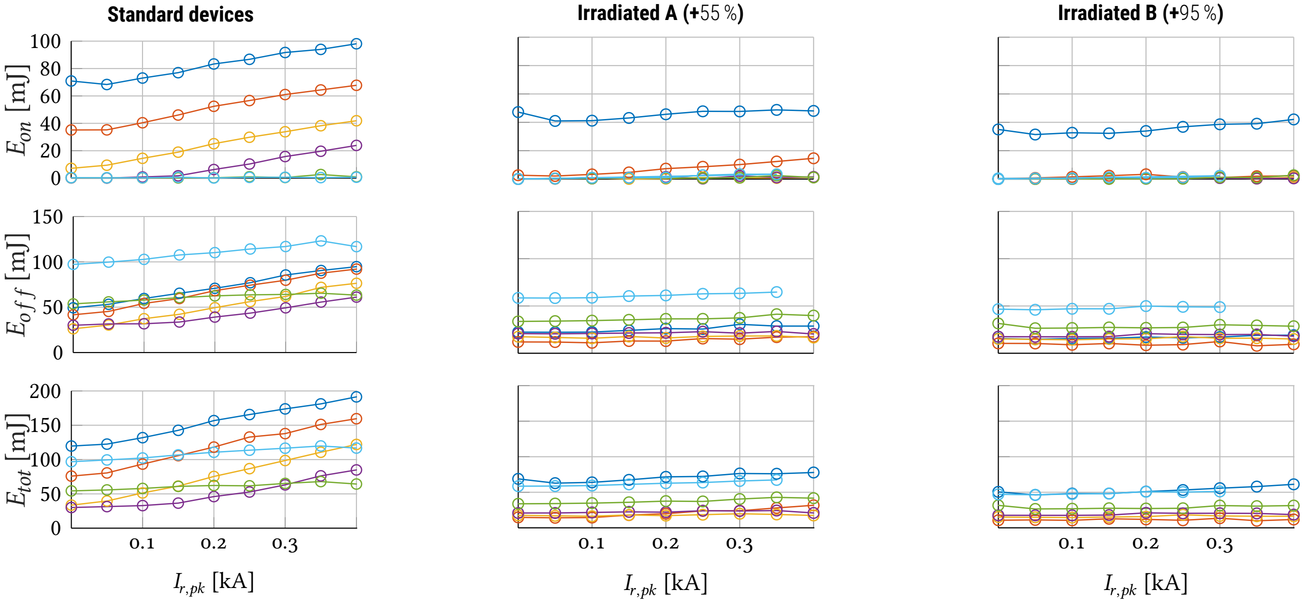

▲ Turn-ON, turn-OFF, and total switching energy for (left) standard commercial RC-IGCTs, (middle) Irradiated A, and (right) Irradiated B devices.

- I_{off} of o 0 A, o 3 A, o 6 A, o 9 A, o 17 A, and o 34 A
- Dead-time of 14 µs

⇒ Compounding benefits with increased irradiation levels!

HIGH FREQUENCY OPERATION (I)

Objective:

- Push IGCT to 5 kHz switching frequency
- Ensure safe operating conditions
- Estimate total losses

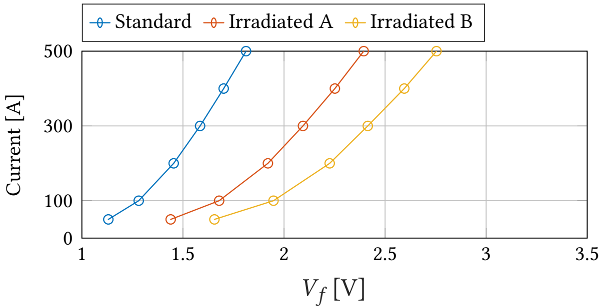

▲ GCT forward voltage

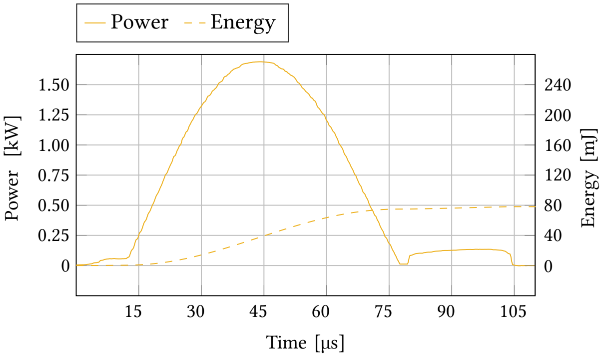

▲ Estimation of losses

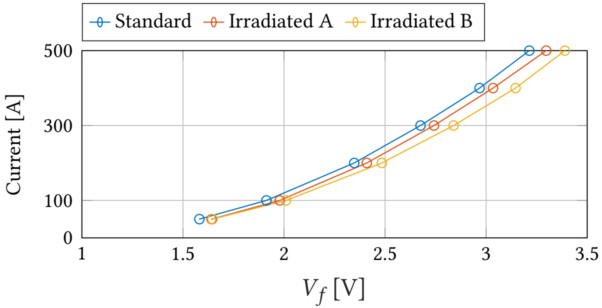

▲ Diode forward voltage

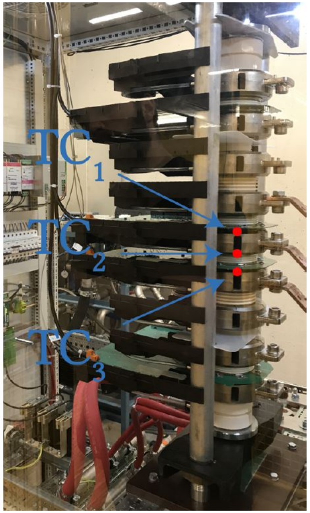

▲ De-ionised water cooling unit - limited temperature control.

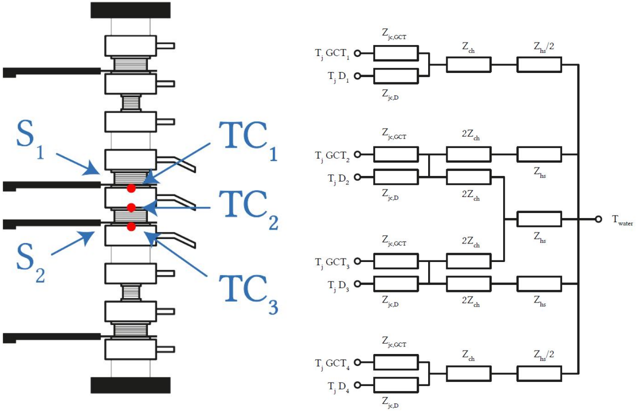

▲ System is modelled and case temperatures sensed for comparison.

Few limitations

- Heatsinks could not be preheated
- Limits of industrial cooling unit

HIGH FREQUENCY OPERATION (III)

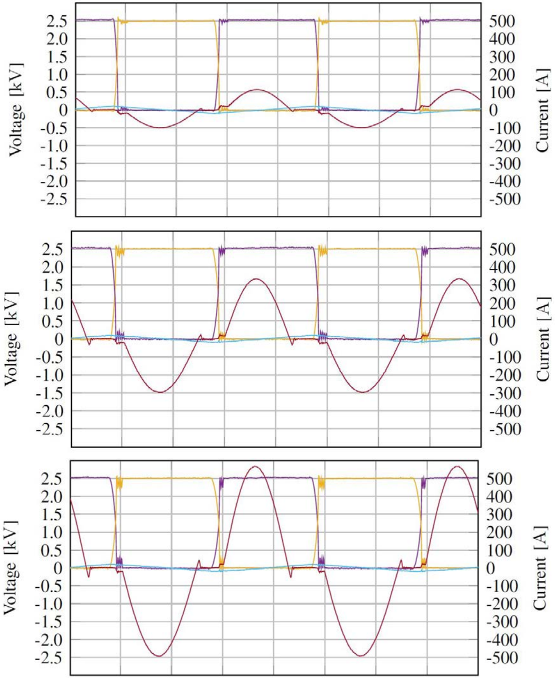

▲ Experimental results at 5 kHz switching and at varying load levels

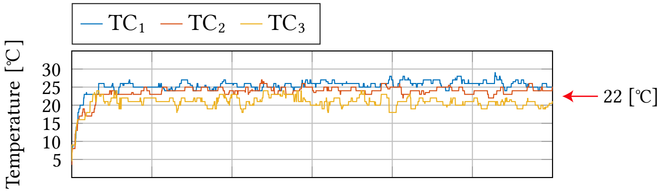

▲ Sensed case temperature for standard device

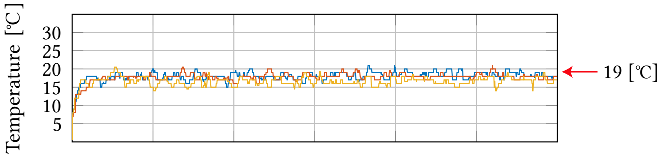

▲ Sensed case temperature for irradiated A device

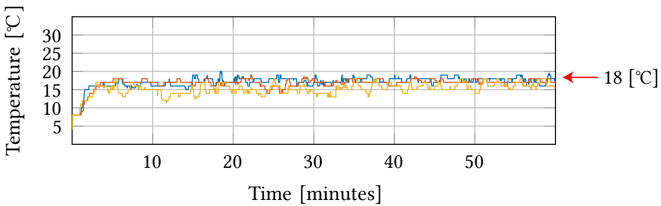

▲ Sensed case temperature for irradiated B device

HIGH FREQUENCY OPERATION (IV)

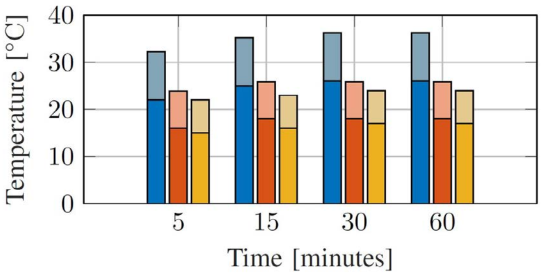

▲ Measured case temperatures and estimated junction temperatures

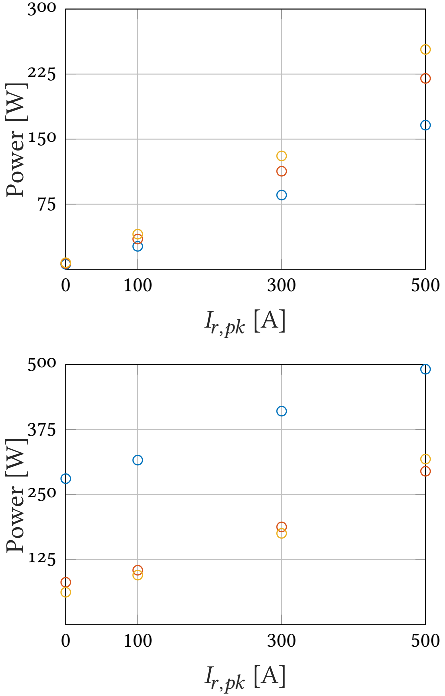

▲ Conduction (top) and total loss (bottom) for o standard, o +55 % irradiated, and o +95 % irradiated devices

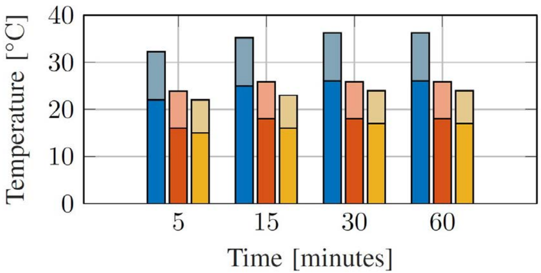

▲ Measured case temperatures and estimated junction temperatures

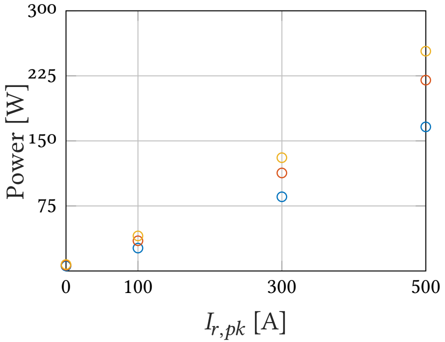

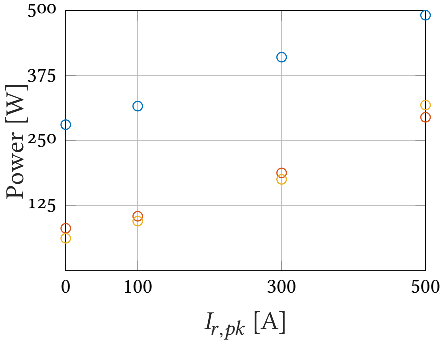

▲ Conduction (top) and total loss (bottom) for o standard, o +55 % irradiated, and o +95 % irradiated devices

⟹ **Optimal IGCT design**

It is possible to minimise total losses!

IGCT IN SERIES CONNECTION - HIGH FREQUENCY OPERATION (1)

Challenges

- Low I_{off}
- Static voltage sharing - not a big problem
- Dynamic voltage sharing
- Snubber capacitance design

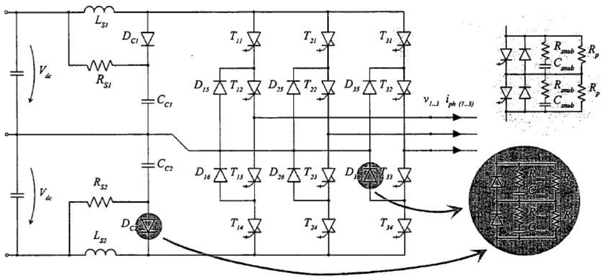

▲ IGCT-based NPC for 6 kV drive [47]

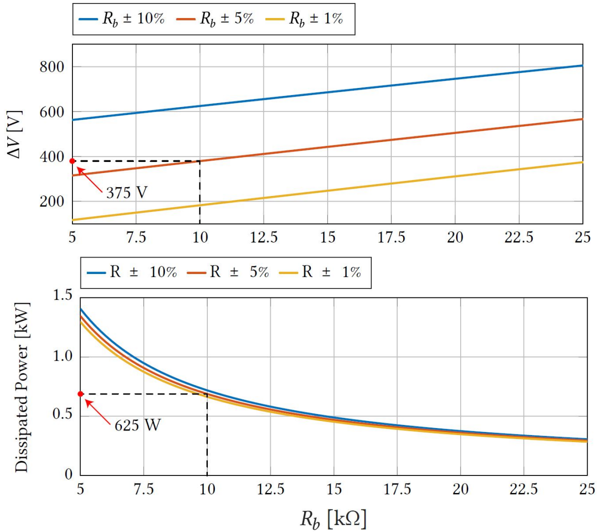

▲ Static balancing determined by max leakage current and accepted voltage difference [47]

IGCT IN SERIES CONNECTION - HIGH FREQUENCY OPERATION (II)

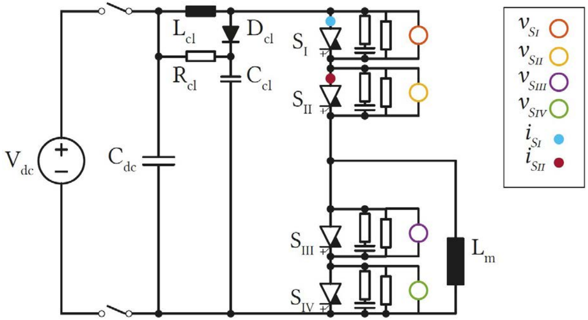

▲ Double Pulse test setup arrangement for series connected IGCT tests

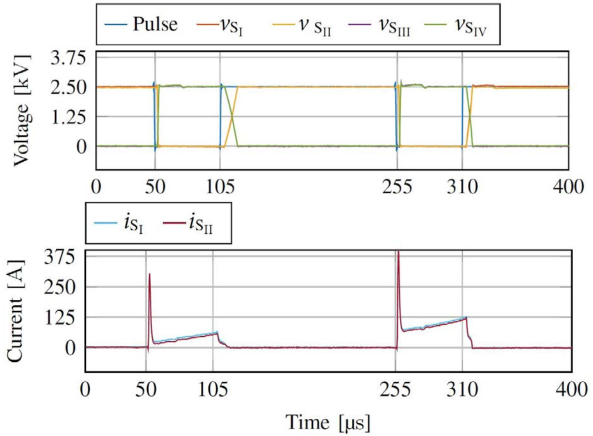

▲ Voltage (top) and current (bottom) waveforms during tests

Snubber capacitance values:

- 40 nF
- 70 nF
- 100 nF

Clamp circuit is in use

IGCT IN SERIES CONNECTION - HIGH FREQUENCY OPERATION (III)

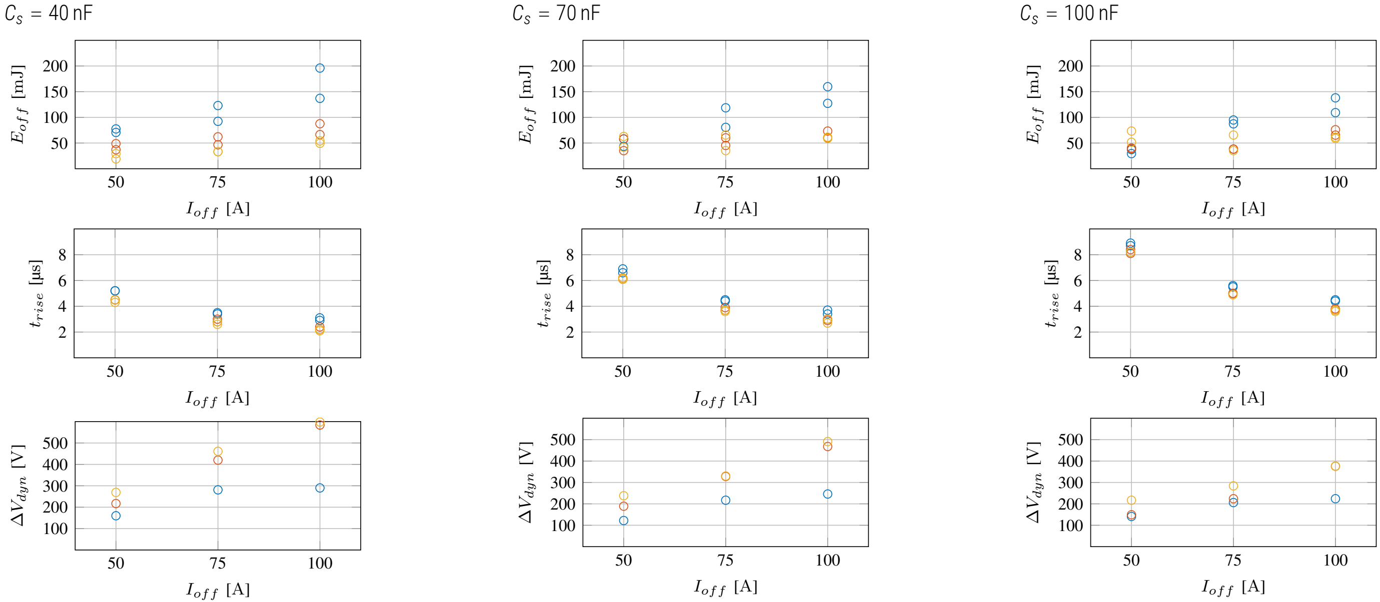

▲ Comparison of switching energy (top), voltage rise time (middle) and ΔV_{dyn} (bottom) during turn-off as a function of I_{off} and for indicated snubber capacitances. o Standard, o +55 % irradiated, and o +95 % irradiated devices.

Operation at 5 kHz demonstrated:

- With standard devices
- With *C* snubbers only [33]

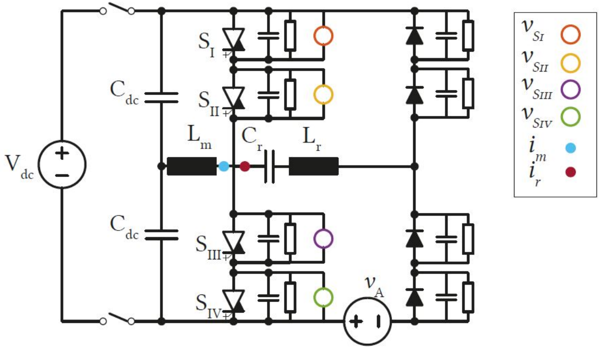

▲ Test setup arrangement for series connected IGCT resonant operation tests

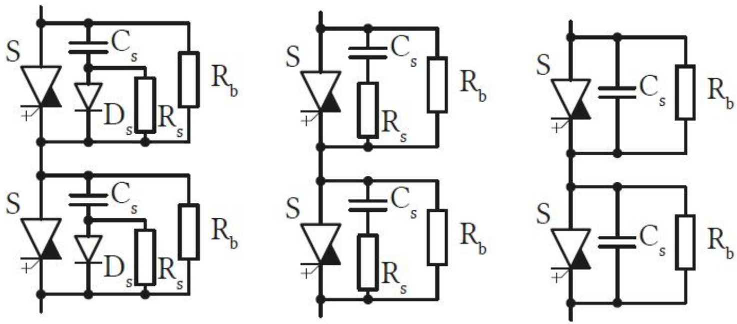

▲ Typical snubber configurations - Only capacitive snubber is used for resonant switching

[33] Gabriele Ulissi et al. "High-Frequency Operation of Series-Connected IGCTs for Resonant Converters." *IEEE Transactions on Power Electronics* 37.5 (2022), pp. 5664–5674

IGCT IN SERIES CONNECTION - HIGH FREQUENCY OPERATION (V)

Operation at 5 kHz demonstrated:

- With standard devices
- With *C* snubbers only [33]

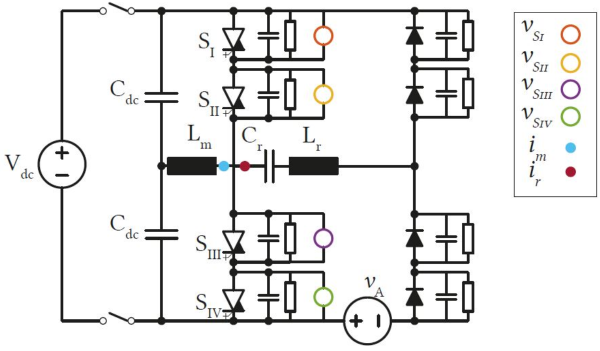

▲ Test setup arrangement for series connected IGCT resonant operation tests

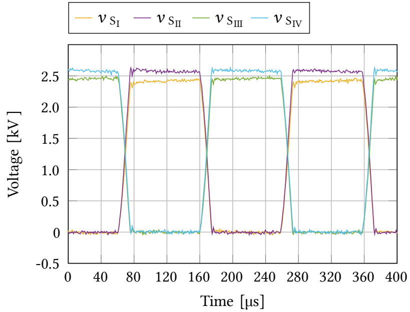

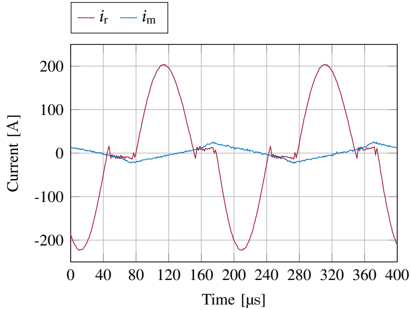

▲ IGCT voltage (top) and resonant current (bottom) during 5 kHz RC-IGCT series-connected resonant operation employing a 17 A turn-off current level and only 20 nF snubber capacitance. The peak dynamic voltage difference between series connected devices is maintained below the value of 500 V despite the ultra-low capacitance value (dead-time is 20 µs).

Ongoing work:

- 10 kV IGCT (engineering samples)
- NPC topology modulation

[33] Gabriele Ulissi et al. "High-Frequency Operation of Series-Connected IGCTs for Resonant Converters." *IEEE Transactions on Power Electronics* 37.5 (2022), pp. 5664–5674

LUNCH BREAK

Finally...

DESIGN OF MW MFTS

What are the design challenges?

PROBLEM DESCRIPTION

Multiphysical optimization problem:

1) Electrical domain:

- Skin and proximity effects due to the increase of the operating frequency
- Accurate electric parameter design

2) Magnetic domain:

- Non-sinusoidal excitation
- Core losses (hysteresis and eddy current losses)

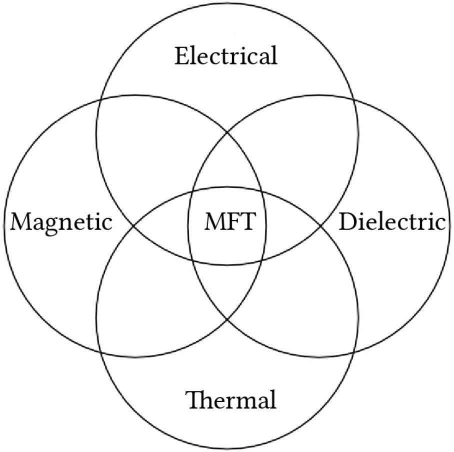

3) Dielectric domain:

- High dV/dt characteristic for the square voltage waveform resulting in over-voltages due to parasitic capacitances
- Insulation coordination

4) Thermal domain:

- Thermal coordination
- Increased hot-spot temperatures
- Thermal anisotropy

⇒ MFT design trade-offs: efficiency vs. power density vs. cost vs. manufacturability vs. ...

Effects:

- Non-uniform current density
- Under-utilization of the conductor material
- Localized H-field distortion within the conductor volume
- Impact on conduction losses
- Impact on leakage inductance

Example of the foil winding MFT geometry cross-section:

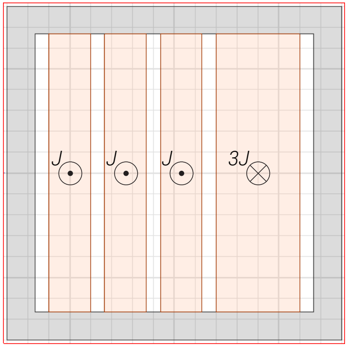

▲ Generic foil winding geometry.

0.1 [Hz] (Δ = 0.01)

*Δ - the penetration ratio

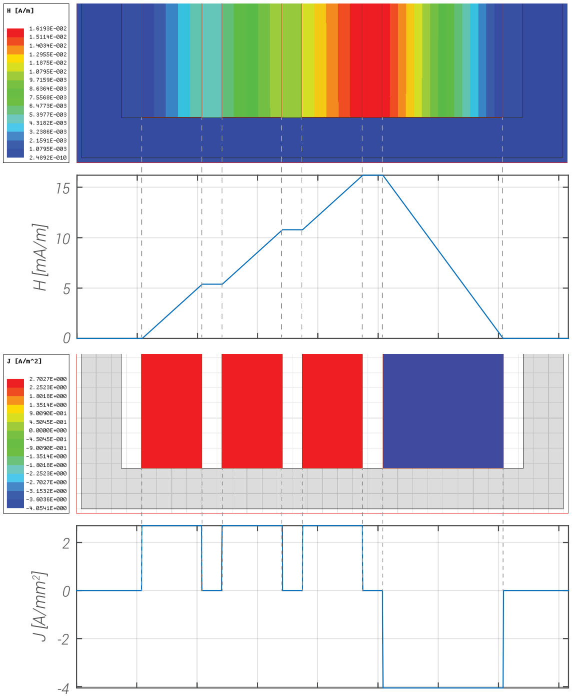

▲ H and J distribution within the core window area.

Effects:

- Non-uniform current density
- Under-utilization of the conductor material
- Localized H-field distortion within the conductor volume
- Impact on conduction losses
- Impact on leakage inductance

Example of the foil winding MFT geometry cross-section:

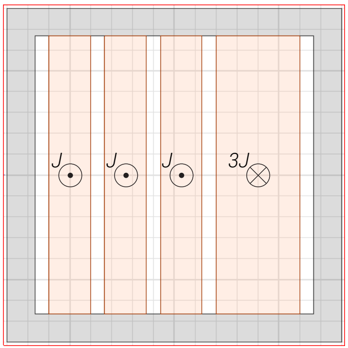

▲ Generic foil winding geometry.

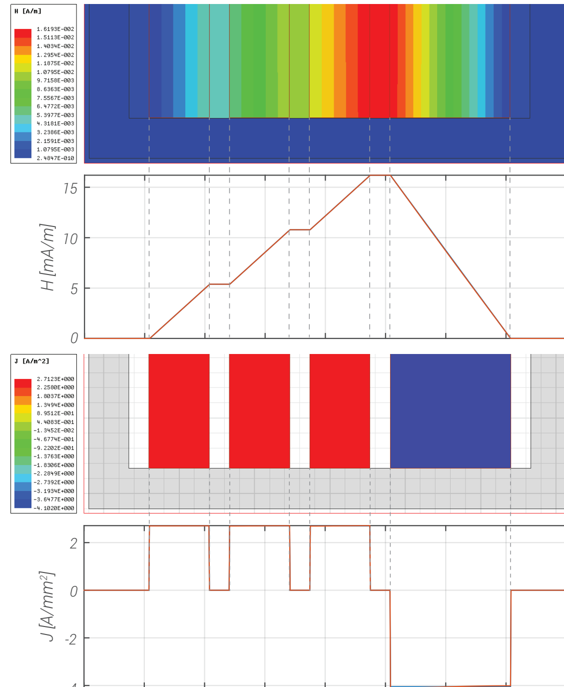

0.1 [Hz] (Δ = 0.01)
100 [Hz] (Δ = 0.3)

*Δ - the penetration ratio

▲ H and J distribution within the core window area.

SKIN AND PROXIMITY EFFECT

Effects:

- Non-uniform current density
- Under-utilization of the conductor material
- Localized H-field distortion within the conductor volume
- Impact on conduction losses
- Impact on leakage inductance

Example of the foil winding MFT geometry cross-section:

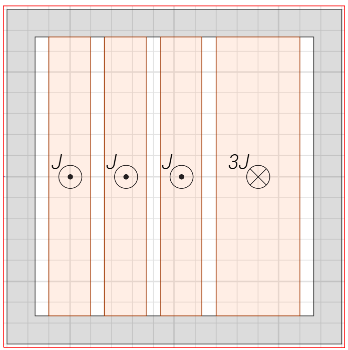

0.1 [Hz] (Δ = 0.01)
100 [Hz] (Δ = 0.3)
1000 [Hz] (Δ = 1)

*Δ - the penetration ratio

▲ Generic foil winding geometry.

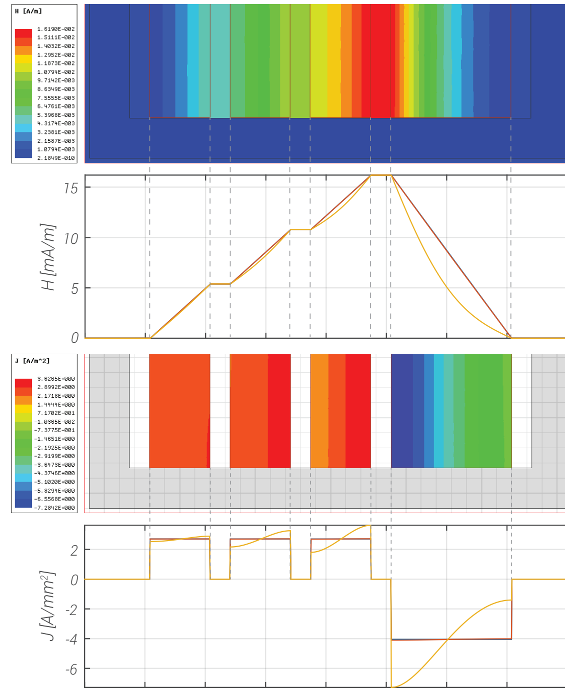

▲ H and J distribution within the core window area.

Effects:

- Non-uniform current density
- Under-utilization of the conductor material
- Localized H-field distortion within the conductor volume
- Impact on conduction losses
- Impact on leakage inductance

Example of the foil winding MFT geometry cross-section:

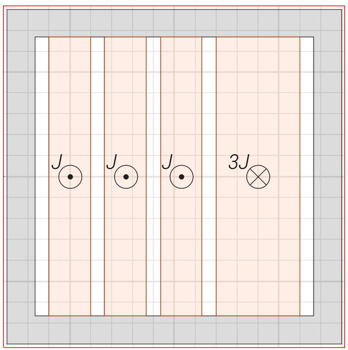

▲ Generic foil winding geometry.

0.1 [Hz] (Δ = 0.01)
100 [Hz] (Δ = 0.3)
1000 [Hz] (Δ = 1)
5000 [Hz] (Δ = 2.15)

*Δ - the penetration ratio

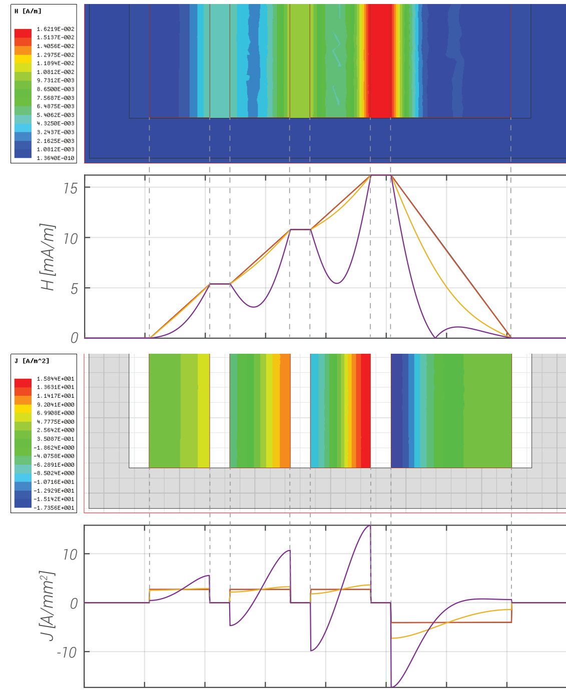

▲ H and J distribution within the core window area.

SKIN AND PROXIMITY EFFECT

Effects:

- Non-uniform current density
- Under-utilization of the conductor material
- Localized H-field distortion within the conductor volume
- Impact on conduction losses
- Impact on leakage inductance

Example of the foil winding MFT geometry cross-section:

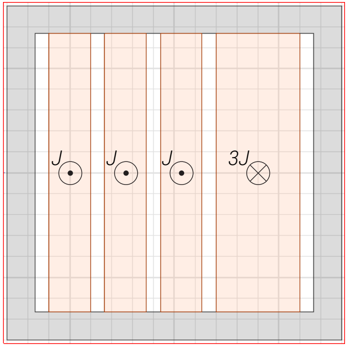

▲ Generic foil winding geometry.

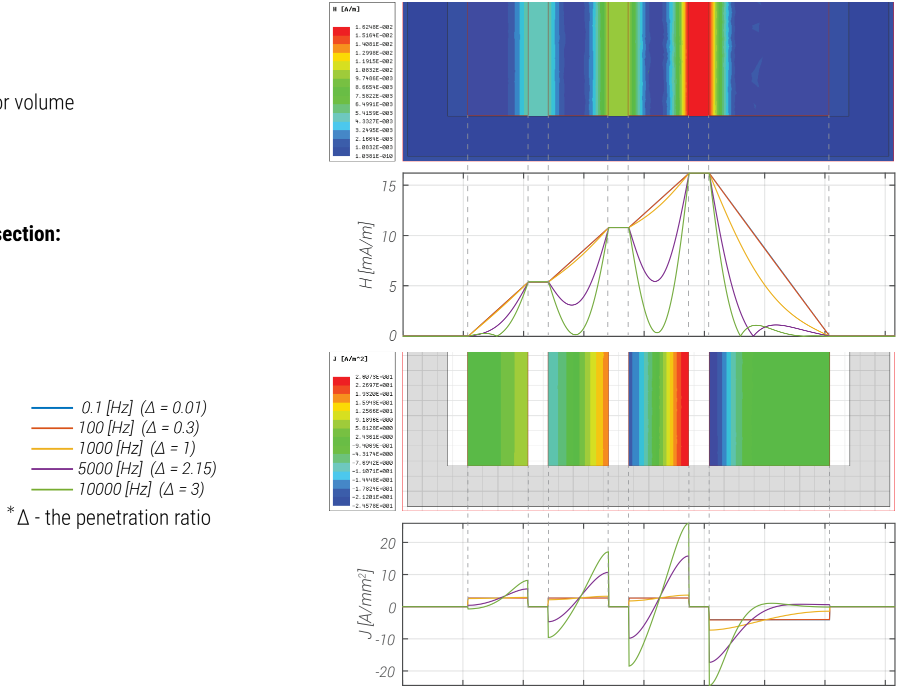

▲ H and J distribution within the core window area.

Effects:

- Non-uniform current density
- Under-utilization of the conductor material
- Localized H-field distortion within the conductor volume
- Impact on conduction losses
- Impact on leakage inductance

Example of the foil winding MFT geometry cross-section:

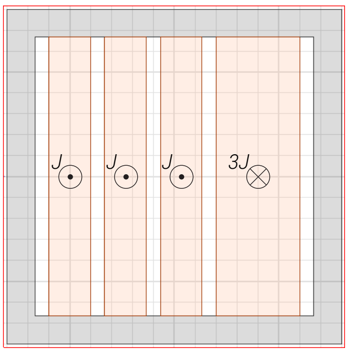

▲ Generic foil winding geometry.

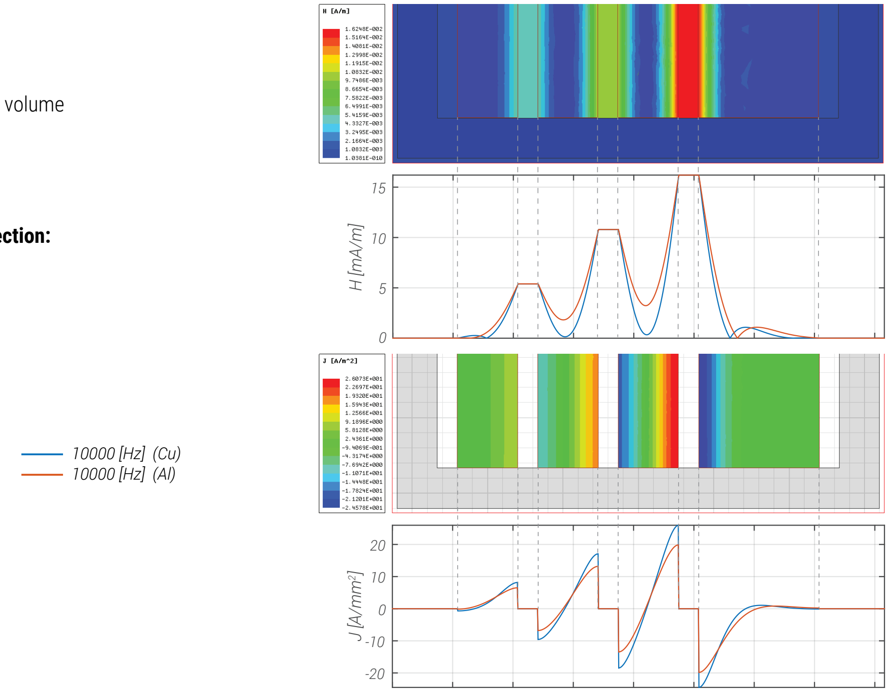

▲ H and J distribution within the core window area.

MFT geometry cross-section:

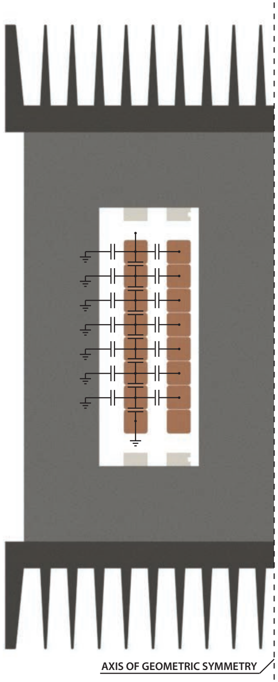

HF winding model:

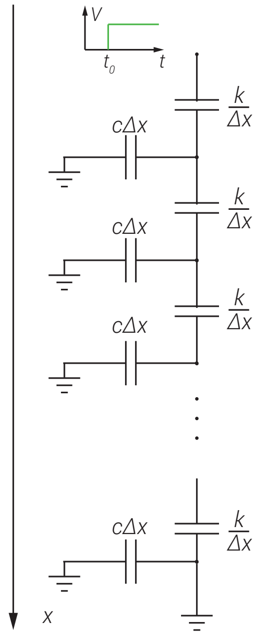

MFT electric parameters:

- Parasitic capacitance cannot be neglected for HF
- Capacitances exist between turns, windings and core
- For pulse excitation voltage distribution is nonlinear
- Higher voltage gradient at the winding input than expected
- Damped oscillatory transient due to turn inductance
- Higher max voltage than expected during transient
- Need for overall insulation reinforcement
- Turn to turn insulation must especially be increased

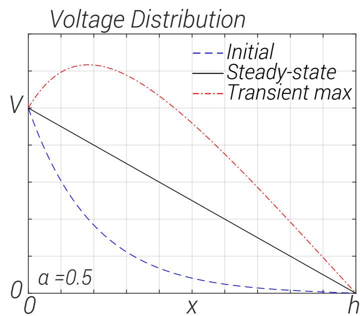

$$V(x) = V\frac{\sinh(ax)}{\sinh(ah)}$$

$$a = \sqrt{\frac{c}{k}}$$

▲ Insulation coordination problem becomes increasingly difficult with high voltages and frequencies.

MFT losses:

- Winding losses
- Core losses

Heat transfer mechanisms:

- Conduction

- Convection

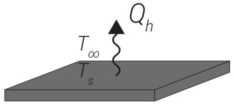

- Radiation

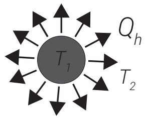

Qualitative analysis:

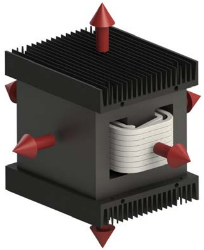

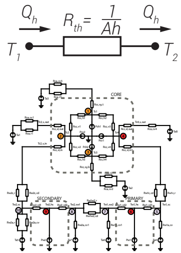

- Heat transfer

$$Q_h = hA\Delta T$$

- Temperature gradient

$$\Delta T = \frac{Q_h}{hA}$$

- Surface decrease ($A \searrow$) implies temperature increase ($\Delta T \nearrow$)

Temperature distribution example:

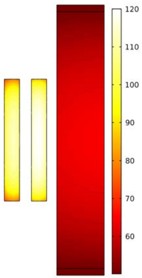

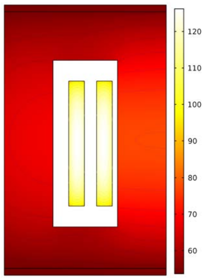

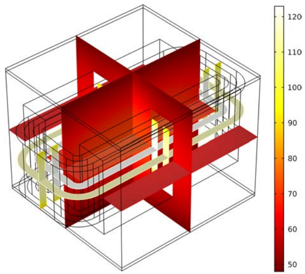

▲ All modes of heat transfer are present. Which one is dominant is the matter of design choices.

Core materials:

- Thermal conductivity varies from $4Wm/K$ (ferrites) to $8.35Wm/K$ (nanocrystalline)
- Isotropic thermal conductivity (e.g. ferrites)

▲ Ferrite core - isotropic.

- Anisotropic thermal conductivity (laminated cores e.g. nanocrystalline)

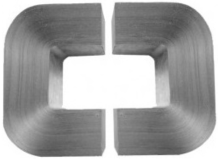

▲ Metglas core - anisotropic.

Windings:

- Copper and Aluminum conductors combined with insulation
- Low R_{th} along the conductor path due low R_{th} of Cu and Al
- High R_{th} in radial direction due to layers of insulation with high R_{th}

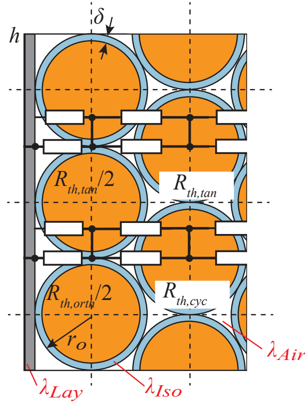

▲ Cross section of a round wire winding [48].

Winding insulation and cooling:

- Much higher insulation level requirement than within the winding insulation
- Good insulators have very low thermal conductivity (solid or fluid)
- Fluid based insulation provides much better cooling due to convection

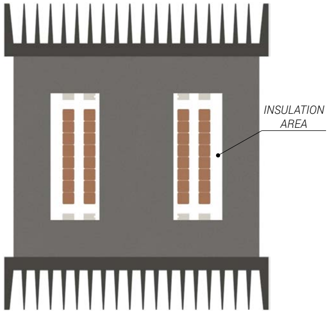

▲ MFT cross section area.

NON-SINUSOIDAL EXCITATION

Series resonant converter (SRC):

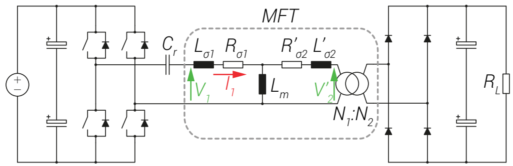

Characteristic SRC waveforms:

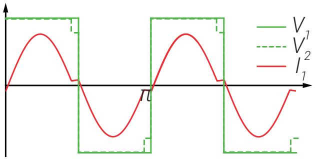

- $V_{1,2}$ square
- I sinusoidal

Core losses:

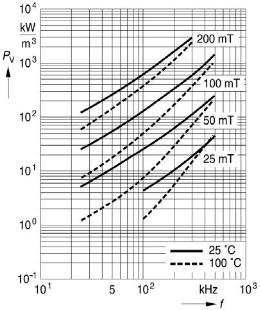

▲ AC core losses.

- Data-sheet data is for sinusoidal excitation
- Derived Steinmetz coefficients describe sinusoidal excitation losses
- Core is excited with square pulses
- Losses are effected
- Generalization of Steinmetz model

Winding losses:

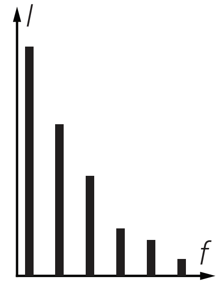

▲ Current harmonics.

- Current waveform impacts the winding losses
- Copper is a linear material
- Losses can be evaluated in harmonic basis
- Current harmonic content must be evaluated
- Total losses are the sum of the individual harmonic losses

ACCURATE ELECTRIC PARAMETER DESIGN

Series resonant converter (SRC):

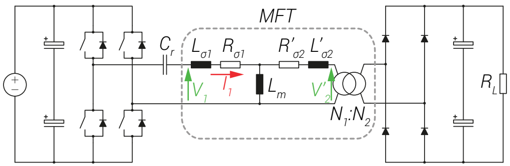

Characteristic SRC waveforms:

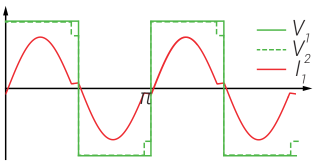

- $V_{1,2}$ square
- I sinusoidal

SRC:

- Leakage inductance is part of the resonant circuit
- It must match the reference:

$$L_{\sigma.ref} = \frac{1}{\omega_0^2 C_r}$$

- ω_0 is the target resonant frequency
- Magnetizing inductance L_m is normally high
- Reduced in the case of LLC converter
- Limits the magnetization current to the reference $I_{m.ref}$
- Limits the switch-off current and losses:

$$L_m = \frac{nV_{DC2}}{4f_s I_{m.ref}}$$

- $I_{m.ref}$ has to be sufficiently high to maintain ZVS

MFT DESIGN SPACE

What are the existing technologies and materials?

DESIGN SPACE EXPLORATION

Construction choices:

- Transformer types:

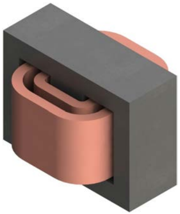

Shell type

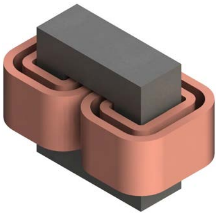

Core type

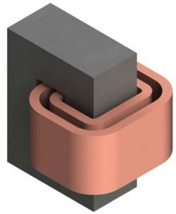

C-type

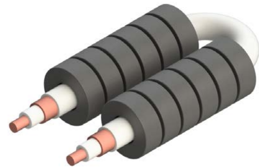

Coaxial type

- Conductor types:

Litz wire

Foil

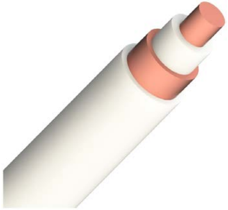

Coaxial

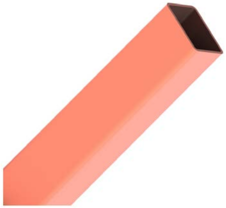

Hollow/Pipes

Materials:

- Core:
  - Silicon steel
  - Amorphous
  - Nanocrystalline
  - Ferrites
- Windings:
  - Copper
  - Aluminum

Technologies:

- Insulation:
  - Air
  - Solid
  - Oil
- Cooling:
  - Air natural/forced
  - Oil natural/forced
  - Deionized water

MAGNETIC MATERIALS - SILICON STEEL

Composition and applications:

- Ferromagnetic material
- Iron based alloy of Silicon provided as isolated laminations
- Mostly used for line frequency transformers

Advantages:

- Wide initial permeability range
- High saturation flux density
- High Curie-termpature
- Relatively low cost
- Mechanically robust
- Various core shapes available (easy to form)

Disadvantages:

- High hysteresis loss (irreversible magnetisation)
- High eddy current loss (high electric conductivity)
- Acoustic noise (magnetostriction)

Saturation B	Init. permeability	Core loss (10 kHz, 0.5T)	Conductivity
0.8 ~ 2.2 T	$0.6 \sim 100 \cdot 10^3$	50 ~ 250 W/kg	$2 \cdot 10^7 \sim 5 \cdot 10^7$ S/m

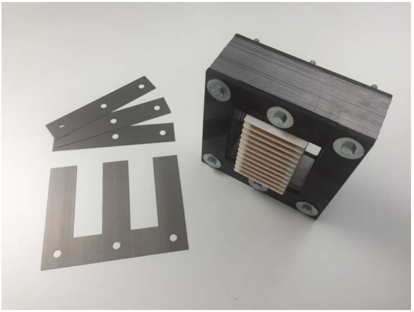

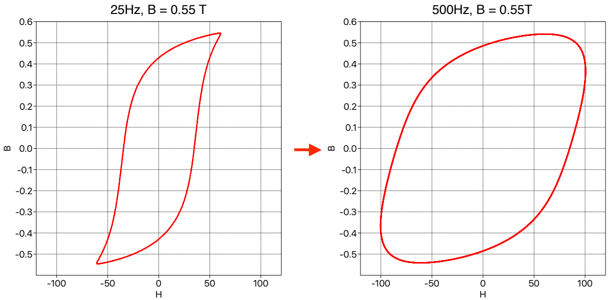

▲ Example: Measured B-H curve of M330-35 laminate.

Composition and applications:

- Ferromagnetic material
- Iron based alloy of Silicon as thin tape without crystal structure
- For both line frequency and switching frequency applications

Advantages:

- High saturation flux density
- Low hysteresis loss
- Low eddy current loss (low electric conductivity)
- High Curie-temperature
- Mechanically robust

Disadvantages:

- Relatively narrow initial permeability range
- Very high acoustic noise (magnetostriction)
- Limited core shapes available (difficult to form)
- Relatively expensive

Saturation B	Init. permeability	Core loss (10kHz, 0.5T)	Conductivity
0.5 ~ 1.6 T	$0.8 \cdot 10^3 \sim 50 \cdot 10^3$	2 ~ 20 W/kg	$< 5 \cdot 10^3$ S/m

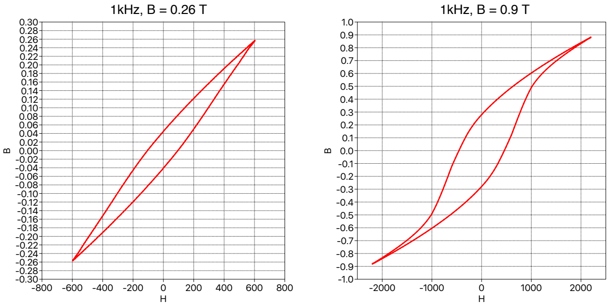

▲ Example: Measured B-H curve of Metglas 2605SA.

MAGNETIC MATERIALS - NANOCRYSTALLINE ALLOY

Composition and applications:

- Ferromagnetic material
- Iron based alloy of silicon as thin tape with minor portion of crystal structure
- For both line frequency and switching frequency applications

Advantages:

- Relatively narrow initial permeability range
- High saturation flux density
- Low hysteresis loss
- High Curie-temperature
- Low acoustic noise

Disadvantages:

- Eddy current loss (compensated thanks to the thin tape)
- Mechanically fragile
- Limited core shapes available (difficult to form)
- Relatively expensive

Saturation B	Init. permeability	Core loss (10kHz, 0.5T)	Conductivity
1 ~ 1.2 T	$0.5 \cdot 10^3 \sim 100 \cdot 10^3$	< 50 W/kg	$3 \cdot 10^3 \sim 5 \cdot 10^4$ S/m

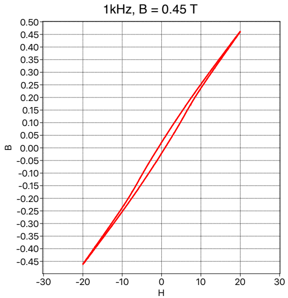

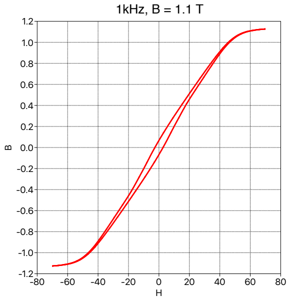

▲ Example: Measured B-H curve of VITROPERM 500F.

Composition and applications:

- Ferrimagnetic material
- Ceramic material made from powder of different oxides and carbons
- For both line frequency and switching frequency applications

Advantages:

- Relatively narrow initial permeability range
- Low hysteresis loss
- Very low eddy current loss
- Low acoustic noise
- Relatively low cost
- Various core shapes available

Disadvantages:

- Low saturation flux density
- Small mechanical size of cores
- Magnetic properties deteriorate with temperature increase
- Mechanically fragile

Saturation B	Init. permeability	Core loss (10kHz, 0.5T)	Conductivity
0.3 ~ 0.5 T	$0.1 \cdot 10^3 \sim 20 \cdot 10^3$	5 ~ 100 W/kg	$< 1 \cdot 10^{-5}$ S/m

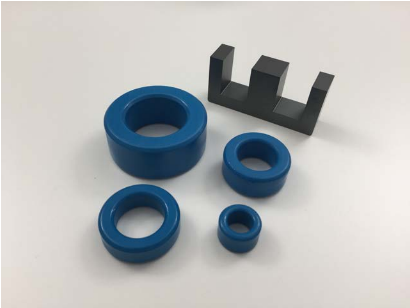

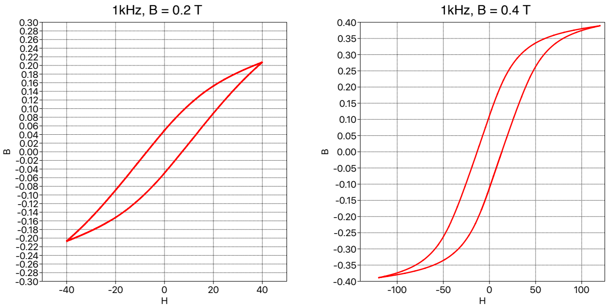

▲ Example: Measured B-H curve of Ferrite N87.

Copper winding:

- Flat wire - low frequency, easy to use
- Litz wire - high frequency, limited bending
- Foil - provide flat windings
- Hollow tubes - provide cooling efficiency
- Better conductor
- More expensive
- Better mechanical properties

Aluminium winding:

- Flat wire
- Foil - skin effect differences compared to Copper
- Hollow tubes
- Difficult to interface with copper
- Offer some weight savings
- Cheaper
- Somewhat difficult mechanical manipulations

Copper parameters:

Electrical conductivity	$58.5 \cdot 10^6\ S/m$
Electrical resistivity	$1.7 \cdot 10^{-8}\ \Omega m$
Thermal conductivity	$401\ W/mK$
TEC (from 0° **to** 100° **C)**	$17 \cdot 10^{-6}\ K^{-1}$
Density	$8.9\ g/cm^3$
Melting point	$1083\ ^\circ C$

Aluminum parameters:

Electrical conductivity	$36.9 \cdot 10^6\ S/m$
Electrical resistivity	$2.7 \cdot 10^{-8}\ \Omega m$
Thermal conductivity	$237\ W/mK$
TEC (from 0° **to** 100° **C)**	$23.5 \cdot 10^{-6}\ K^{-1}$
Density	$2.7\ g/cm^3$
Melting point	$660\ ^\circ C$

INSULATION

Multiple influencing factors:

- Operating voltage levels
- Over-voltage category
- Environment - IP class
- Temperature
- Moisture
- Cooling implications
- Ageing (self-healing?)
- Manufacturing complexity
- Partial Discharge, BIL
- Cost

Dielectric properties:

- Breakdown voltage (dielectric strength)
- Permittivity
- Conductivity
- Loss angle

Dielectric material	Dielectric strength (kV/mm)	Dielectric constant
Air	3	1
Oil	5 - 20	2 - 5
Mica tape	60 - 230	5 - 9
NOMEX 410	18 - 27	1.6 - 3.7
PTFE	60 - 170	2.1
Mylar	80 - 600	3.1
Paper	16	3.85
PE	35 - 50	2.3
XLPE	35 - 50	2.3
KAPTON	118 - 236	3.9

▲ Variety of choices available.

Heat dissipation through heat transfer mechanisms on core and winding surfaces

Three main cooling methods/media for effective dissipation:

Air:

- Natural convection - inefficient for high power designs
- Forced convection - requires a fan
- Increased complexity, reduced reliability
- For both core and windings
- 2 A mm^{-2} current density

Oil:

- Various mineral oils exist - very efficient
- Forced convection, heat exchangers necessary
- Increased cost, complexity
- High power distribution transformers
- For both core and windings
- 4 A mm^{-2} current density

Water:

- Forced convection - very efficient
- Hollow conductors for winding cooling
- Ducts/panels for core cooling
- Traction applications
- Indirect water cooling
- 6-7 A mm^{-2} current density

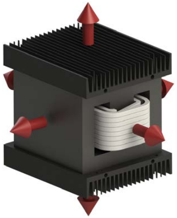
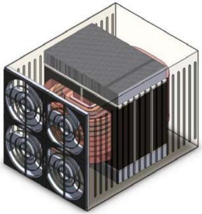

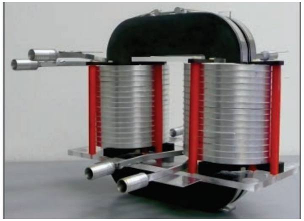

Every cooling method requires modeling, trade-off between accuracy and computational cost

MFT DESIGN DIVERSITY

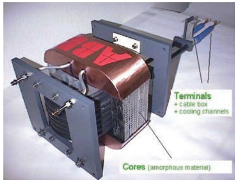

ABB: 350kW, 10kHz

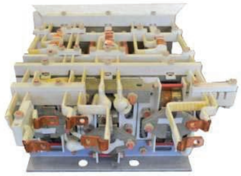

ABB: 3x150kW, 1.8kHz

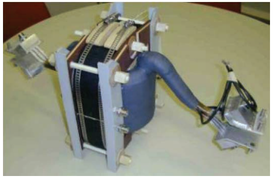

BOMBARDIER: 350kW, 8kHz

CHALMERS: 50kW, 5kHz

IKERLAN: 400kW, 5kHz

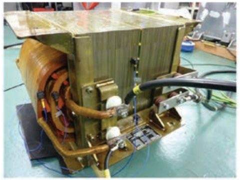

IKERLAN: 400kW, 1kHz

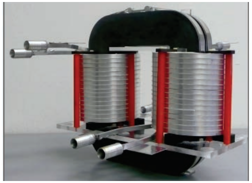

FAU-EN: 450kW, 5.6kHz

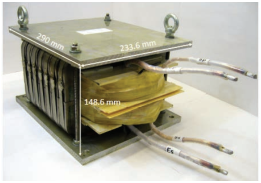

EPFL: 300kW, 2kHz

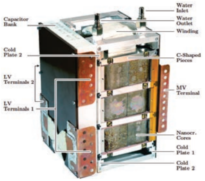

ETHZ: 166kW, 20kHz

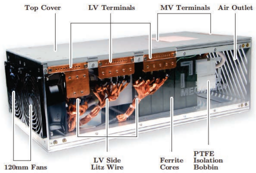

ETHZ: 166kW, 20kHz

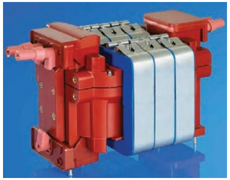

STS: 450kW, 8kHz

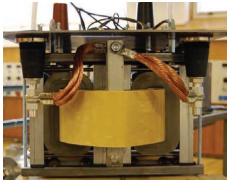

KTH: 170kW, 4kHz

EPFL: 100kW, 10kHz

SCHAFFNER: 5000kW, 1kHz

?

MFT DESIGN DIVERSITY

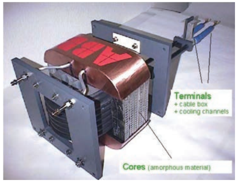

ABB: 350kW, 10kHz

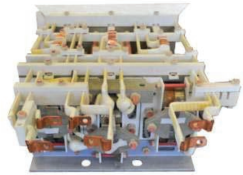
ABB: 3x150kW, 1.8kHz

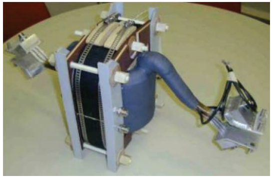
BOMBARDIER: 350kW, 8kHz


CHALMERS: 50kW, 5kHz


IKERLAN: 400kW, 5kHz

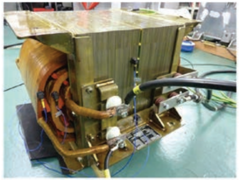
IKERLAN: 400kW, 1kHz

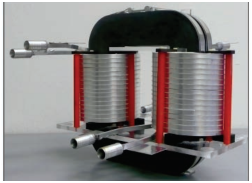
FAU-EN: 450kW, 5.6kHz

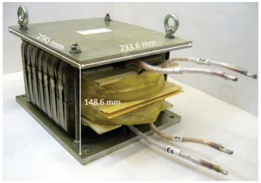

EPFL: 300kW, 2kHz

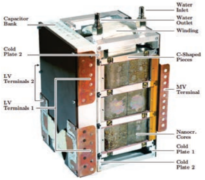

ETHZ: 166kW, 20kHz

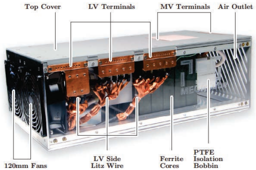

ETHZ: 166kW, 20kHz

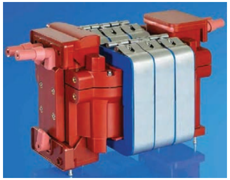
STS: 450kW, 8kHz

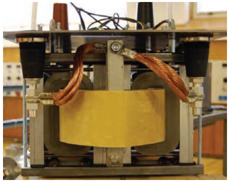
KTH: 170kW, 4kHz


EPFL: 100kW, 10kHz


SCHAFFNER: 5000kW, 1kHz

?

⇒ Large number of MFT designs has been reported, relying on various combinations of technologies!

MFT MODELING

What are the necessary models for fast and accurate MFT design?

Different core loss models:

- Based on characterization of magnetic hysteresis [49], [50], [51]
- Based on loss separation [52]
- Time domain core loss model [53]
- Based on Steinmetz Equation (MSE [54], IGSE [55], iIGSE [56])

Characteristic waveform:

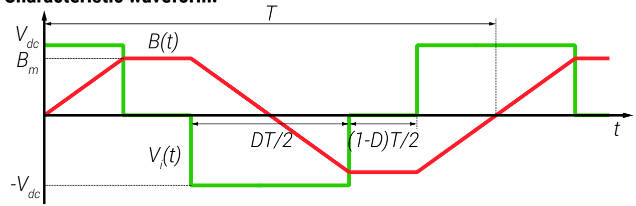

$$\left|\frac{dB(t)}{dt}\right| = \begin{cases} 0 & \text{for } (1-D)T \\ \frac{2\Delta B}{DT} & \text{for } DT \end{cases}$$

Original Steinmetz Equation:

$$P_c = K f^{\alpha} B_m^{\beta}$$

K, α, β - Steinmetz loss coefficients, determined from the core loss dependency graphs ($P_c(B_m)$,$P_c(f)$)

Improved Generalized Steinmetz Equation (IGSE):

$$P_c = \frac{1}{T}\int_0^T k_i \left|\frac{dB(t)}{dt}\right|^{\alpha} (\Delta B)^{\beta-\alpha} dt$$

$$k_i = \frac{K}{(2\pi)^{\alpha-1}\int_0^{2\pi} |cos(\theta)|^{\alpha} 2^{\beta-\alpha} d\theta}$$

Application of IGSE on the Characteristic Waveform:

$$P_s = 2^{\alpha+\beta} k_i f^{\alpha} B_m^{\beta} D^{1-\alpha}$$

$$k_i = \frac{K}{2^{\beta-1}\pi^{\alpha-1}\left(0.2761 + \frac{1.7061}{\alpha+1.354}\right)}$$

Foil winding electromagnetic field analysis:

- Dowell's foil winding loss model [57] provides a frequency dependent expression for AC resistance of the windings
- Porosity factor η ensures an equal magnetic field for both Litz and foil winding

$$\eta = d_{eq}\frac{m_v}{H_w}$$

$$P_\sigma = \frac{1}{\sigma}\int JJ^* dv; \qquad P_\sigma = \underbrace{\frac{\mathrm{MLT}}{\eta\sigma m_h d_{eq} H_w}}_{R_{DC}} I_{DC}^2 + \sum_{n=1}^{\infty} R_{AC,n} I_{RMS,n}^2$$

$$R_{AC} = F_r(f)\cdot R_{DC} = \Delta\left[\varsigma_1 + \frac{2}{3}(m_h^2 - 1)\varsigma_2\right]\cdot R_{DC}, \quad F_r \text{ - Resistance factor}$$

$$\varsigma_1 = \underbrace{\frac{sinh(2\Delta)+sin(2\Delta)}{cosh(2\Delta)-cos(2\Delta)}}_{\text{Skin factor}}; \quad \varsigma_2 = \underbrace{\frac{sinh(\Delta)-sin(\Delta)}{cosh(\Delta)+cos(\Delta)}}_{\text{Proximity factor}}; \quad \Delta = \frac{d_{eq}}{\delta}\sqrt{\eta};$$

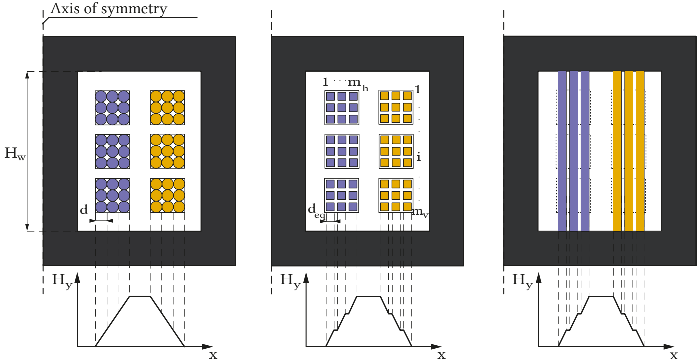

▲ Winding equivalence between the Litz wire (left) and the foil winding (right).

$$d_{eq} = d\sqrt{\frac{\pi}{4}}; \qquad K_w = \frac{h_w}{d_w};$$

$$m_h = \sqrt{\frac{N_s}{K_w}}; \qquad m_v = \sqrt{K_w N_s};$$

h_w, d_w - height and width of a single Litz wire layer;
N_s - number of strands in a layer;
m_v, m_h - equivalent number of vertical and horizontal Litz layers in the winding;

MODELING: LEAKAGE INDUCTANCE

Application of Dowell's model on the equivalent foil winding:

$$L_\sigma = N_1^2 \mu_0 \frac{l_w}{H_w}\Bigg[\underbrace{\frac{d_{w1eq} m_{w1}}{3} F_{w1} + \frac{d_{w2eq} m_{w2}}{3} F_{w2}}_{\text{Frequency dependent portion due to the magnetic energy within the copper volume of the windings}}$$

$$+ \underbrace{d_d}_{\text{Portion due to magnetic energy within the inter-winding dielectric volume}}$$

$$+ \underbrace{d_{w1i} \frac{(m_{w1}-1)(2m_{w1}-1)}{6m_{w1}}}_{\text{Portion due to magnetic energy within the inter-layer dielectric of the primary winding}}$$

$$+ \underbrace{d_{w2i} \frac{(m_{w2}-1)(2m_{w2}-1)}{6m_{w2}}}_{\text{Portion due to magnetic energy within the inter-layer dielectric of the secondary winding}} \Bigg]$$

where:

$$F_w = \frac{1}{2m^2\Delta}\left[(4m^2-1)\varphi_1 - 2(m^2-1)\varphi_2\right]$$

$$\varphi_1 = \frac{sinh(2\Delta) - sin(2\Delta)}{cosh(2\Delta) - cos(2\Delta)}; \qquad \varphi_2 = \frac{sinh(\Delta) - sin(\Delta)}{cosh(\Delta) - cos(\Delta)};$$

Winding equivalence:

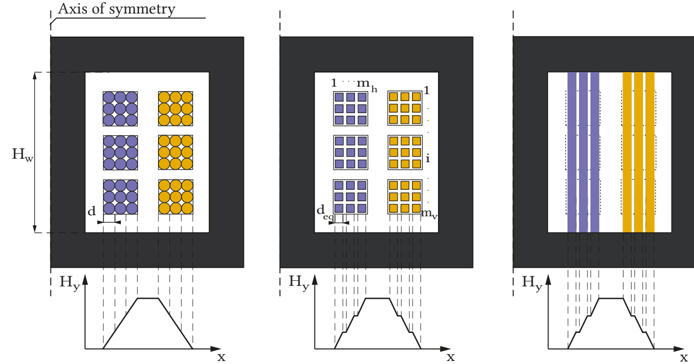

$$\Delta' = \sqrt{\eta}\Delta; \quad \eta = d_{eq}\frac{N_{sv}}{H_w}; \quad m = N_{sh}; \quad d_i = \frac{d_w - N_{sh} d_{eq}}{N_{sh} - 1};$$

Frequency influence:

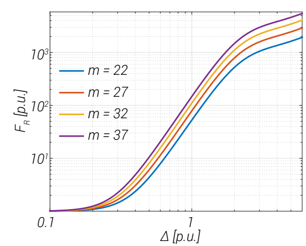

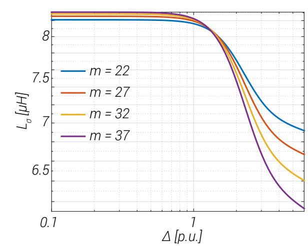

MODELING: MAGNETIZING INDUCTANCE

Magnetic circuit with an air gap:

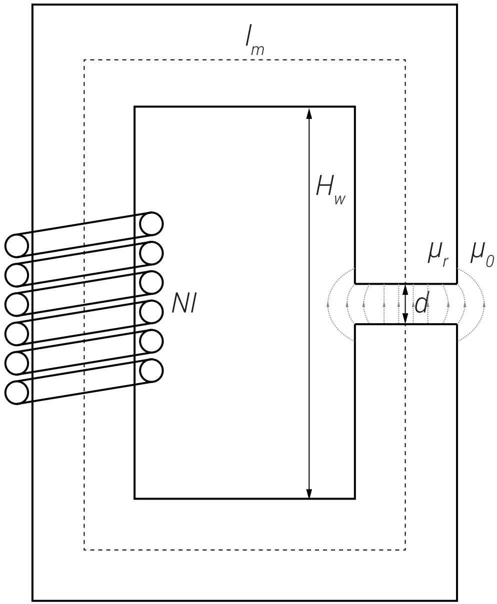

- Fringing flux must be considered and air gap is often distributed

Magnetizing inductance calculation:

$$L_m = \frac{\mu_0 N^2 A_c}{\frac{l_m}{\mu_r} + d}$$

Air gap calculation:

$$d = \mu_0 \frac{N^2 A_c}{L_m} - \frac{l_m}{\mu_r}$$

Fringing effect:

$$L_m^{'} = L_m F_{FR}; \qquad F_{FR} = 1 + \frac{d}{\sqrt{A_c}} ln\left(\frac{2H_w}{d}\right);$$

Core cross section and window height influence:

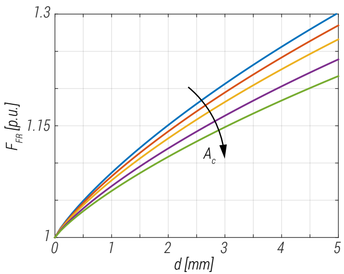

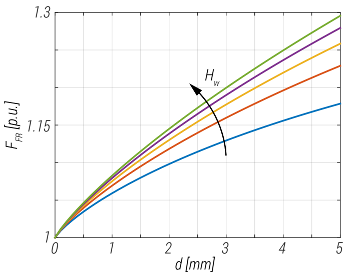

Mechanism	Heat flow	Case	Diagram	Heat transfer coefficient	Characteristic length
Conduction	$Q_h = kA\frac{\Delta T}{L}$				
Convection over Hot-Plate	$Q_h = hA(T_s - T_\infty)$	Top:	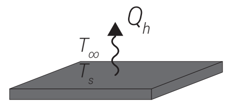	$h = \frac{k(0.65+0.36R_{a_L}^{1/6})^2}{L}$	$L = \frac{\text{Area}}{\text{Perimeter}}$
		Side:	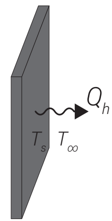	$h = \frac{k}{L}\left(0.825 + \frac{0.387R_{a_L}^{1/6}}{\left(1+(0.492/P_r)^{9/16}\right)^{8/27}}\right)^2$	L = Height
		Bottom:	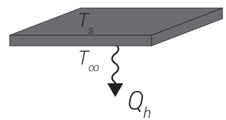	$h = \frac{k0.27R_{a_L}^{1/4}}{L}$	$L = \frac{\text{Area}}{\text{Perimeter}}$
Radiation	$Q_h = hA(T_1 - T_2)$		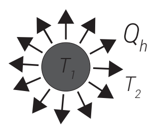	$h = \varepsilon\sigma\frac{(T_1+273.15)^4-(T_2+273.15)^4}{(T_1-T_2)}$	

where: R_{a_L} - Rayleigh number, P_r - Prandtl number, ε - Emissivity, σ - Stefan–Boltzmann constant [58], [59], [60]

Modes of heat transfer:

- Conduction
- Convection
- Radiation

Planes of symmetry:

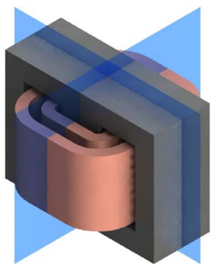

Partitioning into zones:

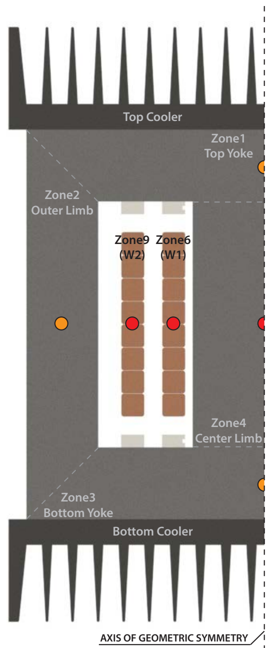

Detailed thermal network model:

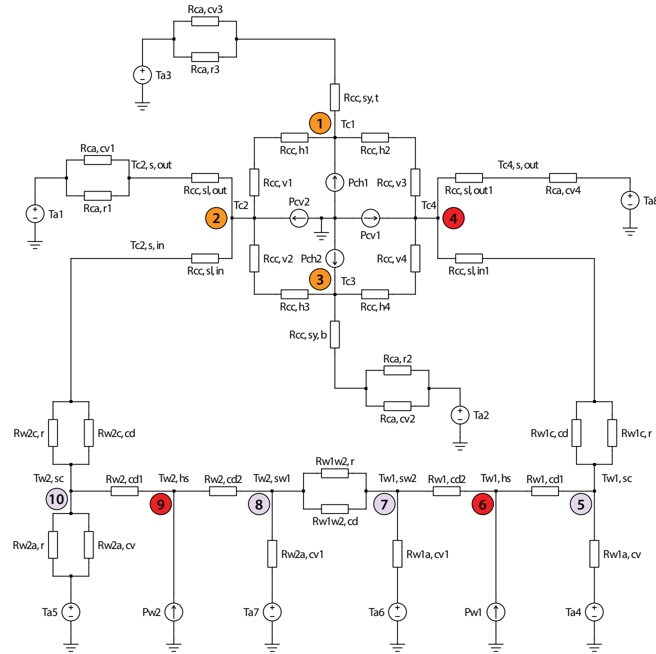

▲ Static thermal model can quickly evaluate maximum temperature rise at critical locations

Modes of heat transfer:

- Conduction
- Convection
- Radiation

Planes of symmetry:

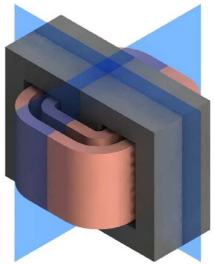

Partitioning into zones:

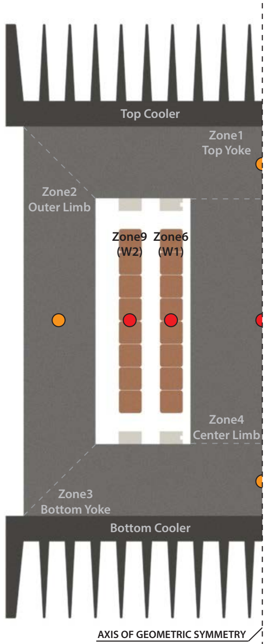

Detailed thermal network model:

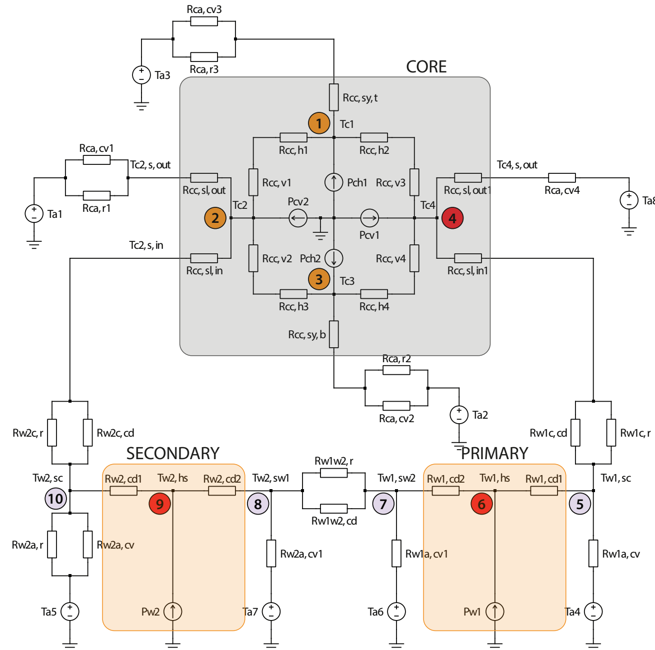

▲ Static thermal model can quickly evaluate maximum temperature rise at critical locations

MODELING: THERMAL MODEL

Modes of heat transfer:

- Conduction
- Convection
- Radiation

Planes of symmetry:

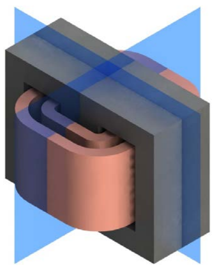

Partitioning into zones:

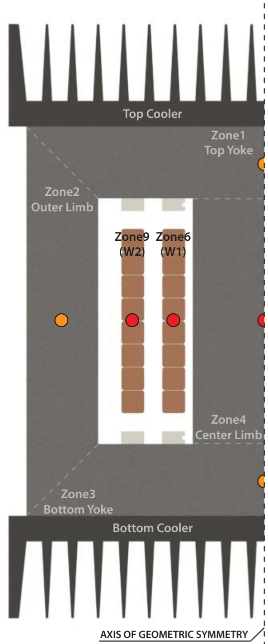

Detailed thermal network model:

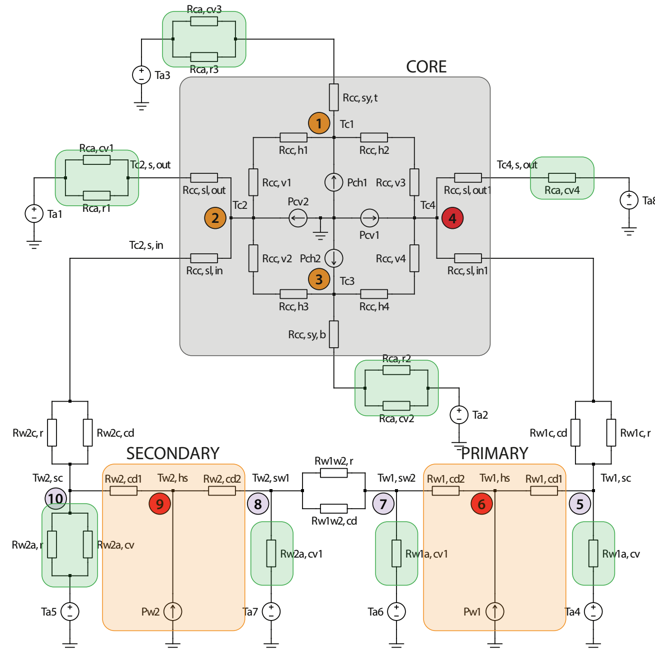

▲ Static thermal model can quickly evaluate maximum temperature rise at critical locations

MODELING: THERMAL MODEL

Modes of heat transfer:

- Conduction
- Convection
- Radiation

Planes of symmetry:

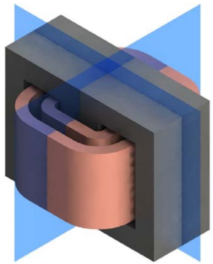

Partitioning into zones:

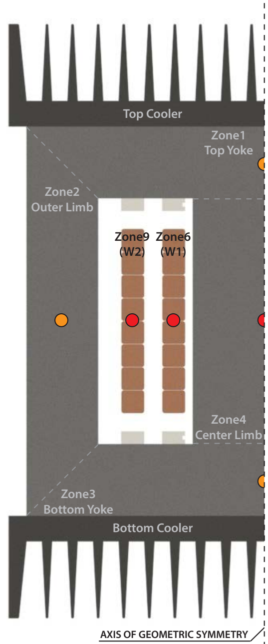

Detailed thermal network model:

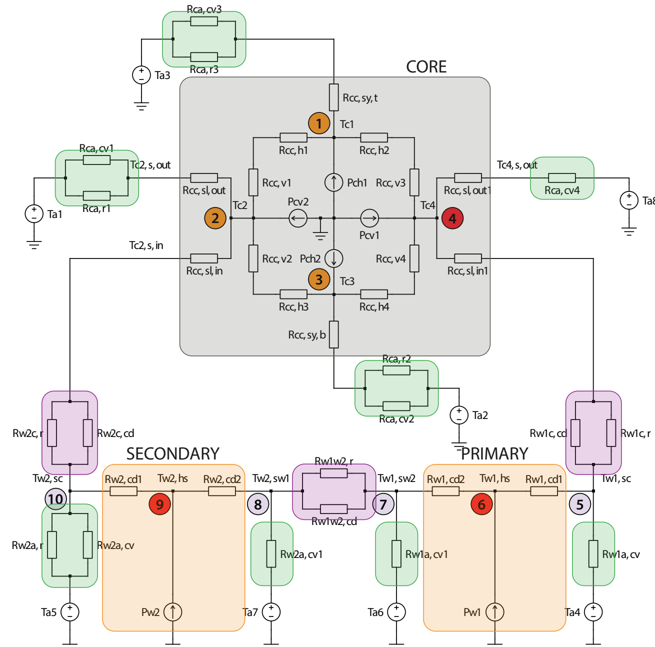

▲ Static thermal model can quickly evaluate maximum temperature rise at critical locations

Implementation of thermal network model:

- Admittance matrix:

$$Q_{(n)} = Y_{th_{(n \times n)}} \Delta T_{(n)}$$

- Rearranging the nodes:

$$\begin{bmatrix} Q_{A_{(m)}} \\ 0_{(p)} \end{bmatrix} = \begin{bmatrix} Y_{thAA_{(m \times m)}} & Y_{thAB_{(m \times p)}} \\ Y_{thBA_{(p \times m)}} & Y_{thBB_{(p \times p)}} \end{bmatrix} \begin{bmatrix} \Delta T_{A_{(m)}} \\ \Delta T_{B_{(p)}} \end{bmatrix}$$

- Kron reduction:

$$\Delta T_{A_{(m)}} = \left(Y_{thAA_{(m \times m)}} - Y_{thAB_{(m \times p)}} Y^{-1}_{thBB_{(p \times p)}} Y_{thBA_{(p \times m)}} \right)^{-1} Q_{A_{(m)}}$$

$$\Delta T_{A_{(m)}} = Y^{-1}_{Kron_{(m \times m)}} Q_{A_{(m)}}$$

- Kron matrix:

$$Y_{Kron_{(m \times m)}} = Y_{thAA_{(m \times m)}} - Y_{thAB_{(m \times p)}} Y^{-1}_{thBB_{(p \times p)}} Y_{thBA_{(p \times m)}}$$

Analytical model results for the optimal MFT prototype:

T_1 [^oC]	T_2 [^oC]	T_3 [^oC]	T_4 [^oC]	T_6 [^oC]	T_9 [^oC]
51.3	59.9	58.4	73.75	124.6	116.3

Detailed thermal network model [61]:

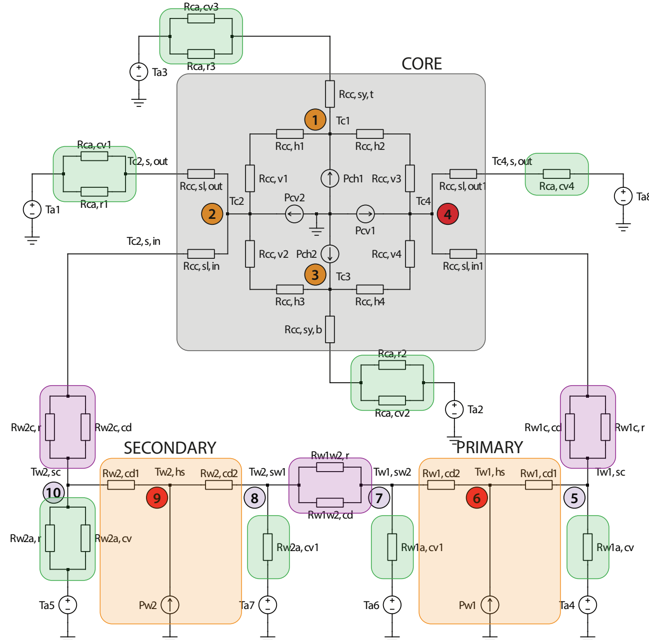

[61] M Mogorovic and D Dujic. "Thermal Modeling and Experimental Verification of an Air Cooled Medium Frequency Transformer." *Proceedings of the 19th European Conference on Power Electronics and Applications (EPE 2017 - ECCE Europe), Warsaw, Poland.* 2017

MFT DESIGN EXAMPLES

Variety of technological combinations

TECHNOLOGIES, MATERIALS, DESIGNS

Construction Choices:

- MFT Types

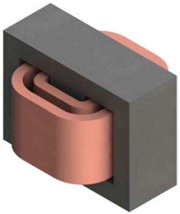

Shell Type

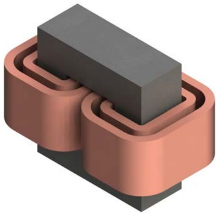

Core Type

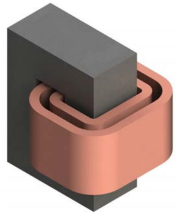

C-Type

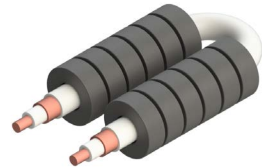

Coaxial Type

- Winding Types

Litz Wire

Foil

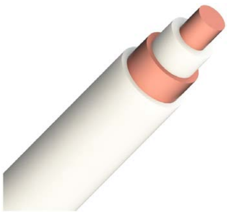

Coaxial

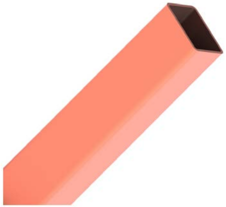

Hollow/Pipes

Materials:

- Magnetic Materials
  - Silicon Steel
  - Amorphous
  - Nanocrystalline
  - Ferrites
- Windings
  - Copper
  - Aluminum
- Insulation
  - Air
  - Solid
  - Oil
- Cooling
  - Air natural/forced
  - Oil natural/forced
  - Water

MFT HALL OF FAME

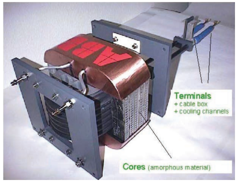

ABB: 350kW, 10kHz

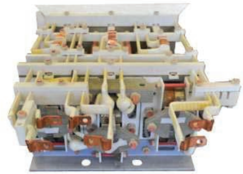
ABB: 3x150kW, 1.8kHz

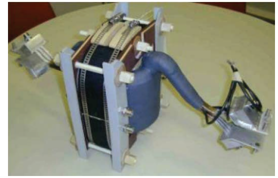
BOMBARDIER: 350kW, 8kHz

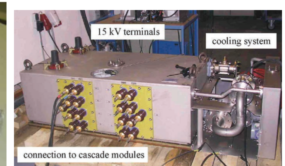

ALSTOM: 1500kW, 5kHz

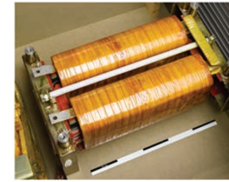
IKERLAN: 400kW, 6kHz

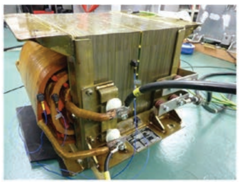
IKERLAN: 400kW, 600Hz

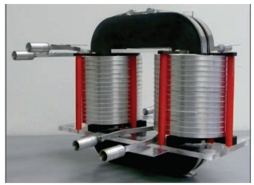
FAU-EN: 450kW, 5.6kHz


CHALMERS: 50kW, 5kHz

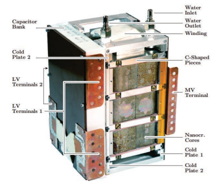

ETHZ: 166kW, 20kHz

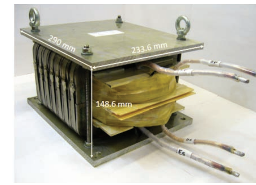

EPFL: 300kW, 2kHz


STS: 450kW, 8kHz

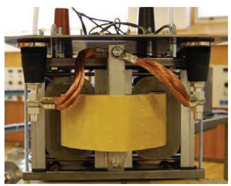
KTH: 170kW, 4kHz

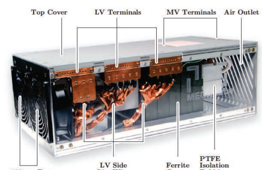

ETHZ: 166kW, 20kHz


EPFL: 100kW, 10kHz

?

ACME: ???kW, ???kHz

ABB MFT - 2002

Construction

- Shell Type
- Coaxial winding

Electrical Ratings

- Power: 350kW
- Frequency: 10kHz
- Input Voltage: ±3000V
- Output Voltage: ±3000V

Core Material

- VAC Vitroperm 500F
- U cores

Windings

- Coaxial (Al inside, Cu outside)

Cooling

- Winding - De-ionized water
- Core - Air

Insulation

- Solid

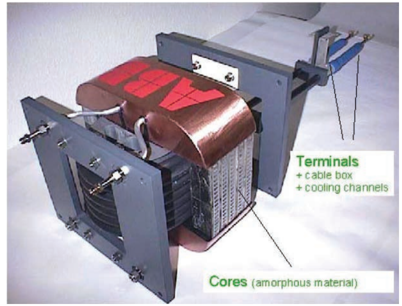

▲ 350kW MFT by ABB [62]

MFT dimensions

- Volume: ≈ 37 l
- V-Density: ≈ 9.5 kW/l
- Weight: < 50 kg
- W-Density: ≈ 7 kW/kg

Insulation Tests

- PD: 38kV, 50Hz, 1 min
- BIL: 95 kV (peak), 10 shots

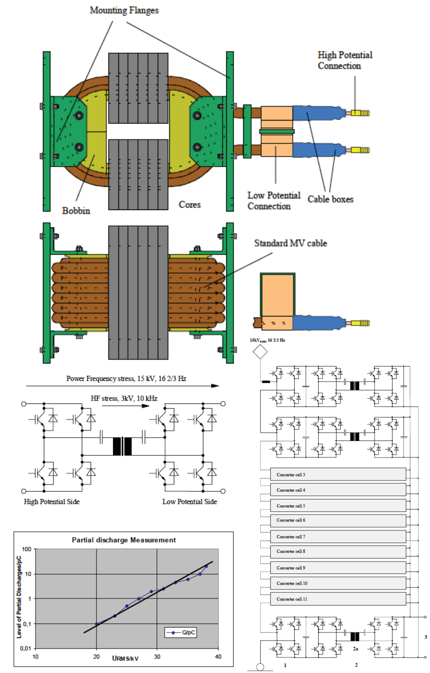

▲ Multilevel line side converter by ABB (2002)

Construction

- Single core with multiple windings

Electrical Ratings

- Power: 1.5MW
- Frequency: 5kHz
- Input Voltage: $\pm 1800V$
- Output Voltage: $\pm 1650V$

Core Material

- Ferrite
- Size and shape unclear

Windings

- Litz wire

Cooling

- Oil (MIDEL)
- Common with power electronics

Insulation

- Oil (MIDEL)
- Immersed

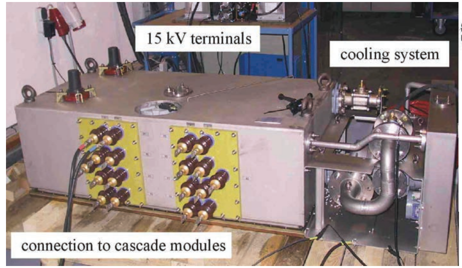

▲ 1.5MW MFT by ALSTOM

MFT dimensions

- Volume: 0.72 m^3 (2.0 x 0.73 x 0.49) m
- V-Density: 2.1 kW/l
- Weight: < 1 t (estimation)
- W-Density: < 1.5 kW / kg (estimation)

e-Transformer dimensions

- (2.1 x 2.62 x 0.58) m
- Volume: 3.22 m^3
- Weight: 3.1 t (50% less)

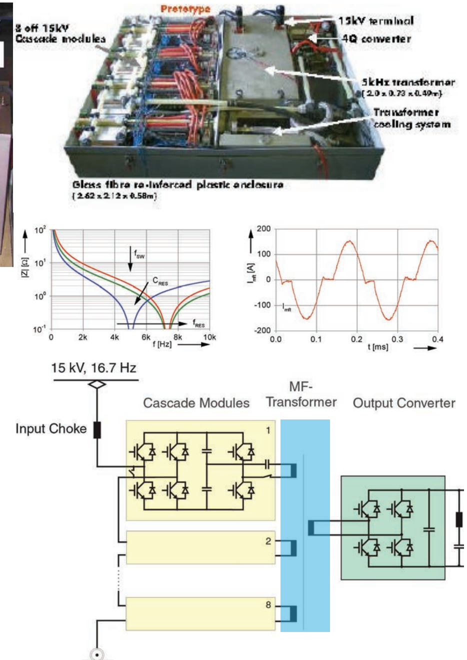

▲ e-Transformer by ALSTOM [63], [64]

ABB MFT - 2007

Construction

- C-type

Electrical Ratings

- Power: 75kW (x16)
- Frequency: 400Hz
- Input Voltage: $\pm 1800V$
- Output Voltage: $\pm 1800V$

Core Material

- SiFe
- Custom made sheets

Windings

- Bar wire

Cooling

- Oil
- Common with power electronics

Insulation

- Oil
- Immersed

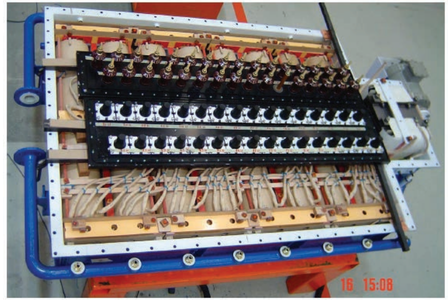

▲ Enclosure with 16 MFTs by ABB

MFT dimensions

- Volume: not reported
- V-Density: ? kW/l
- Weight: not reported
- W-Density: ? kW/kg

PETT dimensions

- Volume: 20% less
- Weight: 50% less
- Efficiency: 3% increase

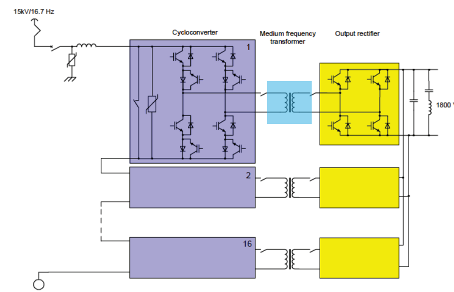

▲ PETT by ABB [65]

Construction
- Core Type
- Hollow conductors

Electrical Ratings
- Power: 350kW (500kW peak)
- Frequency: 8kHz
- Input Voltage: $\pm 1000V$
- Output Voltage: $\pm 1000V$

Core Material
- Nanocrystalline
- U cores

Windings
- Hollow tubes

Cooling
- Winding - De-ionized water
- Core - Water cooled heatsink

Insulation
- Solid

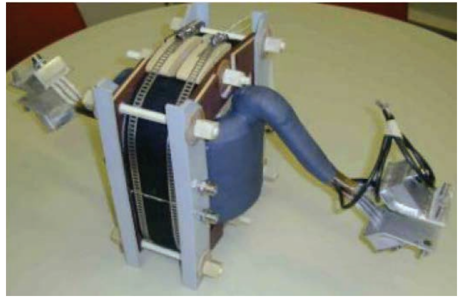

▲ 350kW MFT by Bombardier [66]

MFT dimensions
- Volume: not reported
- V-Density: ? kW/l
- Weight: 18 kg
- Density: ≈ 7 kW/kg

Insulation Tests
- PD: 33kV, 50Hz
- BIL: 100 kV (1.2/50)

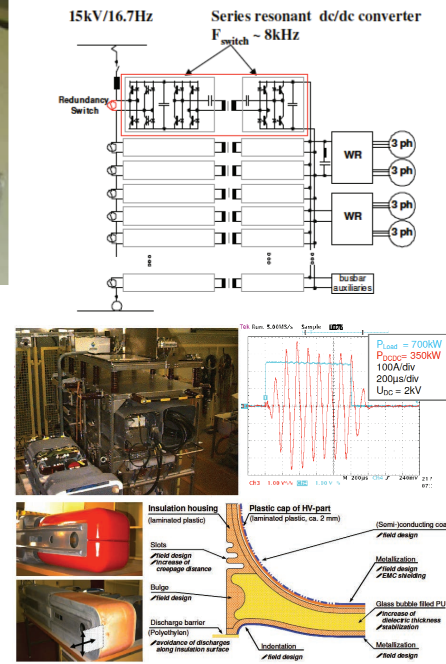

▲ Medium frequency topology by Bombardier

ABB MFT - 2011

Construction
- C-core
- Assembly with 3 MFTs

Electrical Ratings
- Power: 150kW
- Frequency: 1.75kHz
- Input Voltage: $\pm 1800V$
- Output Voltage: $\pm 750V$

Core Material
- Nanocrystalline
- C-cut cores

Windings
- Bar wire

Cooling
- Oil

Insulation
- Oil
- Immersed

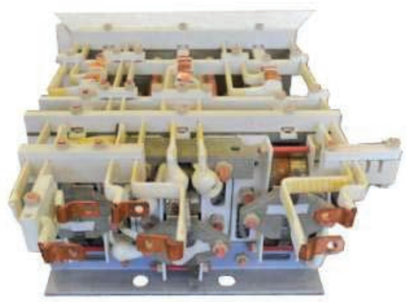

▲ 3 x 150kW MFT by ABB

MFT dimensions
- Volume: ≈ 80 l
- V-Density: ≈ 2.4 kW/l
- Weight: ≈ 170 kg
- W-Density: ≈ 1.1 kW/kg

PETT dimensions
- Weight: 4.5 t

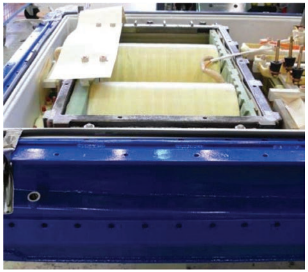

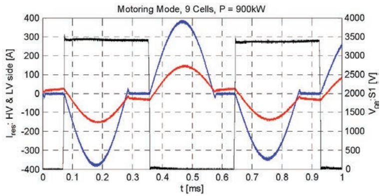

▲ PETT tank with magnetics by ABB [10], [11]

UEN MFT - 2011

Construction
- Core Type

Electrical Ratings
- Power: 450kW
- Frequency: 5.6kHz
- Input Voltage: $\pm 3600V$
- Output Voltage: $\pm 3600V$

Core Material
- Nanocrystalline VITROPERM 500F
- U cores

Windings
- Aluminum
- Hollow profiles

Cooling
- Winding - de-ionized water
- Core - Oil

Insulation
- Oil - Immersed (primary to secondary)
- NOMEX - between turns

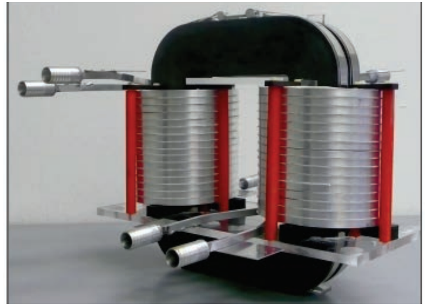

▲ 450kW MFT by UEN [67], [68], [69]

MFT dimensions
- Volume: not reported
- V-Density: ? kW/l
- Weight: 24 - 38.2 kg
- W-Density: ≈ 18.8 - 11.8 kW/kg

Insulation Tests
- Designed for 25kV railway lines
- PD, BIL: not reported

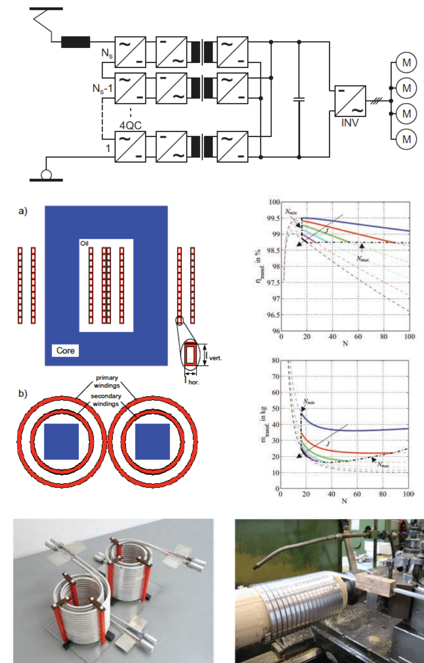

▲ MFT by UEN

Construction

- Shell Type
- for the use with HC-DCM-SRC

Electrical Ratings

- Power: 166kW
- Frequency: 20kHz
- Input Voltage: $\pm 1000V$
- Output Voltage: $\pm 400V$

Core Material

- Nanocrystalline Vitroperm 500F
- C-cores

Windings

- Square Litz Wire

Cooling

- Water-cooled heat sinks

Insulation

- Solid
- Mica tape

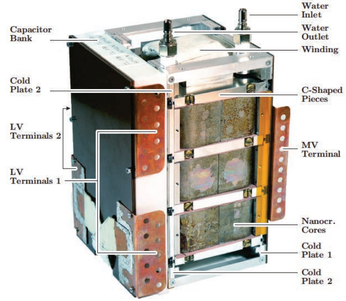

▲ 166kW MFT by ETH [70], [71], [72]

MFT dimensions

- Volume: ≈ 5 l
- V-Density: ≈ 32.7 kW/l
- Weight: ≈ 10 kg
- W-Density: ≈ 16.6 kW/kg

Insulation Tests

- No details provided

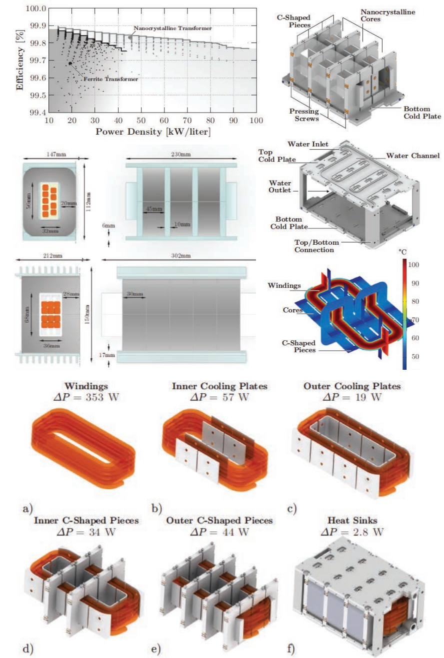

▲ Nanocrystalline MFT by ETHZ

Construction

- Shell Type
- for the use with TCM-DAB

Electrical Ratings

- Power: 166kW
- Frequency: 20kHz
- Input Voltage: ±750*V*
- Output Voltage: ±750*V*

Core Material

- Ferrite N87
- U-cores U96/76/30

Windings

- Square Litz Wire

Cooling

- Winding - Forced air
- Core - Heatsinks (Forced air)

Insulation

- PTFE (teflon)

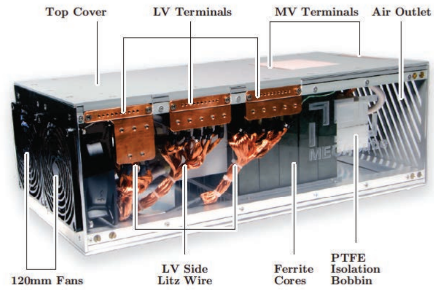

▲ 166kW MFT by ETH [70]

MFT dimensions

- Volume: ≈ 20 l
- V-Density: ≈ 8.21 kW/l
- Weight: not reported
- W-Density: not reported

Insulation Tests

- No details provided

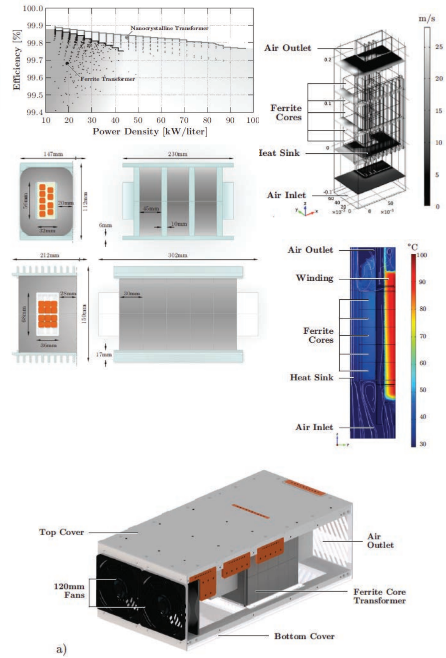

▲ Ferrite MFT by ETHZ

STS MFT - 2015

Construction

- Core Type

Electrical Ratings

- Power: 450kW
- Frequency: 8kHz
- Input Voltage: $\pm 1800V$
- Output Voltage: $\pm 1800V$

Core Material

- Nanocrystalline
- C cores

Windings

- Square Litz Wire

Cooling

- Winding - Oil
- Core - Air cooled

Insulation

- Solid combined with Oil
- Core in the air

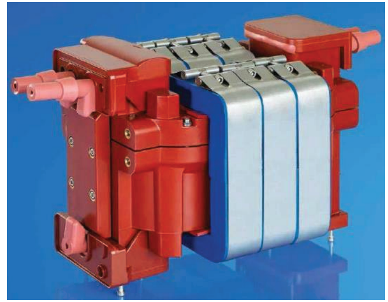

▲ 450kW MFT by STS

MFT dimensions

- Volume: ? l
- V-Density: ≈ ? kW/l
- Weight: 50 kg
- W-Density: ≈ 9 kW/kg

Insulation Tests

- PD: 37kV, 50Hz (PD < 5pC)
- BIL: not specified

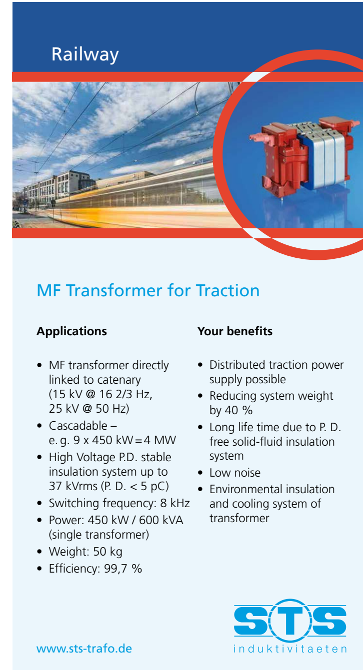

▲ MFT by STS

ABB MFT - 2017

Construction

- Core Type

Electrical Ratings

- Power: 240kW
- Frequency: 10kHz
- Input Voltage: $\pm 600V$
- Output Voltage: $\pm 900V$

Core Material

- Nanocrystalline
- U cores (custom)

Windings

- Litz Wire (4 parallel)

Cooling

- Winding - Air
- Core - Air

Insulation

- Solid - Cast Resin
- Air

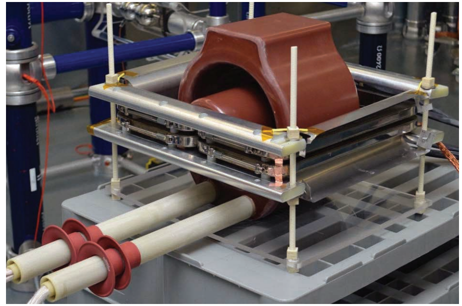

▲ 240kW MFT by ABB [73]

MFT dimensions

- Volume: ≈ 67.7 l
- V-Density: ≈ 3.6 kW/l
- Weight: ≈ 42 kg
- W-Density: ≈ 5.7 kW/kg

Insulation Tests

- PD: 53kV, 50Hz
- BIL: 150kV

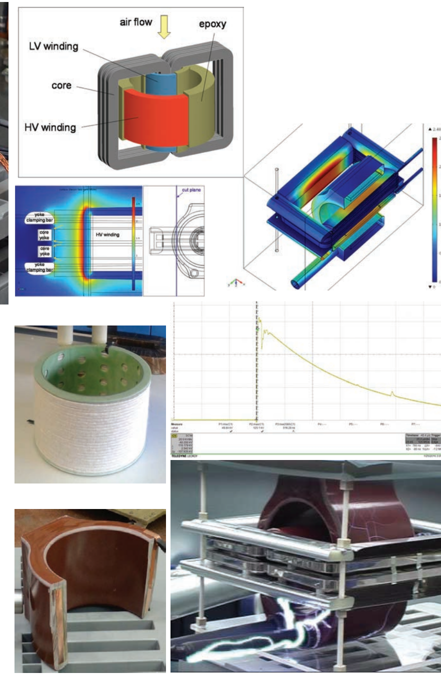

▲ MFT by ABB

ABB CERN MFT - 2017

Construction
- Core Type

Electrical Ratings
- Power: 100kW
- Frequency: 15kHz - 22kHz
- Input Voltage: $\pm 540V$
- Output Voltage: $\pm 540V$ x 24

Core Material
- Nanocrystalline
- U cores

Windings
- Litz Wire

Cooling
- Winding/Core - Oil Immersed
- MFT assembly - Air

Insulation
- Oil (Ester)

▲ 100kW MFT by ABB [74]

MFT dimensions
- Volume: ≈ 91 l (61 l without heatsink)
- V-Density: ≈ 1.1 kW/l
- Weight: ≈ 90 kg
- W-Density: ≈ 1.1 kW/kg

Insulation Tests
- PD: 30kV, 50Hz
- BIL: not reported

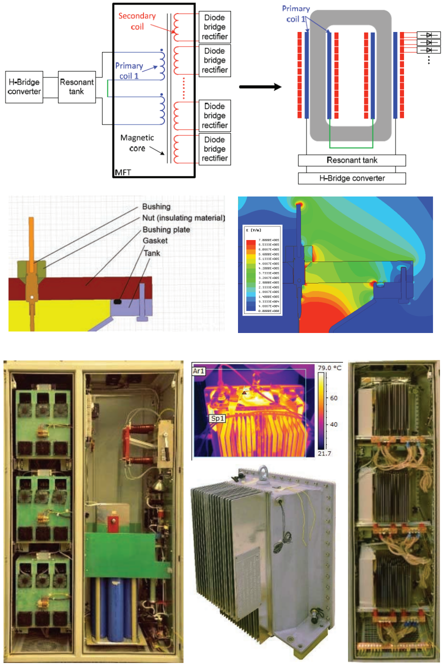

▲ MFT by ABB for CERN

Construction

- Core Type

Electrical Ratings

- Power: 100kW
- Frequency: 10kHz
- Input Voltage: ±750*V*
- Output Voltage: ±750*V*

Core Material

- SiFerrite (UU9316 - CF139)
- U cores

Windings

- Square Litz Wire

Cooling

- Winding - Air
- Core - Air cooled heatsink

Insulation

- Air

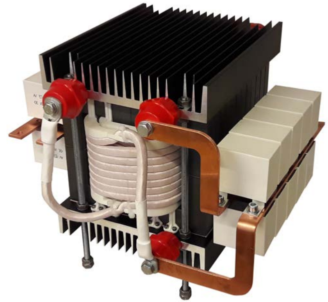

▲ 100kW MFT by EPFL [75], [61], [76]

MFT dimensions

- Volume: ≈ 12.2 l
- V-Density: ≈ 8.2 kW/l
- Weight: ≈ 28 kg
- W-Density: ≈ 3.6 kW/kg

Insulation Tests

- PD: 6kV, 50Hz
- BIL: not performed

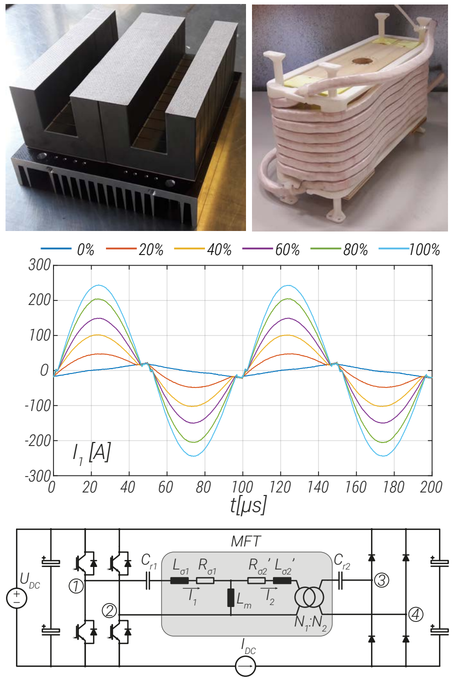

▲ MFT by EPFL

[76] Marko Mogorovic and Drazen Dujic. "100 kW, 10 kHz Medium-Frequency Transformer Design Optimization and Experimental Verification." *IEEE Transactions on Power Electronics* 34.2 (2019), pp. 1696–1708

Construction
- Shell Type
- for the use with DC-DC SRC

Electrical Ratings
- Power: 25kW
- Frequency: 48kHz
- Input Voltage: $\pm 3.5kV$
- Output Voltage: $\pm 400V$

Core Material
- Ferrite BFM8
- U-cores U96/60/30

Windings
- Square Litz Wire

Cooling
- Winding - Forced air
- Core - Forced air

Insulation
- Dry type - Vacuum poting (windings)

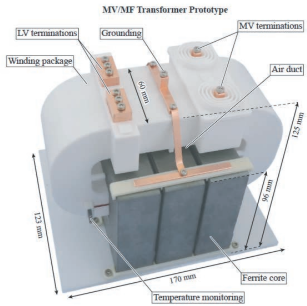

▲ 25kW MFT by ETH [77]

MFT dimensions
- Volume: ≈ 3.4 l
- V-Density: ≈ 7.4 kW/l
- Weight: ≈ 6.2 kg
- W-Density: ≈ 4 kW/kg

Insulation Tests
- 20kV

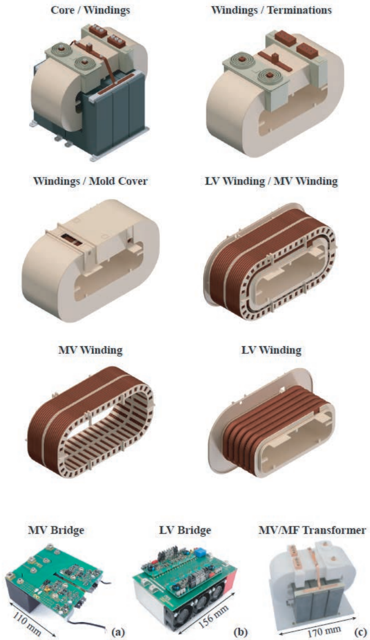

▲ Ferrite MFT by ETHZ

EPFL PEL MFT - 2019

Construction
- Planar type

Electrical ratings
- Power: 100kW
- Frequency: 10kHz
- Input Voltage: $\pm 750V$
- Output Voltage: $\pm 750V$

Core material
- Nanocrystalline VITROPERM 500F
- U cores

Windings
- Copper
- Litz wire

Cooling
- Winding - Forced air
- Core - Heatsinks (Forced air)

Insulation
- Solid - Cast resin

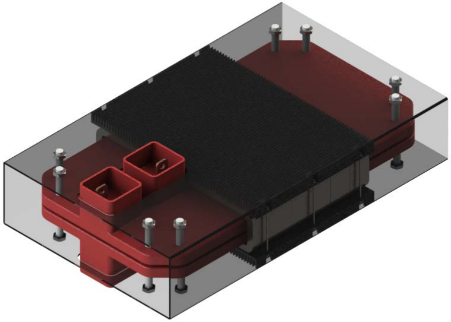

▲ 100kW Planar MFT by PEL.

MFT dimensions
- Volume: 18.5l
- V-Density: 5.4kW/l
- Weight: 26.3kg
- W-Density: 3.8kW/kg

Insulation tests
- PD: 5kV, 50Hz
- BIL: not reported

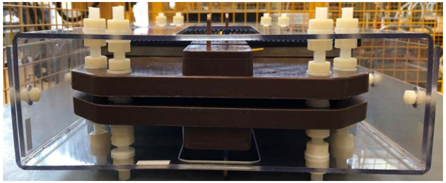

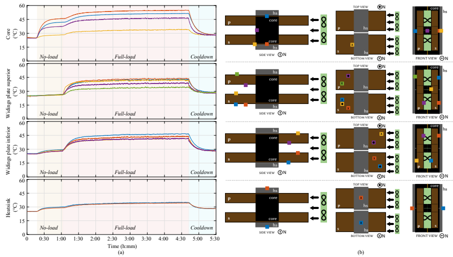

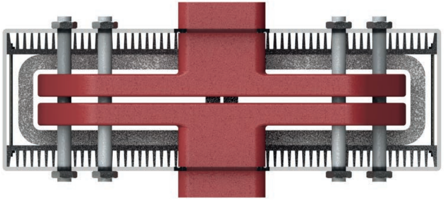

▲ MFT by PEL.

RWTH SCHAFFNER MFT - 2019

Construction

- 3-phase Core type

Electrical ratings

- Power: 5MW
- Frequency: 1kHz
- Input Voltage:
- Output Voltage:

Core material

- Grain oriented silicon steel
- U cores

Windings

- Copper
- Foil

Cooling

- Winding - Air
- Core - Air

Insulation

- Core in the air
- NOMEX/Mica tape?

▲ 5MW 3-phase MFT by Schaffner [78].

MFT dimensions

- Volume: not reported
- V-Density: not reported
- Weight: less than 700kg
- W-Density: > 7.1kW/kg

Insulation tests

- PD, BIL: not reported

▲ MFT by Schaffner.

Construction
- Core type

Electrical ratings
- Power: 100kW
- Frequency: 20kHz
- Input Voltage: ± 1.2kV
- Output Voltage: ± 1.2kV

Core material
- Ferrite
- I cores

Windings
- Copper
- Litz wire

Cooling
- Winding - Forced air

Insulation
- Core in the air

▲ 100kW MFT by Supergrid Institute [79].

MFT dimensions
- Volume: not reported
- V-Density: not reported
- Weight: not reported
- W-Density: not reported

Insulation tests
- PD, BIL: not reported

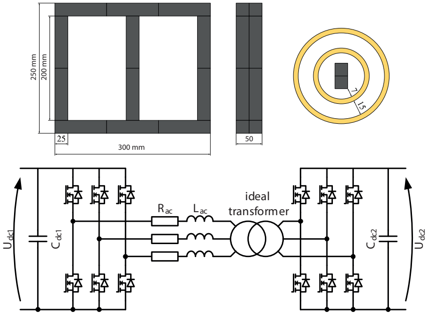

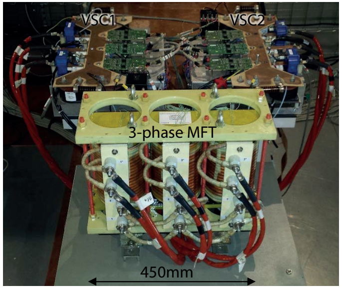

▲ MFT by Supergrid Institute.

EPFL PEL HYOSUNG MFT - 2020

Construction

- Core type

Electrical ratings

- Power: 300kW
- Frequency: 20kHz
- Input Voltage: ± 1.7kV
- Output Voltage: ± 4kV

Core material

- Nanocrystalline
- UU cores

Windings

- Copper
- Litz wire

Cooling

- Winding -Forced air
- Core - Forced air

Insulation

- Winding - Solid, cast resin
- Core - Air

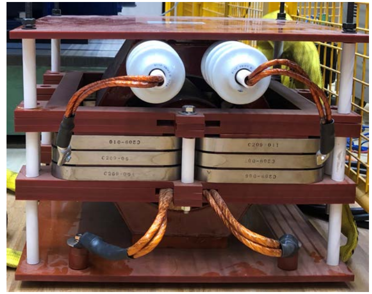

▲ 300kW Planar MFT by PEL and Hyosung.

MFT dimensions

- Volume: 62l
- V-Density: 4.8kW/l
- Weight: 39.7kg
- W-Density: 7.55kW/kg

Insulation tests

- PD: not reported
- BIL: not reported

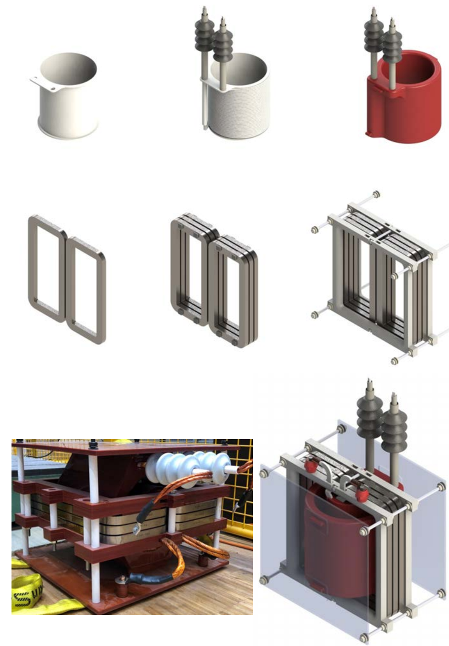

▲ MFT by PEL and Hyosung.

ETH MFT - 2021

Construction
- Air core
- Aluminum conductive shielding

Electrical ratings
- Power: 166kW
- Frequency: 77.4kHz
- Input Voltage: ± 7kV
- Output Voltage: ± 7kV

Windings
- Copper
- Litz wire
- Cylindrical solenoids

Cooling
- Winding - Forced air

Insulation
- NOMEX pressboard

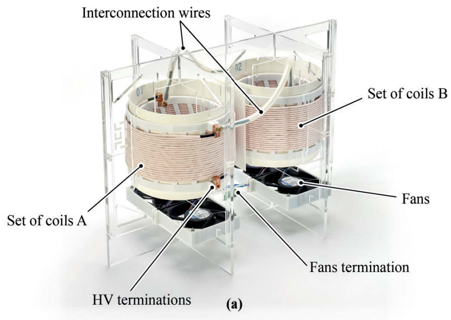

▲ 166kW MFT by ETH [80].

MFT dimensions
- Volume: not reported
- V-Density: not reported
- Weight: 10.1kg
- W-Density: 16.5kW/kg

Insulation tests
- PD, BIL: not reported

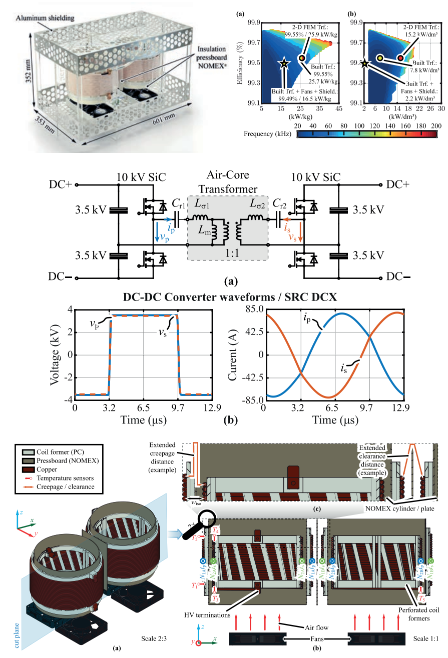

▲ MFT by ETH.

SUMMARY - MFT DESIGNS

Variety of MFT designs

- Shell Type, Core Type, C-Type
- Copper, Aluminum
- Solid wire, Hollow conductors, Litz wire, Foil
- SiFe, Nanocrystalline, Amorphous, Ferrite

Integration with Power Electronics

- Insulation coordination
- Cooling
- Electrical parameters
- Choice of core materials
- Form factor constraints
- Optimization at the system level

Custom designs prevail

There is no best design...

Limited commercial options. Example: STS ⇒

Source/ Type	P_n kVA	Freq. kHz	U_{iso} kV	Core mat.*	Cooling method	Tran. Power density†	Eff.⋆ %	Struct./ Wind.+
GE:1992[65] Dry	50	50	N/A	Ferr.	Air	12(wt)	$99.4^{a,c}$	Coaxial/ Cable
GE:2008[66] Dry	150	10	N/A	Amor.	Air	N/A	N/A	Core/ Ro. Litz
UWM:1995[67] Dry	120	20.4	N/A	Ferr.	Water	59.5(vol)	$99.6^{a,c}$	Coaxial/ Cable
ABB:2002[43] Dry	350	10	15	Nano.	Water	>7(wt)‡	N/A	Coaxial/ Cable
ABB:2007[47] Oil	75	0.4	15	Si-Fe	Oil	N/A	$>95^{b,c}$	So. Cu
ABB:2011[50, 52] Oil	150	1.75	15	Nano.	Oil	N/A	$\approx 96^{b,c}$	Ro. Litz
KTH:2009[68] Oil	170	4	30	Amor.	Water Oil	3.45(wt)	$99^{a,c}$	Shell/ Ro. Litz Foil
TUD:2005[69, 70] Dry	50	25	N/A	Nano.	Water	≈50(vol)	$>97^{b,c}$	Shell/ Foil
Bomb:2007[30] Dry	500	8	15	Nano.	Water	27.8(wt)	N/A	Shell/ Hol. Al
FAU:2011[71] Oil	450	5.6	25	Nano.	Water Oil	N/A	N/A	Core/ Hol. Al
NCSU:2010[72]◇ Dry	10	3	15	Amor.	Air	N/A	$96.76^{a,c}$ $97.3^{a,c}$ $97.16^{a,c}$	Core/ Ro. Litz
NCSU:2012[73] Dry	30	20	9.5	Nano.	Air	N/A	$99.5^{a,d}$	Coaxial/ Ro. Litz So. Cu
EPFL:2010[8] Dry	25	2	8	Amor.	Air	2.5(vol)	$99.13^{a,d}$	Shell/ Rec. Litz
IK4:2012[74]◇ Dry	400	<1 >5	18	Si-Fe Nano.	Air Fan	3.41(vol) 14.88(vol)	$99.36^{a,d}$ $99.76^{a,d}$	Shell Core
ETH:2013[14, 23]◇ Dry	166	20	N/A	Nano. Ferr.	Water Fan	32.7(vol) 8.21(vol)	$99.5^{a,c}$ $99.4^{a,c}$	Shell/ Rec. Litz
ETH:2015[75]◇ Dry	25	25 50 83	N/A	Ferr.	Air	8.2(vol) 13.3(vol) 15.9(vol)	N/A	Matrix/ Litz
Chalm:2016[76]◇ Dry	50	5	6	Nano. Ferr.	Air Air	15.1(vol) 11.5(vol)	$99.66^{a,c}$ $99.58^{a,c}$	Shell/ Rec. Litz
STS:2014[77] Oil/Dry∇	450	8	>30	N/A	Oil Air	9(wt)	$99.7^{a,c}$	Shell/ Litz

▲ Another overview of MFTs reported in literature [81]

MFT DESIGN OPTIMIZATION

Optimal design and realization of a 1MW MFT...

Optimization principles:

- Multi-objective problem: non-linear, non-convex, complex
- Optimization objectives: efficiency, weight, volume, cost ...
- Optimization specifications: known parameters, constants
- Optimization variables: continuous and discrete design parameters
- Optimization constraints: any type of limitations
- Optimization time, accuracy, sensibility, robustness

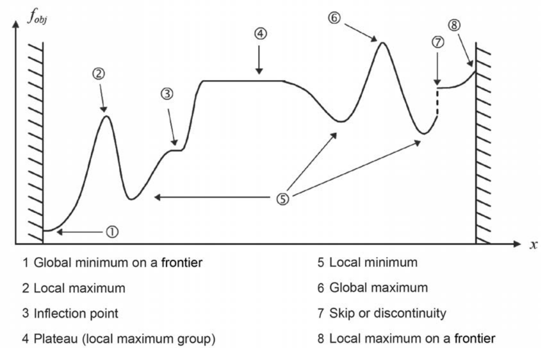

Genetic algorithm:

- Inheritance, mutation, selection and crossover technique

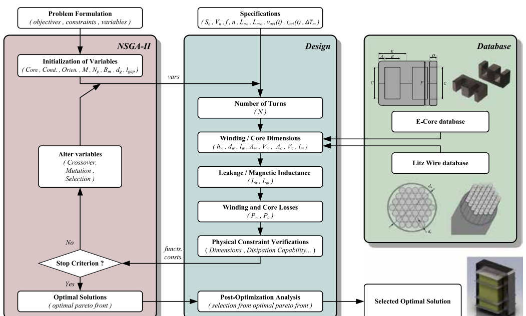

▲ Design flowchart using NSGA-II algorithm [82].

Neural networks based algorithm:

- Specifications and goals as inputs
- ANN trained with measurements, simulations, datasheets...
- No physics-based models
- Pareto front as output

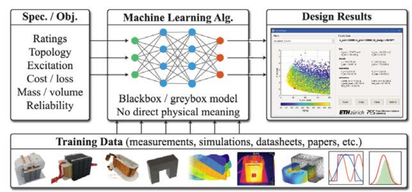

▲ Inductor design with the help of ANN [83].

Brute force algorithm:

- Exhaustive search concept
- Looks into all possible parameter combinations
- Computationally intensive
- Use of heuristics
- Easy to implement

Numerous variants of the brute force algorithm for MFT design exist:

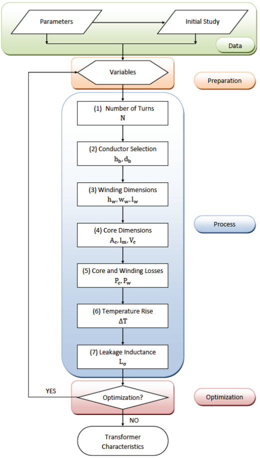

EPFL PhD: Villar [84]

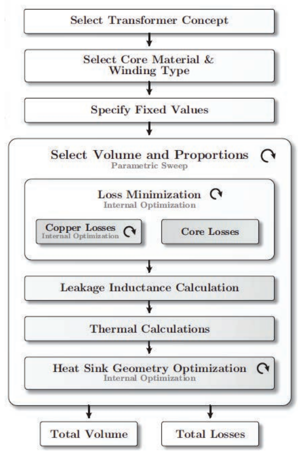

ETHZ PhD: Ortiz [70]

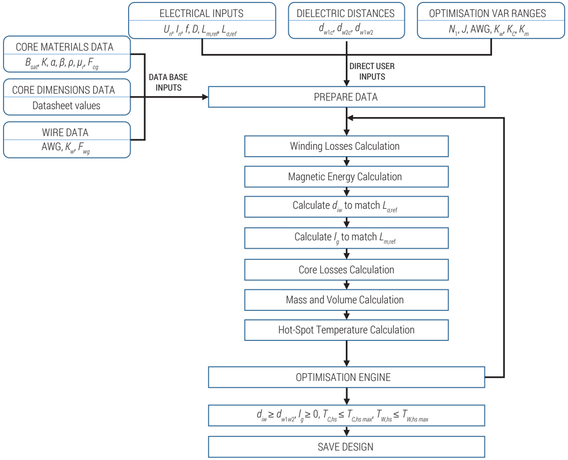

EPFL PhD: Mogorovic [85]

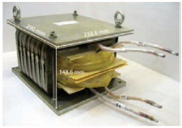

EPFL: 300kW, 2kHz

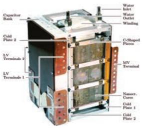

ETHZ: 166kW, 20kHz

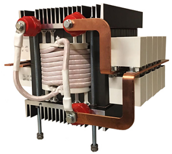

EPFL: 100kW, 10kHz

MFT DESIGN SPECIFICATIONS

1 MW DC transformer for MVDC power distribution networks

- Resonant energy conversion, LLC converter
- Bulk power processing
- Reverse conducting IGCTs as switching devices, DI water cooling
- 10 kV (engineering samples) for the primary and 4.5 kV devices for the secondary converter side

Medium frequency transformer:

- Galvanic isolation, voltage adaptation
- Electrical MFT design requirements:

Characteristics	Unit	Value
Frequency	kHz	5
Nominal Power	MW	1
Turns Ratio	1	2 : 1
Primary Voltage	kV	±5
Secondary Voltage	kV	±2.5
Ref. magn. inductance	mH	25 – 40
Ref. leakage inductance	μH	25 – 50

- Compromise between multiple design criteria - **highest efficiency!**

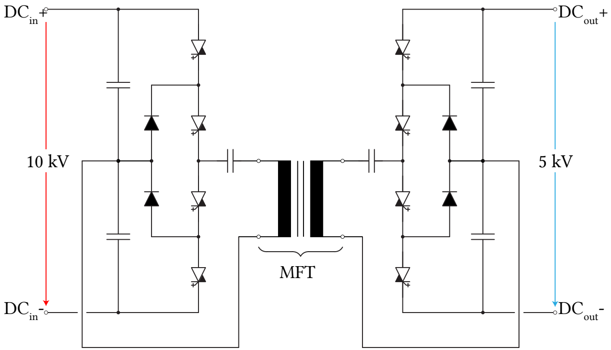

▲ DC transformer with 3-level NPC power stages, IGCT based.

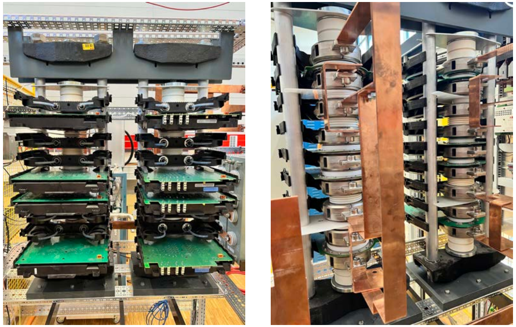

(a) (b)

▲ IGCT stacks used for the two power stages of the 1 MW DCT demonstrator.

TECHNOLOGIES AND MATERIALS

Construction Choices:

- MFT Types

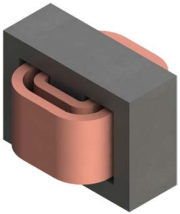

Shell Type

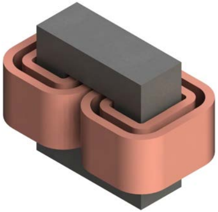

Core Type

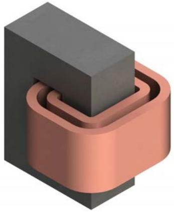

C-Type

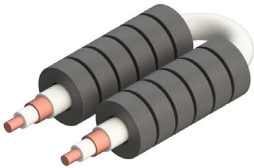

Coaxial Type

- Winding Types

Litz Wire

Foil

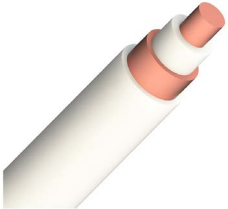

Coaxial

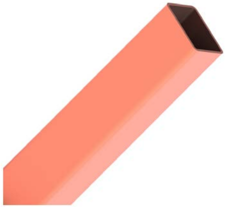

Hollow/Pipes

Materials:

- Magnetic Materials
  - **Silicon Steel**
  - **Amorphous**
  - **Nanocrystalline**
  - Ferrites
- Windings
  - **Copper**
  - Aluminum
- Insulation
  - **Air**
  - Solid
  - **Oil**
- Cooling
  - **Air natural**/forced
  - Oil natural/forced
  - **Water**

MFT WINDING ARRANGEMENTS

1-layer MFT structure:

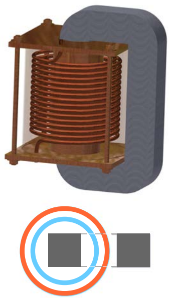

- Single oil vessel with 1 layer of PW and SW
- PW placed closer to the core limb to reduce its length, due to double number of turns
- Lower pressure drop on PW
- For optimal use of the core window area, different conductor's cross section profiles for PW and SW
- By design selection, PW and SW current densities kept equal
- Simple mechanical realization

2-vessel MFT structure:

- Two oil vessels each with 1 layer of PW and SW
- One conductor type for both windings
- Correct turns ratio achieved by external electrical connection, PWs connected in series, SWs in parallel
- Equal current density in both windings
- More complicated realization, requires winding termination panel
- Number of windings doubled compared to 1-layer MFT

3-winding MFT structure:

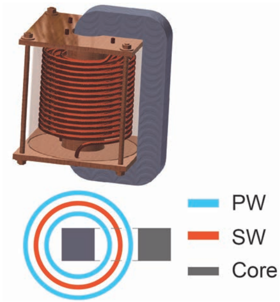

- Single oil vessel with PW interleaved around the SW
- Improved power density with 3 windings
- For optimal use of the core window area, the same conductor type used
- PW current density is 2 times smaller than the SW one
- Necessary turns ratio can be achieved inside or outside the oil vessel

1-layer MFT structure:

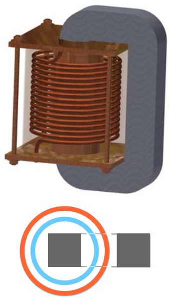

- Single oil vessel with 1 layer of PW and SW
- PW placed closer to the core limb to reduce its length, due to double number of turns
- Lower pressure drop on PW
- For optimal use of the core window area, different conductor's cross section profiles for PW and SW
- By design selection, PW and SW current densities kept equal
- Simple mechanical realization

2-vessel MFT structure:

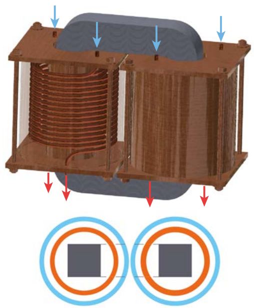

- Two oil vessels each with 1 layer of PW and SW
- One conductor type for both windings
- Correct turns ratio achieved by external electrical connection, PWs connected in series, SWs in parallel
- Equal current density in both windings
- More complicated realization, requires winding termination panel
- Number of windings doubled compared to 1-layer MFT

3-winding MFT structure:

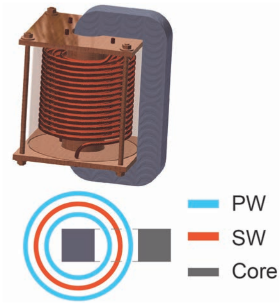

- Single oil vessel with PW interleaved around the SW
- Improved power density with 3 windings
- For optimal use of the core window area, the same conductor type used
- PW current density is 2 times smaller than the SW one
- Necessary turns ratio can be achieved inside or outside the oil vessel

Design optimization algorithm flowchart:

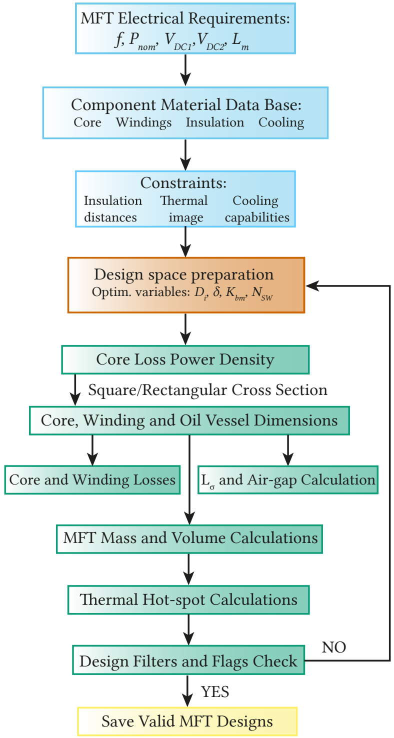

1) User-defined inputs:

- Electrical requirements
- Insulation, thermal, mechanical constraints (flags)
- Data sheets and material characteristics

2) Design optimization variables:

Var.	Min.	Max.	Res.	Description
D_i	3 mm	8 mm	16	Inner diameter
δ	$0.9\delta_{Cu}$	$2.2\delta_{Cu}$	14	Wall thickness
N_{SW}	10	45	36	SW turns number
K_{bm}	0.2	0.9	80	Flux density ratio

3) Design evaluation based on models, design filters and flags:

- Pipe winding loss model
- Thermal-hydraulic model of the oil
- Core to winding loss ratio (R_{WC})
- Minimal current and power density

4) Storing of valid MFT designs

Additional MFT models required!!

THERMAL-HYDRAULIC MODEL (I)

Basic approach of modeling: [86]

- Principles of heat and mass conservation
- Pressure equilibrium in closed oil loops

Thermal part:

- Heat exchange phenomenon
- Four characteristic oil temperatures estimated: $T_{otr}, T_{otw1}, T_{otw2}, T_{ob}$

Energy balance equation for zone Z_0:

$$zP_{\gamma 1} - P_{w,o} - P_{h,t}^{A_0} - P_{h,b}^{A_0} = \rho c_p Q_0 (T_{otr} - T_{ob}),$$

$$Q_0 = A_0 w_0, \quad P_{h,b/t}^{A_0} = A_0 k_p^h (T_{ob/otr} - T_{a,1})$$

- z - ratio of $P_{\gamma 1}$ that heats the oil in zone Z_0
- $P_{\gamma 1}$ - excess PW loss that goes to oil
- $P_{w,o}$ - exchanged heat along the outer vertical wall
- ρ - oil density at T_{ob}
- c_p - specific heat capacity at T_{ob}
- Q_0 - average volumetric oil flow in Z_0
- w_0 - average oil velocity in Z_0
- A_0 - horizontal cross section area of Z_0
- k_p^h - total heat transfer coefficient (HTC)

Many assumptions:

- Foil winding approximation, steady-state
- Stabilized, laminar oil flow, single phase

Hydraulic part:

- Two closed oil circulation paths (ABC_oD_oA and ABC_iD_iA)

Pressure equilibrium:

$$p_{eq,o}: \ p_{T,ABC_oD_oA} = \Delta p_1 + \Delta p_0$$
$$p_{eq,i}: \ p_{T,ABC_iD_iA} = \Delta p_1 + \Delta p_2$$

Produced pressure:

$$p_{T,ABC_oD_oA} = \rho g \beta \left(\frac{1}{2} T_{otr} - T_{a,1} + \frac{1}{2} T_{ob} - \Delta T_{o\text{-}a} \right)$$

- β - oil volume expansion coefficient
- g - gravity

Pressure drop:

$$\Delta p_{0,1,2} = \xi \frac{\rho w_{0,1,2}^2}{2} \quad \text{with} \quad \xi = \lambda \frac{l}{D_h}$$

- ξ - pressure drop coefficient
- λ - friction coefficient
- D_h - hydraulic diameter
- l - conduit length

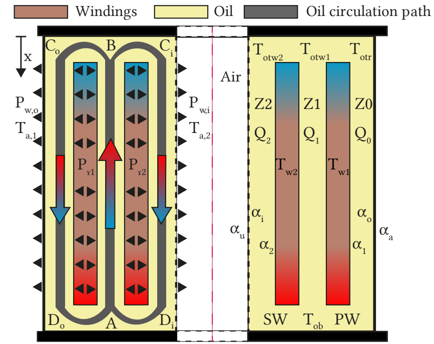

▲ 2D front view of a single oil vessel.

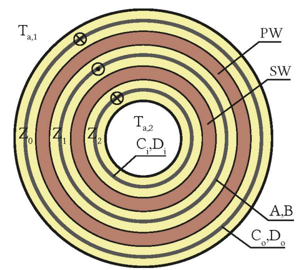

▲ 2D top view of a single oil vessel.

[86] Nikolina Djekanovic and Drazen Dujic. "Modeling and characterisation of natural-convection oil-based insulation for medium frequency transformers." *2022 IEEE Applied Power Electronics Conference and Exposition (APEC)*. 2022

THERMAL-HYDRAULIC MODEL (II)

Analytical part of THM:

- Four oil temperature expressions – $T_{otr}(x)$, $T_{ob}(x)$, $T_{otw1}(x)$, $T_{otw2}(x)$
- Two pressure balance equations – $p_{eq,o}(x)$, $p_{eq,i}(x)$

Multi-objective optimization:

$$\underset{x}{\text{minimize}} \quad f(x), g(x) \qquad f(x) = \sum_{i=\text{otr,otw1,otw2,ob}} \left|T_i(x) - T_i^*\right|$$

$$\text{subject to} \quad B_l \leq x \leq B_h \qquad g(x) = \left|p_{\text{eq,o}}(x) + p_{\text{eq,i}}(x)\right|$$

- x - set of optimizable parameters $\{w_0, w_2, z, y, k_p^o, k_p^i, k_p^h, \alpha_1, \alpha_2\}$
- T_i^* - experimental thermal measurements
- α_1, α_2 - convective HTCs (oil in Z_0 and PW; oil in Z_2 and SW); k_p^o, k_p^i - total HTC (air and oil in Z_0; air and oil in Z_2)

THM Experimental setup:

- DC source used to induce winding losses: (250 A – 450 A) corresponds to (1 kW – 3 kW)

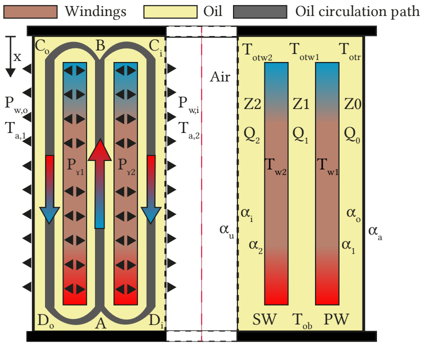

▲ 2D front view of a single oil vessel.

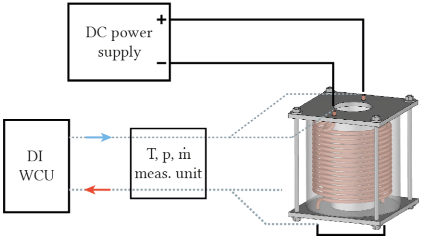

▲ Schematic of the experimental setup.

▲ Oil vessel instrumented with thermocouples.

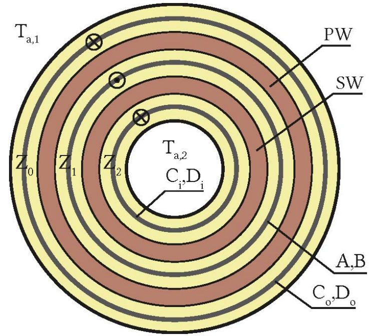

▲ 2D top view of a single oil vessel.

Experimental oil thermal measurements:

- Measured characteristic oil temperatures averaged:

$$T^*_{\text{ob}} = \text{avg}(B_1, B_2, B_3, B_4, B_5, S_8),\ T^*_{\text{otr}} = \text{avg}(T_1, S_1)$$

$$T^*_{\text{otw1}} = \text{avg}(T_2, T_5),\ T^*_{\text{otw2}} = \text{avg}(T_3, T_4)$$

18 thermocouples in the same vertical plane placed equidistantly:

- 5 at the top ($T_1 - T_5$)
- 5 at the bottom ($B_1 - B_5$)
- 8 on the side ($S_1 - S_8$)

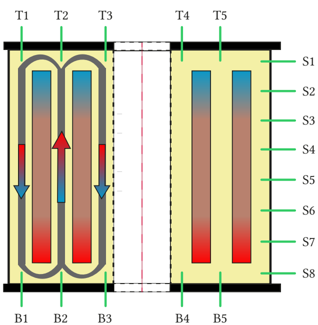

▲ Thermocouples' positions.

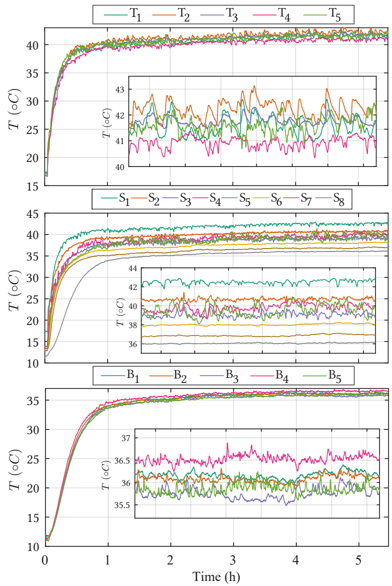

▲ Measurements at 420 A and 23 ml s^{-1}.

Results [86]:

- Overall good agreement between the THM and measured temperatures
- Highest deviation of 4.2 °C for T_{ob} at 310 A operating point
- Improved THM accuracy with higher winding losses, i.e. temperatures
- Experimental measurements versus the THM output for various operating points at 23 mL s^{-1}:

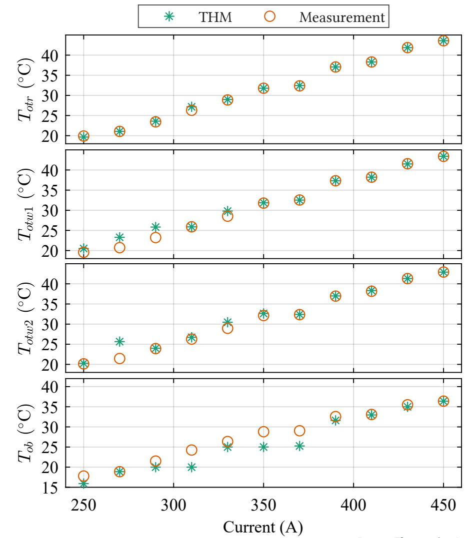

An extension of the existing Dowell's model based on FEM simulations: [87]

- Hollow penetration ratio Δ_h with hollow permeability $x = \frac{t_r}{d_{r,s}}$:

$$\Delta_h = x\Delta \qquad \Rightarrow \qquad \Delta_h = \frac{t_r}{\delta}$$

- Hollow resistance factor F_h - ratio of the AC resistance of the hollow and the solid winding

$$F_h = \frac{R_{AC,h}}{R_{AC,s}}, \qquad R_{AC,s} = F_{rs}(\Delta^{'}) \cdot R_{DC,s}, \quad \text{with} \quad \Delta^{'} = \sqrt{\eta}\Delta$$

- F_h dependency investigated on 4 parameters: m, d, f, Δ_h.
- AC resistance of hollow conductor obtained in simulation of 1080 different models
- Green - square conductor; black - round conductor

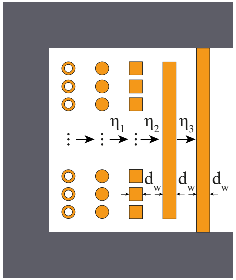

▲ From pipes to foils which extend over the full window height.

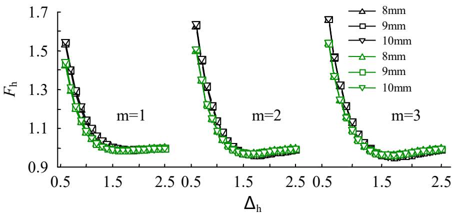

▲ Varied number of layers m in SW.

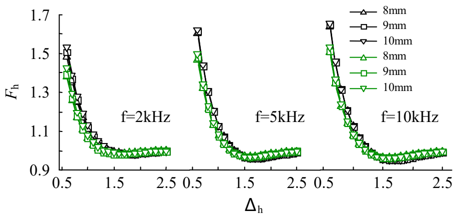

▲ Varied external diameters d in SW, m = 1.

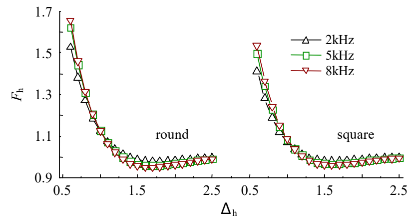

▲ $\Delta_h - F_h$ curves of SW at different frequencies.

- Optimal Δ_h in range $[1.2 - 1.8]$ for both square and round conductors

Optimal selection: 2-vessel core-type MFT with nanocrystalline material

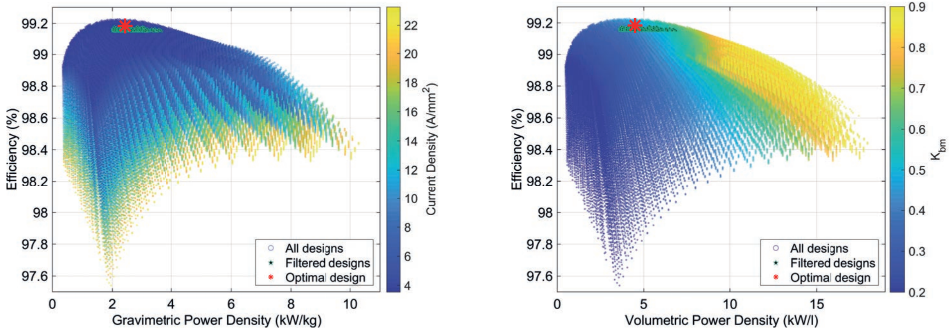

▲ (a) Efficiency vs. weight power density; (b) Efficiency vs. volume power density.

- **Applied design filters:**

R_{wc}	J	kW/kg
≤ 0.33	$\geq 6\,A\,mm^{-2}$	≥ 2

- **Optimal MFT design specifications with the highest efficiency:**

D_i	δ	N_{PW}	N_{SW}	K_{bm}	$P_{loss,PW}$	$P_{loss,SW}$	P_{core}
7.6 mm	1.3 mm	34	17	0.475	2.87 kW	2.67 kW	2.67 kW
R_{wc}	J	kW/kg	kW/l	W	L	H	η
0.32	$6.1\,A\,mm^{-2}$	2.36	3.47	494 mm	851 mm	685 mm	99.18%

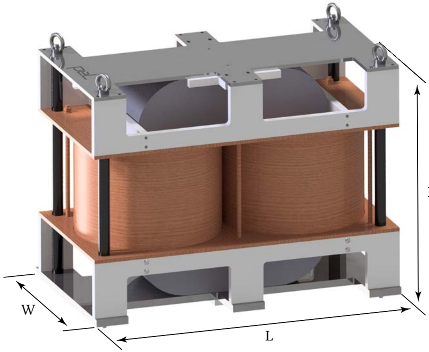

▲ 3D CAD render of the MFT prototype.

Properties of the fully assembled MFT core: [88]

A	*B*	*C*	*D*	M_c
140 mm	256 mm	318 mm	232 mm	≈ 324 kg

- 4 sets put together to assemble the core
- Rectangular cross section
- Core supplied by Hitachi Metals [89]

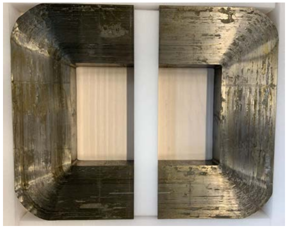

(a)

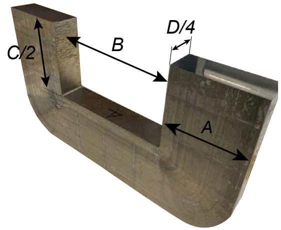

(b)

▲ Nanocrystalline material: (a) Set of two C-cut cores; (b) Single C-cut core.

▲ Full-scale prototype of the 2-vessel MFT.

(c)

(d)

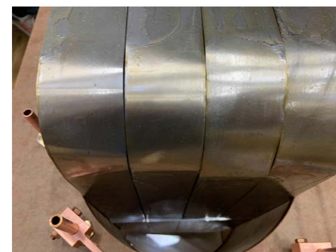

(e)

▲ (a) Side view of the MFT core; (b) Cross section surface of a single C-core; (c) Top view of the upper core half.

[88] Nikolina Djekanovic and Drazen Dujic. "Design Optimization of a MW-level Medium Frequency Transformer." *PCIM Europe 2022.* 2022, pp. 1–10

MFT PROTOTYPE ASSEMBLY (II)

Pipe windings assembly:

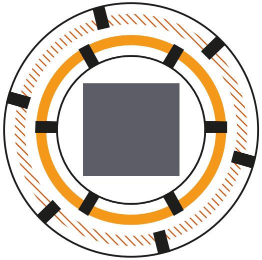

(a)

(b)

▲ (a) Spacer positioning inside the vessel; (b) Comb-alike spacers mounted every 60° on the SW from the inside.

- Soft temper copper, made by Luvata [90], used for winding realization
- Spacers made of thermoplastic POM material
- Oil vessels, made of phenolic paper composite material Etronit I and B66, produced by Elektro-Isola [91]
- Midel 7131 [92] insulation fluid used
- Instead of oil expansion vessel a sufficient air pocket is left in each vessel
- Air breathers filled with silica gel used to keep moisture and particles away

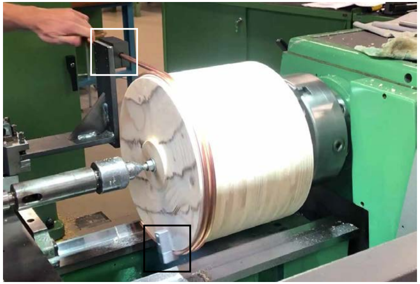

(c)

(d)

(e)

▲ (a) Mandrel bending approach; (b) Left vessel with oil, spacers and pair of windings; (c) In between the vessels.

Comparison of measured and modeled electrical parameters:

- Leakage inductance

L_σ(µH)	An.model	FEM	RLC	Bode 100
0 Hz	43.8	44.3	–	–
5 kHz	–	34	38.2	37.9

- Magnetizing inductance

L_m(mH)	Ref. value	RLC	Bode 100
5 kHz	35.77^*	36.66	36.74

∗ - corresponds to 1 mm total air gap

Final MFT prototype dimensions:

M_{MFT}	kW/kg	kW/l	W^*	L^*	H^*
462 kg	2.17	1.59	778 mm	851 mm	950 mm

▲ 1 MW prototype of the 2-vessel MFT structure.

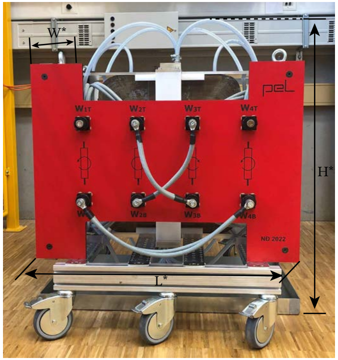

▲ Fully assembled prototype of the 2-vessel MFT.

COFFEE BREAK

Last one...

DC POWER DISTRIBUTION NETWORKS

Modeling, Impact of DCT, Operation Performance Assessment

DC POWER DISTRIBUTION: TRENDS

Exemplary DC Power distribution network

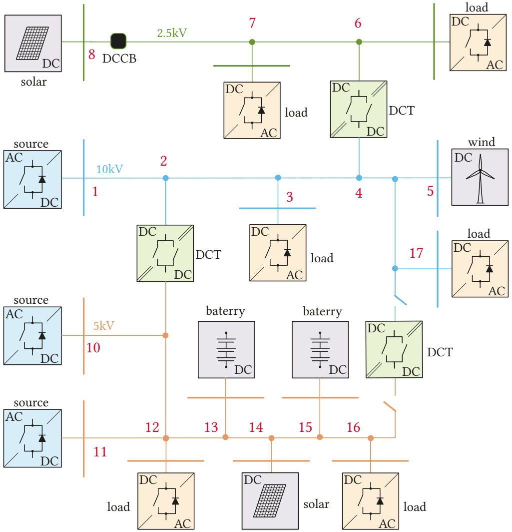

▲ DC power distribution network with multiple nodes and one DCT.

Trends

- DC PDN with integration with renewable and energy storage systems
- DCT connecting different voltage levels
- Interconnected system

Challenges

- System planning and operation
- Solutions to tackle more and more interconnected systems
- Communication?

DC Power distribution network

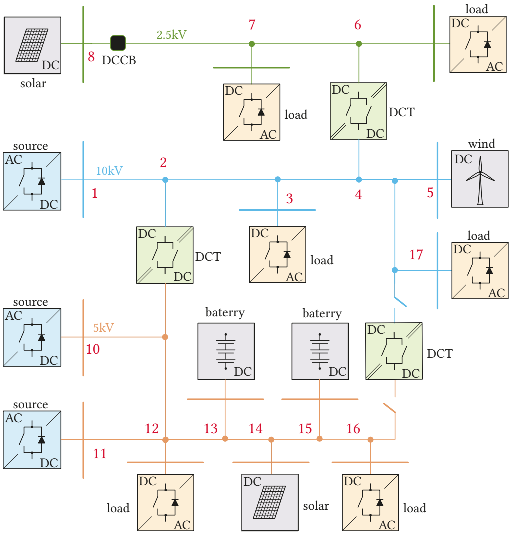

▲ DC power distribution network with six nodes and one DCT.

DC Power Flow

- Integrated solution with AC power flow
- DC network as a point-to-point connection

Solutions:

- Use the advantage of dc systems to solve power flow
- Simple and straightforward solutions

DC Resonance Response

- Power converters with control loop tend to force the system response
- Dynamics between converters and the transient solution are important

Solutions:

- Impedance analysis
- Space state model of complete system
- Eigenanalysis and Nodal analysis.
- ...

DC Power distribution network

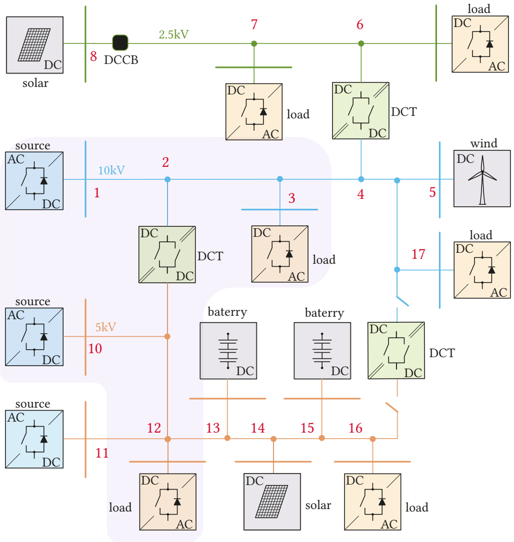

▲ DC power distribution network

DC Power Flow

- Integrated solution with AC power flow
- DC network as a point-to-point connection

Solutions:

- Use the advantage of dc systems to solve power flow
- Simple and straightforward solutions

DC Resonance Response

- Power converters with control loop tend to force the system response
- Dynamics between converters and the transient solution are important

Solutions:

- Impedance analysis
- Space state model of complete system
- Eigenanalysis and Nodal analysis.
- ...

System gets complicated very quickly

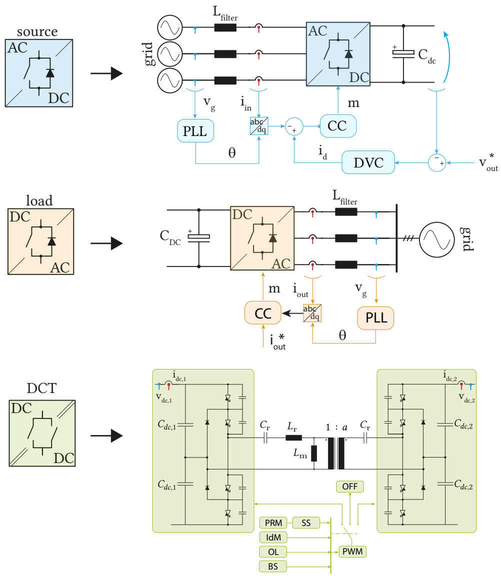

▲ Details inside each power converter box. [93]

Voltage controlled converter (Source)

- Aims to control voltage of dc bus
- Grid Current control (CC)
- Direct Voltage Control (DVC)

Current/Power controlled converter (Load)

- Aims to consume or inject power in the dc PDN
- Model of Loads and Sources that do not regulate output voltage
- Grid Current Control (CC)

DCT (Transformer)

- Link between both dc buses.
- Open loop; rely on extra features to operate.
- Power Reversal Algorithm (PRA)
- Soft-Start (SS)
- Idling Mode (IdM)
- Black-Start (BS)
- Over-Load (OL).

[93] Renan Pillon Barcelos and Dražen Dujić. "Nodal Impedance Assessment in DC Power Distribution Networks." *2021 IEEE 22nd Workshop on Control and Modelling of Power Electronics (COMPEL)*. 2021, pp. 1–8

Example 6 nodes DC PDN

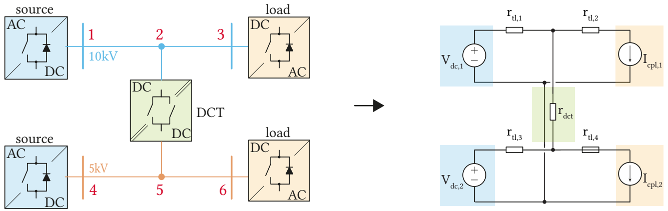

▲ Steady-state representation of the 6 nodes dc PDN.

Example 6 nodes DC PDN

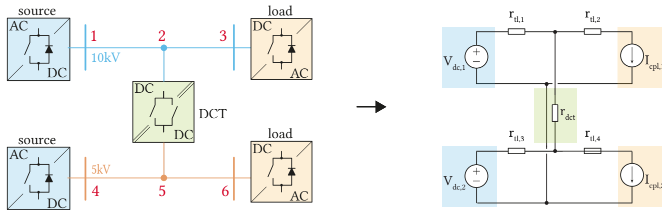

▲ Steady-state representation of the 6 nodes dc PDN.

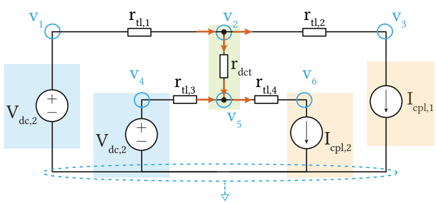

▲ Steady-state circuit and Kirchhoff's Current Law references.

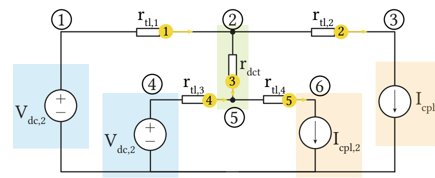

▲ Steady-state circuit Nodal Analysis references.

Example 6 nodes DC PDN

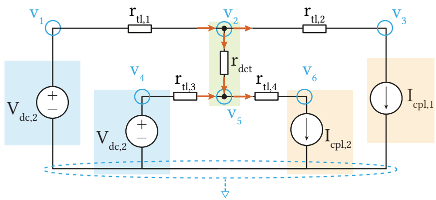

▲ Steady-state circuit and Kirchhoff's Current Law references.

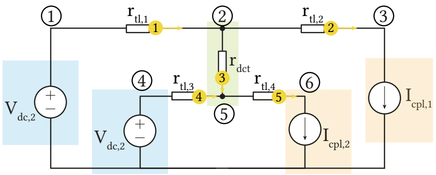

▲ Steady-state circuit Nodal Analysis references.

$$\underbrace{\begin{bmatrix} \left(\frac{1}{r_{lt,1}} + \frac{1}{r_{dct}}\right) & \frac{-1}{r_{dct,1}} \\ \frac{-1}{r_{dct,1}} & \left(\frac{1}{r_{lt,1}} + \frac{1}{r_{dct}}\right) \end{bmatrix}}_{A} \underbrace{\begin{bmatrix} V_2 \\ V_5 \end{bmatrix}}_{x} = \underbrace{\begin{bmatrix} \frac{V_{dc,1}}{r_{lt,1}} - I_{dc,1} \\ \frac{V_{dc,2}}{r_{lt,3}} - I_{dc,2} \end{bmatrix}}_{b}$$

Solve $Ax = b$

$$a = \begin{bmatrix} 1 & -1 & 0 & 0 & 0 & 0 \\ 0 & 1 & -1 & 0 & 0 & 0 \\ 0 & 1 & 0 & 0 & -1 & 0 \\ 0 & 0 & 0 & 1 & -1 & 0 \\ 0 & 0 & 0 & 0 & 1 & -1 \end{bmatrix}$$

$$\underbrace{\begin{bmatrix} Y_{\text{nodal}} & B \\ C & D \end{bmatrix}}_{A} \underbrace{\begin{bmatrix} V \\ I \end{bmatrix}}_{x} = \underbrace{\begin{bmatrix} J \\ F \end{bmatrix}}_{b}$$

Solve $Ax = b$

Example 6 nodes DC PDN

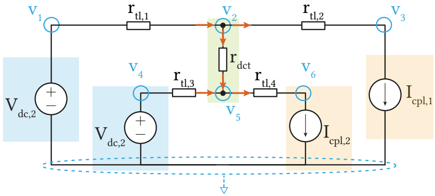

▲ Steady-state circuit and Kirchhoff's Current Law references.

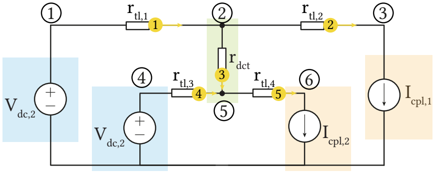

▲ Steady-state circuit Nodal Analysis references.

$$\underbrace{\begin{bmatrix} \left(\frac{1}{r_{lt,1}} + \frac{1}{r_{dct}}\right) & \frac{-1}{r_{dct,1}} \\ \frac{-1}{r_{dct,1}} & \left(\frac{1}{r_{lt,1}} + \frac{1}{r_{dct}}\right) \end{bmatrix}}_{A} \underbrace{\begin{bmatrix} V_2 \\ V_5 \end{bmatrix}}_{x} = \underbrace{\begin{bmatrix} \frac{V_{dc,1}}{r_{lt,1}} - I_{dc,1} \\ \frac{V_{dc,2}}{r_{lt,3}} - I_{dc,2} \end{bmatrix}}_{b}$$

Solve $Ax = b$

Not scalable

$$a = \begin{bmatrix} 1 & -1 & 0 & 0 & 0 & 0 \\ 0 & 1 & -1 & 0 & 0 & 0 \\ 0 & 1 & 0 & 0 & -1 & 0 \\ 0 & 0 & 0 & 1 & -1 & 0 \\ 0 & 0 & 0 & 0 & 1 & -1 \end{bmatrix}$$

$$\underbrace{\begin{bmatrix} Y_{\text{nodal}} & B \\ C & D \end{bmatrix}}_{A} \underbrace{\begin{bmatrix} V \\ I \end{bmatrix}}_{x} = \underbrace{\begin{bmatrix} J \\ F \end{bmatrix}}_{b}$$

Solve $Ax = b$

FREQUENCY RESPONSE OF THE DC PDN (I)

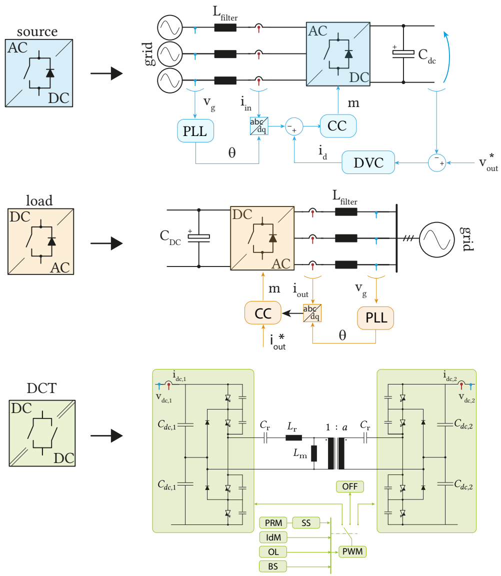

▲ Details inside each power converter box.

Power converters

- Sources, Loads, Transformers
- Every element in the DC PDN is a switched mode converter
- Closed-loop controlled converters tends to force an operational point
- There are no centralized control or communication between converters, nor access to internal parameters.

Transmission line

- Impacts in every point of analysis.
- Have large responsibility in the system dynamics.
- DC cables tend to have high capacitance.

Faults and others

- Faults and extraordinary events cause disturbances in the DC PDN
- Protection of each element is required with proper coordination.

⇒ All elements contribute to the frequency response of DC PDN!

FREQUENCY RESPONSE OF THE DC PDN (II)

How to get the system frequency characteristics?

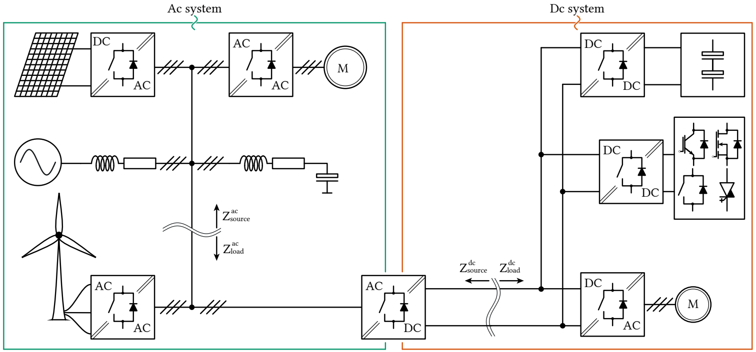

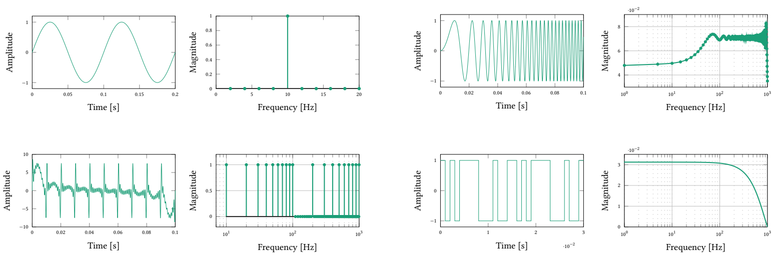

▲ Examples of different perturbation signals.

Interconnection of two independent systems

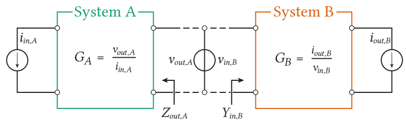

▲ Commercial low voltage, low power, frequency analysers.

▲ Programmable ac sources and grid emulators.

NODAL IMPEDANCE ASSESSMENT (I)

Calculation of $Z_{1,1}$ - DC impedance of DC PDN from Node 1.

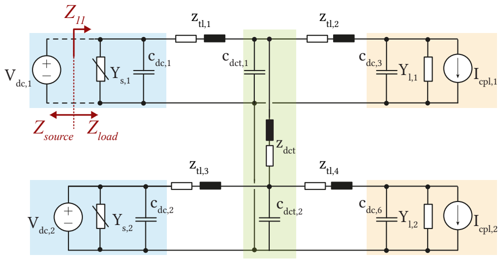

▲ Simplified 6 nodes DC PDN linear equivalent model.

Calculation of $Z_{1,1}$ - DC impedance of dc PDN from Node 1.

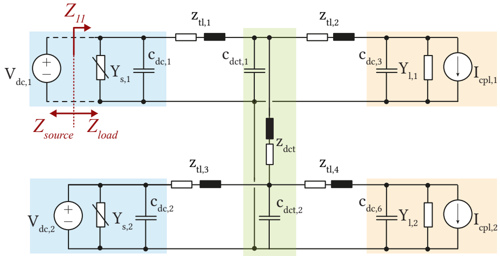

▲ Simplified 6 nodes DC PDN linear equivalent model.

$$Y_{n,3} = c_{dc,3} + Y_{l,1}$$

$$Y_{n,6} = c_{dc,6} + Y_{l,2}$$

$$Y_{eq,sec} = \left[y_{dct}' // \left(y_{tl,3}' + c_{dct,2}' + \left(y_{tl,4}' // Y_{n,6}'\right)\right)\right]$$

$$Y_{eq,pri} = \left(y_{tl,2} // Y_{n,3}\right)$$

$$Y_{eq,n,1} = y_{tl,1} // \left(Y_{eq,sec} + Y_{eq,pri} + c_{dct,2}\right)$$

$$Y_{11} = Y_{s,1} + c_{dc,1} + Y_{eq,n,1}$$

$$Z_{11} = Y_{11}^{-1}$$

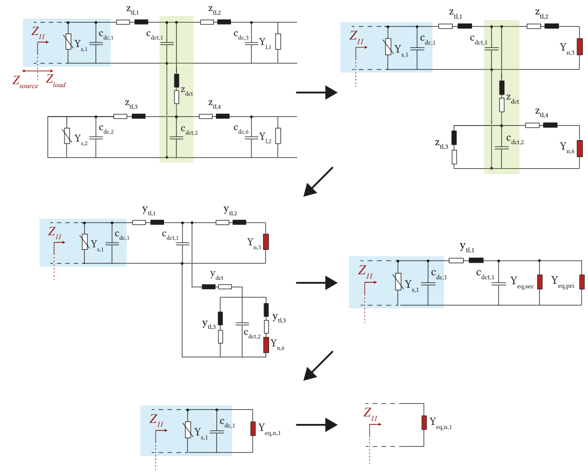

▲ Step-by-step to find equivalent impedance.

NODAL IMPEDANCE ASSESSMENT (I)

Calculation of $Z_{1,1}$ - DC impedance of DC PDN from Node 1.

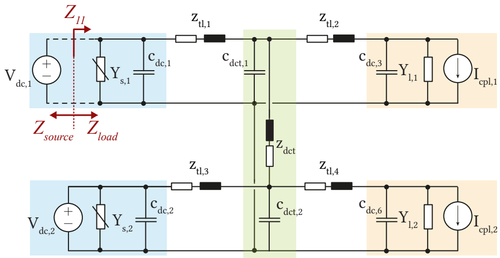

▲ Simplified 6 nodes DC PDN linear equivalent model.

$$Y_{n,3} = c_{dc,3} + Y_{l,1}$$

$$Y_{n,6} = c_{dc,6} + Y_{l,2}$$

$$Y_{eq,sec} = \left[y_{dct}' // \left(y_{tl,3}' + c_{dct,2}' + \left(y_{tl,4}' // Y_{n,6}'\right)\right)\right]$$

$$Y_{eq,pri} = \left(y_{tl,2} // Y_{n,3}\right)$$

$$Y_{eq,n,1} = y_{tl,1} // \left(Y_{eq,sec} + Y_{eq,pri} + c_{dct,2}\right)$$

$$Y_{11} = Y_{s,1} + c_{dc,1} + Y_{eq,n,1}$$

$$Z_{11} = Y_{11}^{-1}$$

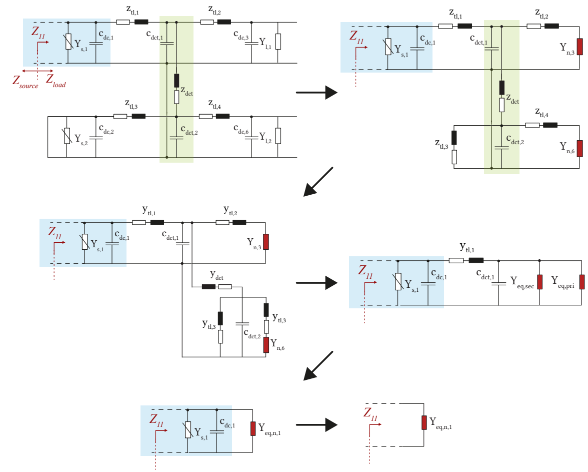

▲ Step-by-step to find equivalent impedance.

Not simple nor scalable!

From mass-spring-damper system to ...

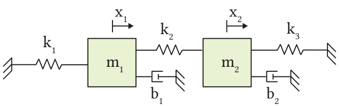

$$\begin{bmatrix} m_1 & 0 \\ 0 & m_2 \end{bmatrix}\begin{bmatrix} \ddot{x}_1 \\ \ddot{x}_2 \end{bmatrix} + \begin{bmatrix} b_1 & 0 \\ 0 & b_2 \end{bmatrix}\begin{bmatrix} \dot{x}_1 \\ \dot{x}_2 \end{bmatrix} + \begin{bmatrix} k_1 + k_2 & -k_2 \\ -k_2 & k_2 + k_3 \end{bmatrix}\begin{bmatrix} x_1 \\ x_2 \end{bmatrix} = \begin{bmatrix} f_1 \\ 0 \end{bmatrix}$$

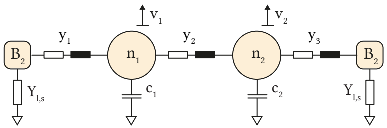

$$\begin{bmatrix} q_1 & 0 \\ 0 & q_2 \end{bmatrix}\begin{bmatrix} \ddot{v}_1 \\ \ddot{v}_2 \end{bmatrix} + \begin{bmatrix} c_1 & 0 \\ 0 & c_2 \end{bmatrix}\begin{bmatrix} \dot{v}_1 \\ \dot{v}_2 \end{bmatrix} + \begin{bmatrix} y_1 + y_2 & -y_2 \\ -y_2 & y_2 + y_3 \end{bmatrix}\begin{bmatrix} v_1 \\ v_2 \end{bmatrix} = \begin{bmatrix} i_1 \\ 0 \end{bmatrix}$$

From mass-spring-damper system to ...

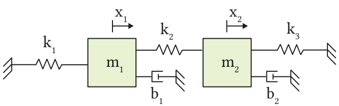

$$\begin{bmatrix} m_1 & 0 \\ 0 & m_2 \end{bmatrix}\begin{bmatrix} \ddot{x}_1 \\ \ddot{x}_2 \end{bmatrix} + \begin{bmatrix} b_1 & 0 \\ 0 & b_2 \end{bmatrix}\begin{bmatrix} \dot{x}_1 \\ \dot{x}_2 \end{bmatrix} + \begin{bmatrix} k_1+k_2 & -k_2 \\ -k_2 & k_2+k_3 \end{bmatrix}\begin{bmatrix} x_1 \\ x_2 \end{bmatrix} = \begin{bmatrix} f_1 \\ 0 \end{bmatrix}$$

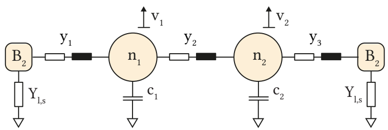

$$\begin{bmatrix} q_1 & 0 \\ 0 & q_2 \end{bmatrix}\begin{bmatrix} \ddot{v}_1 \\ \ddot{v}_2 \end{bmatrix} + \begin{bmatrix} c_1 & 0 \\ 0 & c_2 \end{bmatrix}\begin{bmatrix} \dot{v}_1 \\ \dot{v}_2 \end{bmatrix} + \begin{bmatrix} y_1+y_2 & -y_2 \\ -y_2 & y_2+y_3 \end{bmatrix}\begin{bmatrix} v_1 \\ v_2 \end{bmatrix} = \begin{bmatrix} i_1 \\ 0 \end{bmatrix}$$

$$\cancel{Q\ddot{v}} + C\dot{v} + Yv = I,$$

$$CsVe^{st} + YVe^{st} = Je^{st},$$

$$[Cs + Y]\,V\cancel{e^{st}} = J\cancel{e^{st}}$$

$$V = \underbrace{[Cs + Y]}_{Z}^{-1} J$$

$$V = \underbrace{[Cs + Y_{nodal} + Y_{s,l}]}_{H_Z}^{-1} I$$

Impedance transfer function

$$H_z = \Psi \Lambda \Phi$$

- ⇒ Node's participation factor
- ⇒ Driven points
- ⇒ Eigenanalysis
- ⇒ Mode shape
- ⇒ Sensitivity

- ↯ Includes poles of other voltage controllers
- ↯ It is not the same as state-space model

▼ Example of Node 1 impedance with different controller gains

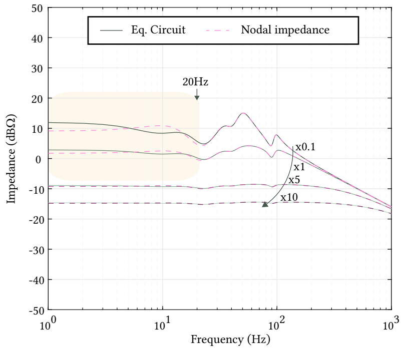

DCT IN MVDC POWER DISTRIBUTION NETWORKS

Operation of the system and impact of DCT in the system.

Power Flow of DC PDN, with different DCT location

- Power flow of dc PDN with different relationship of impedances before and after transformer connection.

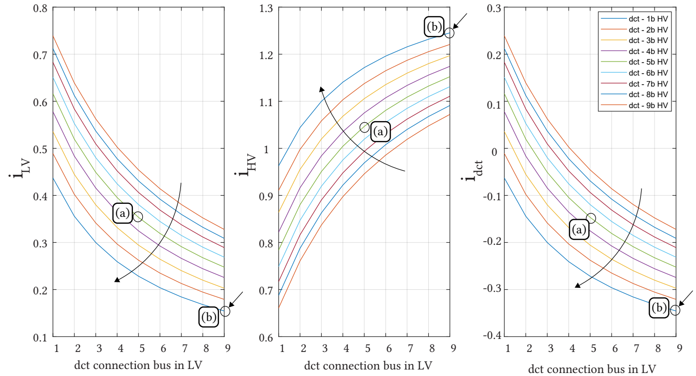

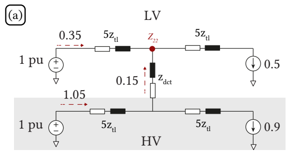

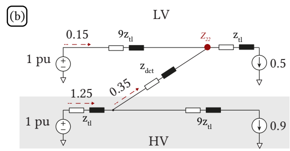

Frequency response of DC PDN, with different location of DCT

- Node impedance of DCT connection for different connection point. [94]

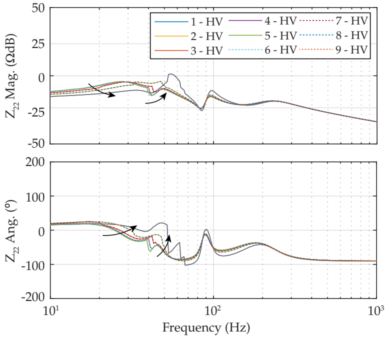

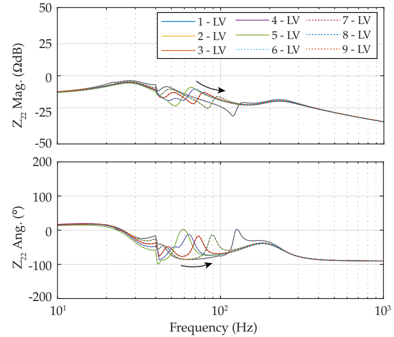

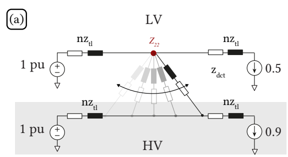

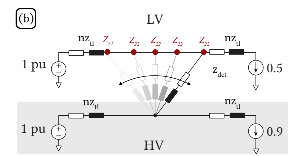

[94] Renan Pillon Barcelos and Drazen Dujic. "Direct Current Transformer Impact on the DC Power Distribution Networks." *IEEE Transactions on Smart Grid* 13.4 (2022), pp. 2547–2556

Connection of extra power converter with...

System operation + model and extra element information

- Set minimum requirements for extra converter
- Add extra dampers to the system
- Limit regions of connections
- ...

Knowledge and control of complete system

- Choose extra converter location
- Change Sources' control loop speed
- Change Impedance characteristic of extra converter
- ...

Interconnected system - "Smart Grid"

- Equipment and dc PDN limits
- ...

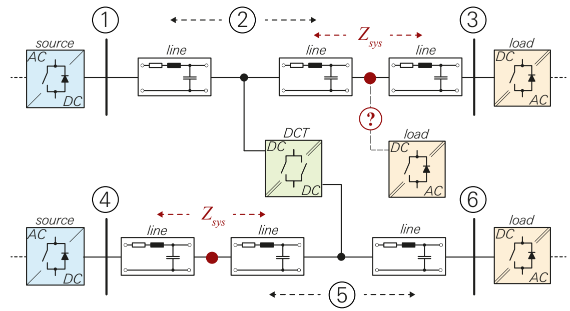

▲ DC PDN with an extra power converter to be connected to the system.

Connection of extra power converter
Choose extra converter location

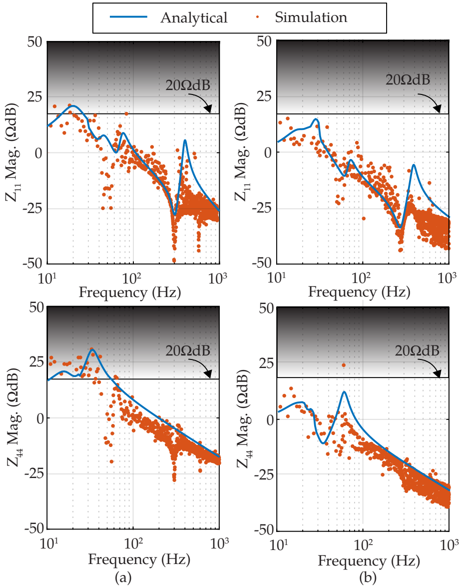

▲ Frequency response for Sources' impedance for extra element connected to (left) Node 3, and (right) Node 2.

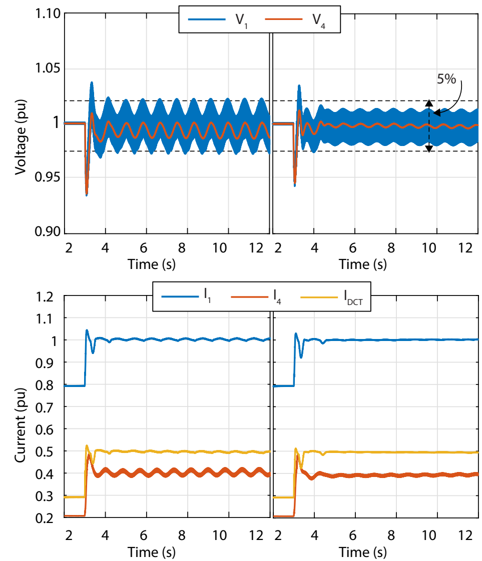

▲ Voltage regulation of the Sources' Nodes with the extra element connected to (left) Node 3, and (right) Node 2.

Connection of extra power converter
Change Sources' control loop speed

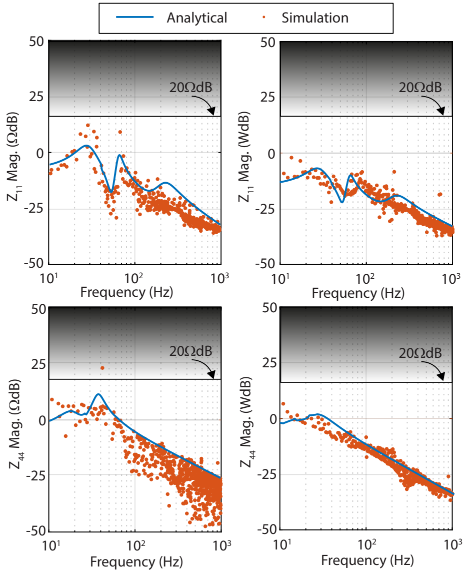

▲ Frequency response for the Sources' impedance with the extra element connected to Node 3 and voltage controller of (left) Node 4, and (right) Node 1, 10x slower.

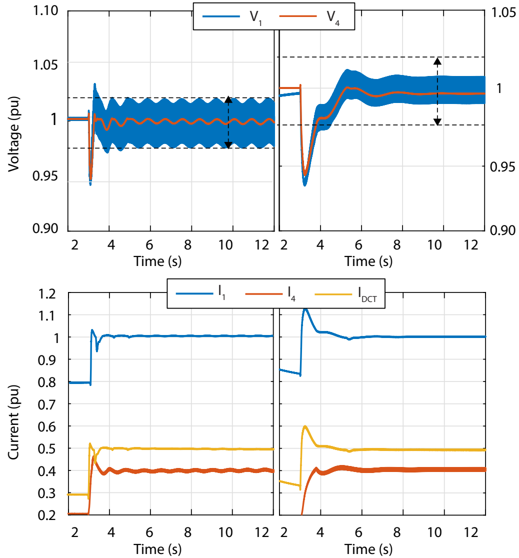

▲ Voltage regulation of the Sources' Nodes with extra element connected to Node 3 and voltage controller of (left) Node 4, and (right) Node 1, 10x slower.

OPERATIONAL PERFORMANCE ASSESSMENT

Nodes, Modes, grid configuration, and impedance assessment.

OPERATIONAL PERFORMANCE ASSESSMENT (I)

Modal response

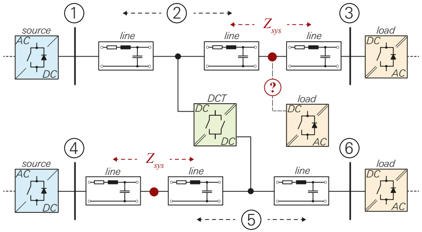

▲ Simple Dc PDN with 6 nodes under consideration.

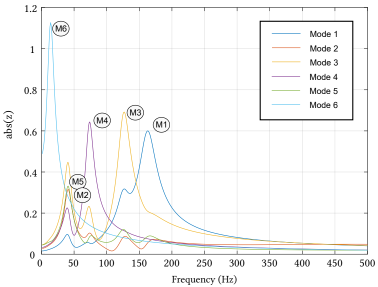

▲ Modes of the system and its magnitude.

Participation Factor

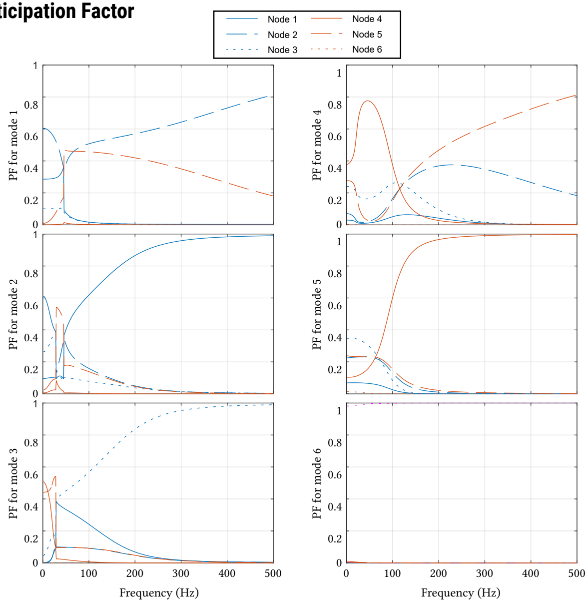

▲ Participation Factor of each Node to the Mode.

OPERATIONAL PERFORMANCE ASSESSMENT (II)

Modal response

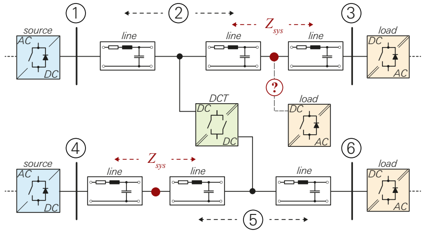

▲ Simple Dc PDN with 6 nodes under consideration.

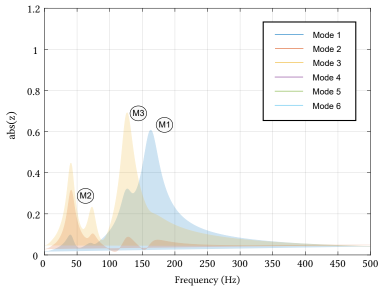

▲ Modes of the system and its magnitude.

Participation Factor

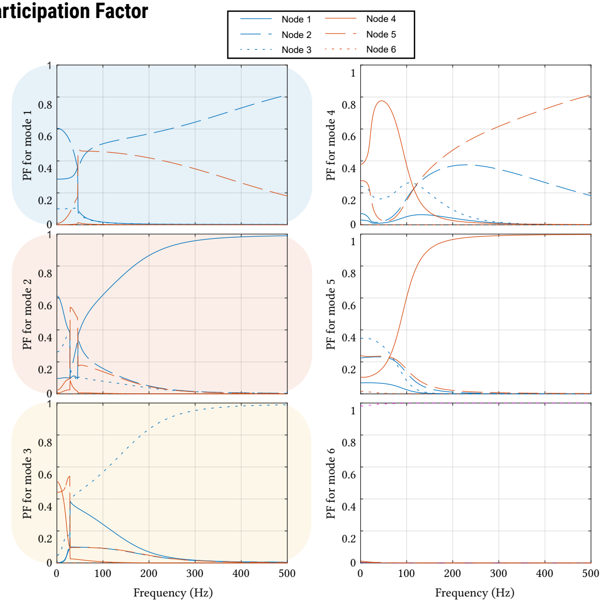

▲ Participation Factor of each Node to the Mode.

Nodes of interest. Nodes' characteristics

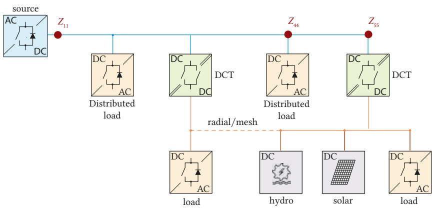

▲ Illustrative example of radial/mesh configuration for a dc PDN with renewables integration.

▲ Aerial view of the illustrative dc PDN for the city of Aigle - Switzerland

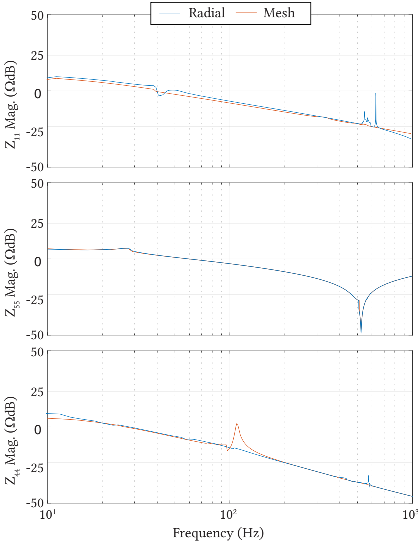

▲ Bode plot of impedance measurements in three different nodes (Source node, Load node, and DCT node).

DIRECT CURRENT TRANSFORMER FEATURES

Operating principles, features, power reversal methods, and practical examples.

DC Transformer

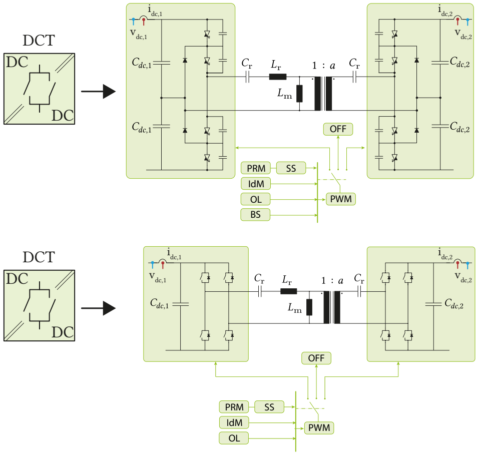

▲ DCT with NPC power stages for high power and Full-bridge power stages for the investigation.

LLC converter benefits

- Open loop operation
- Stiff voltage gain
- High efficiency
- ...

On Features of DC Transformer

- Power Reversal Methods
- Idling Mode Operation
- Soft-start sequence
- Overload Protection
- ...

DC Transformer

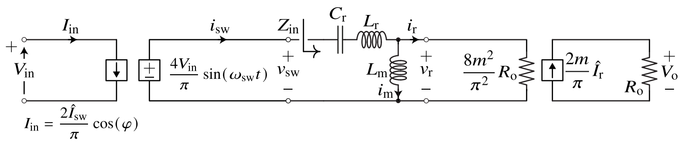

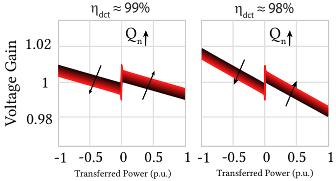

▲ DCT model and characteristic.

DCT 1

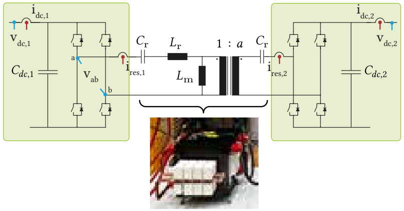

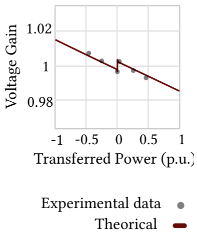

▲ DCT with Full-bridge power stages for the investigation.

DCT 2

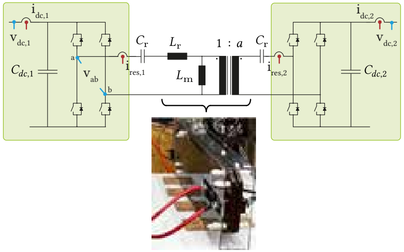

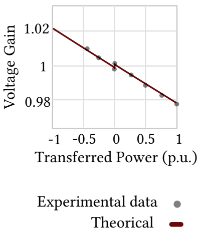

▲ DCT with Full-bridge power stages for the investigation.

Soft-start strategy

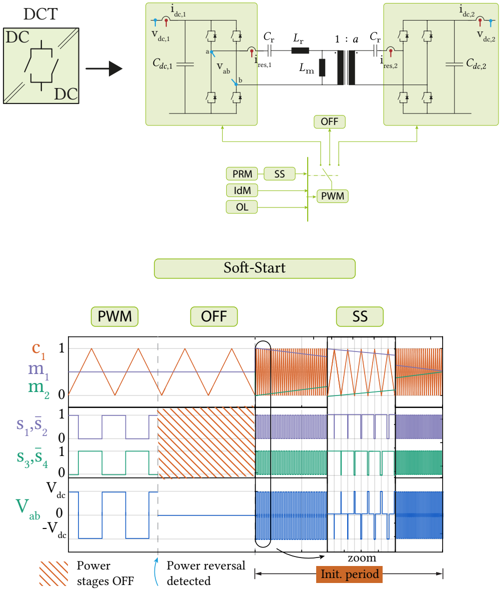

▲ Soft-start strategy

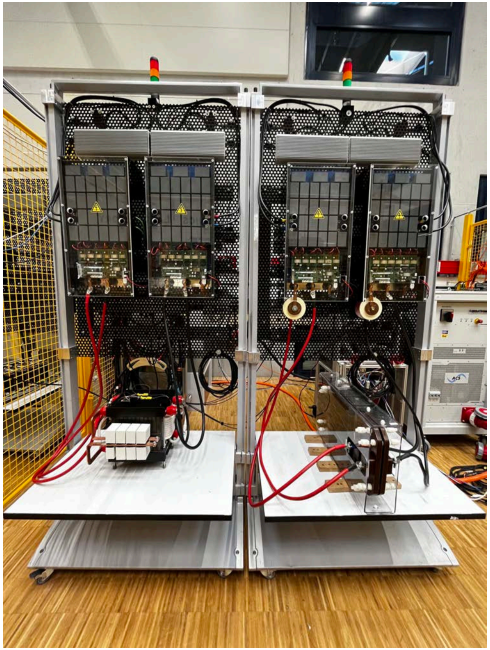

▲ Photo of the two low voltage DCTs of the Laboratory.

Power Reversal Algorithm (I)

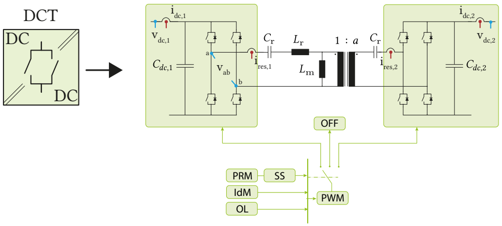

▼ Experimental results for step change.

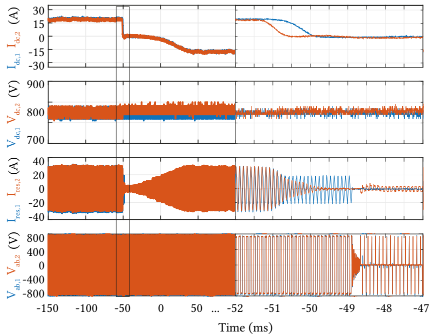

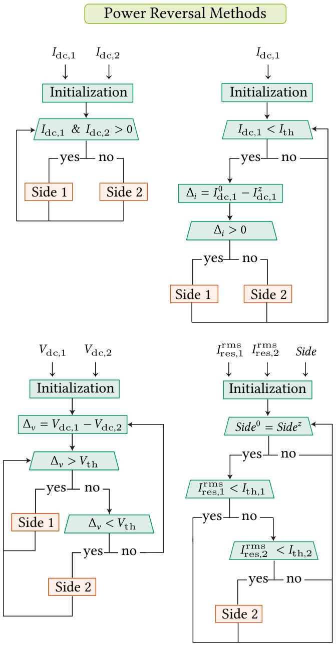

▲ Evaluated Methods.

Power Reversal Algorithm (II)

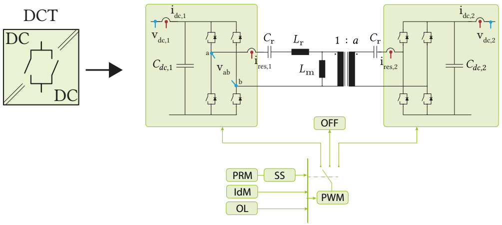

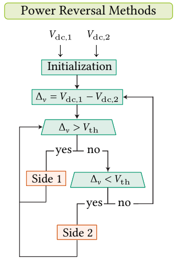

- Experimental results for ramp change and zoom in each stage

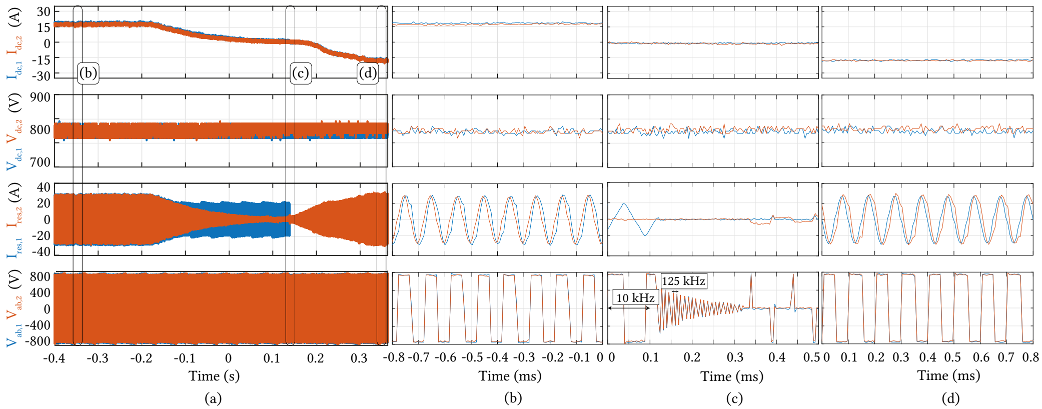

Idling Mode

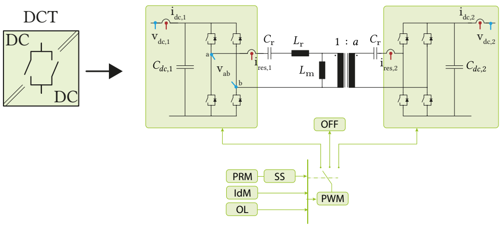

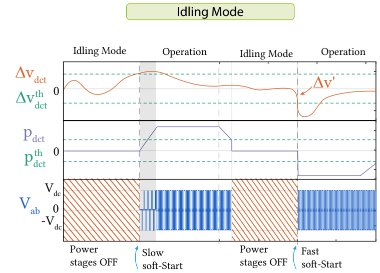

- Experimental results for Idling mode and zoom in each stage

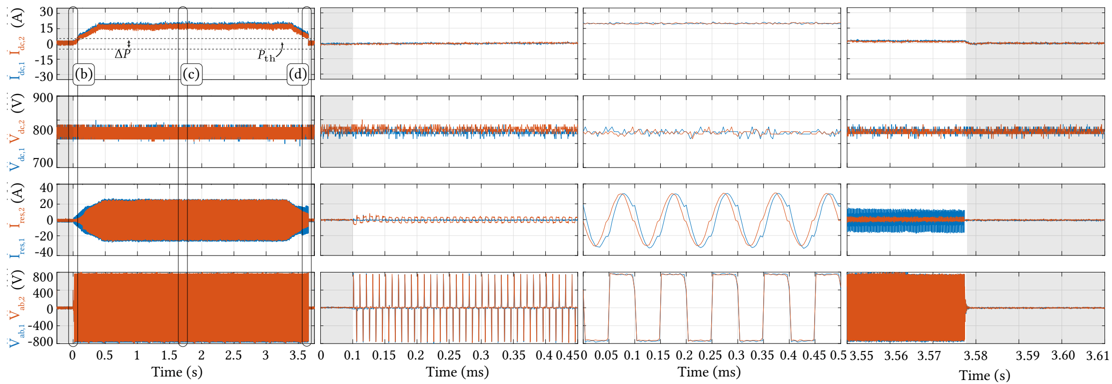

(a) (b) (c) (d)

Current limiting and Overload protection

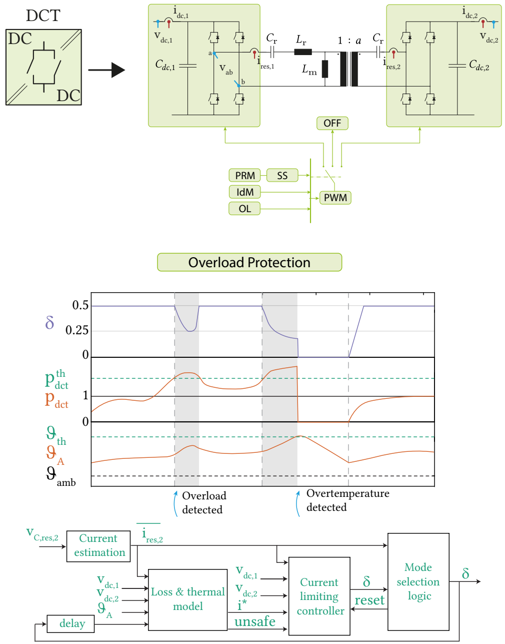

▲ Current limiting strategy

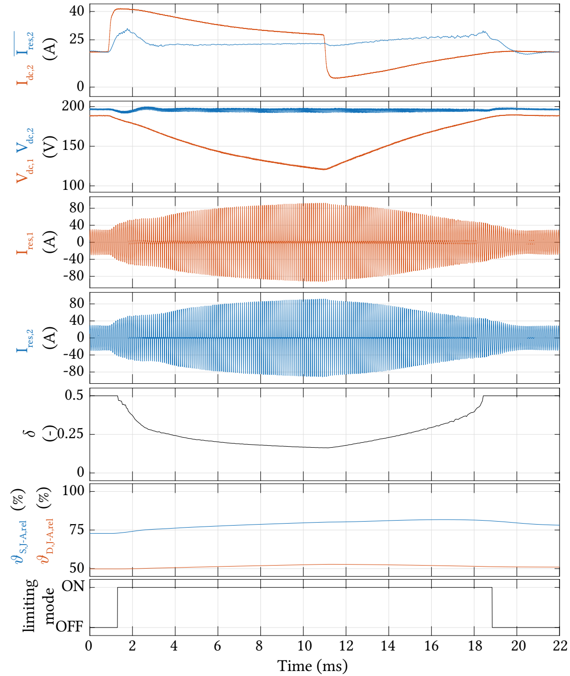

▲ Experimental results for current limiting strategy.

SUMMARY AND CONCLUSIONS

Why DC?, How DC? and When DC?

MVDC BULK POWER CONVERSION

MVDC Power Distribution Networks

- Feasibility
- Technology readiness
- Standards

Conversion

- Modular
- Bulk
- Performances

Applications

- Business Case - Owner
- Business Case - OEM
- Business Case - in general

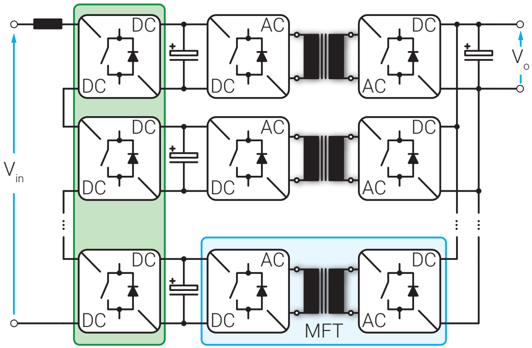

▲ Modular power processing

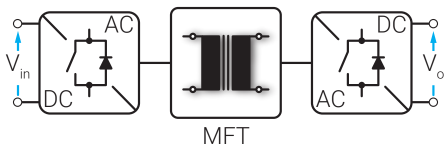

▲ Bulk power processing

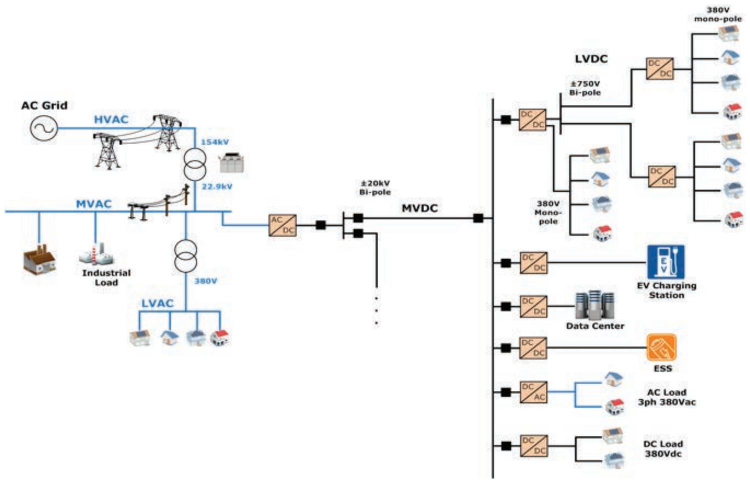

▲ Envisioned future MVDC grids and its links with existing grids

REFERENCES

[1] Uzair Javaid et al. "MVDC supply technologies for marine electrical distribution systems." *CPSS Transactions on Power Electronics and Applications* 3.1 (2018), pp. 65–76.

[2] Alessandro Clerici, Luigi Paris, and Per Danfors. "HVDC conversion of HVAC lines to provide substantial power upgrading." *IEEE transactions on Power Delivery* 6.1 (1991), pp. 324–333.

[3] Michael Häusler, Gernot Schlayer, and Gerd Fitterer. "Converting AC power lines to DC for higher transmission ratings." *ABB review* (1997), pp. 4–11.

[4] D Marene Larruskain et al. "Conversion of AC distribution lines into DC lines to upgrade transmission capacity." *Electric Power Systems Research* 81.7 (2011), pp. 1341–1348.

[5] D Marene Larruskain et al. "VSC-HVDC configurations for converting AC distribution lines into DC lines." *International Journal of Electrical Power & Energy Systems* 54 (2014), pp. 589–597.

[6] ABB. *Tjæreborg*. `http://new.abb.com/systems/hvdc/references/tjaereborg`.

[7] Charles Bodel. *Paimpol-Bréhat tidal demonstrator project*. `http://eusew.eu/sites/default/files/programme-additional-docs/EUSEW1606160PresentationtoEUSEWbyEDF.pdf`. EDF.

[8] G. Bathurst, G. Hwang, and L. Tejwani. "MVDC - The New Technology for Distribution Networks." *11th IET International Conference on AC and DC Power Transmission*. Feb. 2015, pp. 1–5.

[9] SP Energy Networks. *Angle dc*. `https://www.spenergynetworks.co.uk/pages/angle_dc.aspx`.

[10] D. Dujic et al. "Power Electronic Traction Transformer-Low Voltage Prototype." *IEEE Transactions on Power Electronics* 28.12 (Dec. 2013), pp. 5522–5534.

[11] C. Zhao et al. "Power Electronic Traction Transformer-Medium Voltage Prototype." *IEEE Transactions on Industrial Electronics* 61.7 (July 2014), pp. 3257–3268.

[12] M. K. Das et al. "10 kV, 120 A SiC half H-bridge power MOSFET modules suitable for high frequency, medium voltage applications." *2011 IEEE Energy Conversion Congress and Exposition*. Sept. 2011, pp. 2689–2692.

[13] A. Q. Huang. "Medium-Voltage Solid-State Transformer: Technology for a Smarter and Resilient Grid." *IEEE Industrial Electronics Magazine* 10.3 (Sept. 2016), pp. 29–42.

[14] D. Wang et al. "A 10-kV/400-V 500-kVA Electronic Power Transformer." *IEEE Transactions on Industrial Electronics* 63.11 (Nov. 2016), pp. 6653–6663.

[15] Xiaodong Zhao et al. "DC Solid State Transformer Based on Three-Level Power Module for Interconnecting MV and LV DC Distribution Systems." *IEEE Transactions on Power Electronics* 36.2 (2021), pp. 1563–1577.

[16] S. Inoue and H. Akagi. "A Bidirectional Isolated DC-DC Converter as a Core Circuit of the Next-Generation Medium-Voltage Power Conversion System." *IEEE Transactions on Power Electronics* 22.2 (Mar. 2007), pp. 535–542.

[17] Johann W Kolar and Gabriel Ortiz. "Solid-state-transformers: key components of future traction and smart grid systems." *Proc. of the International Power Electronics Conference (IPEC), Hiroshima, Japan*. 2014.

[18] R. W. A. A. De Doncker, D. M. Divan, and M. H. Kheraluwala. "A three-phase soft-switched high-power-density DC/DC converter for high-power applications." *IEEE Transactions on Industry Applications* 27.1 (Jan. 1991), pp. 63–73.

[19] Stefan P Engel, Nils Soltau, and Rik W De Doncker. "Instantaneous current control for the three-phase dual-active bridge DC-DC converter." *Energy Conversion Congress and Exposition (ECCE)*. IEEE. 2012, pp. 3964–3969.

[20] Stefan P Engel et al. "Improved instantaneous current control for the three-phase dual-active bridge DC-DC converter." *ECCE Asia Downunder (ECCE Asia)*. IEEE. 2013, pp. 855–860.

[21] R. Withanage and N. Shammas. "Series Connection of Insulated Gate Bipolar Transistors (IGBTs)." *IEEE Transactions on Power Electronics* 27.4 (Apr. 2012), pp. 2204–2212.

[22] IA Gowaid et al. "Analysis and design of a modular multilevel converter with trapezoidal modulation for medium and high voltage DC-DC transformers." *IEEE Transactions on Power Electronics* 30.10 (2015), pp. 5439–5457.

[23] IA Gowaid et al. "Quasi two-level operation of modular multilevel converter for use in a high-power DC transformer with DC fault isolation capability." *IEEE Transactions on Power Electronics* 30.1 (2015), pp. 108–123.

[24] Stephan Kenzelmann et al. "Isolated DC/DC structure based on modular multilevel converter." *IEEE Transactions on Power Electronics* 30.1 (2015), pp. 89–98.

[25] S. Shao et al. "A Capacitor Voltage Balancing Method for a Modular Multilevel DC Transformer for DC Distribution System." *IEEE Transactions on Power Electronics* 33.4 (Apr. 2018), pp. 3002–3011.

[26] Stefan Milovanovic and Drazen Dujic. "Comprehensive analysis and design of a quasi two-level converter leg." *CPSS Transactions on Power Electronics and Applications* 4.3 (2019), pp. 181–196.

[27] Stefan Milovanovic and Drazen Dujic. "Six-Step MMC-Based High-Power DC-DC Converter." *The 2018 International Power Electronics Conference-IPEC 2018 ECCE Asia*. CONF. 2018.

[28] S. Milovanovic and D. Dujic. "MMC-Based High Power DC-DC Converter Employing Scott Transformer." *PCIM Europe 2018*. June 2018, pp. 1–7.

REFERENCES

[29] Jakub Kucka and Drazen Dujic. "Smooth Power Direction Transition of a Bidirectional LLC Resonant Converter for DC Transformer Applications." *IEEE Transactions on Power Electronics* 36.6 (2021), pp. 6265–6275.

[30] Umamaheswara Vemulapati et al. "Recent advancements in IGCT technologies for high power electronics applications." *2015 17th European Conference on Power Electronics and Applications (EPE'15 ECCE-Europe)*. 2015, pp. 1–10.

[31] Dragan Stamenkovic et al. "Soft Switching Behavior of IGCT for Resonant Conversion." *2019 IEEE Applied Power Electronics Conference and Exposition (APEC)*. 2019, pp. 2714–2719.

[32] Dragan Stamenković et al. "IGCT Low-Current Switching—TCAD and Experimental Characterization." *IEEE Transactions on Industrial Electronics* 67.8 (2020), pp. 6302–6311.

[33] Gabriele Ulissi et al. "High-Frequency Operation of Series-Connected IGCTs for Resonant Converters." *IEEE Transactions on Power Electronics* 37.5 (2022), pp. 5664–5674.

[34] ABB. "Applying IGCT Gate Units." *Application Note 5SYA 2031-05* (2017).

[35] Zhengyu Chen et al. "Stray Impedance Measurement and Improvement of High-Power IGCT Gate Driver Units." *IEEE Transactions on Power Electronics* 34.7 (2019), pp. 6639–6647.

[36] H. Gruening et al. "6 kV 5 kA RCGCT with advanced gate drive unit." *Proceedings of the 13th International Symposium on Power Semiconductor Devices and ICs. IPSD01*. 2001, pp. 133–136.

[37] Luyao Xie, Xinmin Jin, and Yibin Tong. "The design of IGCT Gate-Unit equipped in the three-level NPC converter." *2011 International Conference on Electrical Machines and Systems*. 2011, pp. 1–6.

[38] H.E. Gruening and K. Koyanagi. "A modern low loss, high turn-off capability GCT gate drive concept." *2005 European Conference on Power Electronics and Applications*. 2005, 10 pp.–P.10.

[39] Jakub Kucka and Drazen Dujic. "SOFTGATE – An IGCT Gate Unit for Soft Switching." *PCIM Europe 2022; International Exhibition and Conference for Power Electronics, Intelligent Motion, Renewable Energy and Energy Management*. 2022, pp. 1–9.

[40] Jakub Kucka and Drazen Dujic. "IGCT Gate Unit for Zero-Voltage-Switching Resonant DC Transformer Applications." *IEEE Transactions on Industrial Electronics* 69.12 (2022), pp. 13799–13807.

[41] Jakub Kucka and Drazen Dujic. "Shoot-Through Protection for an IGCT-Based ZVS Resonant DC Transformer." *IEEE Transactions on Industrial Electronics* (2022), pp. 1–1.

[42] Lars Lindenmüller et al. "Loss reduction in a medium frequency series resonance converter by forced evacuation." *2013 IEEE Energy Conversion Congress and Exposition*. 2013, pp. 2044–2051.

[43] Dragan Stamenkovic. "IGCT Based Solid State Resonant Conversion." PhD thesis. EPFL, 2020.

[44] Gabriele Ulissi et al. "Resonant IGCT Soft-Switching: Zero-Voltage Switching or Zero-Current Switching?" *IEEE Transactions on Power Electronics* 37.9 (2022), pp. 10775–10783.

[45] Drazen Dujic et al. "Characterization of 6.5 kV IGBTs for High-Power Medium-Frequency Soft-Switched Applications." *IEEE Transactions on Power Electronics* 29.2 (2014), pp. 906–919.

[46] G. Ortiz et al. "Soft-switching techniques for medium-voltage isolated bidirectional DC/DC converters in solid state transformers." *IECON 2012 - 38th Annual Conference on IEEE Industrial Electronics Society*. 2012, pp. 5233–5240.

[47] A. Nagel et al. "Characterization of IGCTs for series connected operation." *Conference Record of the 2000 IEEE Industry Applications Conference. Thirty-Fifth IAS Annual Meeting and World Conference on Industrial Applications of Electrical Energy (Cat. No.00CH37129)*. Vol. 3. 2000, 1923–1929 vol.3.

[48] M. Jaritz and J. Biela. "Analytical model for the thermal resistance of windings consisting of solid or litz wire." *2013 15th European Conference on Power Electronics and Applications (EPE)*. Sept. 2013, pp. 1–10.

[49] D. C. Jiles and D. L. Atherton. "Theory of ferromagnetic hysteresis (invited)." *Journal of Applied Physics* 55.6 (Mar. 1984), pp. 2115–2120. URL: http://scitation.aip.org/content/aip/journal/jap/55/6/10.1063/1.333582 (visited on 01/15/2016).

[50] F. Preisach. "Über die magnetische Nachwirkung." de. *Zeitschrift für Physik* 94.5-6 (May 1935), pp. 277–302. URL: http://link.springer.com/article/10.1007/BF01349418 (visited on 01/15/2016).

[51] J.H. Chan et al. "Nonlinear transformer model for circuit simulation." *IEEE Transactions on Computer-Aided Design of Integrated Circuits and Systems* 10.4 (Apr. 1991), pp. 476–482.

[52] G. Bertotti. "Some considerations on the physical interpretation of eddy current losses in ferromagnetic materials." *Journal of Magnetism and Magnetic Materials* 54 (Feb. 1986), pp. 1556–1560. URL: http://www.sciencedirect.com/science/article/pii/0304885386909261 (visited on 01/15/2016).

[53] D. Lin et al. "A dynamic core loss model for soft ferromagnetic and power ferrite materials in transient finite element analysis." *IEEE Transactions on Magnetics* 40.2 (Mar. 2004), pp. 1318–1321.

[54] J. Reinert, A. Brockmeyer, and R.W.A.A. De Doncker. "Calculation of losses in ferro- and ferrimagnetic materials based on the modified Steinmetz equation." *IEEE Transactions on Industry Applications* 37.4 (July 2001), pp. 1055–1061.

REFERENCES

[55] Kapil Venkatachalam et al. “Accurate prediction of ferrite core loss with nonsinusoidal waveforms using only Steinmetz parameters.” *2002 IEEE Workshop on Computers in Power Electronics, 2002. Proceedings.* IEEE. 2002, pp. 36–41.

[56] J. Muhlethaler et al. “Improved core loss calculation for magnetic components employed in power electronic system.” *2011 Twenty-Sixth Annual IEEE Applied Power Electronics Conference and Exposition (APEC)*. Mar. 2011, pp. 1729–1736.

[57] P.L. Dowell. “Effects of eddy currents in transformer windings.” *Proceedings of the Institution of Electrical Engineers* 113.8 (1966), p. 1387.

[58] A. Van den Bossche and V. C. Valchev. *Inductors and Transformers for Power Electronics*. Taylor & Francis, Mar. 2005. URL: https://www.crcpress.com/Inductors-and-Transformers-for-Power-Electronics/Valchev-Van-den-Bossche/p/book/9781574446791 (visited on 11/25/2016).

[59] *Convection From a Rectangular Plate*. http://people.csail.mit.edu/jaffer/SimRoof/Convection/.

[60] F. M. White. *Viscous Fluid Flow*. McGraw-Hill Higher Education, 2006.

[61] M Mogorovic and D Dujic. “Thermal Modeling and Experimental Verification of an Air Cooled Medium Frequency Transformer.” *Proceedings of the 19th European Conference on Power Electronics and Applications (EPE 2017 - ECCE Europe), Warsaw, Poland*. 2017.

[62] L. Heinemann. “An actively cooled high power, high frequency transformer with high insulation capability.” *APEC. Seventeenth Annual IEEE Applied Power Electronics Conference and Exposition (Cat. No.02CH37335)*. Vol. 1. Mar. 2002, 352–357 vol.1.

[63] B Engel et al. “15kV/16.7Hz energy supply system with medium frequency transformer and 6.5kV IGBTs in resonant operation.” *Proceedings of the 10th European Conference on Power Electronics and Applications (EPE 2003), Toulouse*. 2003.

[64] J. Taufiq. “Power Electronics Technologies for Railway Vehicles.” *2007 Power Conversion Conference - Nagoya*. Apr. 2007, pp. 1388–1393.

[65] N. Hugo et al. “Power electronics traction transformer.” *2007 European Conference on Power Electronics and Applications*. Sept. 2007, pp. 1–10.

[66] M. Steiner and H. Reinold. “Medium frequency topology in railway applications.” *2007 European Conference on Power Electronics and Applications*. Sept. 2007, pp. 1–10.

[67] H. Hoffmann and B. Piepenbreier. “Medium frequency transformer in resonant switching dc/dc-converters for railway applications.” *Proceedings of the 2011 14th European Conference on Power Electronics and Applications*. Aug. 2011, pp. 1–8.

[68] H. Hoffmann and B. Piepenbreier. “High voltage IGBTs and medium frequency transformer in DC-DC converters for railway applications.” *SPEEDAM 2010*. June 2010, pp. 744–749.

[69] H. Hoffmann and B. Piepenbreier. “Medium frequency transformer for rail application using new materials.” *2011 1st International Electric Drives Production Conference*. Sept. 2011, pp. 192–197.

[70] Gabriel Ortiz. “High-Power DC-DC Converter Technologies for Smart Grid and Traction Applications.” PhD thesis. ETHZ, 2014.

[71] M. Leibl, G. Ortiz, and J. W. Kolar. “Design and Experimental Analysis of a Medium-Frequency Transformer for Solid-State Transformer Applications.” *IEEE Journal of Emerging and Selected Topics in Power Electronics* 5.1 (Mar. 2017), pp. 110–123.

[72] G. Ortiz et al. “Design and Experimental Testing of a Resonant DC-DC Converter for Solid-State Transformers.” *IEEE Transactions on Power Electronics* 32.10 (Oct. 2017), pp. 7534–7542.

[73] T Gradinger, U Drofenik, and S Alvarez. “Novel Insulation Concept for an MV Dry-Cast Medium-Frequency Transformer.” *Proceedings of the 19th European Conference on Power Electronics and Applications (EPE 2017 - ECCE Europe), Warsaw, Poland*. 2017.

[74] S Isler et al. “Development of a 100 kW, 12.5 kV, 22 kHz and 30 kV Insulated Medium Frequency Transformer for Compact and Reliable Medium Voltage Power Conversion.” *Proceedings of the 19th European Conference on Power Electronics and Applications (EPE 2017 - ECCE Europe), Warsaw, Poland*. 2017.

[75] M. Mogorovic and D. Dujic. “Medium Frequency Transformer Design and Optimization.” *PCIM Europe 2017; International Exhibition and Conference for Power Electronics, Intelligent Motion, Renewable Energy and Energy Management*. May 2017, pp. 1–8.

[76] Marko Mogorovic and Drazen Dujic. “100 kW, 10 kHz Medium-Frequency Transformer Design Optimization and Experimental Verification.” *IEEE Transactions on Power Electronics* 34.2 (2019), pp. 1696–1708.

[77] Thomas Guillod. “Modeling and Design of Medium-Frequency Transformers for Future Medium-Voltage Power Electronics Interfaces.” PhD thesis. ETHZ, 2018.

[78] Group Schaffner. *World’s first 5 MW-DC converter*. Accessed 2020.02.13. 2020. URL: https://impulse.schaffner.com/en/worlds-first-5-mw-dc-converter.

[79] Piotr Dworakowski et al. “3-phase medium frequency transformer for a 100kW 1.2 kV 20kHz Dual Active Bridge converter.” *IECON 2019-45th Annual Conference of the IEEE Industrial Electronics Society*. Vol. 1. IEEE. 2019, pp. 4071–4076.

[80] Piotr Czyz et al. “Design and experimental analysis of 166 kW medium-voltage medium-frequency air-core transformer for 1: 1-DCX applications.” *IEEE Journal of Emerging and Selected Topics in Power Electronics* (2021).

REFERENCES

[81] Peng Shuai. "Optimal Design of Highly Efficient, Compact and Silent Medium Frequency Transformers for Future Solid State Transformers." PhD thesis. ETHZ, 2017.

[82] Asier Garcia-Bediaga et al. "Multiobjective Optimization of Medium-Frequency Transformers for Isolated Soft-Switching Converters Using a Genetic Algorithm." *IEEE Transactions on Power Electronics* 32.4 (2017), pp. 2995–3006.

[83] Thomas Guillod, Panteleimon Papamanolis, and Johann W. Kolar. "Artificial Neural Network (ANN) Based Fast and Accurate Inductor Modeling and Design." *IEEE Open Journal of Power Electronics* 1 (2020), pp. 284–299.

[84] Irma Villar. "Multiphysical Characterization of Medium-Frequency Power Electronic Transformers." PhD thesis. EPFL, 2010.

[85] Marko Mogorovic. "Modeling and Design Optimization of Medium Frequency Transformers for Medium-Voltage High-Power Converters." PhD thesis. EPFL, 2019.

[86] Nikolina Djekanovic and Drazen Dujic. "Modeling and characterisation of natural-convection oil-based insulation for medium frequency transformers." *2022 IEEE Applied Power Electronics Conference and Exposition (APEC)*. 2022.

[87] Cheng Lu et al. "AC Resistance Calculation Method for Hollow Conductor Windings in High Power Medium Frequency Transformers." *CSEE* 36.23 (2016).

[88] Nikolina Djekanovic and Drazen Dujic. "Design Optimization of a MW-level Medium Frequency Transformer." *PCIM Europe 2022*. 2022, pp. 1–10.

[89] *Hitachi Metals Ltd. Japan*. `https://www.hitachi-metals.co.jp/e/`. URL: `https://www.hitachi-metals.co.jp/e/`.

[90] *Luvata Pori Oy, Finland*. `https://www.luvata.com/`. URL: `https://www.luvata.com/`.

[91] *Elektro-Isola A/S, Denmark*. `https://www.elektro-isola.com/`. URL: `https://www.elektro-isola.com/`.

[92] *Midel 7131*. `https://www.midel.com/`. URL: `https://www.midel.com/`.

[93] Renan Pillon Barcelos and Dražen Dujić. "Nodal Impedance Assessment in DC Power Distribution Networks." *2021 IEEE 22nd Workshop on Control and Modelling of Power Electronics (COMPEL)*. 2021, pp. 1–8.

[94] Renan Pillon Barcelos and Drazen Dujic. "Direct Current Transformer Impact on the DC Power Distribution Networks." *IEEE Transactions on Smart Grid* 13.4 (2022), pp. 2547–2556.

THANK YOU FOR YOUR ATTENTION

Tutorial pdf can be downloaded from:

- https://www.epfl.ch/labs/pel/publications-2/publications-talks/